# Università degli Studi di Salerno

## Department of Civil Engineering

Doctoral Thesis

# MODELING AND ANALYSIS OF FUNCTIONALLY GRADED NANOBEAMS BASED ON LOCAL/NONLOCAL THEORIES OF ELASTICITY

PhD Program in

**Risk and Sustainability in Civil Engineering, Architecture, Environmental Engineering Systems**

**XXXVI Cycle**

**Supervisor:** Prof.ssa Rosa Penna

**Co-Supervisor:** Prof. Luciano Feo

**PhD Coordinator:** Prof. Fernando Fraternali

**PhD Student:** Giuseppe Lovisi

Academic Year 2022/2023

# Acknowledgements

Desidero esprimere la mia profonda gratitudine a tutte le persone che hanno contribuito con il loro instancabile supporto al completamento di questo percorso di dottorato.

La mia più sentita riconoscenza va ai miei Maestri, la Professoressa Rosa Penna e il Professore Luciano Feo, fonti di ispirazione costante. La loro guida esperta, il sostegno incondizionato e la dedizione alla mia crescita accademica hanno reso possibile il raggiungimento di questo obiettivo.

Alla mia collega di ricerca e amica, Ing. Annavirginia Lambiase, per la collaborazione fruttuosa e la condivisione di idee preziose. Il nostro lavoro di squadra ha reso questa esperienza di ricerca ancora più gratificante.

# Abstract

The aim of this thesis is to introduce the reader to nanotechnologies and functionally graded nanomaterials by providing definitions, classifications and potential applications.

In particular, the thesis summarizes the different theories developed in recent decades to describe the mechanical response of such materials. Functionally graded materials represent an increasingly important class of advanced materials in various engineering applications, such as nano-microelectronic device design, precision sensors, and nanomechanical components.

Initially, a brief introduction to nanotechnology and nanomaterials is provided, highlighting the extraordinary properties emerging at the nanoscale level. In addition, a comprehensive overview of functionally graded materials and micromechanical models used to characterize their thermo-mechanical behavior is presented. This initial overview defines the context and provides the foundation needed to fully understand the challenges and innovations addressed in the thesis.

Subsequently, the document delves into the most commonly used nonlocal theories in scientific literature and their applications in nanoscale material mechanics. It explores the fundamental concepts of non-locality, illustrating how they can be applied to functionally graded nanobeams to capture long-range phenomena and nonlocal interactions that influence structural behavior.

Firstly, the thesis extends the three-parameter nonlocal models of elasticity (L/NStrainG and L/NStressG) proposed in the literature, incorporating hygrothermal effects (L/NStrainGH and L/NStressGH) and evaluates their influence on static and dynamic responses. Moreover, the nonlocal surface stress-driven model of elasticity (SSDM) is extended to study the static response of functionally graded nanobeams, also in presence of discontinuous loads. This aspect provides an in-depth understanding of the behavior of such materials in real-world situations, with significant implications for nanodevice and nanoscale systems engineering. In addition, a rotational hinge-based approach is introduced to assess the effects of cracks, contributing to a comprehensive understanding of the factors influencing structural stability. The focus on these innovative aspects and original results significantly enriches the field of nanoscale material mechanics and opens promising prospects for future development and optimization of nanomechanical devices.

In the analysis process, the Mathematica software was used to solve the governing equations of the problem. In particular, Galerkin's method has been employed to obtain approximate numerical solutions, and a Higher Order Hamiltonian Approach has been proposed to study higher order nonlinear flexural frequencies.

In conclusion, the thesis represents a contribution to the in-depth understanding of functionally graded nanobeams through the use of nonlocal theories. Moreover, the focus on surface energy effects, as well as on hygrothermal environment and cracks, provides a comprehensive and detailed view of the structural and mechanical behavior of these nanostructures. The results obtained and methodologies established have the potential to exert substantial influence on improving the design and engineering of nanodevices and nanoscale systems.

**Keywords:** Nanomaterial, Functionally Graded Material, Nanobeam, Local/Nonlocal Elasticity Theories, Hygrothermal Environments, Surface Effects, Crack.

# Content

# List of Figures

# List of Tables

# List of Publications

I. Rosa Penna, Luciano Feo, **Giuseppe Lovisi**, Hygro-thermal bending behavior of porous FG nano-beams via local/nonlocal strain and stress gradient theories of elasticity, Composite Structures, Volume 263, 2021, 113627, ISSN 0263-8223, https://doi.org/10.1016/j.compstruct.2021.113627.

II. Penna, R.; Feo, L.; **Lovisi, G.**; Fabbrocino, F. Hygro-Thermal Vibrations of Porous FG Nano-Beams Based on Local/Nonlocal Stress Gradient Theory of Elasticity. *Nanomaterials* **2021**, *11*, 910. https://doi.org/10.3390/nano11040910.

III. Penna, R.; **Lovisi, G.**; Feo, L. Dynamic Response of Multilayered Polymer Functionally Graded Carbon Nanotube Reinforced Composite (FG-CNTRC) Nano-Beams in Hygro-Thermal Environment. *Polymers* **2021**, *13*, 2340. https://doi.org/10.3390/polym13142340.

IV. Penna, R.; Feo, L.; **Lovisi, G.**; Fabbrocino, F. Application of the Higher-Order Hamilton Approach to the Nonlinear Free Vibrations Analysis of Porous FG Nano-Beams in a Hygrothermal Environment Based on a Local/Nonlocal Stress Gradient Model of Elasticity. *Nanomaterials* **2022**, *12*, 2098. https://doi.org/10.3390/nano12122098.

V. Rosa Penna, Luciano Feo, **Giuseppe Lovisi**, Arturo Pascuzzo, A stress-driven model incorporating surface energy effects for the bending analysis of functionally graded nanobeams with loading discontinuities, Procedia Structural Integrity, Volume 47, 2023, Pages 789-799, ISSN 2452-3216, https://doi.org/10.1016/j.prostr.2023.07.040.

VI. **Giuseppe Lovisi**, Application of the surface stress-driven nonlocal theory of elasticity for the study of the bending response of FG cracked nanobeams, Composite Structures, Volume 324, 2023, 117549, ISSN 0263-8223, https://doi.org/10.1016/j.compstruct.2023.117549.

VII. Rosa Penna, Annavirginia Lambiase, **Giuseppe Lovisi** and Luciano Feo. Investigating hygrothermal bending behavior of FG nanobeams via local/nonlocal stress gradient theory of elasticity with general boundary conditions, Mechanics of advanced materials and structures, https://doi.org/10.1080/15376494.2023.2269938.

## List of Conference

I. ICCS23 - 23rd International Conference on Composite Structures MECHCOMP6 - 6th International Conference on Mechanics of Composites. FEUP-Faculty of Engineering, University of Porto, Portugal, 1- 4 September 2020. Title: “Nonlinear vibrations analysis of pre-tensioned Bernoulli-Euler functionally graded nanobeams”, Authors: Penna Rosa, Feo Luciano, Fortunato Antonio, **Lovisi Giuseppe**.

II. MECHCOMP7 – 7th International Conference on Mechanics of Composites, Faculty of Engineering, University of Porto, Portugal, 1-3 September 2021. Title: “On the Structural bending response of P-FG nano-beams under hygro-thermo-mechanical loadings”, Authors: Penna Rosa, Feo Luciano, **Lovisi Giuseppe**.

III. 1st International Conference of Mechanics of Solids (MS2022). 3-4 November 2022 - FEUP, Porto – Portugal. Title: “Static analysis of FGM nano-size structures including surface effects based on stress-driven nonlocal theory of elasticity”, Authors: Rosa Penna, **Giuseppe Lovisi**, Annavirginia Lambiase, Luciano Feo.

IV. 1st International Conference of Mechanics of Solids (MS2022), 3-4 November 2022 - FEUP, Porto – Portugal. Title: “Nonlinear free vibrations analysis of porous functionally-graded nano-beams in hygrothermal environment”, Authors: Rosa Penna, **Giuseppe Lovisi**, Annavirginia Lambiase, Luciano Feo.

V. 27th International Conference on Fracture and Structural Integrity, Session 2 – Thursday February 23 - 2023. Title: “A stress-driven model incorporating surface energy effects for the bending analysis of functionally graded nanobeams with discontinuities”, Authors: Rosa Penna, Luciano Feo, **Giuseppe Lovisi**, Artura Pascuzzo.

VI. EUROMSN2023, International Congress and Expo on Materials Science & Nanoscience, June 28-30-2023, Paris, France. Title: “Application of a stress-driven nonlocal model incorporating surface energy effects for the bending analysis of cracked FG nanobeams with loading discontinuities”, Authors: Rosa Penna, **Giuseppe Lovisi**, Annavirginia Lambiase, Luciano Feo.

VII. EMI2023IC, August 27-30 2023, Palermo, Italy. Title: “Application of a stress-driven nonlocal model incorporating surface energy effects for the bending analysis of cracked FG nanobeams”, Author: **Giuseppe Lovisi**.

VIII. EMI2023IC, August 27-30 2023, Palermo, Italy. Title: “On the effect of carbon nanotubes in Ultra-High Performance Fibers Reinforced Concrete: preliminary results”, **Autori**: Annavirginia Lambiase, Luciano Feo, **Giuseppe Lovisi**, Enzo Martinelli, Marco Pepe e Rosa Penna.

IX. Proceedings of the 3rd International Conference on Computations for Science and Engineering, 20-23 September, Naples. Title: “Experiments and micromechanical modeling of the electromechanical properties of carbon nanotube/high performance concrete”, Authors: Feo Luciano, Lambiase Annavirginia, **Lovisi Giuseppe**, Penna Rosa.

## Nomenclature

| *Symbol* | *Definition* |
|---|---|
| $FG$ | Functionally Graded |
| $B$ | Bulk of FG Material |
| $S$ | Surface of FG Material |
| $L$ | Length of FG Nanobeam |
| $\Sigma$ | Cross-Section of FG Nanobeam |
| $\partial\sigma$ | Perimeter of $\Sigma$ |
| $B$ | Width of FG Nanobeam |
| $H$ | Height of FG Nanobeam |
| $O$ | Geometric Center of $\Sigma$ |
| $x'$ | Nanobeam Axis |
| $y', z'$ | The Principal Axes of Geometric Inertia of $\Sigma$ |
| $C$ | Elastic Center of $\Sigma$ |
| $T$ | Temperature |
| $A_E$ | Axial Stiffness of FG Nanobeam |
| $S_E$ | Elastic Static Moment |
| $I_E$ | Bending Stiffness of FG Nanobeam |
| $A_\rho$ | Mass Density of FG Nanobeam |
| $S_\rho$ | Static Moment of Mass (or Couple Rotary) |
| $I_\rho$ | Rotary Inertia of FG Nanobeam |
| $n$ | Gradient Index of FG Material |
| $\zeta$ | Porosity Volume Fraction |
| $E$ | Young's Modulus |

| | |
|---|---|
| $\rho$ | Mass Density |
| $\alpha$ | Thermal Coefficient |
| $\beta$ | Moisture Coefficient |
| $K$ | Thermal Conduction Coefficient |
| $E^B$ | Young’s Modulus of The Bulk Material |
| $E^S$ | Surface Elastic Modulus |
| $\tau^S$ | Residual Surface-Stress |
| $\nu$ | Poisson’s Ratio |
| $m$ | Metal |
| $c$ | Ceramic |
| $\Delta T_{UTR}$ | Uniform Temperature Rise |
| $\Delta T_{HC}$ | Heat-conduction Rise |
| $\varDelta H$ | Uniform Moisture Rise |
| $\varPhi_{L_c}$ | The scalar averaging kernel |
| $L_c$ | Characteristic length of material |
| $L_l$ | Gradient length |
| $\xi_1$， $\xi_2$ | The phase parameters |
| $\lambda_c$ | Nonlocal parameter |
| $\lambda_l$ | Gradient length parameter |
| $u_x, u_y, u_z$ | Cartesian Components of the displacement field of the FG Nanobeam along *x, y a*nd *z* directions |
| $t$ | Time |
| $w = w(x, t)$ | The transverse displacements of *C* |
| $\varepsilon_{xx}^{el}$ | The elastic axial strain component |
| $\varepsilon_{xx}$ | Total axial strain |
| $\varepsilon_{xx}^{*}$ | The non-elastic axial strain |
| $\sigma_{xx}$ | The axial stress component |
| $\sigma_x^B$ | Uniaxial stress state of the *B* |

| | |
|---|---|
| $\sigma_x^S, \tau_{zx}^S$ | Stresses state of *S* |
| $\sigma_z^B$ | The component of the Bulk Stress in *z* direction |
| $\chi$ | Geometrical bending curvature |
| $\delta U$ | Virtual strain energy |
| $\delta W$ | Virtual work done by external forces |
| $\delta K$ | Virtual kinetic energy |
| $N^T, N^H$ | Hygrothermal resultants of axial force |
| $M^T, M^H$ | Hygrothermal resultants of bending moments |
| $q_z$ | Transverse vertical distributed load |
| $C$, $F$ | Concentrated couple and force |
| $M$ | Bending moment |
| $N$ | Axial stress |
| L/NStressG | Local/Nonlocal Stress Gradient Model |
| L/NStrainG | Local/Nonlocal Strain Gradient Model |
| L/NStressGH | Hygrothermal Local/Nonlocal Stress Gradient Model |
| L/NStrainGH | Hygrothermal Local/Nonlocal Strain Gradient Model |
| SDM | Stress-Driven Model |
| EDM | Strain-Driven Model (or Eringen Differential Model) |
| $M^{L/NStressGH}$ | Hygrothermal Nonlocal Stress Gradient Moment Resultant |
| $M^{L/NStrainGH}$ | Hygrothermal Nonlocal Strain Gradient Moment Resultant |
| $N^{L/NStressGH}$ | Hygrothermal Stress Gradient Axial Force |
| $\tilde{V}^{L/NStressGH}$ | Hygrothermal Nonlocal Stress Gradient Shear Force |
| $\widehat{N}$ | Mid-Plane stretching effect |
| $\Omega$ | Natural frequency of flexural vibrations |
| $\widetilde{\omega}_{loc}$ | Dimensionless local natural frequency |
| $\widetilde{W}$ | Non-dimensional spatial shape |
| $W_i(\tilde{x})$ | The *i-th* test function |
| $W_i(t)$ | He unknown *i-th* time-dependent coefficient |

| | |
|---|---|
| $\mathcal{A}_w$ | The amplitude of the nonlinear oscillator |
| $W_1(\tilde{x})$ | The linear spatial mode based on L/NStressGH |
| $\tilde{g}$ | Gyration radious of FG Nanobeam |
| $I_E^*$ | Equivalent bending stiffness |
| $C_m$ | Flexibility constant of rotational spring |
| $\Delta\emptyset$ | Discontinuity in the slope |
| $\bar{\alpha}$ | Crack ratio |
| $\frac{\partial}{\partial x}$ | Derivative with respect to *x* |
| $\frac{\partial}{\partial t}$ | Derivative with respect to t |

## Preface

Due to the considerable interest in the emerging fields of nanotechnology, nanoengineering and nanoscience, small-scale modelling and analysis able to capture size-dependent effects in ultrasmall materials and structures have garnered great attention from academic researchers.

A comprehensive understanding of the mechanical behavior of nanostructures, including nanobeams, nanoplates, and nanoshells, is essential for the design and optimization of small-scale electromechanical devices. Among these small-sized structures, nanobeams are basic structural elements widely used in several engineering applications like nanoactuators and nanosensors. Furthermore, to improve their performance, these devices are often fabricated using functionally graded composite or nanocomposite materials, which overcome typical problems associated with conventional composite materials, such as material interface discontinuities (cracking, delamination, and stress concentration). Furthermore, these materials are suitable for use in environments with severe hygrothermal conditions. Consequently, the mechanical analysis of functionally graded nanostructures has attracted considerable interest within the scientific community.

As demonstrated by nanoscale experiments and atomistic simulations, small-scale phenomena (nonlocal interactions, surface effects, etc.) have a substantial impact, to the point that both static and dynamic structural responses are strongly size-dependent. Classical continuum mechanics is based on the assumption that the constitutive laws obey the local axiom, meaning that the response at one material point of the continuum is not affected by the state of the continuum at distant material points. This is true and produces accurate results for the structural response when the external characteristic length of a continuum (e.g., structural size, wavelength, etc.) is much greater than an internal characteristic length (granular distance, interatomic length, dimensions of heterogeneity, etc.). However, if the external and internal characteristic lengths are comparable, local theories fail to predict effective mechanical behavior, considering the nonlocality necessary to account for long-range interatomic interactions. Therefore, the locality assumption must be removed and nonlocal elasticity models must be considered.

Furthermore, unlike macroscale structures where the surface region can be neglected in the study of mechanical behavior and bulk properties can be used as general properties, nanoscale structures are characterized by a significant surface area relative to the volume of the material. As a result, the energy of atoms near the surface is significant, leading to the formation of surface residual stresses and surface elasticities different from the bulk material. To account for these surface energy-related effects, further theories are needed to capture both nonlocal interactions and surface effects characteristic of nanoscale structures.

As is known, the presence of cracks in structures and nanostructures significantly affects their mechanical properties and stiffness. Many researchers are studying the static and dynamic responses of nanobeams in the presence of cracks. These studies can be developed through rigorous approaches, such as 2-D and 3-D numerical analyses based on the finite element method or using simplified methodologies that require less computational effort.

The present thesis aims to provide an in-depth treatment of the modelling and analysis of functionally graded nanobeams using nonlocal elasticity theories. The document is organized in five Chapters and the main results are summarized in the Conclusions.

Chapter 1 introduces the concepts of nanotechnologies and nanomaterials, providing classification and description of their properties, as well as the most commonly used manufacturing methods. The main small-scale effects characteristic of nanomaterials and their fields of application are then described.

Chapter 2 provides a broad overview of functionally graded materials (FGM), starting from their origins, manufacturing methods and fields of application with practical examples. The micromechanical models used to study their mechanical behavior are described in detail, including the presence of heat sources. The chapter concludes with a series of numerical applications.

Chapter 3 gives an overview of the most commonly used nonlocal theories in the scientific literature. In particular, fundamental concepts of nonlocal mechanics are explained, describing the inapplicability and mathematical inconsistency of the Eringen model (EDM) and the Lim model (NStrainG) for the structural response of nanobeams. This requires the use of well-posed nonlocal models with a single parameter (SDM) or three parameters (L/NStressG and L/NStrainG).

Since functionally graded nanobeams are suitable for use in high-temperature and high-humidity environments, Chapter 4 extends the aforementioned well-posed nonlocal models (L/NStressG and L/NStrainG) to study the static and dynamic structural response of porous functionally graded nanobeams in hygrothermal environments, considering two different types of temperature increase. This chapter introduces local/nonlocal gradient models that take into account hygrothermal boundary conditions. To solve the differential equations that govern the problem, the Mathematica software is first used and the Galerkin method was implemented in it, which allows obtaining approximate numerical solutions; subsequently, to obtain the nonlinear frequencies, the higher order Hamiltonian approach proposed by He was implemented which allows obtaining the frequency expression in closed form. Finally, a parametric analysis was conducted and the results were reported in tables and figures.

The objective of Chapter 5 of this thesis is to consider not only nonlocal effects but also surface energy effects. First of all, the model recently proposed by Penna, based on the coupling of the nonlocal SDM theory with the surface elasticity theory introduced by Gurtin and Murdoch, is presented. An extension was first conceived for the study of functionally graded nanobeams in the presence of discontinuous loads and then for the study of cracked FG nanobeams. The chapter provides a description of the method used to model the crack, a discussion of the applicability and limitations of this approach; finally, results obtained in terms of comparison between the SDM model without surface effects and the proposed SSDM approach with surface effects are presented.

# Chapter 1

# Nanotechnology and Nanomaterials

Nanotechnology is a scientific and technological discipline dealing with the manipulation and engineering of matter at the atomic and molecular level. This extraordinary field of study offers the possibility to create, modify and control nanomaterials and nanostructures, enabling the invention of new paradigms and devices. The importance of this field is evident in the acceleration of scientific discoveries and in the optimization of resources, directly influencing economic competitiveness and social progress.

In the scientific and technological landscape of the 21st century, few disciplines have generated an impact comparable to that of nanotechnology which is radically transforming the entire landscape of applied science and industry, as it shapes our world in ways that challenge traditional concepts and open unimaginable doors to innovation. At the same time, nanomaterials are also emerging as key players in materials science. The combination of nanomaterials and nanotechnology is revolutionizing key industries such as industry, energy, electronics, engineering and medicine.

Due to their nanoscale size, nanomaterials offer unique and amazing properties that set them apart from traditional materials. In this chapter, after a brief overview of nanotechnology, the distinctive features of nanomaterials that differentiate them from traditional materials will explored. Particular emphasis will be placed on practical applications of nanomaterials, including civil engineering in order to demonstrate how their use may offer more efficient and environmentally friendly solutions to global challenges.

## 1.1. Introduction to Nanotechnology

Nanotechnology, as a concept and field of study, began to take shape in the mid-20th century but gained significant attention following a famous lecture entitled

<<*There's Plenty of Room at the Bottom*>> [1] by physicist Richard Feynman at the annual meeting of the American Physical Society at Caltech on December 29, 1959. He urged the audience to focus on understanding phenomena on a very small scale. The term "Nanotechnology" was first used by Taniguchi in 1974 in the article titled "On the basic concept of Nano-Technology: Nanotechnology mainly consists of the processing of separation, consolidation, and deformation of materials by one atom or one molecule" [2]. Since then, nanotechnology has been considered an emerging and multidisciplinary technology and has inspired many scientists to create new materials and devices by manipulating individual atoms and molecules.

The study and practical use of nanotechnology required the development of tools and techniques capable of manipulating and studying structures at the nanoscale. In the 1980s and 1990s, with the advent of scanning tunnelling microscopes (STMs) and atomic force microscopes (AFMs), researchers have taken significant steps in understanding and manipulating nanoscale materials and structures. This period marked the emergence of nanoscience and nanotechnology as recognized scientific disciplines.

The term "Nanotechnology" gained wide recognition at the end of the 20th century. The National Nanotechnology Initiative (NNI) in the United States, established in 2000, has played a key role in coordinating and funding research in the field. Many countries have followed suit by launching their own initiatives in the field of nanotechnology. From a scientific point of view, "*Nanotechnology can be defined as the reference to materials and systems with structures and components that exhibit new and significantly improved physical, chemical, and biological properties, as well as to the phenomena and processes made possible by the ability to control material properties at the nanoscale*" (definition by the National Science and Technology Center, NNI, USA). Advances in nanotechnology research have led to the development of numerous commercial devices using nanomaterials, initially primarily in the field of electronics (NEMs and MEMs). Today, nanotechnology is a thriving field with applications in various fields, including electronics, medicine, physics, biology, engineering, and materials science. This wide use of nanotechnology and the considerable interest in scientific research are due to the exceptional and unique properties exhibited by nanomaterials.

## 1.2. Nanomaterials

### 1.2.1. Definition, classification and properties

Nanomaterials are materials that have at least one dimension ranging from 1 to 100 nanometers (Figure 1.1) [3,4]. At this scale, materials exhibit unique properties and behaviours that differ from their macroscopic counterparts due to quantum effects and increased surface area.

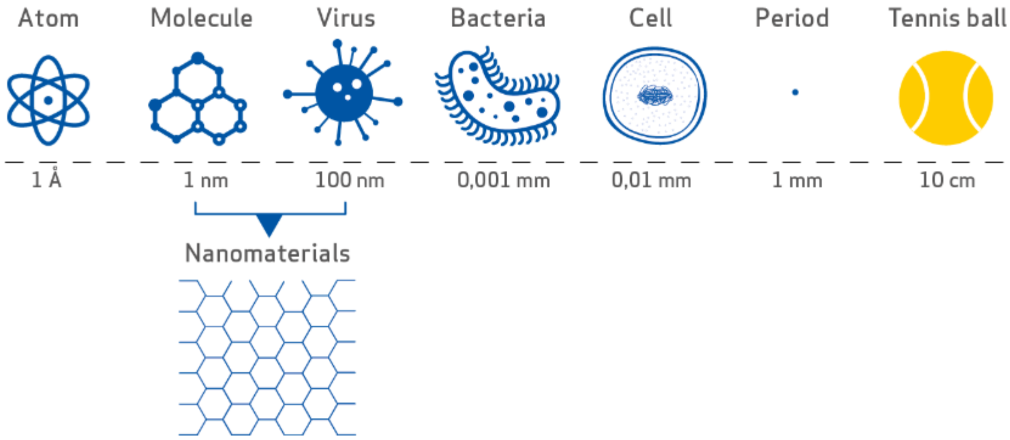

**Figure 1.0.1.** Scale of magnitudes of some common objects and elements. [4]

On October 18, 2011, the European Commission adopted the following definition of nanomaterials: "*A natural, incidental, or manufactured material containing particles, in an unbound state or as an aggregate or as an agglomerate, and where, for 50% or more of the particles in the number size distribution, one or more external dimensions is in the size range 1 nm – 100 nm. In specific cases and where warranted by concerns for the environment, health, safety, or competitiveness, the number size distribution threshold of 50% may be replaced by a threshold between 1% and 50%*".

As illustrated in Figure 1.2, nanomaterials can be classified into different groups according to different criteria [5], such as dimensionality, morphology, state, and chemical composition.

Based on dimensionality, nanomaterials are classified into zero-dimensional structures (0D), when all three dimensions are at the nanoscale level; one-dimensional structures (1D), when only one of the three dimensions is greater than 100 nm, two-dimensional structures (2D), when only one of the three dimensions is at the nanoscale level; three-dimensional structures (3D), if none of the three dimensions is at the nanoscale level [5,6].

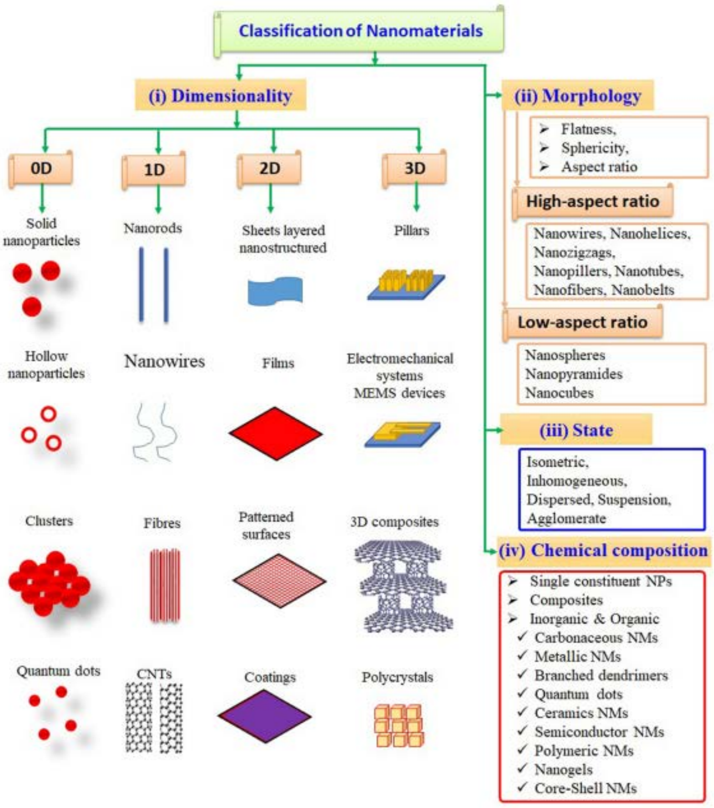

**Figure 1.0.2**. Schematic illustration of the classification of nanomaterials based on different criteria. [6]

These categories can include amorphous or crystalline materials, monocrystalline or polycrystalline materials, composed of one or more chemical elements, isolated or integrated into a matrix, and so on. Nanoscale materials can exhibit different properties compared to their macroscopic counterparts, allowing unique applications: opaque materials become transparent (copper); chemically inert materials acquire catalytic properties (gold, nickel, iron); stable materials become combustible (aluminium); insulating materials become conductive (silicon) [6]. Such changes are related to quantum effects such as variations in electronic structure, a high number of surface atoms, an increase in unsaturated bonds (dangling bonds), and variations in the bandgap. The morphological nature of nanomaterials includes planarity, sphericity, as well as proportions. For uniformity, they can be classified as isotropic and nonhomogeneous or dispersed and agglomerated. Nanomaterials with diverse morphologies include nanotubes, nanozigzags, nanohooks, nanostars, nanocubes, nanoscrews, and nanoplates [6].

### 1.2.2. Methods for synthesis and fabrication of nanomaterials

The production of nanomaterial employs two fundamental approaches that are often used: the chemical approach (also known as bottom-up) and the physical approach (also known as top-down). These two approaches are complementary and are chosen based on the specific needs of the production process and the desired properties of the nanomaterials. The bottom-up approach exploits the ability of some atoms and molecules to self-assemble due to their inherent nature and that of the substrate. On the other hand, the top-down approach involves creating very small structures from bulk materials. This approach entails the removal of material or the modification of existing structures to achieve nanoscale dimensions [6].

Some examples of bottom-up and top-down techniques are given in the following.

**Bottom-up techniques**

- Chemical Synthesis: this is one of the most common methods for production of nanomaterials. It involves the reaction of chemical precursors in solution to form the desired nanomaterials;
- Molecular Self-Assembly: molecules are designed to attract or bond with each other in a specific way to form desired nanoscale structures. One example is the self-assembly of DNA molecules to create nanoscale structures;
- Atomic Layer Deposition (ALD): this technique allows for the growth of thin films of material one atomic layer at a time, carefully controlling the deposition of each layer.

**Top-down techniques**

- Lithography: is a production technique that uses masks or electron beams to sculpt or engrave nanoscale materials. It is widely used in the production of microelectronic devices (MEMs) and nanoelectronics devices (NEMs);

- Milling: this method involves removing material from a larger piece through milling or grinding to obtain nanoscale structures;
- Chemical Etching: it is used to channel or engrave materials in a controlled way on a nanoscale using selective chemical reactions;
- Chemical Vapor Deposition (CVD): this technique allows for the growth of thin films of nanomaterials on solid substrates by depositing atoms or molecules from steam.

These top-down techniques are essential for creating nanoscale structures and models accurately.

The approach chosen depends on the desired properties of the nanomaterials, the intended applications, and the availability of specific tools and technologies. In many cases, both approaches can be used in combination to achieve more sophisticated results. The choice of approach is fundamental for the design and production of nanomaterials with the desired characteristics.

### 1.2.3. Small scale, quantum and surface effects

There are at least three reasons why nanoscale materials exhibit different behaviour than macroscale materials [7]:

1. Due to scaling laws, the dominant forces at the nanoscale and macroscale are markedly different (electromagnetic forces as opposed to gravitational forces). Gravitational force is a function of mass and is weak for nanoscale objects; on the other hand, electromagnetic force depends on charge and dominates at the nanoscale;
2. The surface plays a fundamental role (higher surface-to-volume ratio); the properties of surface atoms are different from those of bulk atoms;
3. Quantum mechanics is the appropriate model for describing the properties of materials at the nanoscale (quantum confinement).

The "small-scale effect" is a general term that refers to a series of phenomena and behaviours that emerge when the size of an object or system is greatly reduced, typically on the nanometer or sub-micrometric scale.

Similarly, quantum effects are phenomena that arise when working with nanomaterials on the nanometric level, where the material dimensions approach or are smaller than the scale of quantum, which is the smallest unit of energy allowed by quantum mechanics.

Surface effects are of great importance in nanomaterials due to the high surface-to-volume ratios. At the nanoscale level, most atoms are located on the surface of the material, leading to significant changes in properties relative to macroscopic materials. These effects can manifest in various fields of science and technology, including physics, chemistry, biology, and materials science. Such effects can involve a wide range of changes in the properties and behaviours of materials compared to their macroscopic counterparts.

The most significant effects in nanomaterials are summarized in the following.

- Energy Quantization: in nanomaterials, energy is quantized into discrete levels due to their limited size. This means that electrons and other charge carriers can only occupy discrete energy levels, resulting in distinct energy spectra. This influences the electronic and optical properties of the material;
- Tunnelling Effect: this quantum phenomenon allows particles, such as electrons, to pass through an energy barrier even when they do not have enough energy to overcome it according to the laws of classical physics. It is essential in devices like tunnel diodes and tunnel transistors;
- Optical Dispersion Effects: in nanomaterials, light can interact differently than materials on a macro-scale due to their small size. This can lead to significant optical dispersion and can affect the coloring and reflectivity of the material;
- Quantum Confinement Effect: when electrons are confined within nanoscale dimensions, their motion is limited. This can affect the density of states and the electrical conduction properties of the material;

- Mechanical Effects: reduced dimensions can significantly influence the mechanical properties of nanomaterials, leading to greater strength, elasticity, or fragility compared to macroscopic materials;
- Thermal Behaviour: in nanomaterials, thermal conduction may differ significantly from macroscopic materials due to the limited diffusion of atoms. This can affect the thermal performance of nanomaterials;
- Chemical Effects: nanomaterial surfaces have a high density of surface atoms, which can influence chemical reactions such as heterogeneous catalysis;
- Quantized Luminescence: some nanomaterials, such as quantum dots, may exhibit quantized luminescence, signifying the emission of light with specific energies related to the quantized energy levels of electrons in the material;
- Chemical Stability: surface effects may result in increased chemical stability or, conversely, greater sensitivity to specific environmental or reactive conditions. This can influence the durability and stability of nanomaterials.

## 1.3. Fields of applications of nanomaterials

Nanomaterials have a wide range of applications thanks to their unique characteristics and properties, which make them reliable and efficient in many industries [8,9], as shown in Figure 1.3.

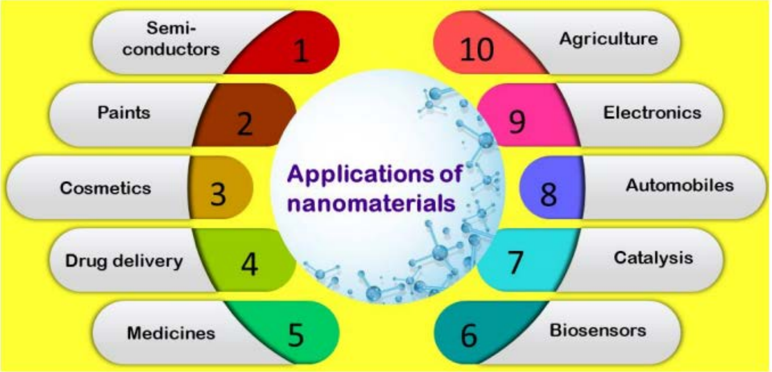

**Figure 1.0.3**. Applications of nanomaterials in different fields. [9]

Below are some of the main fields of application of nanomaterials.

- Electronics: nanomaterials such as graphene and carbon nanotubes are used to develop smaller, faster, and more efficient electronic devices. These materials are valuable for high-performance transistors, flexible displays and advanced sensors;
- Medicine: nanomaterials find applications in the diagnosis and treatment of diseases. Nanoparticles can be used as contrast agents in medical imaging, drug delivery vehicles and therapeutic agents for specific medical conditions;
- Catalysis: nanomaterials act as catalysts in a wide range of chemical reactions. Their high surface area and surface reactivity make them effective for accelerating chemical reactions, such as fuel production and water purification;
- Energy: nanomaterials are employed in energy-related applications, including next-generation solar cells, high-performance batteries, and energy storage devices;
- Composite Materials: nanomaterials are incorporated into composites to improve their mechanical and thermal properties. For example, carbon nanotubes and metallic nanoparticles can be added to polymers or composite materials to increase strength and thermal conductivity;
- Nanoelectronics: nanotechnology is crucial for development of nanoscale electronic devices such as solid-state memory devices, sensors, and tunnel transistors;
- Textiles and Clothing Materials: fabrics enriched with nanomaterials can have antimicrobial, odor-resistant, and stain-resistant properties. In addition, nanotechnological fabrics can be water-repellent or self-regenerating;
- Environment: nanomaterials are used to remove pollutants and contaminants from air and water. For example, titanium nanowires can be used to remove organic pollutants from water;
- Aerospace and Lightweight Materials: nanomaterials can be used to develop lightweight and durable materials for aerospace applications, improving the efficiency of spacecraft and aircraft;
- Nanophotonic: nanomaterials can be used for light manipulation at the nanoscale, allowing optical signal processing and optical devices optimization;

- Food: nanomaterials can be used to improve food packaging, extend shelf life and detect potential contaminants;
- Quantum Electronics: nanomaterials are used in quantum devices, such as superconducting qubits and quantum dots, for the development of quantum computers.

### 1.3.1. Applications in the field of civil engineering

Nanotechnology and nanomaterials have various applications in the field of engineering, including civil engineering. The use of nanomaterials improves the performance of many materials such as glass, steel and concrete [10].

***Nanomaterials and concrete***

One of the most frequent and beneficial uses of nanotechnology in the field of civil engineering concerns its application in concrete production. Concrete is a multi-phase nanostructured composite material that ages over time. It consists of an amorphous phase, nanometric and micrometric size crystals and bound water [11]. There are two main approaches in the application of nanotechnology in concrete research: nanoscience and nano-engineering. Nanoscience deals with the measurement and characterization of the nano and microstructure of cement-based materials to better understand how this structure influences macroscopic properties and performance through the use of advanced characterization techniques and atomic or molecular-level modelling [12]. Nano-engineering involves structure manipulation at the nanometer level to develop a new generation of custom multifunctional cements composites with superior mechanical performance and durability, potentially equipped with new properties such as low electrical resistivity, self-diagnostic ability, self-cleaning, self-repair, high ductility, and crack control. Concrete can be engineered at the nanometric level by incorporating nanoscale elements or entities (e.g., nanoparticles and nanotubes) to control material behaviour and add new properties or by grafting molecules onto cement particles, cementitious phases, aggregates and additives (including nanoscale additives) to provide surface functionalities that can be optimized to promote specific interfacial interactions [12].

For example, nano-silica improves endurance, resistance to water penetration and helps control calcium release. Nano-titanium has proven useful for self-cleaning concrete and offers the additional advantage of contributing to environmental cleaning [11]. Nano-iron and carbon nanotubes have demonstrated the ability to provide self-healing and self-diagnosis capabilities of concrete, as well as increase flexural and compressive strength.

### *Nanomaterials and steel*

As is well known, one of the biggest problems with steel structures is fatigue, which can lead to structural collapse under cyclic loads. This can occur at stresses significantly lower than those of the material. To address this problem, structural practice consists in drastically reducing the rate of work stress of the material, with a consequent economic impact. Stress irregularities are responsible for the onset of cracks and research has shown that the addition of copper nanoparticles reduces the irregularity of steel surface, thus limiting the number of stress start points and, As a result, failure by fatigue. Advances in this technology would lead to increased safety, less monitoring needs and more efficient use of materials in fatigue structures [12].

Another steel problem faced by nanotechnology is welding. Welding strength is an extremely important concern. The heat-affected area in a weld can become brittle and fail unexpectedly. The addition of nanoparticles such as magnesium and calcium can help to solve this problem by making the grains in the area affected by the finest rolled steel heat, resulting in stronger welds [10].

### *Nanomaterials and glass*

Nanotechnology is also used in glass applications. Nano titanium dioxide is used to coat glass, giving it self-cleaning properties. Titanium dioxide decomposes waste and organic compounds, and because it also attracts water, glass can attract rainwater and use it to clean dirt on its own.

Another use of nanotechnology in glass is to make it fire-resistant. This can be achieved when a layer of silica nanoparticles is placed between glass panels. This layer becomes a fire shield when heated [10].

### *Nanosensors*

Nano- and micro-electromechanical sensors have found significant applications in the construction industry for monitoring and controlling environmental conditions and material performance. These sensors can be incorporated into construction materials, such as concrete, to provide valuable information throughout the lifecycle of a structure. In concrete, for example, MEMs sensors can monitor the hardening process by detecting internal temperature and humidity. These data can be integrated into maturity methods to predict the initial strength of the concrete. Knowing the initial strength of concrete increases productivity by reducing formwork removal time and improving the efficiency of prefabricated and prefabricated elements. In addition, continuous monitoring of temperature and humidity during the useful life of a facility may provide information on how environmental factors, such as freeze/thaw cycles, chloride diffusion, alkali-silica reactions, carbonation, and temperature-induced dimensional variations [12]. Nano-sized sensors, with dimensions ranging from 1 nm to 10,000 nm, can also be incorporated in structures during construction. For example, 'smart aggregates' are piezoceramic-based low-cost multifunctional devices used to monitor the properties of early-stage concrete such as humidity, temperature, relative humidity, and strength development. These sensors can also detect corrosion and cracks in the concrete. In addition, they have applications in structural health monitoring, allowing the monitoring of internal stresses, cracks and physical forces within structures throughout their service life. This early indication of structural health can help prevent failures before they occur. Overall, nanotechnology and MEMs sensors play a crucial role in improving the performance, safety, and sustainability of construction projects by providing real-time data and information for better decision-making and maintenance [12].

# Chapter 2

# Functionally Graded Materials: an overview

Materials play a fundamental role in the continuous development of humanity. They have always received great attention from researchers, designers, and innovators because they allow humans beings to shape almost everything, generating a huge sense of value in the objects and products that surround us [13].

The term "*new materials*" is now used to refer to that class of materials that provide better performance and application characteristics and benefits than traditional materials. Through research and experimentation over the years, it has been possible to develop lighter, more durable, intelligent and sustainable materials. Material research has always been recognised as a very important discipline; new materials often influence new ways of designing, producing and even living, creating a significant impact on society [14].

The current landscape of materials has taken on vast dimensions, and new materials can be found in various categories ranging from biology to technology. We are increasingly hearing about new biomaterials, nanomaterials, 3D printing materials, metamaterials, composite materials, smart materials, and many new categories emerging from the intersection of different sciences and within multidisciplinary concepts [13].

In this chapter, the focus will be on a particular class of innovative composite materials: Functionally Graded Materials (FGMs).

## 2.1. Origin and definition of functionally graded materials

Functionally Graded Materials (FGMs) are innovative materials used in engineering for ensure high performance in extreme working environments without losing their functionality [15]. They differ from conventional composite materials in that they exhibit physical and mechanical properties that vary gradually, thus avoiding abrupt transitions of properties resulting in high stress concentrations (Figure 2.1). Indeed, the problem of traditional composite materials stems from the interface between their components, which leads to a high concentration of stresses, promoting crack initiation and propagation, ultimately leading to composite failure. This process is known as "delamination." The interface is eliminated in FGMs through the gradual variation of the volume fractions of their components and, consequently, their properties in a specific direction.

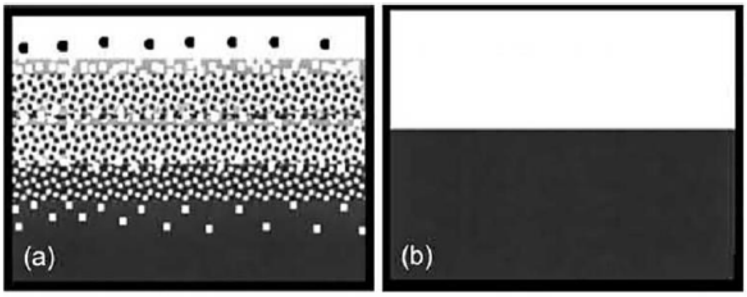

**Figure 2.1.** Schematic diagram of (a) FGM and (b) conventional laminate composite material. [18]

The concept of materials with a graded structure was first introduced in 1972 by Bever and Duwez [16], as well as Shen and Bever [17] (Figure 2.2).

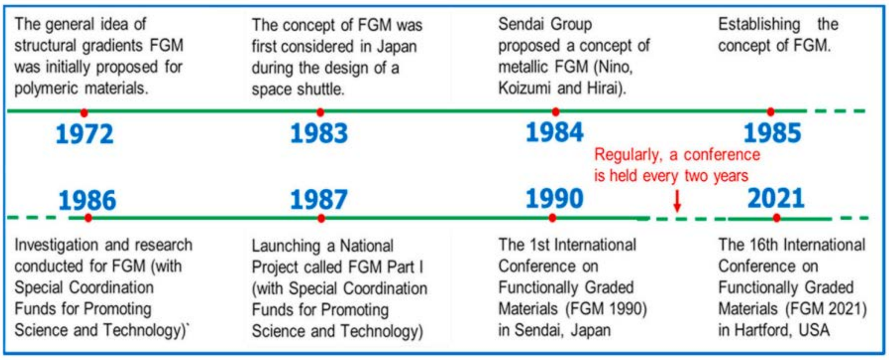

1972 The general idea of structural gradients FGM was initially proposed for polymeric materials.

1983 The concept of FGM was first considered in Japan during the design of a space shuttle.

1984 Sendai Group proposed a concept of metallic FGM (Nino, Koizumi and Hirai).

1985 Establishing the concept of FGM.

1986 Investigation and research conducted for FGM (with Special Coordination Funds for Promoting Science and Technology)`

1987 Launching a National Project called FGM Part I (with Special Coordination Funds for Promoting Science and Technology)

1990 The 1st International Conference on Functionally Graded Materials (FGM 1990) in Sendai, Japan

Regularly, a conference is held every two years

2021 The 16th International Conference on Functionally Graded Materials (FGM 2021) in Hartford, USA

**Figure 2.2.** Historical overview of relevant milestones in the research and development of FGMs. [19]

However, due to the lack of advanced technologies during that period for the production of such materials, their work had limited impact. The first practical application was proposed in 1984 by a group of Japanese scientists during a project on the thermal barrier of a spacecraft [18]. The use of this type of material has been used to reduce thermal stresses in conventional laminated composite materials for reusable rocket engines [20].

Researchers at the National Aerospace Laboratory (STA, Sendai) needed to develop a material that could withstand a huge temperature gradient. The design required that one side of the material be exposed to a temperature of 2000 K (approximately 1700°C) without transferring this temperature to the other part of the composite material. As depicted in Figure 2.3, a material was needed to absorb a thermal gradient of about 1000 K between the inside and outside of the spacecraft [21].

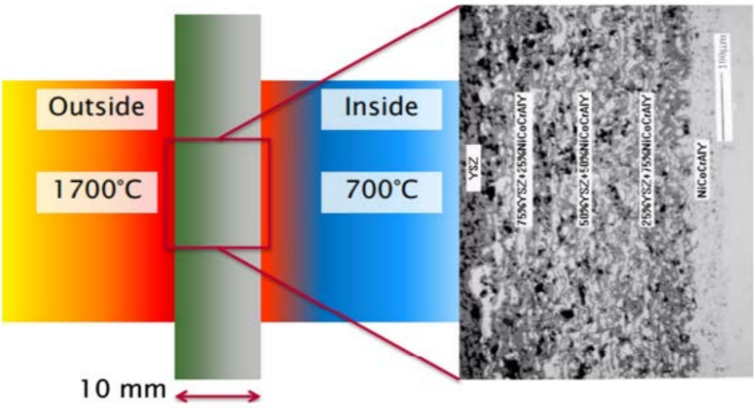

**Figure 2.3.** First example for metallic FGM in Japan. [21]

The presence of interfaces in conventional composite materials has led to delamination of material due to high stress concentration factors. To overcome this problem, researchers transformed the sharp interface into a gradual one, developing a new material called FGM [22]. In summary, the concept of FGM consists in replacing the abrupt change in composition that occurs at the interface between different materials with a gradual composite phase, with the aim of reducing stress concentrations within the structure [21]. Functionally graded materials consist of multiple materials with different properties, and the final properties of MGF material are unique and distinct from each constituent material. To further improve their thermal insulation properties, mechanical impact resistance and catalytic efficiency, the presence of pores plays a key role. These pores may have symmetrical, asymmetric or random distributions [23]. Therefore, the presence of pores can be seen both as a design flaw and as an additional step that can improve certain properties.

Furthermore, FGMs can be classified into continuous and discontinuous materials, as illustrated in Figure 2.4.

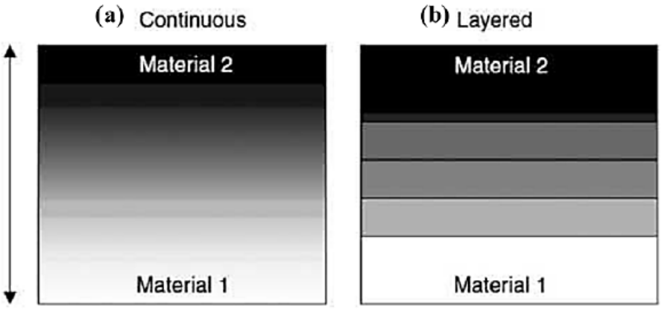

**Figure 2.4.** Types of FGMs (a) continuous FGM (b) discontinuous FGM. [24]

In the case of continuous FGMs, the material composition changes continuously with the position, and there is no visible separation line within the material to distinguish each zone. On the other hand, in discontinuous FGMs, the microstructure and/or the composition material of the material gradually changes, resulting in a multilayer structure with interfaces between discrete layers [24]. Figure 2.5 illustrates how the properties of the FGM material can vary from surface to surface in a continuous or discontinuous manner.

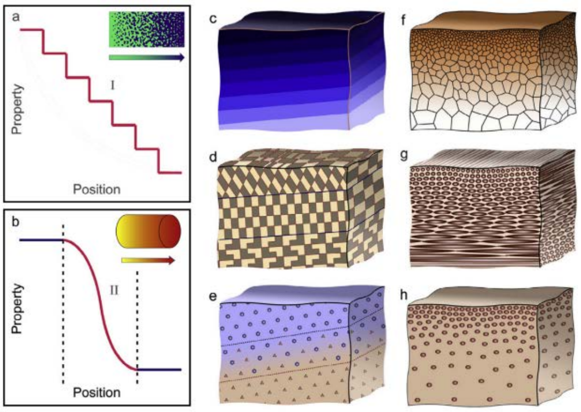

**Figure 2.5.** Schematic diagrams illustrating: (a) discontinuous and (b) continuous FGMs, respectively. (c), (d) and (e) schematic diagrams showing discontinuous FGMs that contain interfaces with gradual change in composition, grain orientation and volume fractions of two types of second-phase particles, respectively. (f), (g) and (h) schematic diagrams showing continuous FGMs in absence of interfaces and with gradual change in grain size, fiber orientation and volume fraction of second-phase particles. [25]

From Figure 2.5 it can be observed that the graded structures are present both in all the material and only in localized regions. Commonly, FGMs are made from isotropic components such as metals and ceramics [26-30]. Ceramics and metals have very different properties. Ceramics are characterized by high compressive strength, high stiffness, and excellent thermal stability, while metals have high tensile strength, good conductivity, and excellent ductility. Therefore, the combination of these two materials allows the creation of a high-strength FGM material even in high-temperature environments and good stiffness that reduces the possibility of catastrophic material fractures.

Having said that, we can summarize the advantages offered by functionally graded materials as follows:

- The presence of graded interfaces helps to overcome the problem of concentration of thermomechanical stress, preventing delamination and increasing the durability of structures.
- The addition of a porous phase contributes to increased impact resistance, provides thermal insulation, improves catalytic efficiency, and reduces electrical and thermal stresses.
- FGMs can be used as an interface layer between two incompatible materials, improving their junction.
- Coating a material with FGMs reduces internal stresses.
- The combination of ceramics and metals results in a high-performance material in terms of stiffness, ductility, strength, and excellent thermal and corrosion protection.

In summary, thanks to their ability to gradually adjust material properties and their versatility in design, functionally graded materials (FGMs) are innovative materials that offer a range of advantages in various applications and across multiple industries.

## 2.2. Methods of manufacturing FGMs

One of the most crucial aspects of promoting a new material is undoubtedly the production process. Over the years, research has devoted significant efforts to exploring and developing new manufacturing techniques for FGM materials, as evidenced by Figure 2.6.

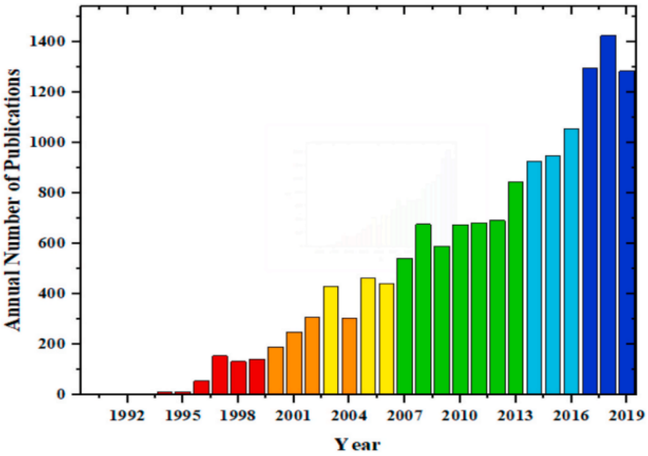

**Figure 2.6.** The annual number of publications using the search titles "functionally graded materials". (Based on the Web of Science search system in the duration of 1990–12/2019). [19]

Figure 2.7 illustrates the contribution of production methods in the fabrication of FGMs based on the Web of Science research system for the period between 1990 and December 2019.

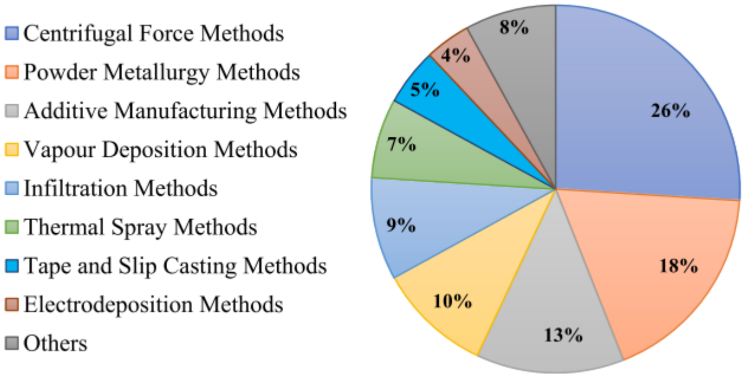

Depending on the specific use of FGM materials, both as surface coatings and as bulk materials, various manufacturing techniques have been developed.

For surface coatings with FGMs, they involve the deposition of thin FGM layers using various vapor-phase deposition techniques [31]. In addition, surface coatings may also be prepared using techniques such as plasma spraying [32], electrodeposition [33], electrophoresis [34], ion beam-assisted deposition (IBAD) [35], and self-propagating high-temperature synthesis (SHS) [36].

Regarding bulk FGMs, they can be fabricated using methods such as powder metallurgy (PM) [37], centrifugal casting [38], slip casting [39], and tape casting [40], among others.

Among the advanced methods available, additive manufacturing [41] is one of the promising processes for FGMs. Additive manufacturing, also known as 3D printing, is an advanced production method that can be used to create three-dimensional objects by layering material using computer-aided design data. Using this technology you can accelerate the production process and maximize the use of the material. Figure 2.8 provides a simplified diagram of the additive manufacturing method.

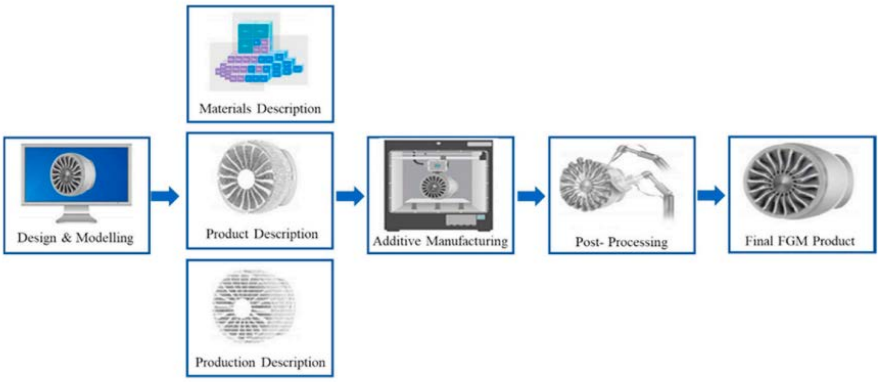

**Figure 2.8.** Concept of functionally graded additive manufacturing method. [19]

## 2.3. Areas of applications of FGMs

FGM is now the ideal solution for the growing demand for applications that require contrasting properties within the same components, where sometimes these components require a high surface hardness compared to the high internal ductility. Furthermore, considering the significant progress and increased flexibility in the production of innovative materials, FGMs find applications in various industries such as aerospace, automotive, coatings, electronics, biomaterials, construction and cutting tools, as shown in Figure 2.9.

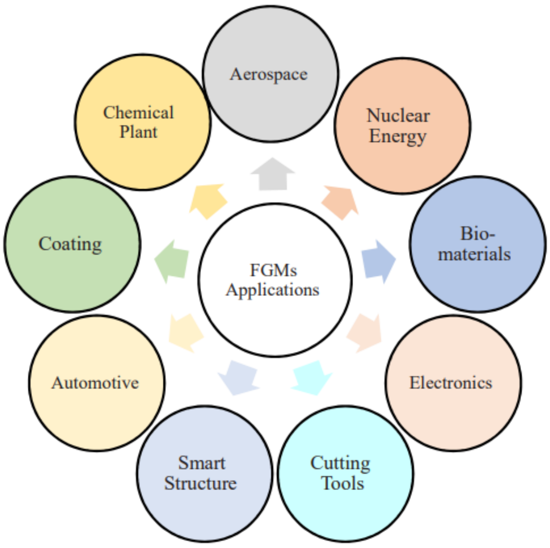

**Figure 2.9**. Areas of practical applications for FGMs. [19]

Below are some examples of application of FGM materials in some areas.

### 2.3.1. Aerospace applications

As discussed earlier, FGMs were initially used in spacecraft to reduce thermal stresses between the interior and exterior of the vehicle. Today, many aircraft and spacecraft components are made from FGMs, as shown in Figure 2.10.

**Figure 2.10.** FGMs parts in aerospace applications. [19]

### 2.3.2. Automotive applications

In the automotive industry, FGMs are also used to manufacture parts of the vehicle that are subjected to high stresses, such as pistons, diesel engine cylinders, combustion chambers, racing car brakes, flywheels, as depicted in Figure 2.11. Additionally, they are applied in the production of automotive body coatings.

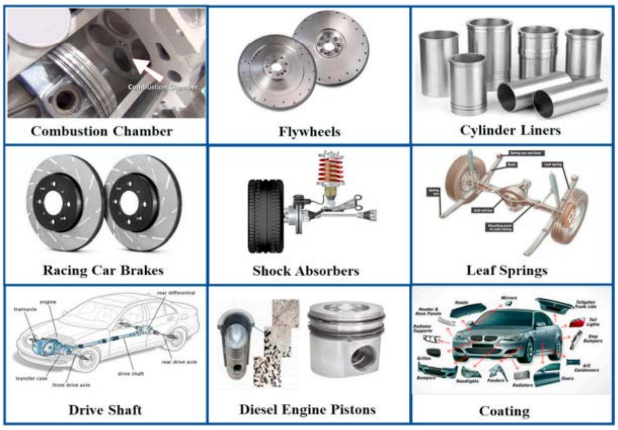

**Figure 2.11.** FGMs parts in automotive applications. [19]

### 2.3.3. Defense applications

One of the most important characteristics of FGMs is their ability to restrict the propagation of cracks, making them valuable in defense applications as penetration-resistant materials used in armored plates, bulletproof vests, and armored vehicle bodies.

### 2.3.4. Electrical and electronical applications

In the electrical and electronic industry, FGM materials are used to reduce stress at the interface between electrodes and spacers, in diodes, semiconductors, insulators, and sensor production. In microelectronics, FGMs based on carbon nanotubes are used as thermal shielding elements.

### 2.3.5. Civil engineering applications

Unlike all other sectors, Functional Graded Materials (FGMs) have received little attention in the field of civil engineering. This can certainly be attributed to the relatively low cost of concrete and, therefore, a widespread culture of over-sizing reinforced concrete structures. However, today the need to increase the durability of structures, minimize energy and use sustainable resources has opened the doors to the use of so-called Functional Graded Concrete (FGC), which uses the same production techniques as FGM materials. Recent advances in robotics have revealed the potential to automate the production of FGC elements to facilitate more efficient and controlled production of custom components. Applications have shown that it is possible to achieve performance improvements in concrete structures [42], reduce mass, improve thermal insulation properties by increasing porosity, as well as introduce multifunctional properties. For example, in flexural components, such as prefabricated slabs, targeted placement of lighter cement mixtures in areas subjected to relatively small loads can reduce the mass by about 60%, which is associated with correspondingly lower $CO_2$ emissions. In addition, the thermal insulation properties can be controlled by changing the porosity along the section height of the component. The highly insulating lightweight aggregates used in the core of the element enable the design of thin wall sections that meet structural and thermal insulation specifications [43].

Figure 2.12 shows an example of FGC material production in which two types of cement were used, one high strength and one light. This approach results in a material that, in addition to having high strength, benefits from the presence of porosity, improving its insulating properties.

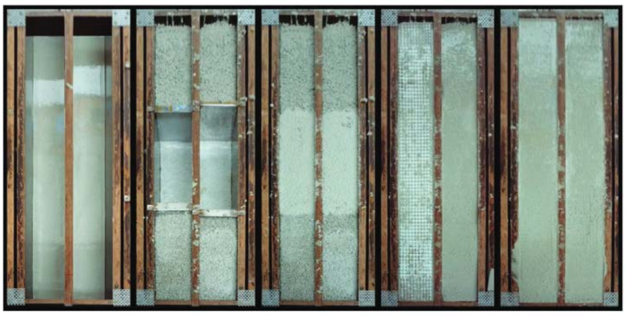

**Figure 2.12.** Production of a functionally graded concrete beam in a layered casting process. [43]

Furthermore, in Figure 2.13, it is demonstrated that as porosity increases, weight and strength tend to decrease, while there is a simultaneous increase in thermal resistance.

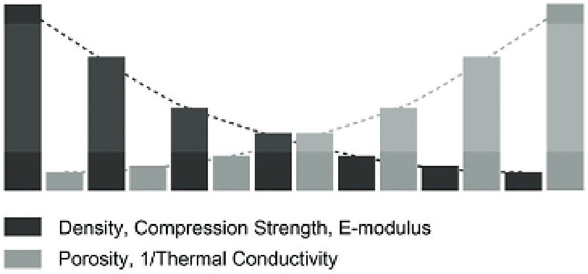

**Figure 2.13.** Curves of hardened concrete characteristics depending on a gradual increase in porosity. [43]

## 2.4. Micromechanical models (homogenization)

As discussed in the previous paragraph, Functional Graded Materials (FGMs) are manufactured in such a way that the composition of the constituent materials gradually varies in one direction, resulting in a uniform variation of mechanical and physical properties such as the normal elastic modulus of the bulk and surface, surface residual stress, tangential modulus, density, coefficient of thermal expansion, moisture coefficient, thermal conductivity coefficient, and so on.

Figure 2.14 depicts the microstructure of an idealised FGM, illustrating the gradual change in the composition of materials. The challenge of analysing an FGM is that the microstructure is often not precisely known. This can be determined through imaging techniques such as computed tomography, but the creation of reasonable computational models remains difficult due to the vast number of degrees of freedom required to characterize the microstructure of FGMs.

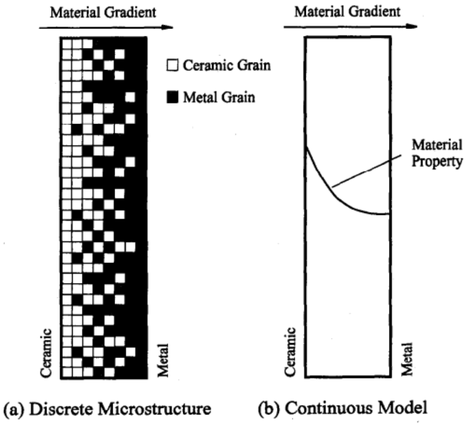

**Figure 2.14.** Schematic drawings of functionally graded materials (FGMs): (a) discrete and random microstructure, and (b) continuous gradient modelling often used. [44]

Since microstructural models for FGMs have a high computational cost, research has developed simplified methods based on homogenization. Homogenization is the process of evaluating a general or effective property for the entire material. These methods were originally developed for non-graded composites where the volume fractions of constituents are more or less uniform throughout the material. This property is called statistical homogeneity. For graded materials, homogenization is performed layer by layer, taking into account the local volume fraction of constituents in each layer rather than using overall volume fractions. Therefore, the homogenised model is a composite material of composites, with each layer having overall uniform but different properties [45]. Figure 2.15 shows a typical homogenised model of an FGM.

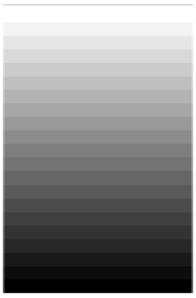

**Figure 2.15.** A homogenized model of a functionally graded material. [45]

Homogenization methods can be divided into three categories: direct methods, variational methods, and approximation methods. Direct methods seek a closed analytical solution to derive average properties in terms of constituent properties. Variational methods provide upper and lower bounds for effective properties in terms of volume fractions of phases. Approximation methods provide a general and effective property of the material.

These methods include the so-called mixture rule, including Voigt's model [46] and Reuss's model [47]. Hashin-Shtrikman composite sphere assembly models [48,49] use the variational principle to determine effective properties. The Mori-Tanaka scheme [50] and Hill's self-consistent scheme [51] estimate the effective properties using local average stress and strain fields of the composite constituents. Further methods developed for the study of these materials include the Wakashima-Tsukamoto model [52], Halpin-Tsai [53], and Tamura [54]. In works [55-60], these models were used and compared with the estimated properties of FGM composite materials.

Below is a brief description of the Mori-Tanaka model and the mixture rule (Voigt's model), which fall into the category of approximation methods, as they are the two most commonly used models for estimating the properties of FGM.

### 2.4.1. The Mori–Tanaka scheme

The Mori-Tanaka model was developed to describe the mechanical behaviour of composite materials consisting of a continuous matrix with dispersed inclusions or reinforcements. This model is based on several fundamental assumptions:

1. Isotropy: the model assumes that both the matrix and the inclusions are isotropic.
2. Elastic linearity: it assumes that the material is elastic.
3. Geometric independence: the inclusions are considered randomly distributed and non-interacting.

In the following equations, the subscript “1” will indicate the phase related to the matrix, while the subscript “2” will denote the phase related to the inclusions.

Based on the Mori-Tanaka model, the effective shear modulus ($G$) and bulk moduli ($E$) can be expressed in the following form:

$$G = G_1 + \frac{V}{\frac{1}{G_2 - G_1} + \frac{6(K_1 + 2G_1)(1 - V)}{5G_1(3K_1 + 4G_1)}} \tag{2.1}$$

$$K = K_1 + \frac{V}{\frac{1}{K_2 - K_1} + \frac{3(1 - V)}{3K_1 + 4G_1}} \tag{2.2}$$

where $V$ denotes the volumetric fraction of the phase relating to inclusions.

Using effective shear and bulk modulus, the effective Young's modulus ($E$) and Poisson's ratio ($v$) are expressed as follows:

$$E = \frac{9GK}{G + 3K} \tag{2.3}$$

$$K = \frac{3K - 2G}{2G + 3K} \tag{2.4}$$

### 2.4.2. The rule of the mixture (Voigt Model)

The Voigt model is based on the idea of defining the elastic properties of a composite material by averaging the stresses across all phases, assuming uniform strain. According to this rule, any property of the generic material, denoted as *P*, is considered to vary uniformly along a direction depending on the volume fractions and the properties of the constituent materials. The generic property *P* can be expressed as a linear combination:

$$P = \sum_{i=1}^{n} P_i \, V_i \tag{2.5}$$

where $P_i$ and $V_i$ are respectively the material property and the volume fraction of the *i*-th constituent of the FGM, where:

$$\sum_{i=1}^{n} V_i = 1 \tag{2.6}$$

## 2.5. Gradation Laws

FGM can be studied by assuming that the material properties, such as Young's modulus, density, or thermal expansion coefficient, vary in the grading directions according to different gradation laws. Therefore, it is possible to choose the laws governing the variations in properties of an FGM along any direction based on design requirements. Various gradation laws can be found in the literature, such as the power law (P-FGM), the sigmoid law (S-FGM), and the exponential law (E-FGM).

### 2.5.1. Power-law (P-FGM)

The power law (P-FGM) was introduced by Wakashima et al. [61] and is widely used by researchers for the analysis of stresses in FGM structures.

Referring to a nanobeam of thickness $h$, as shown in Figure 2.16, the generic effective material property $P(z)$ in a specific direction (along $z$) can be determined using the following relationship:

$$P(z) = P_m + (P_c - P_m)\left(\frac{1}{2} + \frac{z}{h}\right)^n \tag{2.7}$$

where $P_m$ and $P_C$ denote the generic properties of the metal and ceramic constituent of the FG nanobeam, respectively; $n$ represents the material gradient index and is a quantity that satisfies the following relationship:

$$0 \leq n \leq \infty \tag{2.8}$$

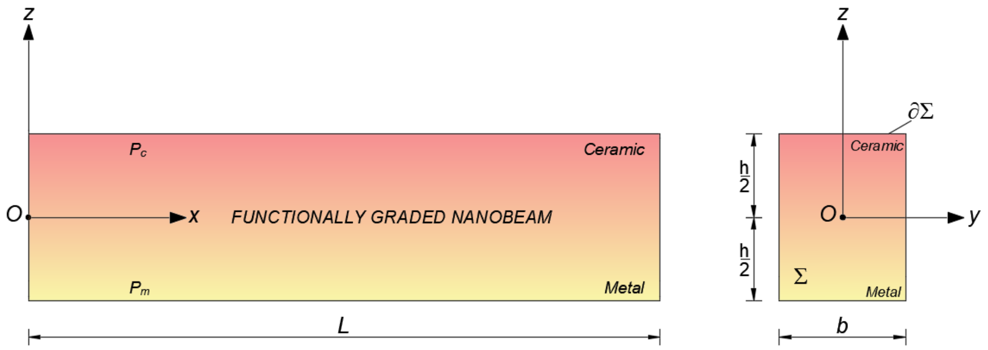

**Figure 2.16**. FG nanobeam made of ceramic ($c$) and metal ($m$).

Specifically, when $n = 0$, it results in a homogeneous nanobeam exhibiting ceramic properties. Conversely, when $n = \infty$, the nanobeam becomes homogeneous with exclusively metallic properties.

### 2.5.2. Sigmoid Law (S-FGM)

In the case where an FGM with a single power law function is added to the multi-layered composite, stress concentrations occur at one of the interfaces where the material is continuous but changes rapidly [62,63]. Therefore, Chung and Chi [64] defined the volume fraction using two power law functions to ensure a uniform stress distribution across all interfaces [65]. According to the Sigmoid law (S-FGM), the two power laws can be defined as:

$$V_c(z) = 1 - \frac{1}{2}\left(\frac{\frac{h}{2} - z}{\frac{h}{2}}\right)^n \qquad 0 \leq z \leq \frac{h}{2} \tag{2.9}$$

$$V_m(z) = \frac{1}{2}\left(\frac{\frac{h}{2} + z}{\frac{h}{2}}\right)^n \qquad -\frac{h}{2} \leq z \leq 0 \tag{2.10}$$

Using the mixture rule in Eq. 2.5, the effective properties of an FGM can be calculated as follows:

$$P(z) = P_m + (P_c - P_m)\left(1 - \frac{1}{2}\left(\frac{\frac{h}{2} - z}{\frac{h}{2}}\right)^n\right) \qquad 0 \leq z \leq \frac{h}{2} \tag{2.11}$$

$$P(z) = P_m + (P_c - P_m)\left(\frac{1}{2}\left(\frac{\frac{h}{2} + z}{\frac{h}{2}}\right)^n\right) \qquad -\frac{h}{2} \leq z \leq \tag{2.12}$$

### 2.5.3. Exponential Law (E-FGM)

Kim and Paulino in [66] proposed an exponential law (E-FGM) for the effective properties of FG material to address issues related to fracture mechanisms. The distribution of the generic property along the thickness of a nanobeam, in accordance with the power law, is defined as follows:

$$P(z) = P_m e^{\frac{1}{h}\left(\ln\frac{P_m}{P_c}\right)\left(z+\frac{h}{2}\right)} \tag{2.13}$$

## 2.6. Porous FG nanobeams

Due to the significant differences in the solidification temperatures between ceramic and metallic constituents, FGMs may have some micro-cavities during preparation for sintering [67]. In addition, based on the principle of the multi-step sequential infiltration technique that can be employed to fabricate FGM samples, porosities occur mainly in the central zone due to the different infiltration process. The presence of pores can have a significant impact on the properties and performance of materials, so it is important to manage and control them in applications where porosity is undesirable. In other cases, porosity may be intentionally designed to modify the thermal and conductivity properties of FGM materials. Suppose that the FG nanobeam in Figure 2.17 is equipped with both even and uneven porosity distributions that spread within the cross-sectional area of the FG nanobeam due to defects during the production processes.

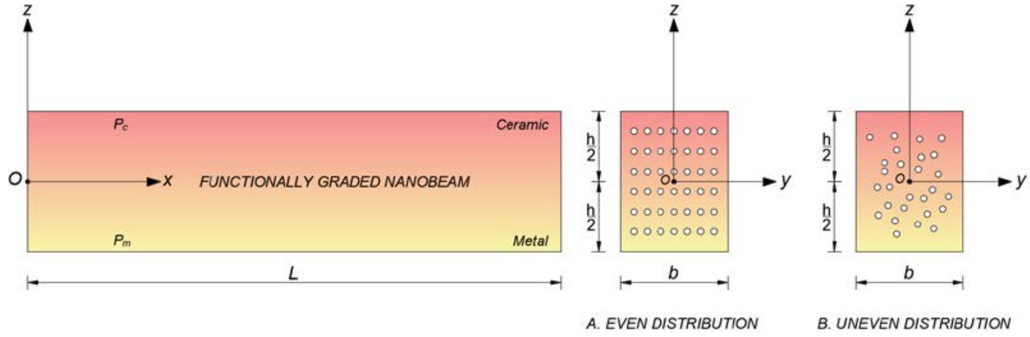

**Figure 2.17.** Coordinate system and configuration of a porous FG Bernoulli–Euler nanobeam: even (A) and uneven (B) porosity distributions across the thickness of the FG nanobeam.

Wattanasakulpong et al. in [68] proposed an amendment of the P-FGM law to estimate the generic effective properties of a porous FGM material, both for a scenario with even porosity (Eq. 2.14) and uneven porosity (Eq. 2.15):

$$P(z) = P_m + (P_c - P_m)\left(\frac{1}{2} + \frac{z}{h}\right)^n - (P_c + P_m)\frac{\zeta}{2} \tag{2.14}$$

$$P(z) = P_m + (P_c - P_m)\left(\frac{1}{2} + \frac{z}{h}\right)^n - (P_c + P_m)\frac{\zeta}{2}\left(1 - \frac{2|z|}{h}\right) \tag{2.15}$$

where the term $\zeta \ll 1$ denotes the porosity volume fraction.

## 2.7. Thermo-mechanical properties of FG nanobeam

Very often, FG materials are used in environments with high temperature and absorbed humidity, such as aerospace and marine structures. This has attracted particular attention from numerous scientists because the increase in temperature and humidity can lead to a reduction in their mechanical properties, potentially resulting in catastrophic failure of the structures. Therefore, it is crucial to consider the effects of humidity and temperature for accurate prediction of mechanical response.

Toulokian in [69] proposed that the generic thermoelastic properties, $P_j(T)$, of the constituents of FG materials, such as Young's modulus, thermal expansion coefficient, humidity coefficient, etc., can be expressed as a nonlinear function of temperature:

$$P_j(T) = P_{0_j}\left(X_{-1_j}T^{-1} + X_{1_j}T + X_{2_j}T^2 + X_{3_j}T^3\right), \quad j = m, c \tag{2.16}$$

in which $P_{0_j}$ denotes the characteristic values of the thermo-elastic and physical properties of material and $X_{-1_j}$, $X_{1_j}$, $X_{2_j}$ and $X_{3_j}$ are the coefficients of the two material phases $(j = m, c)$.

Mass density is weakly temperature dependent and is generally considered to be only a function of $z$ for FGM materials.

The thermoelastic properties and phase coefficients of an FG material composed of metal ($SuS_3O_4$) and ceramic ($Si_3N_4$) are reported in Tables 2.1 and 2.2.

**Table 2.1.** Characteristic values of thermos-elastic properties of metal (*SuS3O4)* and ceramic (*Si3N4*). [70]

| Ceramic ($Si_3N_4$) - $P_{0_c}$ | | | | | Metal ($SuS_3O_4$) - $P_{0_m}$ | | | | |
|---|---|---|---|---|---|---|---|---|---|
| $E_c$ | $\rho_c$ | $\alpha_c$ | $\beta_c$ | $K_c$ | $E_m$ | $\rho_m$ | $\alpha_m$ | $\beta_m$ | $K_m$ |
| *(GPa)* | (kg/m$^3$) | (K$^{-1}$) | (wt. % $H_2O$)$^{-1}$ | (Wm$^{-1}$K$^{-1}$) | *(GPa)* | (kg/m$^3$) | (K$^{-1}$) | (wt. % $H_2O$)$^{-1}$ | (Wm$^{-1}$K$^{-1}$) |
| 348.43 | 2170 | 5.87273E-06 | 0 | 13.723 | 201.04 | 8166 | 12.33 E-06 | 0.0005 | 15.379 |

**Table 2.2.** Coefficients of material phases for metal (*SuS3O4)* and ceramic (*Si3N4*). [70]

| Coefficients | Unit | Ceramic ($Si_3N_4$) | | | | | Metal ($SuS_3O_4$) | | | | |
|---|---|---|---|---|---|---|---|---|---|---|---|
| | | $E_c$ | $\rho_c$ | $\alpha_c$ | $\beta_c$ | $K_c$ | $E_m$ | $\rho_m$ | $\alpha_m$ | $\beta_m$ | $K_m$ |
| $X_{-1}$ | (K) | 0 | 0 | 0 | 0 | 0 | 0 | 0 | 0 | 0 | 0 |
| $X_1$ | (K$^{-1}$) | -3.07 E-04 | 0 | 9.095 E-04 | 0 | -1.032 E-03 | 3.079 E-04 | 0 | 8.086 E-04 | 0 | -1.264 E-03 |
| $X_2$ | (K$^{-2}$) | 2.16 E-07 | 0 | 0 | 0 | -5.466 E-07 | -6.534 E-07 | 0 | 0 | 0 | 2.092 E-06 |
| $X_3$ | (K$^{-3}$) | -8.946 E-11 | 0 | 0 | 0 | -7.876 E-11 | 0 | 0 | 0 | 0 | -7.223 E-10 |

where $\rho_c$, $\rho_m$ and $E_c$, $E_m$ are the material densities and the Euler-Young moduli of ceramic and metal, respectively; $\alpha_c$, $\alpha_m$ and $\beta_c$, $\beta_m$ are the thermal expansion coefficients and the moisture expansion coefficients of the two aforementioned materials, respectively; $K_c$ and $K_m$ denote the bottom and top thermal conduction coefficients, respectively.

As is well known, the presence of a heat source causes a change in the thermoelastic and physical properties of a material. Table 2.3 shows the values of the thermo-elastic and physical characteristics of the metal ($SuS_3O_4$) and ceramic ($Si_3N_4$) examined for four temperature values ($T = 305, 405, 505, 605\ [K]$).

**Table 2.3.** Thermo-elastic properties of metal (SuS3O4) and ceramic (Si3N4) at different temperatures.

| Material | Properties | Unit | P(305 K) | P(405 K) | P(505 K) | P(605 K) |
|---|---|---|---|---|---|---|
| Ceramic ($Si_3N_4$) | $E_c$ | (GPa) | 321.92 | 315.38 | 309.59 | 304.36 |
| | $\rho_c$ | (kg/m3) | 2170 | 2170 | 2170 | 2170 |
| | $\alpha_c$ | (K-1) | 7.502 E-06 | 8.036 E-06 | 8.570 E-06 | 9.104 E-06 |
| | $\beta_c$ | (wt. % H2O)-1 | 0.00 | 0.00 | 0.00 | 0.00 |
| | $K_c$ | (Wm-1K-1) | 8.6751 | 6.6852 | 4.5190 | 2.1700 |
| Metal ($SuS_3O_4$) | $E_m$ | (GPa) | 207.70 | 204.56 | 198.80 | 190.41 |
| | $\rho_m$ | (kg/m3) | 8166 | 8166 | 8166 | 8166 |
| | $\alpha_m$ | (K-1) | 1.537 E-05 | 1.637 E-05 | 1.736 E-05 | 1.836 E-05 |
| | $\beta_m$ | (wt. % H2O)-1 | 0.0005 | 0.0005 | 0.0005 | 0.0005 |
| | $K_m$ | (Wm-1K-1) | 12.1278 | 12.0454 | 12.3366 | 12.9346 |

As can be seen from Table 2.3, as the temperature increases the Young's modulus and the thermal conduction coefficient always decrease while with increasing temperature the thermal expansion coefficient increases. In addition, since the density mass and the moisture coefficient are independent of temperature and they do not change as the temperature increases.

It can be concluded that for a correct study of the structural response it is necessary to take into account the influence of temperature.

## 2.8. Determination of neutral axis position and its effects on FG nanobeam

Consider a functionally graded (FG) nanobeam of length $L$ in a Cartesian coordinate system $\{O, x', y', z'\}$ with origin in the geometric center $O$ of its rectangular cross-section $\Sigma$ $(b \times h)$, being $x'$ $(0 \leq x' \leq L)$ the nanobeam axis and $y'$ and $z'$ the principal axes of geometric inertia of $\Sigma$ (Figure 18).

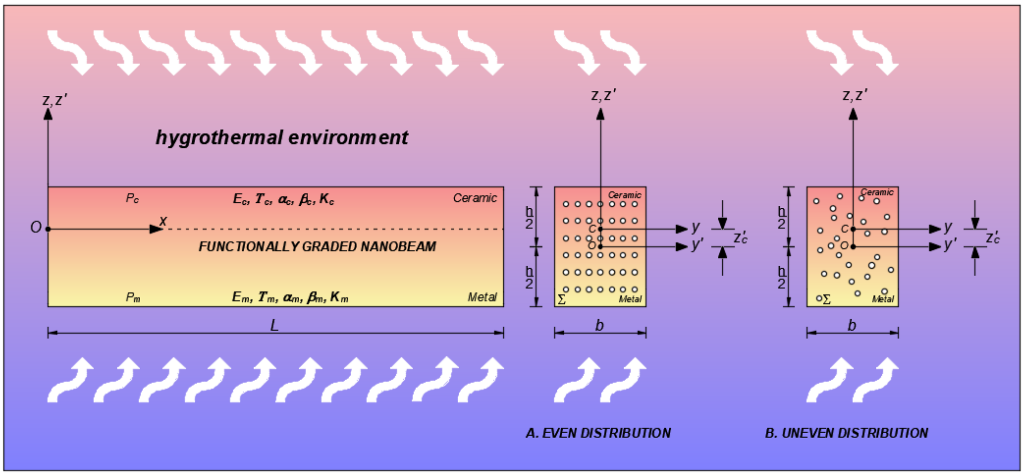

**Figure 2.18.** Coordinate system and configuration of FG Bernoulli-Euler nanobeam in a hygrothermal environment for two different types of porosity distributions: A. even porosity distribution, B. uneven porosity distribution.

In functionally graded materials, the position of the neutral axis varies with the material distribution throughout the thickness. Due to the variation in Young's modulus, the neutral surface does not coincide with the midplane [71], which means that the elastic center *C* does not coincide with the geometric center *O*.

In order to remove any bending-stretching coupling due to the variation of the FG material, it is convenient to evaluate the effective thermoelastic properties of the material with respect to the elastic center *C*. The position of the elastic center *C*, depending on the current temperature *T* and is shifted relative to the geometric center *O* by an amount:

$$z_c' = \frac{\int_\Sigma E(z',T)z'd\Sigma}{\int_\Sigma E(z',T)d\Sigma} \tag{2.17}$$

In the new Cartesian coordinate system with elastic coordinates, the original $z$-coordinate at $C$ is given by $z = z' - z_c'$, and $y = y'$ as shown in Figure 2.18. Consequently, the axial stiffness $A_E$, the elastic static moment $S_E$, and the bending stiffness $I_E$ with respect to the elastic center $C$ of the porous FG nanobeam are expressed as follows:

$$A_E = b\int_{-\frac{h}{2}-z_c'}^{\frac{h}{2}-z_c'} E(z,T)dz \tag{2.18}$$

$$S_E = b\int_{-\frac{h}{2}-z_c'}^{\frac{h}{2}-z_c'} E(z,T)\, z\, dz \tag{2.19}$$

$$I_E = b\int_{-\frac{h}{2}-z_c'}^{\frac{h}{2}-z_c'} E(z,T)\, z^2\, dz \tag{2.20}$$

It is worth noting that, with respect to the elastic center $C$, the elastic static moment, $S_E$, is always zero. The shifted position of the elastic center also affects the expressions of mass density, $A_\rho$, rotary inertia, $I_\rho$, and static moment of mass (or couple rotary), $S_\rho$, which are defined as follows:

$$A_\rho = b\int_{-\frac{h}{2}-z_c'}^{\frac{h}{2}-z_c'} \rho(z) dz \tag{2.21}$$

$$I_\rho = b\int_{-\frac{h}{2}-z_c'}^{\frac{h}{2}-z_c'} \rho(z)\, z^2\, dz \tag{2.22}$$

$$S_\rho = b\int_{-\frac{h}{2}-z_c'}^{\frac{h}{2}-z_c'} \rho(z)\, z\, dz \tag{2.23}$$

For the sake of comprehensiveness, the quantities related to Eqs. 2.18-2.23 are explicitly presented in Appendix A, both for even and uneven porosity distribution.

## 2.9 Numerical application

Now, let's consider the porous functionally graded nanobeam represented in Figure 2.18. The following are the results of the effects of the gradient index, the porosity volume fraction, and temperature on the following dimensionless quantities are shown:

$$\bar{z}_c' = \frac{z_c'}{h} \tag{2.24}$$

$$\bar{A}_E = \frac{A_E}{A_{E_C}} \tag{2.25}$$

$$\bar{I}_E = \frac{I_E}{I_{E_C}} \tag{2.26}$$

$$\bar{A}_\rho = \frac{A_\rho}{A_{\rho_C}} \tag{2.27}$$

$$\bar{I}_\rho = \frac{I_\rho}{I_{\rho_C}} \tag{2.28}$$

where $A_{E_C}, I_{E_C}, A_{\rho_C}$, e $I_{\rho_C}$ refer to the values of axial stiffness, bending stiffness, mass density and rotary inertia of a non-porous fully ceramic FG nanobeam ($n$=0, $\zeta$=0) at the temperature reference $T$=305[K].

In Figures 2.19, we observe the influence of the gradient index ($n$) on the dimensionless position of the elastic center $C$ ($\bar{z}_c'$) for a rectangular cross-section of an FG nanobeam, considering both non-porous and porous materials. A notable observation is that as the gradient index ($n$) increases, the dimensionless distance $\bar{z}_c'$ also increases, reaching a maximum value at $n^*$, which depends on the value of $\zeta$ and $T$. It's worth noting that for $k$ values greater than $n^*$, the distance $\bar{z}_c'$ gradually approaches zero as $n$ tends infinity. Additionally, Figures 2.19 reveals that the curves representing uneven porosity distribution show a less significant increase compared to those of the even porosity distribution. Furthermore, from Figure 2.19b it is possible to notice that as the temperature $T$ increases the dimensionless position of the elastic center $\bar{z}_c'$ increases.

The effect of porosity volume fraction, $\zeta$, on the mechanical properties of the FG nanobeam is even more evident from the graphs of Figures 2.20 and 2.21. As can be observed, the increase in the gradient index, $n$, as well as in the value of the porosity volume fraction, $\zeta$, cause a decrease of the dimensionless axial stiffnesses, $\bar{A}_E$, and bending stiffness, $\bar{I}_E$, of porous FG nanobeam, for both the two types of porosity distribution considered. Furthermore, the uneven porosity distribution always provides greater values of the dimensionless axial and bending stiffness than the even porosity distribution. Additionally, from Figures 2.20b and 2.21b, an increase in temperature, $T$, always leads to a reduction of the mechanical properties of the FG nanobeam.

In Figure 2.22, the effects of the gradient index, $n$, porosity, $\zeta$, and temperature, $T$, on dimensionless rotary inertia, $\bar{I}_\rho$, are depicted. It is evident that with an increase in the gradient index, the dimensionless rotary inertia always increases, while it decreases with an increase in the porosity volume fraction. Specifically, an even porosity distribution exhibits higher values of dimensionless rotational inertia compared to an uneven porosity distribution. Furthermore, by observing Figure 2.22b, it can be noted that the influence of temperature on dimensionless rotary inertia is relatively insignificant.

As can be expected from Figure 2.23, as the porosity volume fraction, $\zeta$, increases, the dimensionless values of mass density, $\bar{A}_\rho$, decrease. Furthermore, an even porosity distribution always exhibits higher values of dimensionless mass density compared to an uneven porosity distribution.

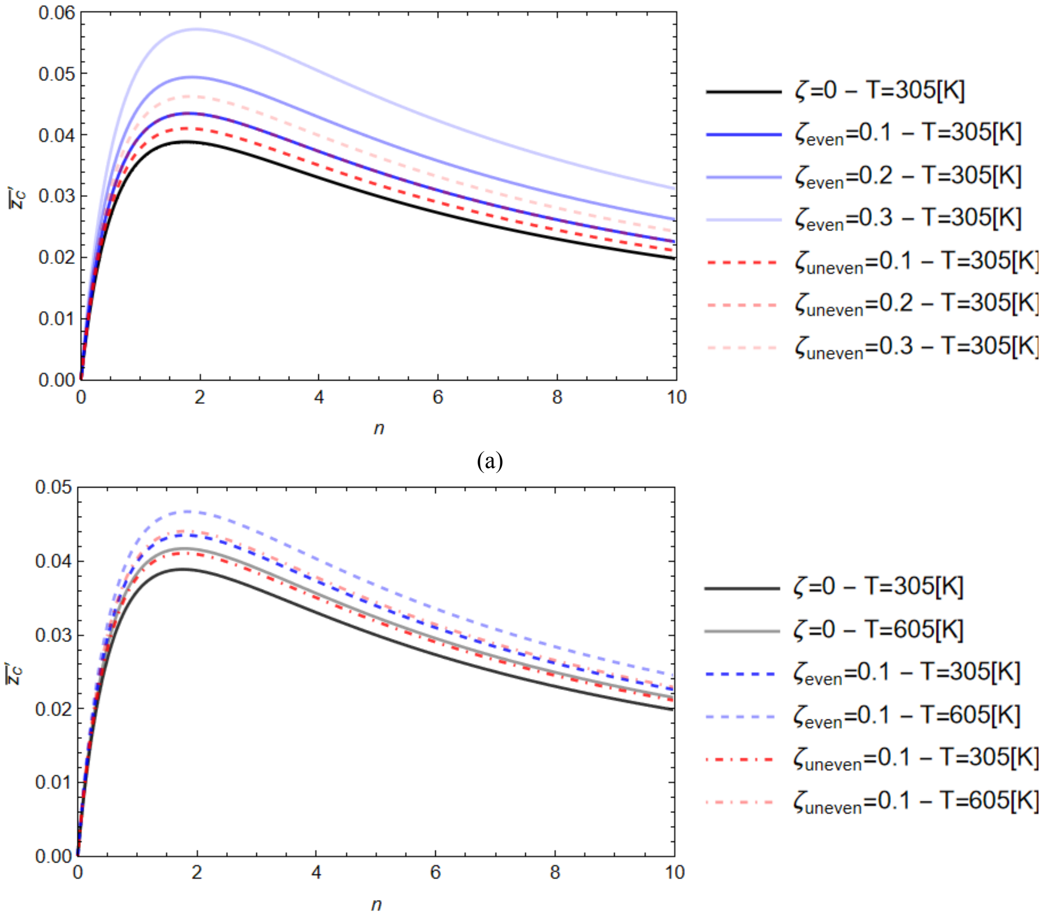

(b)

**Figures 2.19.** Effects of the gradient index ($n$) of the FG material on the dimensionless position of the elastic center $C$ varying the porosity volume fraction ($\zeta$) for both even and uneven porosity distribution and for two values of temperature $T$={305,605}[K].

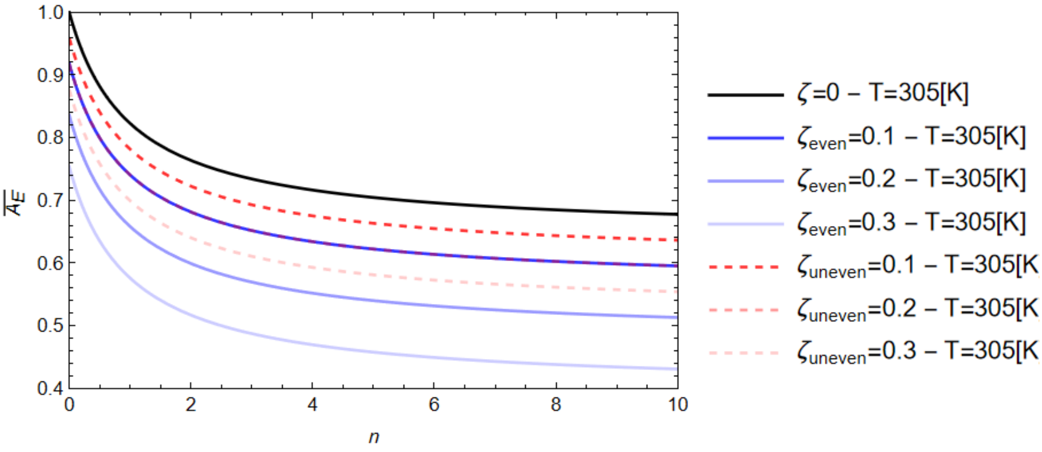

(a)

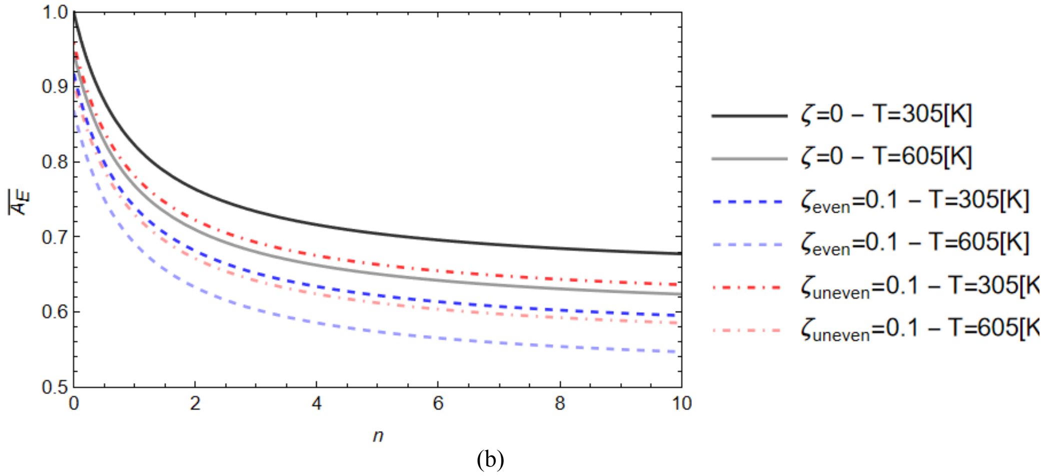

(b)

**Figures 2.20.** Effects of the gradient index (*n*) of the FG material on the dimensionless axial stiffness $\bar{A}_E$ varying the porosity volume fraction ($\zeta$) for both even and uneven porosity distribution and for two values of temperature *T*={305,605}[K].

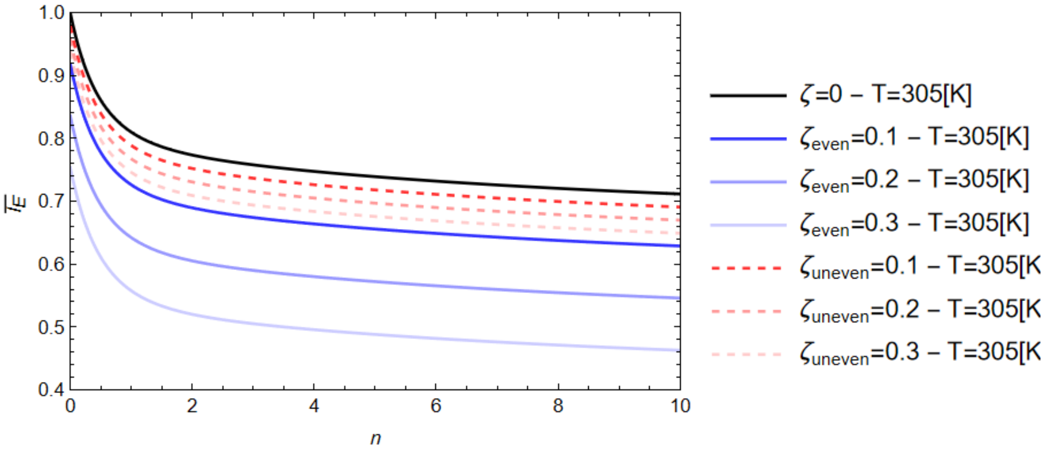

(a)

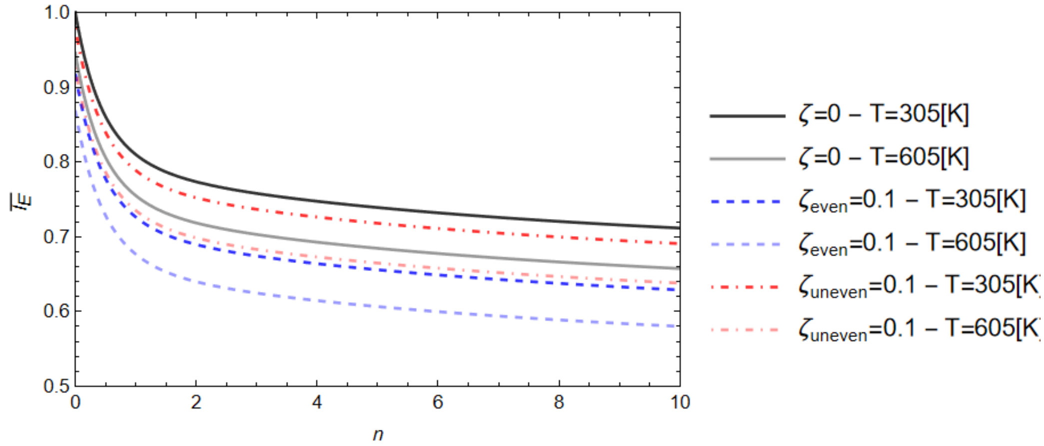

(b)

**Figures 2.21.** Effects of the gradient index ($n$) of the FG material on the dimensionless bending stiffness $\bar{I}_E$ varying the porosity volume fraction ($\zeta$) for both even and uneven porosity distribution and for two values of temperature $T$={305,605}[K].

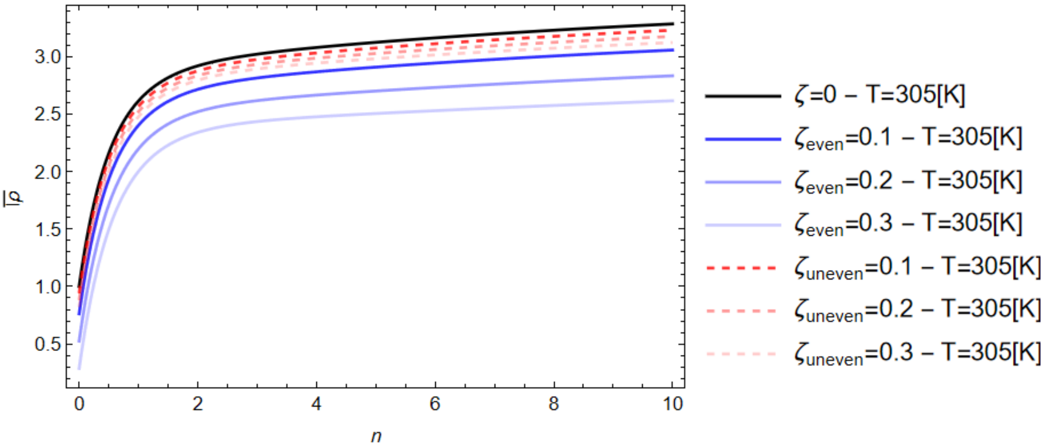

(a)

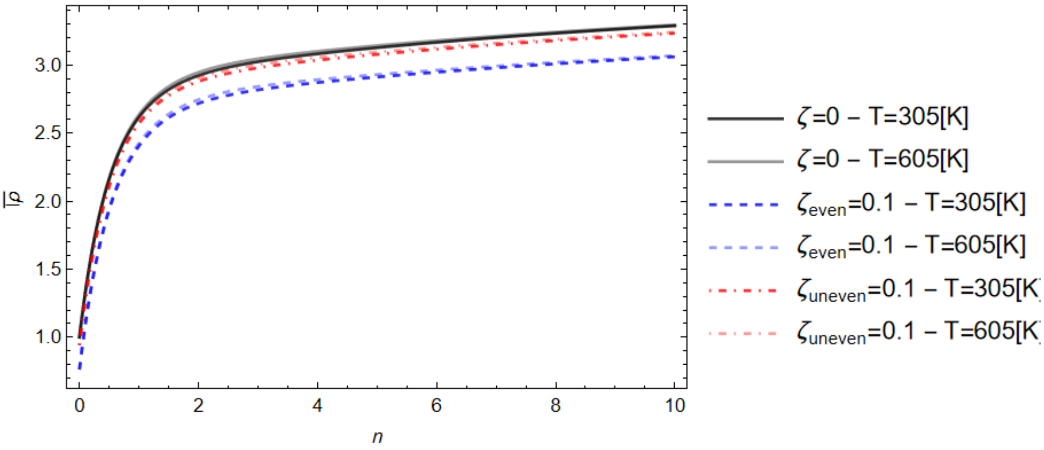

(b)

**Figures 2.22.** Effects of the gradient index ($n$) of the FG material on the dimensionless rotary inertia $\bar{I}_\rho$ varying the porosity volume fraction ($\zeta$) for both even and uneven porosity distribution and for two values of temperature $T = \{305,605\}[K]$.

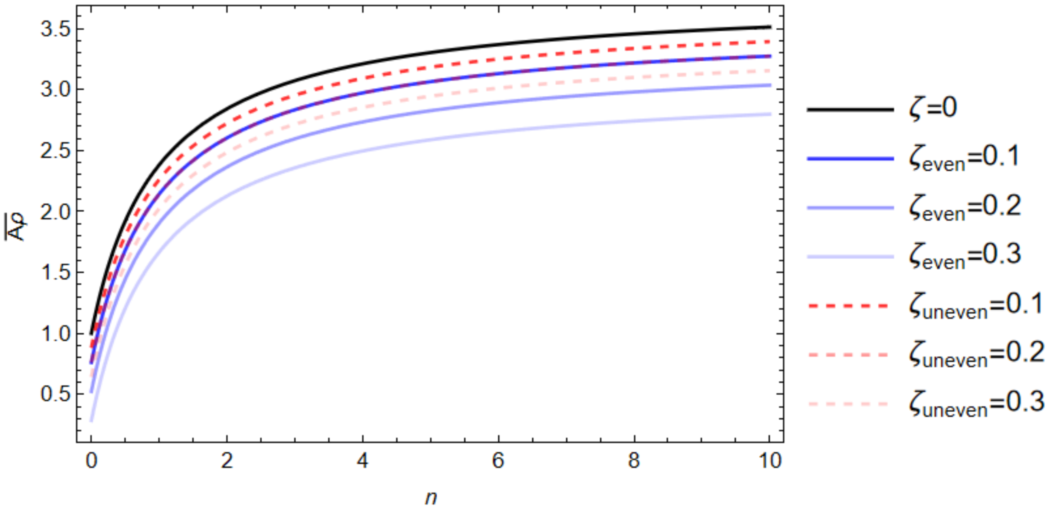

**Figures 2.23.** Effects of the gradient index ($n$) of the FG material on the dimensionless mass density $\bar{A}_\rho$ varying the porosity volume fraction ($\zeta$) for both even and uneven porosity distribution.

The variation of the Euler-Young modulus ($E$), thermal coefficient ($\alpha$), mass density (ρ), moisture coefficient ($\beta$) and thermal conduction coefficient ($K$) across the thickness of a porous and non-porous FG nanobeam are illustrated in Figures 2.24-2.26 varying $n$ in in the set {0, 0.2, 0.3, 0.5, 1, 2, 3, 5, ∞} at the reference temperature $T_0$=305 [K]. As expected, when $n = 0$ the FG material reduces to pure ceramic while, on the contrary for $n = \infty$, the material properties tend to pure metal. The variations of physical and thermos-elastic properties through the thickness of the FG nanobeam cross section, assuming ζ=0.1, are illustrated in Figure 2.25,2.26 for even and uneven porosity distribution, respectively. As can be noted, the curves of the variation of physical and thermos-elastic properties relative to the even distribution (Figure 2.25) have the same behavior of those illustrated in Figure 2.26, corresponding to a non-porous FG material, but with lower property values. Finally, Figure 2.26 shows that the maximum of the FG material properties for the uneven distribution of porosity is reached at the top and bottom of the cross-section and decrease in the direction of the middle zone.

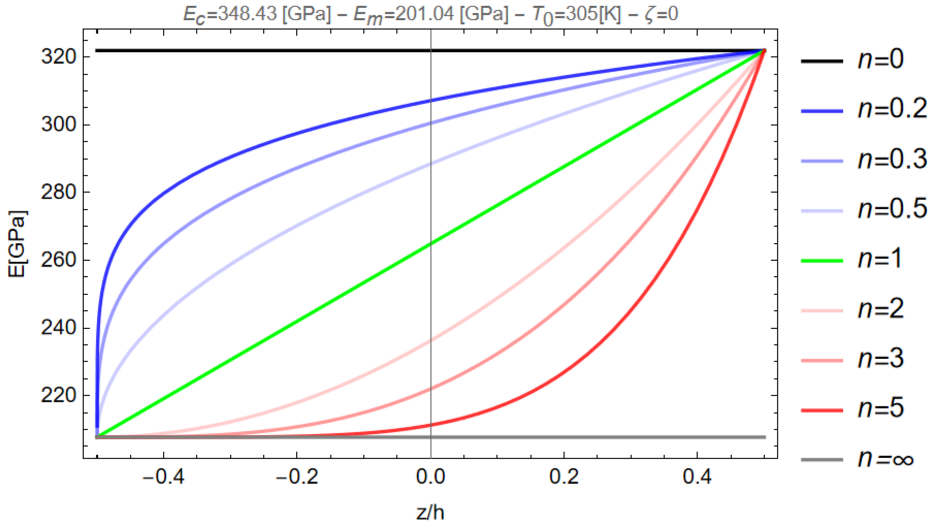
$E_c$=348.43 [GPa] – $E_m$=201.04 [GPa] – $T_0$=305[K] – $\zeta$=0
E[GPa]
320
300
280
260
240
220
−0.4
−0.2
0.0
0.2
0.4
z/h
$n$=0
$n$=0.2
$n$=0.3
$n$=0.5
$n$=1
$n$=2
$n$=3
$n$=5
$n$=∞

(a)

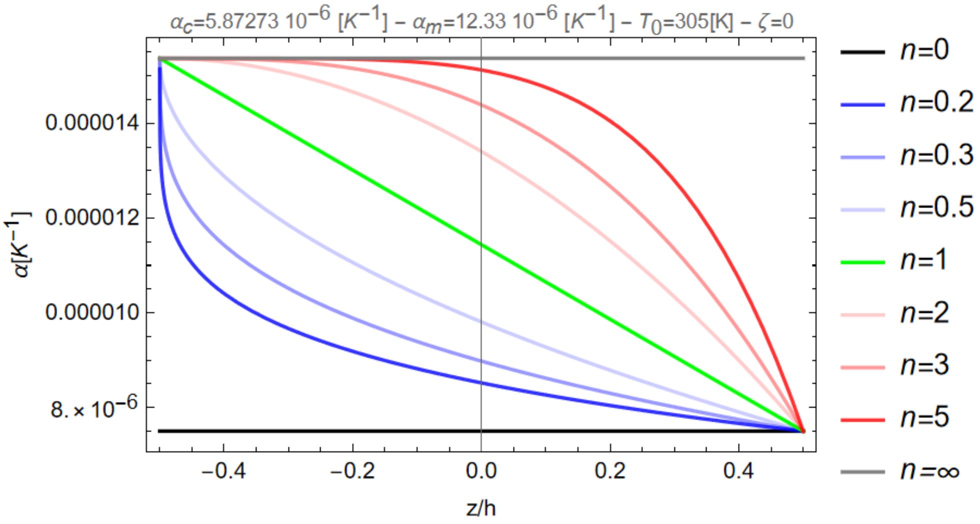
$\alpha_c$=5.87273 $10^{-6}$ [$K^{-1}$] – $\alpha_m$=12.33 $10^{-6}$ [$K^{-1}$] – $T_0$=305[K] – $\zeta$=0
$\alpha$[$K^{-1}$]
0.000014
0.000012
0.000010
8. × $10^{-6}$
−0.4
−0.2
0.0
0.2
0.4
z/h
$n$=0
$n$=0.2
$n$=0.3
$n$=0.5
$n$=1
$n$=2
$n$=3
$n$=5
$n$=∞

(b)

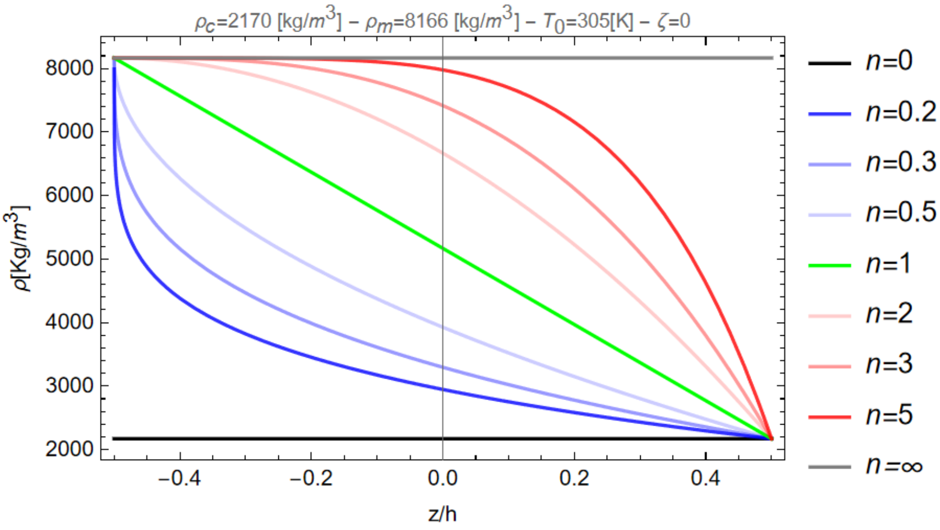
$\rho_c$=2170 [kg/$m^3$] – $\rho_m$=8166 [kg/$m^3$] – $T_0$=305[K] – $\zeta$=0
$\rho$[Kg/$m^3$]
8000
7000
6000
5000
4000
3000
2000
−0.4
−0.2
0.0
0.2
0.4
z/h
$n$=0
$n$=0.2
$n$=0.3
$n$=0.5
$n$=1
$n$=2
$n$=3
$n$=5
$n$=∞

(c)

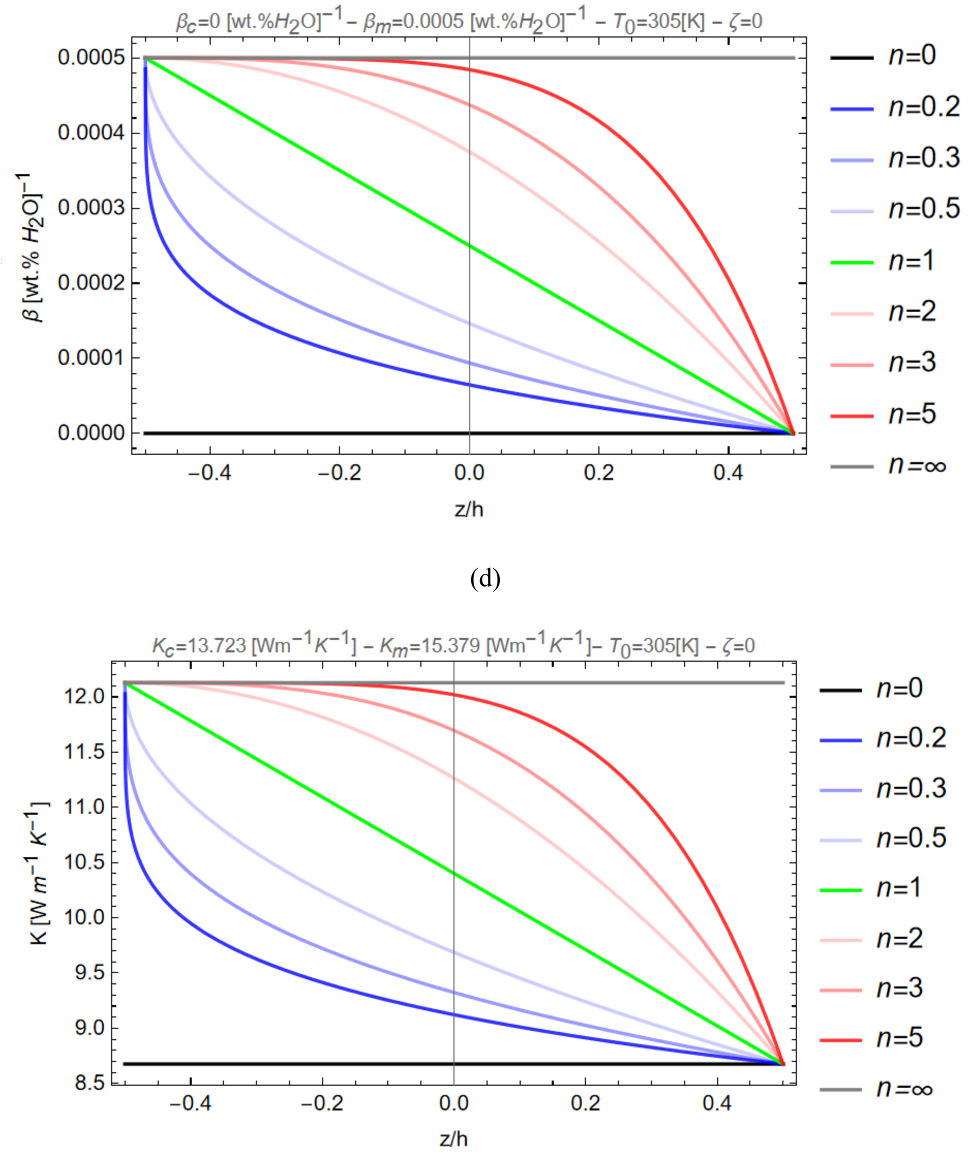

(d)

(e)

**Figures 2.24.** Variations of the: a- Euler-Young modulus ($E$), b- thermal coefficient ($\alpha$), c- mass density ($\rho$), d- moisture coefficient ($\beta$) and e- thermal conduction coefficient ($K$) in terms of dimensionless thickness ($z = z/h$) with $n$ ranging in the set {0, 0.2, 0.3, 0.5, 1, 2, 3, 5, ∞} for a non-porous FG nanobeam ($\zeta = 0$) at the temperature reference $T_0$=305 [K].

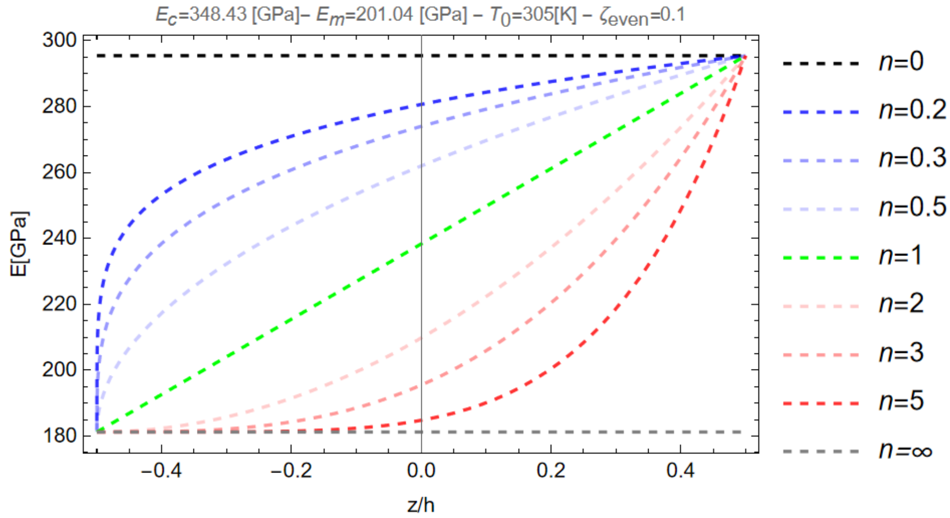
$E_c$=348.43 [GPa]– $E_m$=201.04 [GPa] – $T_0$=305[K] – $\zeta_{even}$=0.1
E[GPa]
300
280
260
240
220
200
180
−0.4
−0.2
0.0
0.2
0.4
z/h
n=0
n=0.2
n=0.3
n=0.5
n=1
n=2
n=3
n=5
n=∞

(a)

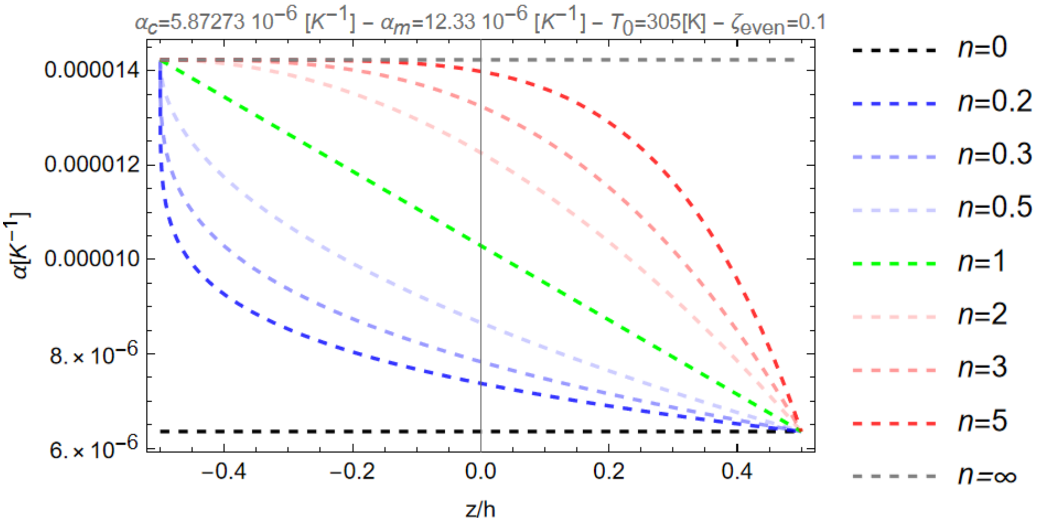
$\alpha_c$=5.87273 $10^{-6}$ [$K^{-1}$] – $\alpha_m$=12.33 $10^{-6}$ [$K^{-1}$] – $T_0$=305[K] – $\zeta_{even}$=0.1
α[$K^{-1}$]
0.000014
0.000012
0.000010
8.×$10^{-6}$
6.×$10^{-6}$
−0.4
−0.2
0.0
0.2
0.4
z/h
n=0
n=0.2
n=0.3
n=0.5
n=1
n=2
n=3
n=5
n=∞

(b)

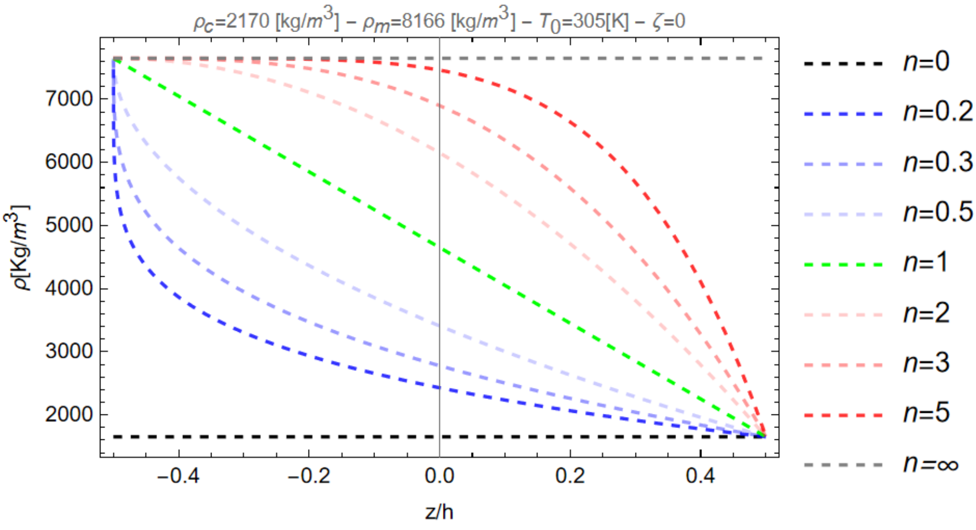
$\rho_c$=2170 [kg/$m^3$] – $\rho_m$=8166 [kg/$m^3$] – $T_0$=305[K] – ζ=0
ρ[Kg/$m^3$]
7000
6000
5000
4000
3000
2000
−0.4
−0.2
0.0
0.2
0.4
z/h
n=0
n=0.2
n=0.3
n=0.5
n=1
n=2
n=3
n=5
n=∞

(c)

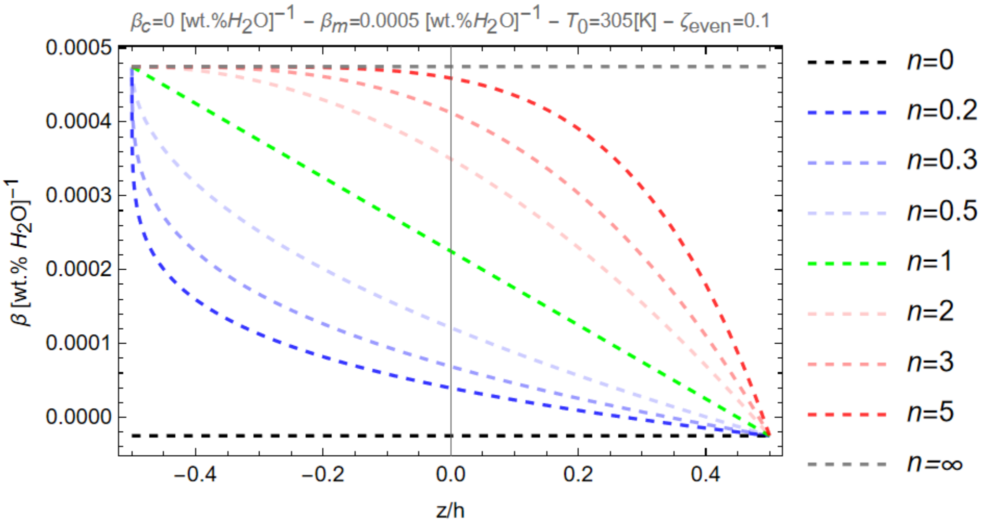

(d)

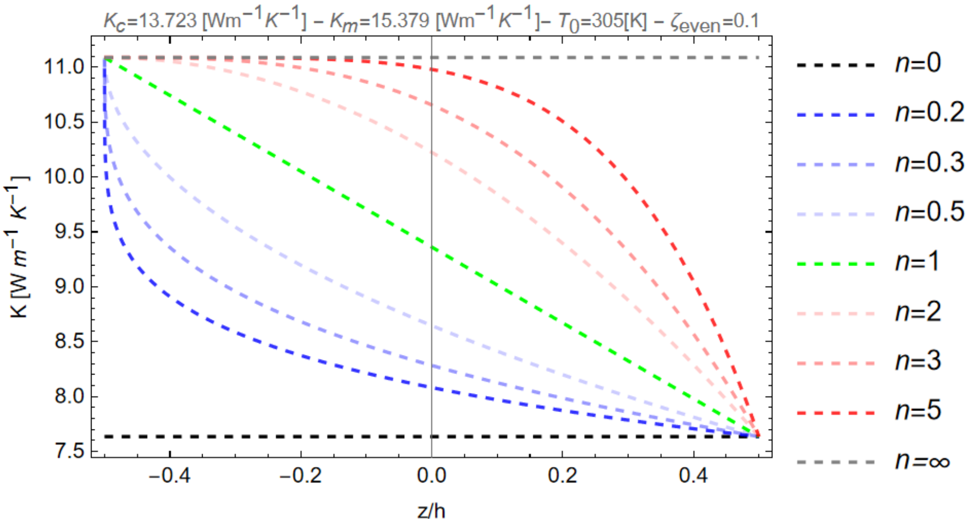

(e)

**Figures 2.25.** Variations of the: a- Euler-Young modulus (*E*), b- thermal coefficient (*α*), c- mass density (*ρ*), d- moisture coefficient (*β*) and e- thermal conduction coefficient (*K*) in terms of dimensionless thickness ($z = z/h$) with *n* ranging in the set {0, 0.2, 0.3, 0.5, 1, 2, 3, 5, ∞} for a porous FG nanobeam with an even porosity distribution ($\zeta_{even} = 0.1$) at the temperature reference *T₀=305 [K]*.

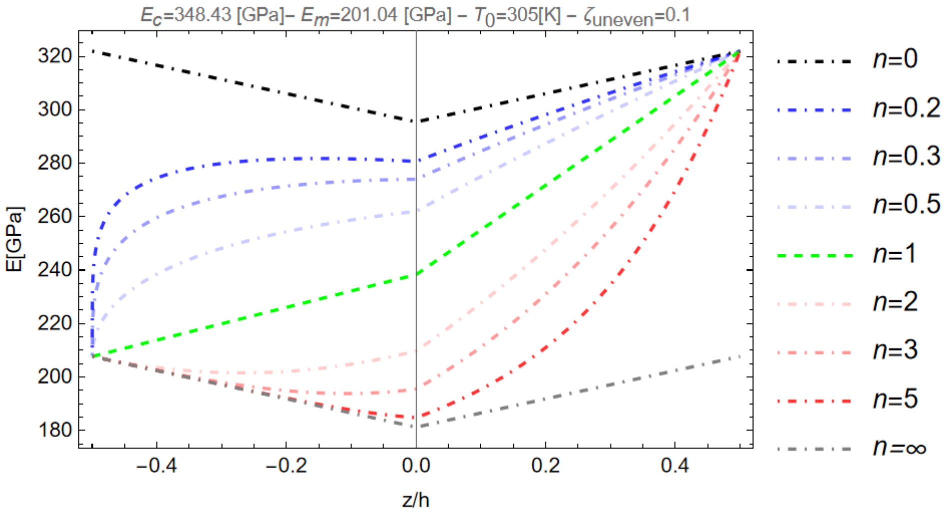
$E_c$=348.43 [GPa]– $E_m$=201.04 [GPa] – $T_0$=305[K] – $\zeta_{uneven}$=0.1
E[GPa]
320
300
280
260
240
220
200
180
−0.4
−0.2
0.0
0.2
0.4
z/h
n=0
n=0.2
n=0.3
n=0.5
n=1
n=2
n=3
n=5
n=∞

(a)

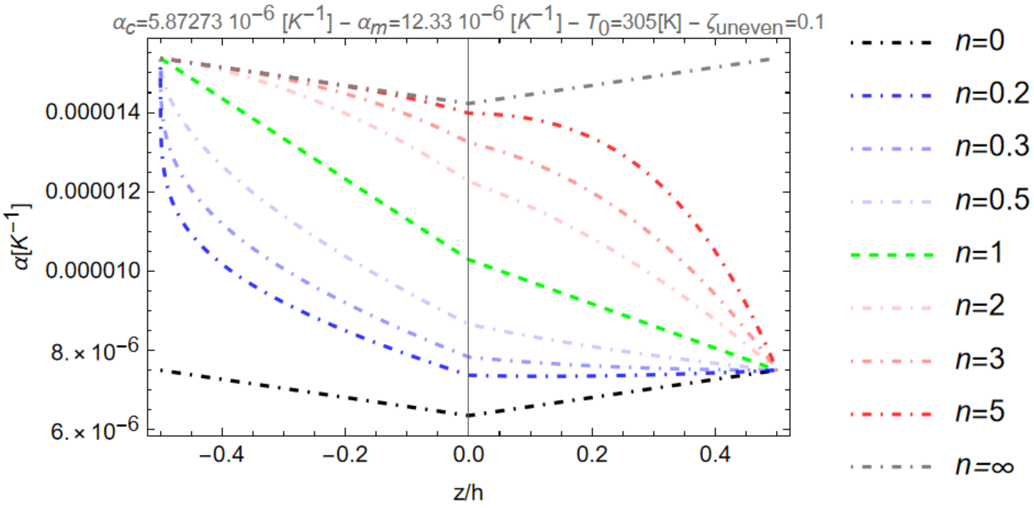
$\alpha_c$=5.87273 $10^{-6}$ [$K^{-1}$] – $\alpha_m$=12.33 $10^{-6}$ [$K^{-1}$] – $T_0$=305[K] – $\zeta_{uneven}$=0.1
α[$K^{-1}$]
0.000014
0.000012
0.000010
$8.\times10^{-6}$
$6.\times10^{-6}$
−0.4
−0.2
0.0
0.2
0.4
z/h
n=0
n=0.2
n=0.3
n=0.5
n=1
n=2
n=3
n=5
n=∞

(b)

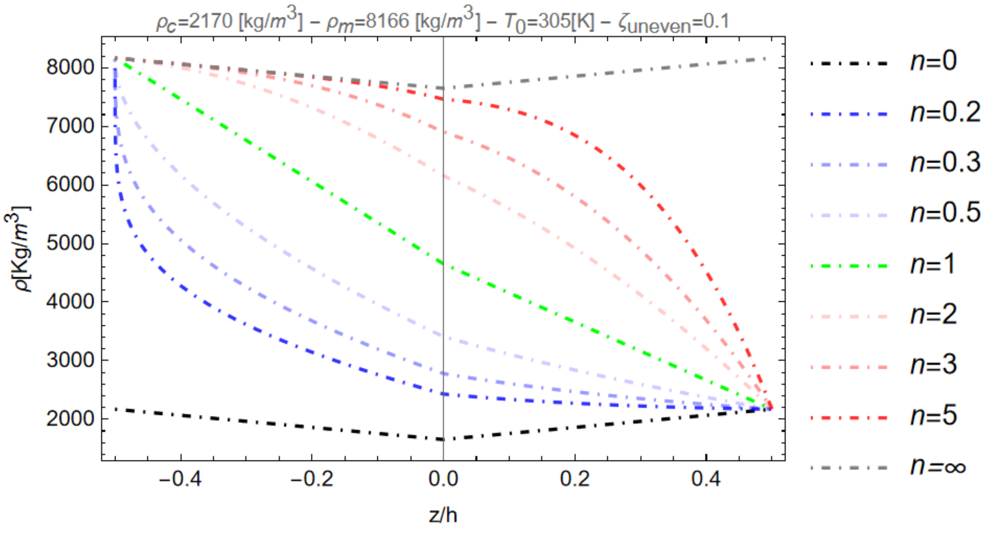
$\rho_c$=2170 [kg/$m^3$] – $\rho_m$=8166 [kg/$m^3$] – $T_0$=305[K] – $\zeta_{uneven}$=0.1
ρ[Kg/$m^3$]
8000
7000
6000
5000
4000
3000
2000
−0.4
−0.2
0.0
0.2
0.4
z/h
n=0
n=0.2
n=0.3
n=0.5
n=1
n=2
n=3
n=5
n=∞

(c)

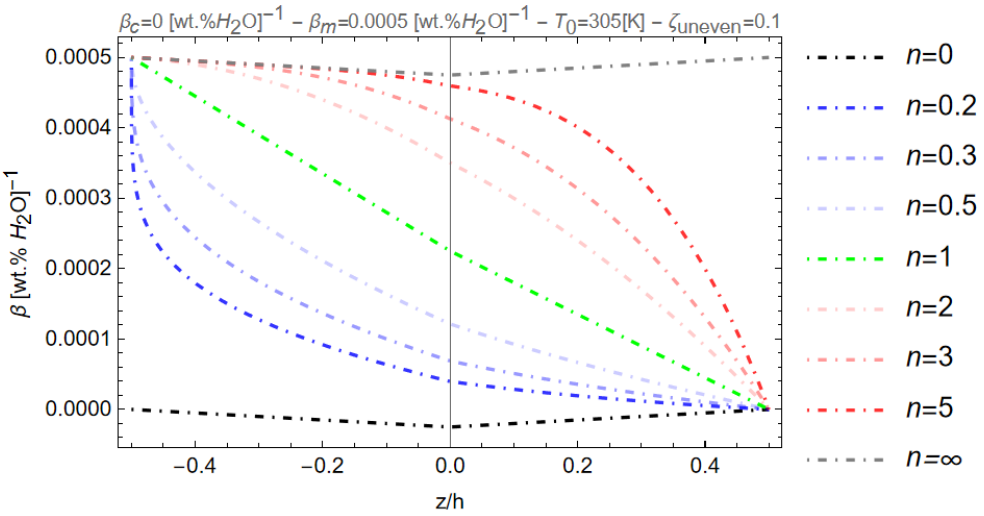

(d)

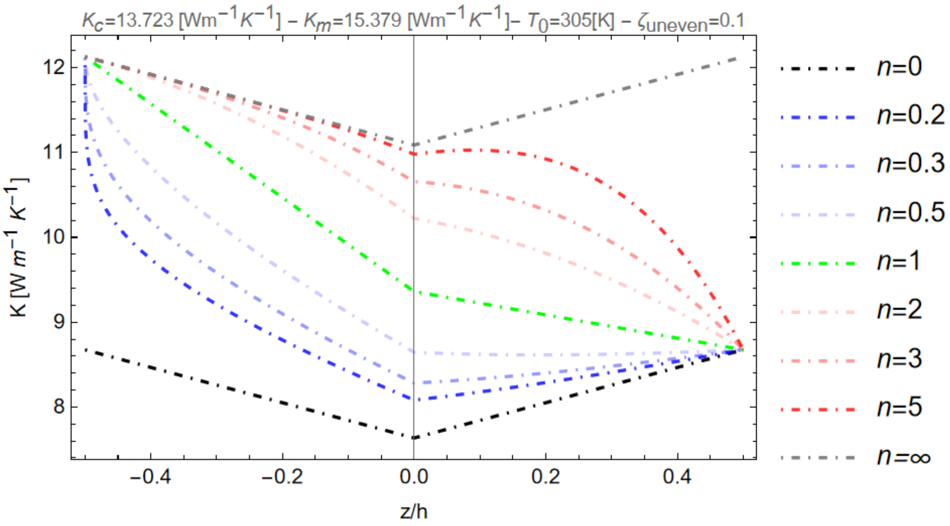

(e)

**Figures 2.26.** Variations of the: a- Euler-Young modulus ($E$), b- thermal coefficient ($\alpha$), c- mass density ($\rho$), d- moisture coefficient ($\beta$) and e- thermal conduction coefficient ($K$) in terms of dimensionless thickness ($z = z/h$) with $n$ ranging in the set {0, 0.2, 0.3, 0.5, 1, 2, 3, 5, ∞} for a porous FG nanobeam with an uneven porosity distribution ($\zeta_{uneven} = 0.1$) at the temperature reference $T_0$=*305 [K]*.

# Chapter 3

## Local/nonlocal gradient formulations

Due to the growing interest in nanoscience and nanotechnology, as discussed in Chapter 1, the modeling and optimization of nanoscale devices has generated significant interest within the scientific community to develop increasingly effective mathematical tools. Since atomic approaches [72,73] require substantial computational effort and considerably longer lead times, the development of simple and computationally convenient methodologies is the main motivation behind many recent scientific research efforts. The behavior of nanostructures can be considered similar to that of macrostructures, meaning that equivalent continuum models can be applied to study the mechanical behavior of nanostructures. However, nanostructures exhibit a discrete nature due to atomic interactions and the atomic lattice, necessitating appropriate adjustments within the realm of continuum mechanics. Moreover, as observed through experimental tests and atomistic simulations, completely negligible forces on a macroscale play a fundamental role on a nanoscale [74].

Since the classical theories of the local continuum fail to reproduce small-scale mechanical behaviors, it becomes necessary to use the mechanics of the nonlocal continuum to explain specific phenomena that emerge at the nanoscale and provide a more accurate description of the mechanical behavior of nanostructures. Classical local theories are incapable of capturing effective mechanical behavior when external and internal characteristic lengths are comparable, and nonlocality is thus required to take into account for long-range interaction forces [75].

In summary, while classical local theories state that the stress at a given point depends exclusively on the strain at that point, nonlocal theories also allow us to capture the effects of the surrounding region.

The use of nonlocal theories is necessary to model the mechanical behavior of nanostructures for several reasons:

- Small-Scale Effects: at the nanoscale, small-scale effects are significant, and nonlocal theories can describe them more accurately than classical elastic theories.
- Surface Effects: surface atoms behave differently from internal atoms, affecting the mechanical behavior of the structure. Nonlocal theories may also consider the contribution of interactions between surface atoms, which can be crucial for understanding the behavior of nanostructures.
- Long-Range Behavior: classical local theories assume that atomic interactions vanish with distance. However, at the nanoscale, long-range interactions can become significant. Nonlocal theories incorporate these interactions, allowing for a more accurate description of the mechanical behavior of nanostructures.
- Improved Experimental Correspondence: nonlocal theories provide a better match between theoretical and experimental results, meaning they can be used for designing nanomaterials and nanodevices more accurately.

Therefore, the use of nonlocal elastic laws is necessary to achieve consistent results. From a mathematical perspective, nonlocal theories, starting from their early formulations [76,77], are based on the idea that stress at a point depends on the local strain field over the whole domain. Nonlocal approaches provide enriched constitutive laws in which long-range interactions within the body are described by internal parameters [75].

One of the first integral nonlocal theories was proposed by Eringen [78], with an equivalent differential formulation in [79], where nonlocal stress results from an integral convolution between the input elastic strain field and an attenuation function that depends on the material's characteristic internal length. It has been demonstrated that the use of Eringen's model (Eringen Differential Model "EDM" or Strain-Driven Model) provides consistent results for studying problems such as screw dislocations and surface waves in unlimited domains. However, when applied to structural problems, it leads to inconsistencies between constitutive requirements and equilibrium.

Indeed, as demonstrated by Peddieson et al. in [80] and subsequently by other researchers in [81-83], the EDM model leads to known incorrect results, referred to as mechanical paradoxes within the scientific community.

To overcome the problems associated with the EDM model in limited domains, various theories have been developed, including two-phase mixture models (local/nonlocal). This model was first introduced by Eringen in [78,84] and is based on a combination of local and nonlocal responses through a mixing parameter. To obtain well-posed results, it is necessary to assume that the local fraction of the constitutive law is not negligible.

To address the difficulties of Eringen's formulation, Romano and Barretta in [85] introduced a new Stress-Driven Model (SDM) that is mathematically well-posed and provides a coherent approach to the study of nanostructures. This theory defines the nonlocal elastic strain field at a given point as a convolution integral between the local elastic strain and a scalar averaging kernel. In addition, Barretta et al. in [86] extended the Stress-Driven Model by combining it with the mixture model, which is well-posed for any local fraction.

Lim et al. in [87] introduced the nonlocal strain-gradient law (NStrainGT) by coupling Eringen's integral law with Mindlin's elasticity strain-gradient model [88,89]. Although this model has been widely applied for many years by various researchers in numerous investigations, Zaera et al. [90] recently demonstrated that nonlocal strain-gradient theory leads to ill-posed structural problems because constitutive boundary conditions conflict with both non-standard kinematic boundary conditions and higher-order static boundary conditions. The mathematical ill-posedness of Lim's NStrainGT model can be advantageously circumvented by using variational-consistent formulations of nonlocal gradient theories, such as the local/nonlocal strain-driven gradient theories (L/NStrainG) and the local/nonlocal stress-driven gradient theories (L/NStressG), conceived by Barretta et al. [91] and Pinnola et al. [92] for both static and dynamic problems. These new constitutive formulations lead to well-posed structural problems in nanomechanics. In order to study the structural response of nanostructures in a hygrothermal environment, some researchers have extended the aforementioned theories to include hygrothermal effects [93-98].

The aim of this chapter is to provide an overview of the nonlocal theories commonly employed by the scientific community. In particular, in Chapter 3.1, the local/nonlocal gradient abstract formulation is introduced. In subsections 3.1.1 and 3.1.2, the two mixture theories most commonly utilized by the scientific community, L/NStressG and L/NStrainG, respectively, are summarized. From the previously mentioned formulations, it is demonstrated how, by setting the mixture parameter and gradient length parameter to zero, the two models reduce to the pure nonlocal models SDM and EDM.

## 3.1. Local/Nonlocal Gradient formulation

The abstract formulation of local/nonlocal gradient elasticity is expressed by the following integro-differential law relating a source field, $s(x)\colon [0, L] \rightarrow R,$ and an output field, $f(x)\colon [0, L] \rightarrow R$ [91]

$$\begin{aligned} f(x) \\ = \xi_1\, s(x) + \xi_2 \int_0^L \Phi_{L_c}(x-\xi)\, \mathrm{s}(\xi) d\xi - L_l^2 \frac{\partial}{\partial x} \int_0^L \Phi_{L_c}(x-\xi)\, \frac{\partial\, \mathrm{s}(\xi)}{\partial x} d\xi \end{aligned} \tag{3.1}$$

where $\Phi_{L_c}$ is the scalar averaging kernel, depending on the length-scale parameter, $L_c$, which describes the nonlocal effects; $L_l$ denotes the gradient length parameter, introduced to capture the effects of the higher-order axial strain; $\xi_1$ and $\xi_2$ are the two-phase parameters.

It is well-known how the aforementioned constitutive mixture equation can be seen as the competition between the classical local elasticity (with volume fraction $\xi_1$) and the nonlocal elasticity (with volume fraction $\xi_2$) where the two-phase parameters must fulfil the conditions: $0 < (\xi_1, \xi_2) < 1$ and $\xi_1 + \xi_2 = 1$. Thus, the pure nonlocal law is obtained by setting $\xi_1 = 0$ (or $\xi_2 = 1$), while the well-known classical local law corresponds to $\xi_1 = 1$ (or $\xi_2 = 0$).

In the following paragraphs, both the local/nonlocal stress-driven and strain-driven gradient models of elasticity are introduced.

### 3.1.1. Local/Nonlocal Stress Gradient formulation (L/NStressG)

Local/nonlocal stress gradient formulation is obtained by setting in the Eq. 3.1 the source field, $s(x) = \frac{\sigma_{xx}(x)}{E}$ and the output field $f(x) = \varepsilon_{xx}^{el}$, being $\sigma_{xx}$ the axial stress component, subjected to equilibrium conditions, $E$ is the Young's modulus and $\varepsilon_{xx}^{el}$ the elastic axial strain component. It follows that Eq. 3.1 is transformed into the following local/nonlocal constitutive mixture equation, expressing the elastic axial strain as the function of strains at both the reference point $x$ and its nearby points $\xi$:

$$\varepsilon_{xx}^{el} = \xi_1 \frac{\sigma_{xx}(x)}{E} + \frac{\xi_2}{E} \int_0^L \Phi_{L_c}(x-\xi)\, \sigma_{xx}(\xi) d\xi - \frac{1}{E} L_l^2 \frac{\partial}{\partial x} \int_0^L \Phi_{L_c}(x-\xi)\, \frac{\partial \sigma_{xx}(\xi)}{\partial x} d\xi \tag{3.2}$$

where $\frac{\partial \sigma_{xx}}{\partial x}$ denotes the gradient of the axial stress component and $E$ is the Young's modulus.

Choosing the bi-exponential function for the kernel $\Phi_{L_c}$ depending on a positive nonlocal parameter, $L_c$, and satisfies the properties of symmetry, positivity and limit impulsivity on the real axis as:

$$\Phi_{L_c}(x, L_c) = \frac{1}{2L_c} \exp\left(-\frac{|x|}{L_c}\right) \tag{3.3}$$

and substituting the relations $\xi_2 = 1 - \xi_1$, the integro-differential relation of Eq. 3.2 admits the following set of solutions:

$$\varepsilon_{xx}^{el} - L_c^2 \frac{\partial^2 \varepsilon_{xx}^{el}}{\partial x^2} = \frac{\sigma_{xx}}{E} - \frac{L_c^2}{E}\left(\xi_1 + \frac{L_l^2}{L_c^2}\right) \frac{\partial^2 \sigma_{xx}}{\partial x^2} \tag{3.4}$$

with $x \in$ [0, L], if and only if the following two pairs of constitutive boundary conditions (CBCs) are satisfied at the nanobeam ends:

$$\frac{\partial \varepsilon_{xx}^{el}(0)}{\partial x} - \frac{1}{L_c} \varepsilon_{xx}^{el}(0) = -\frac{1}{E}\frac{\xi_1}{L_c} \sigma_{xx}(0) + \frac{1}{E}\left(\xi_1 + \frac{L_l^2}{L_c^2}\right) \frac{\partial \sigma_{xx}(0)}{\partial x} \tag{3.5}$$

$$\frac{\partial \varepsilon_{xx}^{el}(L)}{\partial x} + \frac{1}{L_c} \varepsilon_{xx}^{el}(L) = \frac{1}{E}\frac{\xi_1}{L_c} \sigma_{xx}(L) + \frac{1}{E}\left(\xi_1 + \frac{L_l^2}{L_c^2}\right) \frac{\partial \sigma_{xx}(L)}{\partial x} \tag{3.6}$$

Now, by setting $\xi_1 = 0$ and $L_l = 0$ in Eq. 3.4, we get the differential equation of a purely nonlocal stress-driven model [85]:

$$\varepsilon_{xx}^{el} - L_c^2 \frac{\partial^2 \varepsilon_{xx}^{el}}{\partial x^2} = \frac{\sigma_{xx}}{E} \tag{3.7}$$

with the corresponding constitutive boundary conditions at the nanobeam ends:

$$\frac{\partial \varepsilon_{xx}^{el}(0)}{\partial x} - \frac{1}{L_c} \varepsilon_{xx}^{el}(0) = 0 \tag{3.8}$$

$$\frac{\partial \varepsilon_{xx}^{el}(L)}{\partial x} + \frac{1}{L_c} \varepsilon_{xx}^{el}(L) = 0 \tag{3.9}$$

### 3.1.2. Local/Nonlocal Strain Gradient formulation (L/NStrainG)

Local/nonlocal strain gradient formulation is obtained by setting in Eq. 3.1 the source field, $s(x) = \varepsilon_{xx}^{el}$ and the output field $f(x) = \frac{\sigma_{xx}(x)}{E}$. It follows that Eq. 3.1 is transformed into the following local/nonlocal constitutive mixture L/NStrainG formulation:

$$\frac{\sigma_{xx}(x)}{E} = \xi_1 \varepsilon_{xx}^{el} + \xi_2 \int_0^L \Phi_{L_c}(x-\xi)\, \varepsilon_{xx}^{el}(\xi) d\xi - L_l^2 \frac{\partial}{\partial x} \int_0^L \Phi_{L_c}(x-\xi) \frac{\partial \varepsilon_{xx}^{el}(\xi)}{\partial x} d\xi \tag{3.10}$$

Eq. 3.10 is equivalent to the following differential law:

$$\sigma_{xx} - L_c^2 \frac{\partial^2 \sigma_{xx}}{\partial x^2} = E \varepsilon_{xx}^{el} - E L_c^2 \left( \xi_1 + \frac{L_l^2}{L_c^2} \right) \frac{\partial^2 \varepsilon_{xx}^{el}}{\partial x^2} \tag{3.11}$$

equipped with the following two pairs of constitutive boundary conditions:

$$\frac{\partial \sigma_{xx}(0)}{\partial x} - \frac{1}{L_c} \sigma_{xx}(0) = -E \frac{\xi_1}{L_c} \varepsilon_{xx}^{el}(0) + E \left( \xi_1 + \frac{L_l^2}{L_c^2} \right) \frac{\partial \varepsilon_{xx}^{el}(0)}{\partial x} \tag{3.12}$$

$$\frac{\partial \sigma_{xx}(L)}{\partial x} + \frac{1}{L_c} \sigma_{xx}(L) = E \frac{\xi_1}{L_c} \varepsilon_{xx}^{el}(L) + E \left( \xi_1 + \frac{L_l^2}{L_c^2} \right) \frac{\partial \varepsilon_{xx}^{el}(L)}{\partial x} \tag{3.13}$$

Now, by setting $\xi_1 = 0$ and $L_l = 0$ in Eq. 3.11, we get the differential equation of a purely nonlocal strain-driven model [70]:

$$\sigma_{xx} - L_c^2 \frac{\partial^2 \sigma_{xx}}{\partial x^2} = E\varepsilon_{xx}^{el} \tag{3.14}$$

equipped with the corresponding constitutive boundary conditions at the nanobeam ends:

$$\frac{\partial \sigma_{xx}(0)}{\partial x} - \frac{1}{L_c}\sigma_{xx}(0) = 0 \tag{3.15}$$

$$\frac{\partial \sigma_{xx}(L)}{\partial x} + \frac{1}{L_c}\sigma_{xx}(L) = 0 \tag{3.16}$$

# Chapter 4

## Hygrothermal effects on the static and dynamic response of porous functionally graded nanobeams

As widely discussed in previous chapters, nanostructures, including functionally graded nanobeams, are employed in a wide range of advanced technological applications, many of which involve hygrothermal effects. Therefore, it is of paramount importance to understand how these effects influence the structural response of nanostructures. Because of their nanoscale size, these structures are highly sensitive to the effects of temperature and humidity, which can cause deformations, stresses, and cracks that compromise their durability and reliability. To ensure optimal performance even under difficult conditions, researchers use models that explain how hygrothermal effects influence the nanostructures bending response [26,100,101]. In addition, as it is well known, free transverse vibrations represent a critical aspect of the structural behavior of any structure, including nanobeams [27,28]. In particular, the coupled effect of temperature and humidity significantly influences the natural frequency and vibration modes of the structure, as well as the stability of the structure itself. Understanding their effect is crucial to ensuring their proper functioning under specific environmental conditions. Due to the extremely small scale, vibrations in nanobeams can become inherently nonlinear. Nonlinear effects can significantly influence the structural response of nanodevices, making it essential to understand and study nonlinear vibrations to ensure that devices can perform their intended functions safely and effectively. In order to study nonlinear vibrations, many researchers have addressed this issue by proposing a higher-order Hamiltonian approach [29,102-105]. This provides a more accurate description of these phenomena that are overlooked by linear models, allowing for the capture of complex behaviors and the optimization of device designs, whereas hygrothermal effects influence not only linear but also nonlinear vibrations. In addition, as widely discussed in [106-111], in the case of an FG nanobeam, due to dependency of Young's modulus, thermal coefficient, and moisture expansion coefficients from $z$ coordinate, hygrothermal moments are generated and, therefore, the "*original boundary conditions*", including the hygrothermal moments, must be employed. On the contrary, in the case of a homogeneous isotropic nanobeam under uniform temperature and moistures rises, the hygrothermal resultants of axial forces are uniform along the thickness direction and the hygrothermal bending moments vanish and the corresponding boundary conditions coincide with the so called "*simplified boundary conditions*". It should be noted that under heat-conduction between the bottom and the top surface of nanobeams cross-section, the thermal bending moment doesn't disappear from the boundary conditions of both homogeneous isotropic and functionally graded nanobeams due to the fact that the temperature is a function of $z$ coordinate. Therefore, in the study of a homogeneous isotropic nanobeam under heat-conduction it is necessary to consider the original boundary conditions in order to take into account the effects of thermal bending moment on its bending response.

To the author's knowledge, hygrothermal size-dependent mechanical models in which the hygrothermal moments appear at the flexural boundary conditions are less studied. Therefore, a well-posed Hygrothermal Local/Nonlocal Stress Gradient model (L/NStressGH) and Hygrothermal Local/Nonlocal Strain Gradient model (L/NStrainGH) based on the use of original boundary conditions for the bending and dynamic analysis of porous FG nanobeams subjected to in-plane hygrothermal loadings are proposed. In particular, the main results of a parametric investigation varying the nonlocal parameter, the gradient length parameter, the mixture parameter, the nonlinear oscillator amplitude and the material gradient index are presented and discussed for both uniform temperatures rise and heat-conduction across the thickness.

The chapter is structured as follows. Section 4.1 describes the functionally graded material under examination and the corresponding laws governing its thermoelastic properties. Briefly, in Section 4.2, the two types of hygrothermal loads considered in this study are outlined. Chapter 4.3 presents case studies on the use of L/NStressGH and L/NStrainGH theories for studying the static behavior of a porous functionally graded nanobeam in a hygrothermal environment, with a summary of the most significant results. Finally, Section 4.3 explore the linear and nonlinear free oscillations (employ a higher-order Hamiltonian approach), of functionally graded porous nanobeams in a hygrothermal environment using the L/NStressGH model.

## 4.1. Material

Let us consider a functionally graded (FG) nanobeam of length "$L$" in a Cartesian coordinate system $\{O, x', y', z'\}$ having the origin in the geometric center $O$ of its rectangular cross-section $\Sigma$ $(b \times h)$, being $x'$ $(0 \leq x' \leq L)$ the nanobeam axis and $y'$, $z'$ the principal axes of geometric inertia of $\Sigma$ (Figure 4.1).

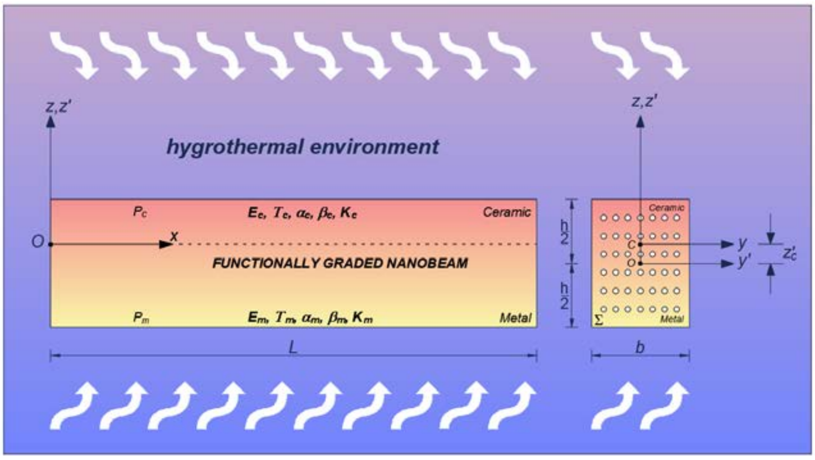

**Figure 4.1.** Coordinate system and configuration of a porous FG Bernoulli-Euler nanobeam in a hygrothermal environment.

It is supposed that the FG nanobeam material is made of a metal-ceramic mixture spatially varying from the bottom surface (metal) to the top surface (ceramic); furthermore, the subscripts "$m$" and "$c$" refer to metal and ceramic, respectively. It is further assumed the nanobeam structure to have an even porosity distribution across the thickness, generated during its manufacturing process. Consequently, the effective mechanical and hygrothermal properties of the FG material, here described by the mass density, $\rho = \rho(z')$, Young's modulus, $\rho = E(z', T)$, thermal expansions coefficient, $\alpha = \alpha(z', T)$, moisture expansion coefficient, $\beta = \beta(z', T)$, and thermal conduction coefficient, $K = K(z', T)$, can be calculated according to the mixture rule of Eq. 2.7:

$$\rho = \rho_m + (\rho_c - \rho_m)\left(\frac{1}{2} + \frac{z'}{h}\right)^n - \frac{\zeta}{2}\,(\rho_c + \rho_m) \tag{4.1}$$

$$E = E_m + (E_c - E_m)\left(\frac{1}{2} + \frac{z'}{h}\right)^n - \frac{\zeta}{2}\,(E_c + E_m) \tag{4.2}$$

$$\alpha = \alpha_m + (\alpha_c - \alpha_m)\left(\frac{1}{2} + \frac{z'}{h}\right)^n - \frac{\zeta}{2}\,(\alpha_c + \alpha_m) \tag{4.3}$$

$$\beta = \beta_m + (\beta_c - \beta_m)\left(\frac{1}{2}+\frac{z'}{h}\right)^n - \frac{\zeta}{2}\,(\beta_c + \beta_m) \tag{4.4}$$

$$K = K_m + (K_c - K_m)\left(\frac{1}{2}+\frac{z'}{h}\right)^n - \frac{\zeta}{2}\,(K_c + K_m) \tag{4.5}$$

where $\rho_c$, $\rho_m$ and $E_c$, $E_m$ are the material densities and the Euler-Young moduli of ceramic and metal, respectively; $\alpha_c$, $\alpha_m$ and $\beta_c$, $\beta_m$ are the thermal expansion coefficients and the moisture expansion coefficients of the two aforementioned materials, respectively; $K_c$ and $K_m$ denote the bottom and top thermal conduction coefficients, respectively. Furthermore, the symbols $n$ ($n \geq 0$) and $\zeta$ ($\zeta << 1$) denote the gradient index and the porosity volume fraction of the FG material, respectively. The characteristic values of thermo-elastic properties of the constituent nanobeam materials, metal ($SuS_3O_4$) and ceramic ($Si_3N_4$), as well as the values of the coefficients of material phases are listed in Table 2.1 and Table 2.2 (§2.7), respectively. It is well-known that under an extreme temperature environment, the material properties are also assumed to be temperature-dependent in according to Eq. 2.16.

In order to eliminate the bending–extension coupling due to the variation of the functionally graded material, the thermo-elastic material properties are evaluated with respect to a new elastic Cartesian coordinate system originating at the elastic center $C$ (Figure 4.1), whose position, $z'_c$, is given by Eq. 2.17.

## 4.2. Types of hygrothermal loadings

In this investigation, both a uniform temperature rise (UTR) [26,27] and heat-conduction (HC) between the bottom and the top surface of the FG nanobeam cross-section, under the hypothesis of absence of heat sources [99], are considered:

- (UTR)

$$\Delta T_{UTR} = T_{UTR} - T_0 = const \tag{4.6}$$

- (HC)

$$\Delta T_{HC}(z) = T_{HC}(z) - T_0 \tag{4.7}$$

where

$$T_{HC}(z) = T_m + \frac{(T_c - T_m)}{\sum_{i=0}^{k}\left[\frac{(-1)^i}{n\,i+1}\left(\frac{K_c - K_m}{K_m - \frac{\zeta}{2}(K_c + K_m)}\right)^i\right]} \sum_{i=0}^{k}\left[\frac{(-1)^i}{n\,i+1}\left(\frac{1}{2} + \frac{z}{h}\right)^{n\,i+1}\left(\frac{K_c - K_m}{\frac{\zeta}{2}(K_c + K_m)}\right)^i\right] \tag{4.8}$$

being $T_0$ the reference value of temperature of FG nanobeam, $T_m$ and $T_c$ the bottom and top temperatures, respectively, and $K_m$ and $K_c$ the thermal conduction coefficients of the two constituent nanobeam materials. Furthermore, the index $i$ represents an adequate number of terms that must be taken into account in the solution procedure to ensure the convergence of series in Eq. 4.8. Whereas, for the moisture concentration we considered only the case of Uniform Moisture Rise, $\Delta H = H_{UMR} - H_0 = const$, in which $H_0$ denotes the reference value of the moisture concentration.

It is now possible to introduce the hygrothermal resultants of axial force and bending moments respectively for both uniform temperature rise and heat-conduction as follows:

- (UTR)

$$N^T = N_{UTR}^T(z,T) = \int_{\Sigma} E\alpha\Delta T_{UTR}\,dz \tag{4.9}$$

$$M^T = M_{UTR}^T(z,T) = \int_{\Sigma} E\alpha\Delta T_{UTR}\,z\,dz \tag{4.10}$$

- (HC)

$$N^T = N_{HC}^T(z,T) = \int_{\Sigma} E\alpha\Delta T_{HC}(z)\,dz \tag{4.11}$$

$$M^T = M_{HC}^T(z,T) = \int_{\Sigma} E\alpha\Delta T_{HC}(z)\,z\,dz \tag{4.12}$$

- (UMR)

$$N^H = N^H(z,T) = \int_{\Sigma} E\beta\Delta H dz \tag{4.13}$$

$$M^H = M^H(z,T) = \int_{\Sigma} E\beta\Delta H z dz \tag{4.14}$$

in which $E = E(z,T)$, $\alpha = \alpha(z,T)$ and $\beta = \beta(z,T)$ are the Young's modulus, the thermal and the moisture expansion coefficients, respectively.

## 4.3. Hygrothermal bending behavior of porous FG nanobeams via L/NStressGH and L/NStrainGH theories of elasticity

Based on Bernoulli-Euler theory, in the elastic coordinate reference system $\{C, x, y, z\}$, the Cartesian components of the displacement field of the nanobeam, $u_x = u_x(x,z)$, $u_y = u_y(x,z)$ and $u_z = u_z(x,z)$, along *x, y* and *z* directions, respectively, can be expressed as:

$$u_x = -z\frac{\partial w}{\partial x} \tag{4.15}$$

$$u_y = 0 \tag{4.16}$$

$$u_z = w \tag{4.17}$$

where $w = w(x)$ is the transverse displacements of the elastic centre *C*. Consequently, the only nonzero component deformation associated with the displacement field is the axial strain, defined as:

$$\varepsilon_{xx} = -z\frac{\partial^2 w}{\partial x^2} \tag{4.18}$$

where $\frac{\partial^2 w}{\partial x^2}$ refers to the geometrical bending curvature $\chi$.

By using the principle of virtual work, we can derive the governing equations, as follows:

$$\delta U + \delta W = 0 \tag{4.19}$$

being $\delta U$ and $\delta W$ the virtual strain energy and the virtual work done by external forces, respectively. The virtual strain energy $\delta U$ is given by:

$$\delta U = \int_0^L \int_\Sigma \sigma_{xx} \delta \varepsilon_{xx} \, d\Sigma \, dx = -\int_0^L M \frac{\partial^2 \delta w}{\partial x^2} \, dx \tag{4.20}$$

where $\sigma_{xx} = \sigma_{xx}(z, T) = E(z, T)\varepsilon_{xx} = E\varepsilon_{xx}$, is the temperature-dependent axial stress, and $M$, is the moment stress resultant defined as follows:

$$M = M(x) = -I_E \, \chi \tag{4.21}$$

in which $I_E$ denotes the bending stiffness defined Eq. 2.20.

The expression of the virtual work of the external force $\delta W$ is:

$$\delta W = -\int_0^L \left( q_z \delta w + (N^T + N^H) \frac{\partial w}{\partial x} \frac{\partial \delta w}{\partial x} \right) dx \tag{4.22}$$

where $q_z = q_z(x)$ is the transverse distributed load.

By substituting Eq. 4.20 and Eq. 4.22 into Eq. 4.19, and using the fundamental lemma of variational calculus, the following equation of equilibrium can be obtained:

$$\frac{\partial^2 M}{\partial x^2} - (N^T + N^H) \frac{\partial^2 w}{\partial x^2} + q_z = 0 \tag{4.23}$$

The corresponding boundary conditions at the nanobeam's ends ($x = 0$ and $x = L$) can be chosen by specifying one element of each of the following two pairs (standard kinematic or static boundary conditions, SBC) at $x = 0, L$:

$$w = w^*|_{x=0,L} \quad \text{or} \quad \frac{\partial M}{\partial x} - (N^T + N^H) \frac{\partial w}{\partial x} = V^*|_{x=0,L} \tag{4.24}$$

$$\frac{\partial w}{\partial x} = \frac{\partial w^*}{\partial x}|_{x=0,L} \quad \text{or} \quad M = M^*|_{x=0,L} \tag{4.25}$$

being $M^*$ and $V^*$ assigned moment and vertical force acting at the nanobeam ends, respectively, and $w^*$ an assigned vertical displacement at the nanobeam ends.

### 4.3.1. Constitutive laws

- *Local/Nonlocal Hygrothermal Stress Gradient model of elasticity (L/NStressGH)*

Reference is made to the differential constitutive law of the L/NStressG model, with the corresponding constitutive boundary conditions previously developed in §3.1.1.:

$$\varepsilon_{xx}^{el} - L_c^2 \frac{\partial^2 \varepsilon_{xx}^{el}}{\partial x^2} = \frac{\sigma_{xx}}{E} - \frac{L_c^2}{E}\left(\xi_1 + \frac{L_l^2}{L_c^2}\right)\frac{\partial^2 \sigma_{xx}}{\partial x^2} \tag{4.26}$$

$$\frac{\partial \varepsilon_{xx}^{el}(0)}{\partial x} - \frac{1}{L_c}\varepsilon_{xx}^{el}(0) = -\frac{1}{E}\frac{\xi_1}{L_c}\sigma_{xx}(0) + \frac{1}{E}\left(\xi_1 + \frac{L_l^2}{L_c^2}\right)\frac{\partial \sigma_{xx}(0)}{\partial x} \tag{4.27}$$

$$\frac{\partial \varepsilon_{xx}^{el}(L)}{\partial x} + \frac{1}{L_c}\varepsilon_{xx}^{el}(L) = \frac{1}{E}\frac{\xi_1}{L_c}\sigma_{xx}(L) + \frac{1}{E}\left(\xi_1 + \frac{L_l^2}{L_c^2}\right)\frac{\partial \sigma_{xx}(L)}{\partial x} \tag{4.28}$$

In a hygrothermal environment, the elastic axial strain is expressed as the difference between the total strain, $\varepsilon_{xx}$, and the non-elastic axial strain, $\varepsilon_{xx}^* = \alpha\Delta T + \beta\Delta H$, depending on the increases in temperature, $\Delta T$, and moisture concentration, $\Delta H$, (i.e. hygrothermal effects):

$$\varepsilon_{xx}^{el} = \varepsilon_{xx} - \varepsilon_{xx}^* \tag{4.29}$$

By manipulating Eq. 4.18 with Eq. 4.29 and substituting into Eqs. 4.26-4.29, then multiplying by *z*, the integration over the nanobeam cross section provides the following "*L/NStressGH*" equation in terms of transverse displacement:

$$\begin{aligned} &- I_E \frac{\partial^2 w}{\partial x^2} + I_E L_c^2 \frac{\partial^4 w}{\partial x^4} - M^T - M^H \\ &\qquad = M^{L/NStressGH} - L_c^2\left(\xi_1 + \frac{L_l^2}{L_c^2}\right)\frac{\partial^2 M^{L/NStressGH}}{\partial x^2} \end{aligned} \tag{4.30}$$

with the corresponding constitutive boundary conditions (CBCs) (at $x = 0, L$):

$$\begin{aligned} &- I_E \frac{\partial^3 w(0)}{\partial x^3} + \frac{I_E}{L_c}\frac{\partial^2 w(0)}{\partial x^2} + \frac{M^T + M^H}{L_c} \\ &\qquad = -\frac{\xi_1}{L_c} M^{L/NStressGH}(0) \\ &\qquad + \left(\xi_1 + \frac{L_l^2}{L_c^2}\right)\frac{\partial M^{L/NStressGH}(0)}{\partial x} \end{aligned} \tag{4.31}$$

$$
\begin{aligned}
&- I_E \frac{\partial^3 w(L)}{\partial x^3} - \frac{I_E}{L_c}\frac{\partial^2 w(L)}{\partial x^2} - \frac{M^T + M^H}{L_c} \\
&\qquad = \frac{\xi_1}{L_c} M^{L/NStressGH}(L) + \left(\xi_1 + \frac{L_l^2}{L_c^2}\right) \frac{\partial M^{L/NStressGH}(L)}{\partial x}
\end{aligned}
\tag{4.32}
$$

in which $M^{L/NStressGH} = M^{L/NStressGH}(x)$ denotes the hygrothermal local/nonlocal gradient moment. Substituting Eq. 4.23 into Eq. 4.37, the expression of the abovementioned moment can be expressed as follows:

$$
\begin{aligned}
M^{L/NStressGH} &= - I_E \frac{\partial^2 w}{\partial x^2} + I_E L_c^2 \frac{\partial^4 w}{\partial x^4} \\
&\quad + L_c^2 \left(\xi_1 + \frac{L_l^2}{L_c^2}\right)\left((N^T + N^H)\frac{\partial^2 w}{\partial x^2} - q_z\right) - (M^T + M^H)
\end{aligned}
\tag{4.33}
$$

equipped with standard boundary conditions (Eqs. 4.24 and 4.25) together with aforementioned constitutive boundary conditions at the ends of FG nanobeam given by Eqs. 4.28 and 4.29.

- *Hygrothermal Local/Nonlocal Strain Gradient model of elasticity (L/NStrainGH)*

Now, reference is made to the set of differential constitutive law of the L/NStrainG model, previously developed in §3.1.2.:

$$
\sigma_{xx} - L_c^2 \frac{\partial^2 \sigma_{xx}}{\partial x^2} = E\varepsilon_{xx}^{el} - E L_c^2 \left(\xi_1 + \frac{L_l^2}{L_c^2}\right) \frac{\partial^2 \varepsilon_{xx}^{el}}{\partial x^2}
\tag{4.34}
$$

$$
\frac{\partial \sigma_{xx}(0)}{\partial x} - \frac{1}{L_c}\sigma_{xx}(0) = -E\frac{\xi_1}{L_c}\varepsilon_{xx}^{el}(0) + E\left(\xi_1 + \frac{L_l^2}{L_c^2}\right)\frac{\partial \varepsilon_{xx}^{el}(0)}{\partial x}
\tag{4.35}
$$

$$
\frac{\partial \sigma_{xx}(L)}{\partial x} + \frac{1}{L_c}\sigma_{xx}(L) = E\frac{\xi_1}{L_c}\varepsilon_{xx}^{el}(L) + E\left(\xi_1 + \frac{L_l^2}{L_c^2}\right)\frac{\partial \varepsilon_{xx}^{el}(L)}{\partial x}
\tag{4.36}
$$

By repeating the same steps developed in the previous paragraph related to the stress gradient formulation, the following "*L/NStrainGH*" ordinary differential governing equation are obtained:

$$
\begin{aligned}
&-I_E\frac{\partial^4 w}{\partial x^4}+I_E L_c^2\left(\xi_1+\frac{L_l^2}{L_c^2}\right)\frac{\partial^6 w}{\partial x^6}+L_c^2\,\frac{\partial^2}{\partial x^2}\left((N^T+N^H)\frac{\partial^2 w}{\partial x^2}-q_z\right)\\
&\qquad -(N^T+N^H)\frac{\partial^2 w}{\partial x^2}+q_z=0
\end{aligned}
\tag{4.37}
$$

which can be solved by prescribing the standard boundary conditions (SBCs) expressed by Eqs. 4.24 and 4.25 and the following constitutive ones at $x=0,L$ (CBCs):

$$
\begin{aligned}
&\frac{\partial M^{L/NStrainGH}}{\partial x}(0)-\frac{M^{\frac{L}{NStrainGH}}}{L_c}(0)\\
&\qquad=\frac{\xi_1}{L_c}\left(I_E\frac{\partial^2 w}{\partial x^2}(0)+M^T+M^H\right)-I_E\left(\xi_1+\frac{L_l^2}{L_c^2}\right)\frac{\partial^3 w}{\partial x^3}(0)
\end{aligned}
\tag{4.38}
$$

$$
\begin{aligned}
&\frac{\partial M^{L/NStrainGH}}{\partial x}(L)+\frac{M^{L/NStrainGH}}{L_c}(L)\\
&\qquad=-\frac{\xi_1}{L_c}\left(I_E\frac{\partial^2 w}{\partial x^2}(L)+M^T+M^H\right)\\
&\qquad-I_E\left(\xi_1+\frac{L_l^2}{L_c^2}\right)\frac{\partial^3 w}{\partial x^3}(L)
\end{aligned}
\tag{4.39}
$$

where the expression of $M^{NStrainG}=M^{NStrainG}(x)$ is reported in the following equation:

$$
\begin{aligned}
M^{L/NStrainGH}&=-I_E\,\frac{\partial^2 w}{\partial x^2}+I_E L_c^2\left(\xi_1+\frac{L_l^2}{L_c^2}\right)\frac{\partial^4 w}{\partial x^4}+L_c^2(N^T+N^H)\frac{\partial^2 w}{\partial x^2}\\
&-L_c^2 q_z-(M^T+M^H)
\end{aligned}
\tag{4.40}
$$

**Remark 4.1.**

*It's worth observing that when dealing with homogeneous isotropic nanobeams, we can derive the governing differential equation and corresponding boundary conditions by setting the material gradient index 'n' to either zero or infinity. Furthermore, in scenarios where a homogeneous isotropic nanobeam is exposed to both uniform temperature and moisture rise, the hygrothermal axial forces* $\widetilde{N}^T$ *and* $\widetilde{N}^H$ *remain constant across the thickness direction (denoted as 'z'). Additionally, the hygrothermal bending moments* $\widetilde{M}^T$ *and* $\widetilde{M}^H$ *are eliminated from the expressions of the* *nonlocal stress and strain gradient hygrothermal moments, Eq. 4.33 and Eq. 4.40, respectively. Consequently, the associated boundary conditions align with the standard ones, often referred to as simplified boundary conditions. Conversely, in the case of functionally graded (FG) nanobeams, due to the dependence of Young's modulus, thermal coefficient, and moisture expansion coefficients on the 'z' coordinate, hygrothermal moments are generated. Consequently, the original boundary conditions must be applied. It's important to note that for both homogeneous isotropic and functionally graded nanobeams undergoing heat-conduction, the thermal bending moment* $\widetilde{M}^T$ *remains present in the boundary conditions due to the temperature's dependency on the 'z' coordinate (as shown in Eq. 4.7). Hence, even when studying homogeneous isotropic nanobeams under heat-conduction, it's essential to use the original boundary conditions to consider the influence of the thermal bending moment on their mechanical behavior. Finally, in cases where static schemes do not involve hygrothermal bending moments in the boundary conditions, like in clamped-clamped nanobeams, the results obtained from simplified and original boundary conditions are equivalent. Conversely, when hygrothermal bending moments are present in the boundary conditions for both FG and homogeneous isotropic nanobeams, as in the cases of clamped-pinned and pinned-pinned configurations, relying on simplified boundary conditions can lead to inaccurate outcomes.*

### 4.3.2. Static of inflected porous FG nanobeams

In this section, the dimensionless equations governing the elastic equilibrium of L/NStressGH and L/NStrainGH inflected nanobeams are obtained. By introducing the following dimensionless quantities:

$$\begin{array}{llll} \tilde{x} = \dfrac{x}{L} & \widetilde{w} = \dfrac{w}{L} & \widetilde{w}^* = \dfrac{w^*}{L} & \lambda_c = \dfrac{L_c}{L} \\ \lambda_l = \dfrac{L_l}{L} & \widetilde{N}^T = \dfrac{N^T}{I_E} L^2 & \widetilde{N}^H = \dfrac{N^H}{I_E} L^2 & \widetilde{M}^T = \dfrac{M^T}{I_E} L \\ \tilde{V}^* = \dfrac{V^*}{I_E} L^2 & \tilde{q}_z = \dfrac{q_z}{I_E} L^3 & \widetilde{M}^H = \dfrac{M^T}{I_E} L & \widetilde{M}^* = \dfrac{M^*}{I_E} L \end{array} \tag{4.41}$$

the dimensionless equations of the elastostatic problems associated with L/NStressGH and L/NStrainGH inflected beams can be formulated as follows.

### - *Elastostatic problem of L/NStressGH inflected nanobeams*

*Equilibrium equation*

$$\lambda_c^2 \frac{\partial^6 \tilde{w}}{\partial \tilde{x}^6} - \frac{\partial^4 \tilde{w}}{\partial \tilde{x}^4} + \lambda_c^2 \left( \xi_1 + \frac{\lambda_l^2}{\lambda_c^2} \right) \frac{\partial^2}{\partial \tilde{x}^2} \left( \left( \tilde{N}^T + \tilde{N}^H \right) \frac{\partial^2 \tilde{w}}{\partial \tilde{x}^2} - \tilde{q}_z \right) - \left( \tilde{N}^T + \tilde{N}^H \right) \frac{\partial^2 \tilde{w}}{\partial \tilde{x}^2} + \tilde{q}_z = 0 \tag{4.42}$$

*Standard boundary conditions*

$$\tilde{w} = \tilde{w}^* |_{0,1} \quad \text{or} \quad \frac{\partial \tilde{M}^{L/NStressGH}}{\partial x} - \left( \tilde{N}^T + \tilde{N}^H \right) \frac{\partial \tilde{w}}{\partial \tilde{x}} = \tilde{V}^* |_{0,1} \tag{4.43}$$

$$\frac{\partial \tilde{w}}{\partial \tilde{x}} = \frac{\partial \tilde{w}^*}{\partial \tilde{x}} |_{0,1} \quad \text{or} \quad \tilde{M}^{L/NStressGH} = \tilde{M}^* |_{0,1} \tag{4.44}$$

*Constitutive boundary conditions*

$$-\frac{\partial^3 \tilde{w}(0)}{\partial \tilde{x}^3} + \frac{1}{\lambda_c} \frac{\partial^2 \tilde{w}(0)}{\partial \tilde{x}^2} + \frac{\tilde{M}^T + \tilde{M}^H}{\lambda_c} = -\frac{\xi_1}{\lambda_c} \tilde{M}^{L/NStressGH}(0) + \left( \xi_1 + \frac{\lambda_l^2}{\lambda_c^2} \right) \frac{\partial \tilde{M}^{L/NStressGH}(0)}{\partial \tilde{x}} \tag{4.45}$$

$$-\frac{\partial^3 \tilde{w}(1)}{\partial \tilde{x}^3} - \frac{1}{\lambda_c} \frac{\partial^2 \tilde{w}(1)}{\partial \tilde{x}^2} - \frac{\tilde{M}^T + \tilde{M}^H}{\lambda_c} = \frac{\xi_1}{\lambda_c} \tilde{M}^{L/NStressGH}(1) + \left( \xi_1 + \frac{\lambda_l^2}{\lambda_c^2} \right) \frac{\partial \tilde{M}^{L/NStressGH}(1)}{\partial \tilde{x}} \tag{4.46}$$

being

$$\tilde{M}^{L/NStressGH} = -\frac{\partial^2 \tilde{w}}{\partial \tilde{x}^2} + \lambda_c^2 \frac{\partial^4 \tilde{w}}{\partial \tilde{x}^4} + \lambda_c^2 \left( \xi_1 + \frac{\lambda_l^2}{\lambda_c^2} \right) \left( \left( \tilde{N}^T + \tilde{N}^H \right) \frac{\partial^2 \tilde{w}}{\partial \tilde{x}^2} - \tilde{q}_z \right) - \left( \tilde{M}^T + \tilde{M}^H \right) \tag{4.47}$$

- ***Elastostatic problem of L/NStrainG inflected nanobeams***

*Equilibrium equation*

$$-\frac{\partial^4 \tilde{w}}{\partial \tilde{x}^4} + \lambda_c^2\left(\xi_1 + \frac{\lambda_l^2}{\lambda_c^2}\right)\frac{\partial^6 \tilde{w}}{\partial \tilde{x}^6} + \lambda_c^2\frac{\partial^2}{\partial \tilde{x}^2}\left(\left(\tilde{N}^T + \tilde{N}^H\right)\frac{\partial^2 \tilde{w}}{\partial \tilde{x}^2} - \tilde{q}_z\right) - \left(\tilde{N}^T + \tilde{N}^H\right)\frac{\partial^2 \tilde{w}}{\partial \tilde{x}^2} + \tilde{q}_z = 0 \tag{4.48}$$

*Standard boundary conditions*

$$\tilde{w} = \tilde{w}^*|_{0,1} \quad \text{or} \quad \frac{\partial \tilde{M}^{L/NStrainGH}}{\partial x} - \left(\tilde{N}^T + \tilde{N}^H\right)\frac{\partial \tilde{w}}{\partial \tilde{x}} = \tilde{V}^*|_{0,1} \tag{4.49}$$

$$\frac{\partial \tilde{w}}{\partial \tilde{x}} = \frac{\partial \tilde{w}^*}{\partial \tilde{x}}|_{0,1} \quad \text{or} \quad \tilde{M}^{L/NStrainGH} = \tilde{M}^*|_{0,1} \tag{4.50}$$

*Constitutive boundary conditions*

$$\frac{\partial \tilde{M}^{L/NStrainGH}}{\partial \tilde{x}}(0) - \frac{\tilde{M}^{L/NStrainGH}}{\lambda_c}(0) = \frac{\xi_1}{\lambda_c}\frac{\partial^2 \tilde{w}(0)}{\partial \tilde{x}^2} - \left(\xi_1 + \frac{\lambda_l^2}{\lambda_c^2}\right)\frac{\partial^3 \tilde{w}(0)}{\partial \tilde{x}^3} \tag{4.51}$$

$$\frac{\partial \tilde{M}^{L/NStrainGH}}{\partial \tilde{x}}(1) + \frac{\tilde{M}^{L/NStrainGH}}{\lambda_c}(1) = -\frac{\xi_1}{\lambda_c}\frac{\partial^2 \tilde{w}(0)}{\partial \tilde{x}^2} - \left(\xi_1 + \frac{\lambda_l^2}{\lambda_c^2}\right)\frac{\partial^3 \tilde{w}(0)}{\partial \tilde{x}^3} \tag{4.52}$$

being

$$\tilde{M}^{L/NStrainGH} = -\frac{\partial^2 \tilde{w}}{\partial \tilde{x}^2} + \lambda_c^2\left(\xi_1 + \frac{\lambda_l^2}{\lambda_c^2}\right)\frac{\partial^4 \tilde{w}}{\partial \tilde{x}^4} + \lambda_c^2\left(\tilde{N}^T + \tilde{N}^H\right)\frac{\partial^2 \tilde{w}}{\partial \tilde{x}^2} - \lambda_c^2\tilde{q}_z - \left(\tilde{M}^T + \tilde{M}^H\right) \tag{4.53}$$

### 4.3.3. Results and discussion

In this paragraph, the numerical investigation of FG porous Bernoulli-Euler nanobeams, with length $L$= 10 nm and square cross-section ($b$=$h$=0.1$L$) considering two static schemes: a Simply-Supported (S-S) nanobeam and a Doubly-Clamped (C-

C), both subjected to hygrothermal loadings and a uniformly distributed dimensionless load across the complete span, $\tilde{q}_z$, has been developed for both L/NStressGH and L/NStrainGH models of nonlocal elasticity.

To assess the accuracy and reliability of the proposed approach, in Tables 4.1 and 4.2, both the pure nonlocal L/NStrainGH and L/NStressGH dimensionless values ($\xi_1 = 0$) of the of the midpoint deflection, $\tilde{w}(1/2)$, of the simply supported and doubly clamped nanobeam, are summarized varying the nonlocal parameter, $\lambda_c$. It is worth noting that, when the hygrothermal loadings are neglected, and considering $\tilde{q}_z = 1$, the results obtained for $\lambda_l = 0$ coincide with those obtained in [112] and with the results presented in [91] for $\lambda_l = 0.5$.

**Table 4.1.** Simply-Supported FG nanobeam under uniformly distributed load: non-dimensional midpoint deflection $\tilde{w}(1/2)$, vs. nonlocal parameter $\lambda_c$. Comparison between L/NStressGH and L/NStrainGH, assuming $\xi_1 = 0.0$, $\Delta T_{UTR} = \Delta T_{HC} = 0$ and varying $\lambda_l$ in the set (0.0, 0.5).

| $\lambda_c$ | L/NStrainG | | | | L/NStressG | | | |
|---|---|---|---|---|---|---|---|---|
| | $\lambda_l = 0.0^+$ | Ref. [112] | $\lambda_l = 0.5$ | Ref. [91] | $\lambda_l = 0.0^+$ | Ref. [112] | $\lambda_l = 0.5$ | Ref. [91] |
| $0.00^+$ | 0.01302 | 0.01302 | 0.01065 | 0.01065 | 0.01302 | 0.01302 | 0.04427 | 0.04427 |
| 0.10 | 0.01471 | 0.01471 | 0.01075 | 0.01075 | 0.01207 | 0.01207 | 0.03592 | 0.03592 |
| 0.20 | 0.01802 | 0.01802 | 0.01103 | 0.01103 | 0.01038 | 0.01038 | 0.02689 | 0.02689 |
| 0.30 | 0.02427 | 0.02427 | 0.01151 | 0.01151 | 0.00888 | 0.00888 | 0.02039 | 0.02039 |
| 0.40 | 0.03302 | 0.03302 | 0.01217 | 0.01217 | 0.00768 | 0.00768 | 0.01602 | 0.01602 |
| 0.50 | 0.04427 | 0.04427 | 0.01302 | 0.01302 | 0.00674 | 0.00674 | 0.01302 | 0.01302 |

**Table 4.2.** Doubly-Clamped FG nanobeam under uniformly distributed load: non-dimensional midpoint deflection $\tilde{w}(1/2)$, vs. nonlocal parameter $\lambda_c$. Comparison between L/NStressGH and L/NStrainGH, assuming $\xi_1 = 0.0$, $\Delta T_{UTR} = \Delta T_{HC} = 0$ and varying $\lambda_l$ in the set (0.0, 0.5).

| $\lambda_c$ | L/NStrainG | | | | L/NStressG | | | |
|---|---|---|---|---|---|---|---|---|
| | $\lambda_l = 0.0^+$ | Ref. [112] | $\lambda_l = 0.5$ | Ref. [91] | $\lambda_l = 0.0^+$ | Ref. [112] | $\lambda_l = 0.5$ | Ref. [91] |
| $0.00^+$ | 0.00260 | 0.00260 | 0.00024 | 0.00024 | 0.00260 | 0.00260 | 0.01823 | 0.01823 |
| 0.10 | 0.00260 | 0.00260 | 0.00046 | 0.00046 | 0.00148 | 0.00148 | 0.01199 | 0.01199 |
| 0.20 | 0.00260 | 0.00260 | 0.00084 | 0.00084 | 0.00078 | 0.00078 | 0.00700 | 0.00700 |
| 0.30 | 0.00260 | 0.00260 | 0.00138 | 0.00138 | 0.00045 | 0.00045 | 0.00430 | 0.00430 |
| 0.40 | 0.00260 | 0.00260 | 0.00210 | 0.00210 | 0.00029 | 0.00029 | 0.00284 | 0.00284 |
| 0.50 | 0.00260 | 0.00260 | 0.00300 | 0.00300 | 0.00020 | 0.00020 | 0.00200 | 0.00200 |

As said before, starting from a reference value of temperature equal to $T_0 = 300\ [K]$ and an initial value of moisture concentration $H_0 = 0.0\ [wt.\%\mathrm{H_2O}]$, both a uniform temperature rise and a heat-conduction have been considered in the parametric thermo-elastic analysis. In particular, two different values of the uniform temperature rise, $\Delta\mathrm{T_{UTR}} = \{0,50,100\}[K]$ and three heat-conduction scenarios, $\Delta T_{HC}$, corresponding to following choices of the bottom and top temperatures: $\{T_m = 300\ [K], T_\mathrm{c} = 300\ [K]\}, \{T_m = 350\ [K], T_\mathrm{c} = 300\ [K]\}$ and $\{T_m = 400\ [K], T_\mathrm{c} = 300\ [K]\}$ have been taken into account while a moisture rise, $\Delta H$, is always assumed to be equal to $0.1\ [wt.\%\mathrm{H_2O}]$. The convergence of series in Eq. 4.8 has been ensured by setting $k = 10$. A uniform distributed load value $q_z = -10\ nN/nm$ was considered in the analysis.

Furthermore, the coupled effects of the mixture parameter $\xi_1$, the nonlocal parameter, $\lambda_c$, the gradient length parameter, $\lambda_l$, the material gradient index, $n$, as well as of the porosity volume fraction, $\zeta$, on the structural responses exhibited FG nanobeams under investigations in terms of absolute value of dimensionless deflection are shown in the following figures:

- *Simply-Supported porous FG nanobeam subjected to a uniformly distributed load*

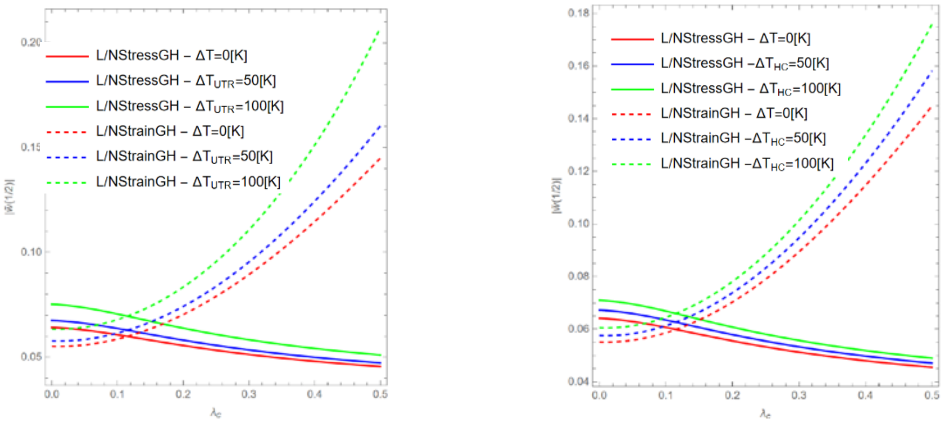

(a) (b)

**Figures 4.2.** Simply-Supported non-porous FG nanobeam under a uniformly distributed load: non-dimensional midpoint deflection $\tilde{w}(1/2)$ vs. nonlocal parameter $\lambda_c$, with $\lambda_l = 0.1$, $\xi_1 = 0.5$, $n = 1$ and $\zeta = 0$ evaluated by a uniform temperature rise (a) and a heat-conduction (b) via L/NStrainGH and L/NStressGH varying $\Delta\mathrm{T_{UTR}}$ in the set $\{0,50,100\}[K]$ and for three heat-conduction scenarios, $\Delta T_{HC}$, corresponding to following choices of the bottom and top temperatures: $\{T_m = 300\ [K], T_\mathrm{c} = 300\ [K]\}$, $\{T_m = 350\ [K], T_\mathrm{c} = 300\ [K]\}$ and $\{T_m = 400\ [K], T_\mathrm{c} = 300\ [K]\}$.

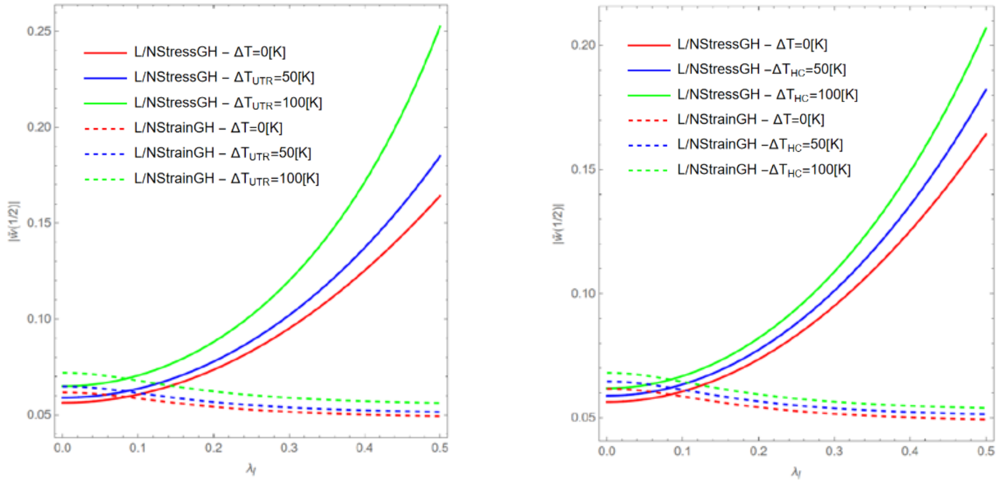

(a) (b)

**Figures 4.3.** Simply-Supported non-porous FG nanobeam under a uniformly distributed load: absolute values of non-dimensional midpoint deflection $\tilde{w}(1/2)$ vs. gradient length parameter $\lambda_l$, with $\lambda_c = 0.1$, $\xi_1 = 0.5$, $n = 1$ and $\zeta = 0$ evaluated by a uniform temperature rise (a) and a heat-conduction (b) via L/NStrainGH and L/NStressGH varying $\Delta\mathrm{T}_{\mathrm{UTR}}$ in the set $\{0,50,100\}[K]$ and for three heat-conduction scenarios, $\Delta T_{HC}$, corresponding to following choices of the bottom and top temperatures: $\{T_m = 300\ [K], T_c = 300\ [K]\}$, $\{T_m = 350\ [K], T_c = 300\ [K]\}$ and $\{T_m = 400\ [K], T_c = 300\ [K]\}$.

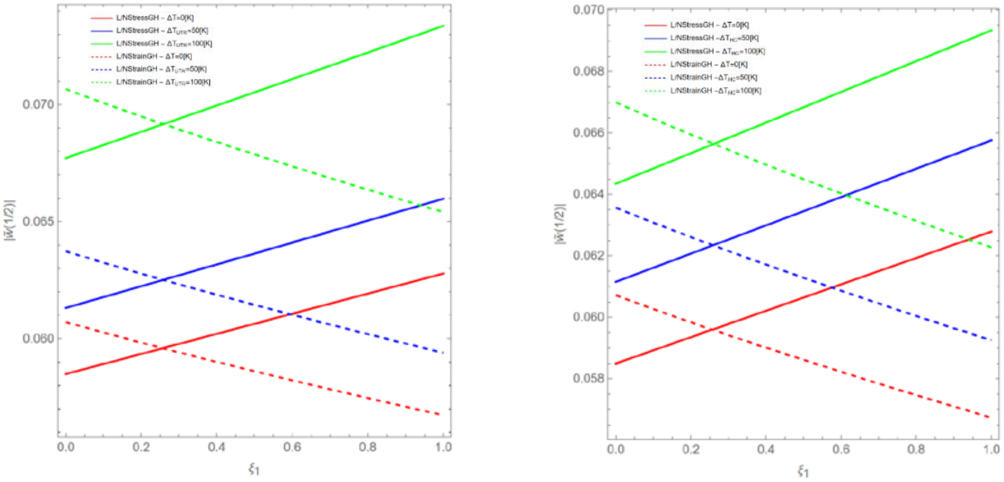

(a) (b)

**Figures 4.4.** Simply-Supported non-porous FG nanobeam under a uniformly distributed load: absolute values of non-dimensional midpoint deflection $\tilde{w}(1/2)$ vs. mixture parameter $\xi_1$, with $\lambda_c = 0.1$, $\lambda_l = 0.1$, $n = 1$ and $\zeta = 0$ evaluated by a uniform temperature rise (a) and a heat-conduction (b) via L/NStrainGH and L/NStressGH varying $\Delta\mathrm{T}_{\mathrm{UTR}}$ in the set $\{0,50,100\}[K]$ and for three heat-conduction scenarios, $\Delta T_{HC}$, corresponding to following choices of the bottom and top temperatures: $\{T_m = 300\ [K], T_c = 300\ [K]\}$, $\{T_m = 350\ [K], T_c = 300\ [K]\}$ and $\{T_m = 400\ [K], T_c = 300\ [K]\}$.

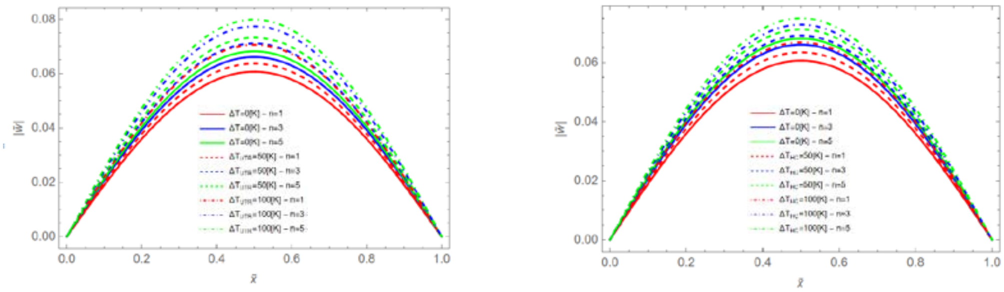

(a) (b)

**Figures 4.5.** Absolute value of dimensionless deflection, $\tilde{w}$, for a non-porous Simply-Supported FG nanobeam with $\xi_1 = 0.5$, $\lambda_c = 0.1$, $\lambda_l = 0.1$ and $\zeta = 0$ evaluated by a uniform temperature rise (a) and a heat-conduction (b) via L/NStressGH varying $n$ in the set $\{1,3,5\}$ $\Delta T_{UTR}$ in the set $\{0, 50, 100\}[K]$ and for three heat-conduction scenarios, $\Delta T_{HC}$, corresponding to following choices of the bottom and top temperatures: $\{T_m = 300\ [K], T_c = 300\ [K]\}$, $\{T_m = 350\ [K], T_c = 300\ [K]\}$ and $\{T_m = 400\ [K], T_c = 300\ [K]\}$.

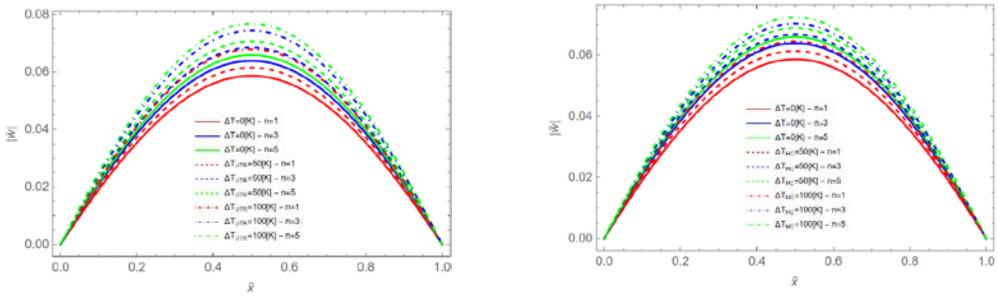

(a) (b)

**Figures 4.6.** Absolute value of dimensionless deflection, $\tilde{w}$, for a non-porous Simply-Supported FG nanobeam with $\xi_1 = 0.5$, $\lambda_c = 0.1$, $\lambda_l = 0.1$, $n = 1$ and $\zeta = 0$ evaluated by a uniform temperature rise (a) and a heat-conduction (b) via L/NStrainGH varying $\Delta T_{UTR}$ in the set $\{0, 50, 100\}[K]$ and for three heat-conduction scenarios, $\Delta T_{HC}$, corresponding to following choices of the bottom and top temperatures: $\{T_m = 300\ [K], T_c = 300\ [K]\}$, $\{T_m = 350\ [K], T_c = 300\ [K]\}$ and $\{T_m = 400\ [K], T_c = 300\ [K]\}$.

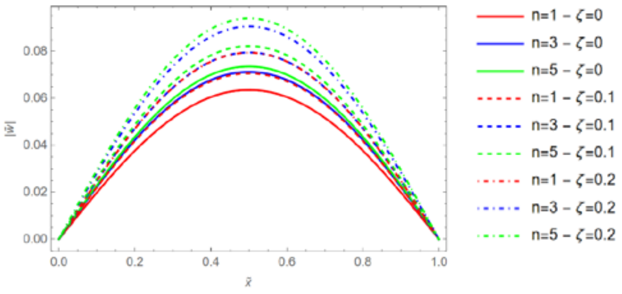

(a)

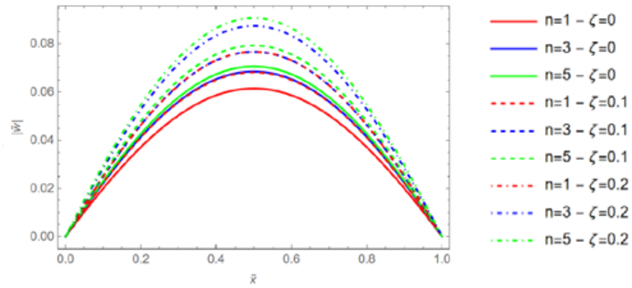

(b)

**Figures 4.7.** Absolute value of dimensionless deflection, $\tilde{w}$, for a non-porous and porous Simply-Supported FG nanobeam with $\xi_1 = 0.5$, $\lambda_c = 0.1$, $\lambda_l = 0.1$, evaluated by a uniform temperature rise (a) and a heat-conduction (b) via L/NStressGH assuming $\Delta \mathrm{T_{UTR}} = 50[K]$ and a heat-conduction scenarios, $\Delta T_{HC}$, corresponding to following choice of the bottom and top temperatures: $\{T_m = 350\ [K], T_c = 300\ [K]\}$ and varying $n$ and $\zeta$ in the set $\{1,3,5\}$ and $\{0,0.1,0.2\}$, respectively.

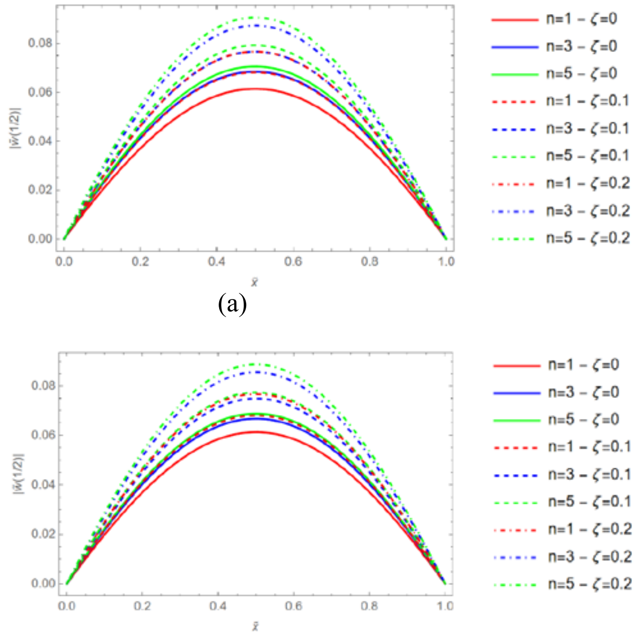

(a)

(b)

**Figures 4.8.** Absolute value of dimensionless deflection, $\tilde{w}$, for a non-porous and porous Simply-Supported FG nanobeam with $\xi_1 = 0.5$, $\lambda_c = 0.1$, $\lambda_l = 0.1$, evaluated by a uniform temperature rise (a) and a heat-conduction (b) via L/NStrainGH assuming $\Delta \mathrm{T_{UTR}} = 50[K]$ and a heat-conduction scenarios, $\Delta T_{HC}$, corresponding to following choice of the bottom and top temperatures: $\{T_m = 350\ [K], T_c = 300\ [K]\}$ and varying $n$ and $\zeta$ in the set $\{1,3,5\}$ and $\{0,0.1,0.2\}$, respectively.

- *Doubly-Clamped porous FG nanobeam subjected to a uniformly distributed load*

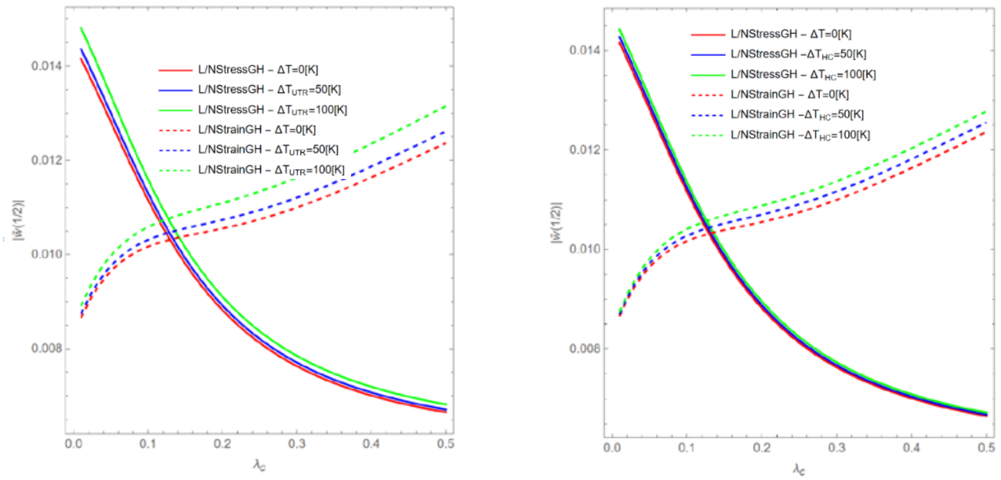

(a) (b)

**Figures 4.9.** Doubly-Clamped non-porous FG nanobeam under a uniformly distributed load: non-dimensional midpoint deflection $\widetilde{w}(1/2)$ vs. nonlocal parameter $\lambda_c$, with $\lambda_l = 0.1$, $\xi_1 = 0.5$, $n = 1$ and $\zeta = 0$ evaluated by a uniform temperature rise (a) and a heat-conduction (b) via L/NStrainGH and L/NStressGH varying $\Delta T_{\text{UTR}}$ in the set $\{0,50,100\}[K]$ and for three heat-conduction scenarios, $\Delta T_{HC}$, corresponding to following choices of the bottom and top temperatures: $\{T_m = 300\ [K], T_c = 300\ [K]\}$, $\{T_m = 350\ [K], T_c = 300\ [K]\}$ and $\{T_m = 400\ [K], T_c = 300\ [K]\}$.

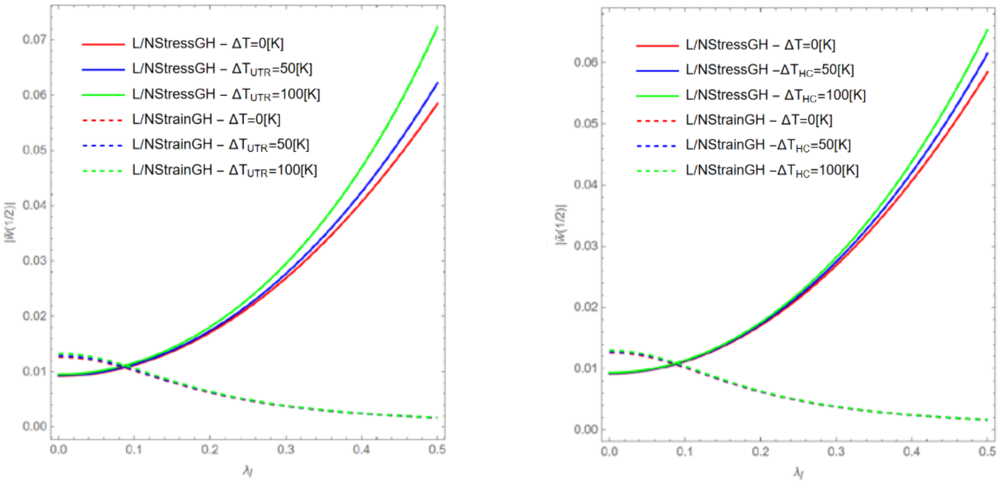

(a) (b)

**Figures 4.10.** Doubly-Clamped non-porous FG nanobeam under a uniformly distributed load: absolute values of non-dimensional midpoint deflection $\widetilde{w}(1/2)$ vs. gradient length parameter $\lambda_l$, with $\lambda_c = 0.1$, $\xi_1 = 0.5$, $n = 1$ and $\zeta = 0$ evaluated by a uniform temperature rise (a) and a heat-conduction (b) via L/NStrainGH and L/NStressGH varying $\Delta T_{\text{UTR}}$ in the set $\{0,50,100\}[K]$ and for three heat-conduction scenarios, $\Delta T_{HC}$, corresponding to following choices of the bottom and top temperatures: $\{T_m = 300\ [K], T_c = 300\ [K]\}$, $\{T_m = 350\ [K], T_c = 300\ [K]\}$ and $\{T_m = 400\ [K], T_c = 300\ [K]\}$.

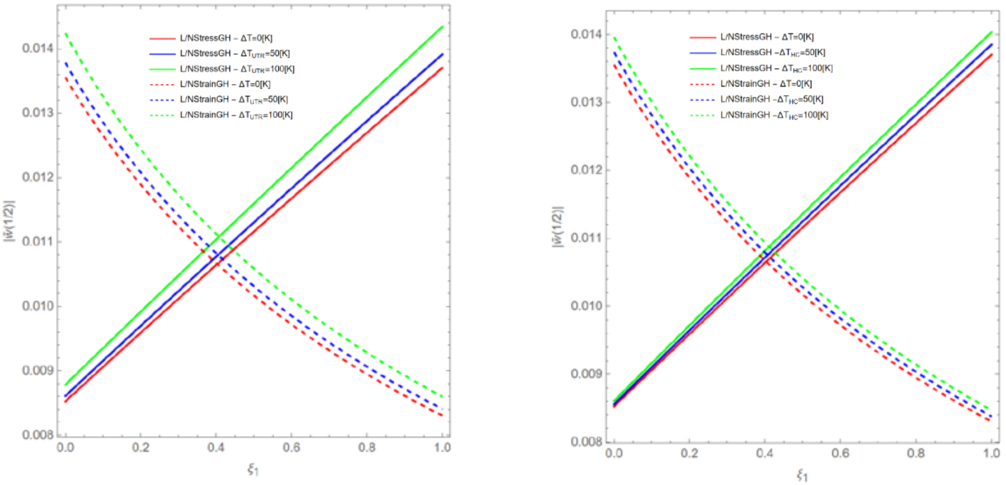

(a) (b)

**Figures 4.11.** Doubly-Clamped non-porous FG nanobeam under a uniformly distributed load: absolute values of non-dimensional midpoint deflection $\tilde{w}(1/2)$ vs. mixture parameter $\xi_1$, with $\lambda_c = 0.1$, $\lambda_l = 0.1$, $n = 1$ and $\zeta = 0$ evaluated by a uniform temperature rise (a) and a heat-conduction (b) via L/NStrainGH and L/NStressGH varying $\Delta \mathrm{T_{UTR}}$ in the set $\{0,50,100\}[K]$ and for three heat-conduction scenarios, $\Delta T_{HC}$, corresponding to following choices of the bottom and top temperatures: $\{T_m = 300\ [K], T_c = 300\ [K]\}, \{T_m = 350\ [K], T_c = 300\ [K]\}$ and $\{T_m = 400\ [K], T_c = 300\ [K]\}$.

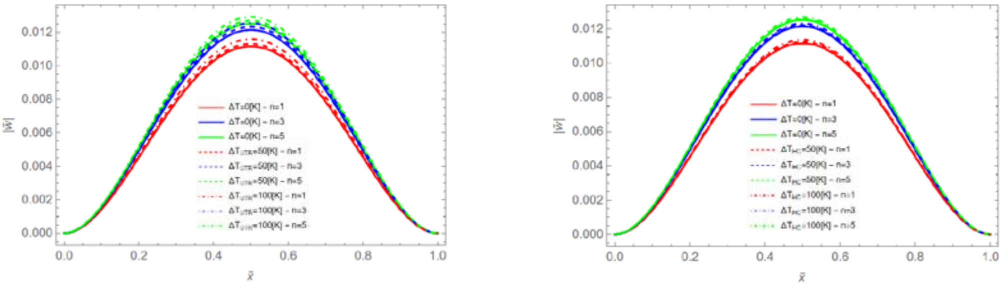

(a) (b)

**Figures 4.12.** Absolute value of dimensionless deflection, $\tilde{w}$, for a non-porous Doubly-Clamped FG nanobeam with $\xi_1 = 0.5$, $\lambda_c = 0.1$, $\lambda_l = 0.1$ and $\zeta = 0$ evaluated by a uniform temperature rise (a) and a heat-conduction (b) via L/NStressGH varying $n$ in the set $\{1,3,5\}$ $\Delta \mathrm{T_{UTR}}$ in the set $\{0, 50, 100\}[K]$ and for three heat-conduction scenarios, $\Delta T_{HC}$, corresponding to following choices of the bottom and top temperatures: $\{T_m = 300\ [K], T_c = 300\ [K]\}, \{T_m = 350\ [K], T_c = 300\ [K]\}$ and $\{T_m = 400\ [K], T_c = 300\ [K]\}$.

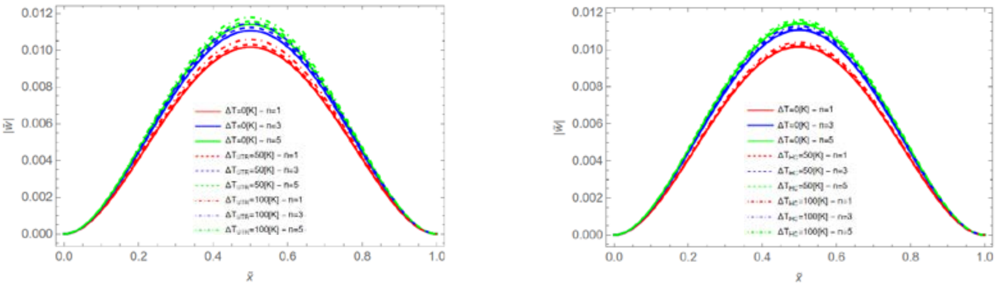

(a) (b)

**Figures 4.13.** Absolute value of dimensionless deflection, $\widetilde{w}$, for a non-porous Doubly-Clamped FG nanobeam with $\xi_1 = 0.5$, $\lambda_c = 0.1$, $\lambda_l = 0.1$, $n = 1$ and $\zeta = 0$ evaluated by a uniform temperature rise (a) and a heat-conduction (b) via L/NStrainGH varying $\Delta\mathrm{T}_{\mathrm{UTR}}$ in the set $\{0, 50, 100\}[K]$ and for three heat-conduction scenarios, $\Delta T_{HC}$, corresponding to following choices of the bottom and top temperatures: $\{T_m = 300\ [K], T_c = 300\ [K]\}$, $\{T_m = 350\ [K], T_c = 300\ [K]\}$ and $\{T_m = 400\ [K], T_c = 300\ [K]\}$.

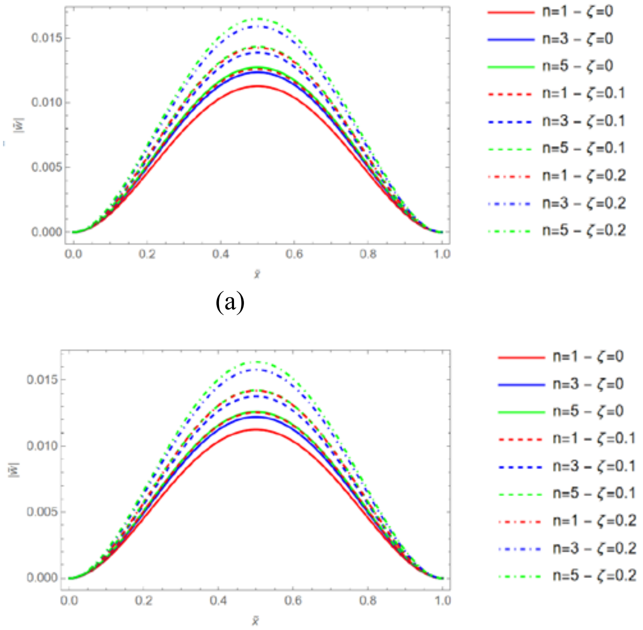

(a)

(b)

**Figures 4.14.** Absolute value of dimensionless deflection, $\widetilde{w}$, for a non-porous and porous Doubly-Clamped FG nanobeam with $\xi_1 = 0.5$, $\lambda_c = 0.1$, $\lambda_l = 0.1$, evaluated by a uniform temperature rise (a) and a heat-conduction (b) via L/NStressGH assuming $\Delta\mathrm{T}_{\mathrm{UTR}} = 50[K]$ and a heat-conduction scenarios, $\Delta T_{HC}$, corresponding to following choice of the bottom and top temperatures: $\{T_m = 350\ [K], T_c = 300\ [K]\}$ and varying $n$ and ζ in the set {1,3,5} and {0,0.1,0.2}, respectively.

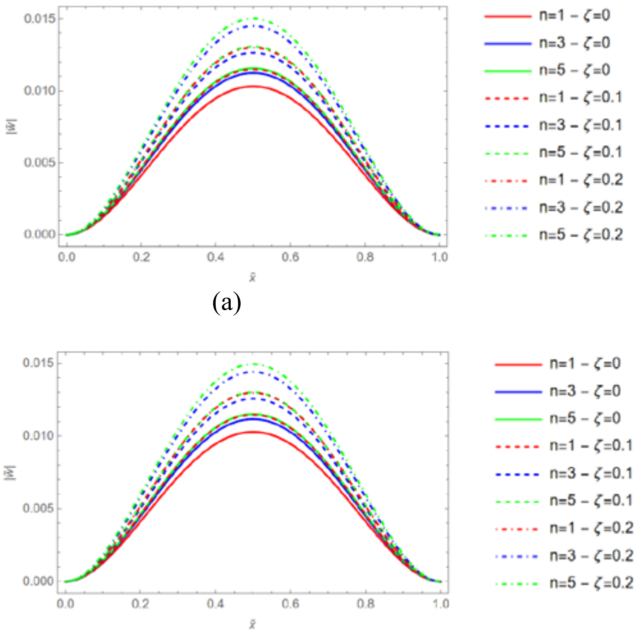

(a)

(b)

**Figures 4.15.** Absolute value of dimensionless deflection, $\tilde{w}$, for a non-porous and porous Doubly-Clamped FG nanobeam with $\xi_1 = 0.5$, $\lambda_c = 0.1$, $\lambda_l = 0.1$, evaluated by a uniform temperature rise (a) and a heat-conduction (b) via L/NStrainGH assuming $\Delta T_{\mathrm{UTR}} = 50[K]$ and a heat-conduction scenarios, $\Delta T_{HC}$, corresponding to following choice of the bottom and top temperatures: $\{T_m = 350\ [K], T_{\mathrm{c}} = 300\ [K]\}$ and varying $n$ and ζ in the set {1,3,5} and {0,0.1,0.2}, respectively.

From the curves plotted in Figures 4.2-4.4 and Figures 4.9-4.11, it is interesting to underline that stress-driven and strain-driven hygrothermal local/nonlocal gradient theories are able to simulate both a softening and stiffening size-dependent structural response of inflected nanobeams with internal uniform porosity under hygro-thermo-mechanical loadings. A softening response is exhibited by L/NStrainGH formulation when increasing the nonlocal parameter, $\lambda_c$, (see Figures 4.2 and 4.9) and a stiffening behavior is observed when increasing the gradient length parameter, $\lambda_l$ (see Figures 4.3 and 4.10) and the mixture parameter $\xi_1$ (see Figures 4.4 and 4.11). On the contrary, a stiffening response is exhibited by L/NStressGH theory when increasing the nonlocal parameter, $\lambda_c$ (see Figures 4.2 and 4.9) and a softening behavior is observed when increasing the gradient length parameter, $\lambda_l$ (see Figures 4.3 and 4.10) and the mixture parameter $\xi_1$ (see Figures 4.4 and 4.11). Furthermore, from Figures 4.5, 4.6 and Figures 4.12, 4.13, it can be noted that an increase in the material gradient index always leads to an increase in the dimensionless deflection. In addition, the graphs of Figures 4.2-4.6 together with in Figures 4.9-4.13 show that an increase in temperature always leads to a softening behavior due to an abatement of the mechanical properties of the

FG material. Moreover, as was to be expected from figures 4.7,4.8 together with Figures 4.14,4.15, an increase in the porosity volume fraction always provides, for both elasticity models, an increase in dimensionless deflections. Finally, in the case studies examined, the curves relating to the uniform temperature rise always show higher values than those obtained by heat-conduction.

### 4.3.4. Summary and conclusions

It was analyzed the bending response of a non-porous and porous Bernoulli-Euler FG nanobeam subjected to hygro-thermo-mechanical loadings using both hygrothermal local/nonlocal stress-driven and strain-driven gradient formulations. The governing equations were derived by using the virtual work principle. A Wolfram language code in Mathematica was then written to carry out a parametric investigation for different boundary conditions including Simply-Supported and Doubly-Clamped configurations.

A parametric investigation on the structural bending behavior of FG nanobeams varying the nonlocal parameter, the gradient length parameter, the hygro-thermo-mechanical loadings and the mixture parameter of both local/nonlocal hygrothermal strain- (L/NStrainGH) and stress- gradient (L/NStressGH) formulations was presented.

From the above investigation, we can draw some conclusions as follows:

- increasing the porosity volume fraction, the gradient index and the thermal rise reduces the bending and axial stiffnesses of the FG nanobeam with it generally leading to an increase in bending flexibility;
- a softening response has been exhibited by L/NStrainGH formulation when increasing the nonlocal parameter and a stiffening behavior is observed when increasing the gradient length parameter and the mixture parameter;
- a stiffening behavior is exhibited by L/NStressGH theory when increasing the nonlocal parameter and a softening behavior is observed when increasing the gradient length parameter and the mixture parameter;
- an increase in material gradient index and porosity volume fraction always leads to an increase in the dimensionless deflection;

- upon increasing the temperature always leads to an increase in the bending deflection of the nanobeams related to a decrease in the bending stiffness due to an abatement of the thermos-elastic properties of the non-porous and porous FG material;
- for the cases studies examines, a uniform temperature rise always shows higher values than those obtained by heat-conduction.

The results obtained in the study confirm that hygrothermal stress-driven and strain-driven local/nonlocal gradient formulations are able to simulate both a softening and stiffening size-dependent structural response of inflected nanobeams with internal uniform porosity under severe thermal loadings.

In conclusion, the proposed approach represents a cost-effective method to capture the bending behavior of inflected porous and non-porous functionally graded Bernoulli–Euler nanobeams subjected to severe environmental conditions.

## 4.4. Linear and nonlinear free vibrations analysis of porous FG nanobeams in a hygrothermal environment based on L/NStressGH

In this section, the functionally graded porous nanobeam illustrated in Figure 4.1 is analyzed to study the dynamic behavior in a hygrothermal environment based on hygrothermal local/nonlocal stress gradient model of elasticity introduced in previously paragraph.

Based on Bernoulli-Euler theory, the Cartesian components of the displacement field of the FG nanobeam in the elastic coordinate reference system $(C, x, \mathrm{y}, z)$ can be expressed by:

$$u_x(x,z,t) = u(x,t) - z\frac{\partial w}{\partial x}(x,t) \tag{4.54}$$

$$u_z(x,z,t) = w(x,t) \tag{4.55}$$

being $u_x(x,z,t), u_z(x,z,t)$ the displacement components along $x$ and $z$ directions, $u = u(x,t)$ and $w = w(x,t)$ the axial and transverse displacements of the elastic centre $C$, at time $t$, respectively.

According to conventional Von-Kármán geometrical nonlinearity, which includes small strains but moderately large rotation, the only nonzero kinematically compatible strain is given by:

$$\varepsilon_{xx} = \varepsilon_{xx}(x,t) = \frac{\partial u}{\partial x} + \frac{1}{2}\left(\frac{\partial w}{\partial x}\right)^2 - z\frac{\partial^2 w}{\partial x^2} \tag{4.56}$$

The nonlinear equations of motion, are derived by using the Hamilton's principle:

$$\int_{t_1}^{t_2} \delta(U - K)\, dt = 0 \tag{4.57}$$

The expression of the virtual strain energy $\delta U$ is:

$$\delta U = \int_0^L \int_\Sigma \sigma_{xx}\delta\varepsilon_{xx}\, d\Sigma\, dx = \int_0^L \left(N\frac{\partial \delta u}{\partial x} + N\frac{\partial w}{\partial x}\frac{\partial \delta w}{\partial x} - M\frac{\partial^2 \delta w}{\partial x^2}\right) dx \tag{4.58}$$

where $\sigma_{xx} = \sigma_{xx}(z,T) = E(z,T)\varepsilon_{xx} = E\varepsilon_{xx}$, is the temperature-dependent axial stress, while $M$ and $N$ are the moment and axial stress resultant, respectively, defined as follows:

$$M = M(x,t) = -I_E\frac{\partial^2 w}{\partial x^2} \tag{4.59}$$

$$N = N(x,t) = \frac{A_E}{2}\left(\frac{\partial w}{\partial x}\right)^2 \tag{4.60}$$

in which $I_E$ and $A_E$ indicate the bending stiffness and axial stiffness defined in Eq. 2.18 and Eq. 2.20, respectively; $M^T$ and $M^H$ are the hygrothermal moments previously defined.

In addition, the expression of virtual kinetic energy $\delta K$ is defined as follows:

$$\begin{aligned}\delta K &= \int_0^L \int_\Sigma \rho(z)\left[\frac{\partial u_x}{\partial t}\frac{\partial \delta u_x}{\partial t} + \frac{\partial u_z}{\partial t}\frac{\partial \delta u_z}{\partial t}\right] d\Sigma\, dx = \\ &= \int_0^L \left(A_\rho\frac{\partial u}{\partial t}\frac{\partial \delta u}{\partial t} + I_\rho\frac{\partial^2 w}{\partial x\partial t}\frac{\partial^2 \delta w}{\partial x\partial t} + A_\rho\frac{\partial w}{\partial t}\frac{\partial \delta w}{\partial t}\right) dx\end{aligned} \tag{4.61}$$

where $A_\rho, S_\rho$ and $I_\rho$ are the mass density, couple rotary normal and rotary inertia terms defined in Eqs. 2.21-2.23, respectively.

By substituting Eq. 4.58 and Eq. 4.61 into Eq. 4.57, by applying the fundamental lemma of calculus of variations we obtain the following equations of motion:

$$\frac{\partial N}{\partial x} = A_\rho \frac{\partial^2 u}{\partial t^2} - S_\rho \frac{\partial^3 w}{\partial x \partial t^2} \tag{4.62}$$

$$\frac{\partial^2 M}{\partial x^2} + \frac{\partial}{\partial x}\left(N \frac{\partial w}{\partial x}\right) = A_\rho \frac{\partial^2 w}{\partial t^2} + S_\rho \frac{\partial^3 u}{\partial x \partial t^2} - I_\rho \frac{\partial^4 w}{\partial x^2 \partial t^2} \tag{4.63}$$

with the natural or standard boundary conditions (SBCs) (at $x = 0, L$) expressed as:

$$u = u^*|_{0,L} \qquad \text{or} \qquad N = N^*|_{0,L} \tag{4.64}$$

$$\frac{\partial w}{\partial x} = \frac{\partial w^*}{\partial x}|_{0,L} \qquad \text{or} \qquad M = M^*|_{0,L} \tag{4.65}$$

$$w = w^*|_{0,L} \qquad \text{or} \qquad \begin{aligned} &\frac{\partial M}{\partial x} + (N - N^T - N^H)\frac{\partial w}{\partial x} + I_\rho \frac{\partial^3 w}{\partial x \partial t^2} \\ &= V^*|_{0,L} \end{aligned} \tag{4.66}$$

being $M^*$ and $V^*$ assigned moment and vertical force acting at the nanobeam ends, respectively, and $u^*, w^*$ an assigned horizontal and vertical displacements at the nanobeam ends, respectively.

As shown in §3.1.1., by using the local/nonlocal stress gradient model of elasticity, the elastic axial strain, $\varepsilon_{xx}^{el}$, can be expressed by the following differential equation:

$$\varepsilon_{xx}^{el} - L_c^2 \frac{\partial^2 \varepsilon_{xx}^{el}}{\partial x^2} = \frac{\sigma_{xx}}{E} - \frac{L_c^2}{E}\left(\xi_1 + \frac{L_l^2}{L_c^2}\right)\frac{\partial^2 \sigma_{xx}}{\partial x^2} \tag{4.67}$$

with the following two pairs of constitutive boundary conditions (CBCs) are satisfied at the nanobeam ends:

$$\frac{\partial \varepsilon_{xx}^{el}(0,t)}{\partial x} - \frac{1}{L_c}\varepsilon_{xx}^{el}(0,t) = -\frac{1}{E}\frac{\xi_1}{L_c}\sigma_{xx}(0,t) + \frac{1}{E}\left(\xi_1 + \frac{L_l^2}{L_c^2}\right)\frac{\partial \sigma_{xx}(0,t)}{\partial x} \tag{4.68}$$

$$\frac{\partial \varepsilon_{xx}^{el}(L,t)}{\partial x} + \frac{1}{L_c}\varepsilon_{xx}^{el}(L,t) = \frac{1}{E}\frac{\xi_1}{L_c}\sigma_{xx}(L,t) + \frac{1}{E}\left(\xi_1 + \frac{L_l^2}{L_c^2}\right)\frac{\partial \sigma_{xx}(L,t)}{\partial x} \tag{4.69}$$

In hygrothermal environment, the elastic axial strain, $\varepsilon_{xx}^{el}$, is expressed as the difference between the total strain, $\varepsilon_{xx}$, and the non-elastic axial strain, $\varepsilon_{xx}^* = \alpha\,\Delta T + \beta \Delta H$:

$$\varepsilon_{xx}^{el} = \varepsilon_{xx} - \varepsilon_{xx}^* \tag{4.70}$$

By manipulating Eq. 4.56 with Eq. 4.70 and substituting into Eqs. 4.67-4.69 then multiplying by (1, *z*), the integration over the nanobeam cross section provides the following L/NStressGH equations in terms of displacements:

$$\begin{aligned} A_E\left(\frac{\partial u}{\partial x}+\frac{1}{2}\left(\frac{\partial w}{\partial x}\right)^2\right)-A_E L_c^2\frac{\partial^2}{\partial x^2}\left(\frac{\partial u}{\partial x}+\frac{1}{2}\left(\frac{\partial w}{\partial x}\right)^2\right)-\left(N^T+N^H\right) \\ = N^{L/NStressGH}-L_c^2\left(\xi_1+\frac{{L_l}^2}{L_c^2}\right)\frac{\partial^2 N^{L/NStressGH}}{\partial x^2} \end{aligned} \tag{4.71}$$

$$\begin{aligned} -I_E\frac{\partial^2 w}{\partial x^2}+I_E L_c^2\,\frac{\partial^4 w}{\partial x^4}-\left(M^T+M^H\right) \\ = M^{L/NStressGH}-L_c^2\left(\xi_1+\frac{{L_l}^2}{L_c^2}\right)\frac{\partial^2 M^{L/NStressGH}}{\partial x^2} \end{aligned} \tag{4.72}$$

with the corresponding constitutive boundary conditions:

$$\begin{aligned} \frac{\partial}{\partial x}\left(\frac{\partial u(0,t)}{\partial x}+\frac{1}{2}\left(\frac{\partial w(0,t)}{\partial x}\right)^2\right)-\frac{A_E}{L_c}\left(\frac{\partial u(0,t)}{\partial x}+\frac{1}{2}\left(\frac{\partial w(0,t)}{\partial x}\right)^2\right) \\ +\frac{N^T+N^H}{L_c} \\ =-\frac{\xi_1}{L_c}N^{L/NStressGH}(0,t)+\left(\xi_1+\frac{L_l^2}{L_c^2}\right)\frac{\partial N^{NStressGH}(0,t)}{\partial x} \end{aligned} \tag{4.73}$$

$$\begin{aligned} A_E\frac{\partial}{\partial x}\left(\frac{\partial u(L,t)}{\partial x}+\frac{1}{2}\left(\frac{\partial w(L,t)}{\partial x}\right)^2\right)+\frac{A_E}{L_c}\left(\frac{\partial u(L,t)}{\partial x}+\frac{1}{2}\left(\frac{\partial w(L,t)}{\partial x}\right)^2\right) \\ -\frac{N^T+N^H}{L_c} \\ =\frac{\xi_1}{L_c}N^{L/NStressGH}(L,t)+\left(\xi_1+\frac{L_l^2}{L_c^2}\right)\frac{\partial N^{L/NStressGH}(L,t)}{\partial x} \end{aligned} \tag{4.74}$$

$$\begin{aligned} -I_E\frac{\partial^3 w(0,t)}{\partial x^3}+\frac{I_E}{L_c}\frac{\partial^2 w(0,t)}{\partial x^2}+\frac{M^T+M^H}{L_c} \\ =-\frac{\xi_1}{L_c}M^{L/NStressGH}(0,t) \\ +\left(\xi_1+\frac{L_l^2}{L_c^2}\right)\frac{\partial M^{L/NStressGH}(0,t)}{\partial x} \end{aligned} \tag{4.75}$$

$$
\begin{aligned}
&-I_E\frac{\partial^3 w(L,t)}{\partial x^3}-\frac{I_E}{L_c}\frac{\partial^2 w(L,t)}{\partial x^2}-\frac{M^T+M^H}{L_c}\\
&\qquad=\frac{\xi_1}{L_c}M^{L/NStressGH}(L,t)+\left(\xi_1+\frac{L_l^2}{L_c^2}\right)\frac{\partial M^{L/NStressGH}(L,t)}{\partial x}
\end{aligned}
\tag{4.76}
$$

in which $N^{L/NStressGH}=N^{L/NStressGH}(x,t)$ and $M^{L/NStressGH}=M^{L/NStressGH}(x,t)$ denote the hygrothermal stress gradient axial force and moment resultants, respectively.

Substituting Eq. 4.62 and Eq. 4.63 into Eq. 4.71 and 4.72, respectively, the nonlocal stress gradient hygrothermal axial force and moment resultants can be expressed as follows:

$$
\begin{aligned}
N^{L/NStressGH}&=A_E\left(\frac{\partial u}{\partial x}+\frac{1}{2}\left(\frac{\partial w}{\partial x}\right)^2\right)-A_E L_c^2\frac{\partial^2}{\partial x^2}\left(\frac{\partial u}{\partial x}+\frac{1}{2}\left(\frac{\partial w}{\partial x}\right)^2\right)\\
&\quad+L_c^2\left(\xi_1+\frac{{L_l}^2}{L_c^2}\right)\left(A_\rho\frac{\partial^3 u}{\partial x\partial t^2}-S_\rho\frac{\partial^4 w}{\partial x^2\partial t^2}\right)-\left(N^T+N^H\right)
\end{aligned}
\tag{4.77}
$$

$$
\begin{aligned}
M^{L/NStressGH}&=-I_E\frac{\partial^2 w}{\partial x^2}+I_E L_c^2\frac{\partial^4 w}{\partial x^4}\\
&\quad+L_c^2\left(\xi_1+\frac{{L_l}^2}{L_c^2}\right)\left(A_\rho\frac{\partial^2 w}{\partial t^2}-I_\rho\frac{\partial^4 w}{\partial x^2\partial t^2}-\frac{\partial}{\partial x}\left(N\frac{\partial w}{\partial x}\right)\right)\\
&\quad-\left(M^T+M^H\right)
\end{aligned}
\tag{4.78}
$$

**Remark 4.2.** *It is supposed a nanobeam with immovable ends* $(u|_{x=0}=u|_{x=L}=0\ and\ w|_{x=0}=w|_{x=L}=0)$*; in order to examine the flexural response of system, it is assumed that the axial and the axial-rotational inertia terms have insignificant influence on the flexural response of system.*

Therefore, Eq. 4.77 can be rewritten as:

$$
\begin{aligned}
N^{L/NStressGH}&=\frac{A_E}{2}\left(\frac{\partial w}{\partial x}\right)^2-\frac{A_E}{2}L_c^2\frac{\partial^2}{\partial x^2}\left(\frac{\partial w}{\partial x}\right)^2-\left(N^T+N^H\right)\\
&=\widehat{N}-\left(N^T+N^H\right)
\end{aligned}
\tag{4.79}
$$

in which

$$\widehat{N}=\frac{A_E}{2}\left(\frac{\partial w}{\partial x}\right)^2-\frac{A_E}{2}L_c^2\frac{\partial^2}{\partial x^2}\left(\frac{\partial w}{\partial x}\right)^2=const. \tag{4.80}$$

By integrating both sides of Eq. 4.80 over the domain [*0*, *L*] yields to the following expression:

$$\widehat{N}=\frac{1}{L}\int_0^L\left(\frac{A_E}{2}\left(\frac{\partial w}{\partial x}\right)^2-\frac{A_E}{2}L_c^2\frac{\partial^2}{\partial x^2}\left(\frac{\partial w}{\partial x}\right)^2\right)dx \tag{4.81}$$

which coincides with the "mid-plane stretching effect" [29].

In addition, by substituting Eq. 4.78 into Eq. 4.63 and taking into account the assumption of Eq. 4.81 gives the following L/NStressGH ordinary differential governing equations in terms of transverse displacements:

$$\begin{aligned}&-I_E\frac{\partial^4 w}{\partial x^4}+I_E L_c^2\frac{\partial^6 w}{\partial x^6}\\&\qquad+L_c^2\left(\xi_1+\frac{{L_l}^2}{L_c^2}\right)\frac{\partial^2}{\partial x^2}\left(A_\rho\frac{\partial^2 w}{\partial t^2}-I_\rho\frac{\partial^4 w}{\partial x^2\partial t^2}-\frac{\partial}{\partial x}\left(\widehat{N}\frac{\partial w}{\partial x}\right)\right.\\&\qquad\left.+\left(N^T+N^H\right)\frac{\partial^2 w}{\partial x^2}\right)+\frac{\partial}{\partial x}\left(\widehat{N}\frac{\partial w}{\partial x}\right)-\left(N^T+N^H\right)\frac{\partial^2 w}{\partial x^2}\\&\qquad=A_\rho\frac{\partial^2 w}{\partial t^2}-I_\rho\frac{\partial^4 w}{\partial x^2\partial t^2}\end{aligned} \tag{4.82}$$

which describes the nonlinear transverse free vibrations of porous FG nanobeams in a hygrothermal environment.

By introducing the following dimensionless quantities:

$$\tilde{A}_\rho=\frac{A_\rho L^4}{I_E} \qquad\qquad \tilde{g}^2=\frac{1}{L^2}\frac{I_\rho}{A_\rho} \tag{4.83}$$

in conjunction with those reported in Eq. 4.41, the dimensionless governing equations of the nonlinear transverse free vibrations associated with L/NStressGH constitutive formulation can be obtained as follows:

$$\lambda_c^2\frac{\partial^6\tilde{w}}{\partial\tilde{x}^6}-\frac{\partial^4\tilde{w}}{\partial\tilde{x}^4}+\tilde{A}_\rho\lambda_c^2\left(\xi_1+\frac{\lambda_l^2}{\lambda_c^2}\right)\left(\frac{\partial^4\tilde{w}}{\partial\tilde{x}^2\partial t^2}-\tilde{g}^2\frac{\partial^6\tilde{w}}{\partial\tilde{x}^4\partial t^2}\right)$$
$$+\lambda_c^2\left(\xi_1+\frac{\lambda_l^2}{\lambda_c^2}\right)\left(\left(\tilde{N}^T+\tilde{N}^H\right)\frac{\partial^4\tilde{w}}{\partial\tilde{x}^4}-\tilde{r}^2\frac{\partial^3}{\partial\tilde{x}^3}\left(\tilde{N}\frac{\partial\tilde{w}}{\partial\tilde{x}}\right)\right)$$
$$+\tilde{r}^2\frac{\partial}{\partial\tilde{x}}\left(\tilde{N}\frac{\partial\tilde{w}}{\partial\tilde{x}}\right)-\left(\tilde{N}^T+\tilde{N}^H\right)\frac{\partial^2\tilde{w}}{\partial\tilde{x}^2}$$
$$=\tilde{A}_\rho\left(\frac{\partial^2\tilde{w}}{\partial t^2}-\tilde{g}^2\frac{\partial^4\tilde{w}}{\partial\tilde{x}^2\partial t^2}\right) \tag{4.84}$$

where:

$$\tilde{N}=\int_0^1\left(\frac{1}{2}\left(\frac{\partial\tilde{w}}{\partial\tilde{x}}\right)^2-\frac{1}{2}\lambda_c^2\frac{\partial^2}{\partial\tilde{x}^2}\left(\frac{\partial\tilde{w}}{\partial\tilde{x}}\right)^2\right)d\tilde{x} \tag{4.85}$$

$$\tilde{r}^2=\frac{L^2A_E}{I_E} \tag{4.86}$$

with the following dimensionless standard boundary conditions at the nanobeam ends:

$$\frac{\partial\tilde{w}}{\partial\tilde{x}}=\frac{\partial\tilde{w}^*}{\partial\tilde{x}}\Big|_{0,1} \quad \text{or} \quad \tilde{M}^{L/NStressGH}=\tilde{M}^*\big|_{0,1} \tag{4.87}$$

$$\tilde{w}=\tilde{w}^*\big|_{0,1} \quad \text{or} \quad \tilde{V}^{L/NStressGH}=\tilde{V}^*\big|_{0,1} \tag{4.88}$$

together with the dimensionless constitutive boundary conditions at $\tilde{x}=0,1$:

$$-\frac{\partial^3\tilde{w}(0,t)}{\partial\tilde{x}^3}+\frac{1}{\lambda_c}\frac{\partial^2\tilde{w}(0,t)}{\partial\tilde{x}^2}+\frac{\tilde{M}^T+\tilde{M}^H}{\lambda_c}$$
$$=-\frac{\xi_1}{\lambda_c}\tilde{M}^{L/NStressGH}(0,t)$$
$$+\left(\xi_1+\frac{\lambda_l^2}{\lambda_c^2}\right)\frac{\partial\tilde{M}^{L/NStressGH}(0,t)}{\partial\tilde{x}} \tag{4.89}$$

$$-\frac{\partial^3\tilde{w}(1,t)}{\partial\tilde{x}^3}-\frac{1}{\lambda_c}\frac{\partial^2\tilde{w}(1,t)}{\partial\tilde{x}^2}-\frac{\tilde{M}^T+\tilde{M}^H}{\lambda_c}$$
$$=\frac{\xi_1}{\lambda_c}\tilde{M}^{L/NStressGH}(1,t)$$
$$+\left(\xi_1+\frac{\lambda_l^2}{\lambda_c^2}\right)\frac{\partial\tilde{M}^{L/NStressGH}(1,t)}{\partial\tilde{x}} \tag{4.90}$$

where $\widetilde{M}^{L/NStressGH} = \widetilde{M}^{L/NStressGH}(\tilde{x},t)$ and $\tilde{V}^{L/NStressGH} = \tilde{V}^{L/NStressGH}(\tilde{x},t)$ denote the hygrothermal resultant moment and shear force, respectively.

In addition, the hygrothermal bending moment and shear force in dimensionless form can be rewritten as:

$$\begin{aligned}\widetilde{M}^{L/NStressGH} &= -\frac{\partial^2\widetilde{w}}{\partial\tilde{x}^2} + \lambda_c^2\frac{\partial^4\widetilde{w}}{\partial\tilde{x}^4} \\ &\quad + \tilde{A}_\rho(\lambda_c^2\,\xi_1 + \lambda_l^2)\left(\frac{\partial^2\widetilde{w}}{\partial t^2} - \tilde{g}^2\frac{\partial^4\widetilde{w}}{\partial\tilde{x}^2\partial t^2}\right) \\ &\quad + (\lambda_c^2\,\xi_1 + \lambda_l^2)\left(\left(\widetilde{N}^T + \widetilde{N}^H\right)\frac{\partial^2\widetilde{w}}{\partial\tilde{x}^2}\right) - \left(\widetilde{M}^T + \widetilde{M}^H\right)\end{aligned} \tag{4.91}$$

$$\begin{aligned}\tilde{V}^{L/NStressGH} &= -\frac{\partial^3\widetilde{w}}{\partial\tilde{x}^3} + \lambda_c^2\,\frac{\partial^5\widetilde{w}}{\partial\tilde{x}^5} \\ &\quad + \tilde{A}_\rho(\lambda_c^2\xi_1 + \lambda_l^2)\left(\frac{\partial^3\widetilde{w}}{\partial\tilde{x}\partial t^2} - \tilde{g}^2\frac{\partial^5\widetilde{w}}{\partial\tilde{x}^3\partial t^2}\right. \\ &\quad \left. + \frac{\tilde{g}^2}{(\lambda_c^2\xi_1 + \lambda_l^2)}\frac{\partial^3\widetilde{w}}{\partial\tilde{x}\partial t^2}\right) \\ &\quad + (\lambda_c^2\xi_1 + \lambda_l^2)\left(\left(\widetilde{N}^T + \widetilde{N}^H\right)\frac{\partial^3\widetilde{w}}{\partial\tilde{x}^3} - \tilde{r}^2\frac{\partial^2}{\partial\tilde{x}^2}\left(\widetilde{N}\frac{\partial\widetilde{w}}{\partial\tilde{x}}\right)\right) \\ &\quad + \left(\tilde{r}^2\widetilde{N} - \widetilde{N}^T - \widetilde{N}^H\right)\frac{\partial\widetilde{w}}{\partial\tilde{x}}\end{aligned} \tag{4.92}$$

It should be noted that by setting the dimensionless term $\tilde{r}^2$ to zero, on which the nonlinear nature of the equations depends, from the previous equation, we obtain the linear transverse free vibrations associated with L/NStressGH:

$$\begin{aligned}\lambda_c^2\frac{\partial^6\tilde{w}}{\partial\tilde{x}^6}-\frac{\partial^4\tilde{w}}{\partial\tilde{x}^4}+\tilde{A}_\rho\lambda_c^2\left(\xi_1+\frac{\lambda_l^2}{\lambda_c^2}\right)\left(\frac{\partial^4\tilde{w}}{\partial\tilde{x}^2\partial t^2}-\tilde{\mathrm{g}}^2\frac{\partial^6\tilde{w}}{\partial\tilde{x}^4\partial t^2}\right)\\ +\lambda_c^2\left(\xi_1+\frac{\lambda_l^2}{\lambda_c^2}\right)\left(\tilde{N}^T+\tilde{N}^H\right)\frac{\partial^4\tilde{w}}{\partial\tilde{x}^4}-\left(\tilde{N}^T+\tilde{N}^H\right)\frac{\partial^2\tilde{w}}{\partial\tilde{x}^2}\\ =\tilde{A}_\rho\left(\frac{\partial^2\tilde{w}}{\partial t^2}-\tilde{\mathrm{g}}^2\frac{\partial^4\tilde{w}}{\partial\tilde{x}^2\partial t^2}\right)\end{aligned} \tag{4.93}$$

### 4.4.1. Linear free vibrations: solution procedure

Natural frequencies and mode shapes of flexural vibrations can be evaluated by employing the classical separation of the spatial and time variables:

$$\tilde{w}(\tilde{x},t)=\tilde{W}(\tilde{x})\,e^{i\omega t} \tag{4.94}$$

being *ω* the natural frequency of flexural vibrations. Enforcing the separation of the variables Eq. 4.93 to the differential condition of dynamic equilibrium, the following dimensionless governing equations of the linear transverse free vibrations based on L/NStressGH can be rewritten in terms of non-dimensional spatial shape $\tilde{W}=\tilde{W}(\tilde{x})$ as:

- *Dimensionless free vibration equation in terms of spatial mode*

$$\begin{aligned}\lambda_c^2\,\frac{\partial^6\tilde{W}}{\partial\tilde{x}^6}+\frac{\partial^4\tilde{W}}{\partial\tilde{x}^4}\left(\tilde{\omega}^2\,(\lambda_c^2\,\xi_1+\lambda_l^2)\tilde{g}^2+(\lambda_c^2\,\xi_1+\lambda_l^2)\left(\tilde{N}^T+\tilde{N}^H\right)-1\right)\\ -\frac{\partial^2\tilde{W}}{\partial\tilde{x}^2}\left(\tilde{\omega}^2(\lambda_c^2\,\xi_1+\lambda_l^2)+\tilde{g}^2\tilde{\omega}^2+\left(\tilde{N}^T+\tilde{N}^H\right)\right)\\ +\tilde{\omega}^2\tilde{W}=0\end{aligned} \tag{4.95}$$

- *Dimensionless standard boundary conditions in terms of spatial shape*

$$\frac{\partial\tilde{W}}{\partial\tilde{x}}=\frac{\partial\tilde{W}^*}{\partial\tilde{x}}\big|_{0,1} \quad \text{or} \quad \tilde{M}^{L/NStressGH}=\tilde{M}^*\big|_{0,1} \tag{4.96}$$

$$\tilde{W}=\tilde{W}^*\big|_{0,1} \quad \text{or} \quad \tilde{V}^{L/NStressGH}=\tilde{V}^*\big|_{0,1} \tag{4.97}$$

- *Dimensionless constitutive boundary conditions in terms of spatial shape*

$$-\frac{\partial^3\widetilde{W}(0)}{\partial\tilde{x}^3}+\frac{1}{\lambda_c}\frac{\partial^2\widetilde{W}(0)}{\partial\tilde{x}^2}+\frac{\widetilde{M}^T+\widetilde{M}^H}{\lambda_c} = -\frac{\xi_1}{\lambda_c}\widetilde{M}^{L/NStressGH}(0) + \left(\xi_1+\frac{\lambda_l^2}{\lambda_c^2}\right)\frac{\partial\widetilde{M}^{L/NStressGH}(0)}{\partial\tilde{x}} \tag{4.98}$$

$$-\frac{\partial^3\widetilde{W}(1)}{\partial\tilde{x}^3}-\frac{1}{\lambda_c}\frac{\partial^2\widetilde{W}(1)}{\partial\tilde{x}^2}-\frac{\widetilde{M}^T+\widetilde{M}^H}{\lambda_c} = \frac{\xi_1}{\lambda_c}\widetilde{M}^{L/NStressGH}(1)+\left(\xi_1+\frac{\lambda_l^2}{\lambda_c^2}\right)\frac{\partial\widetilde{M}^{L/NStressGH}(1)}{\partial\tilde{x}} \tag{4.99}$$

- *Dimensionless bending moment in terms of spatial shape*

$$\widetilde{M}^{L/NStressGH} = -\frac{\partial^2\widetilde{W}}{\partial\tilde{x}^2}+\lambda_c^2\frac{\partial^4\widetilde{W}}{\partial\tilde{x}^4} + \tilde{\omega}^2(\lambda_c^2\,\xi_1+\lambda_l^2)\left(\tilde{g}^2\frac{\partial^2\widetilde{W}}{\partial\tilde{x}^2}-\widetilde{W}\right) + (\lambda_c^2\,\xi_1+\lambda_l^2)\left(\widetilde{N}^T+\widetilde{N}^H\right)\frac{\partial^2\widetilde{W}}{\partial\tilde{x}^2}-\left(\widetilde{M}^T+\widetilde{M}^H\right) \tag{4.100}$$

- *Dimensionless shear force in terms of spatial shape*

$$\widetilde{V}^{L/NStressGH} = -\frac{\partial^3\widetilde{W}}{\partial\tilde{x}^3}+\lambda_c^2\frac{\partial^5\widetilde{W}}{\partial\tilde{x}^5} + \tilde{\omega}^2\left(\lambda_c^2\xi_1+\lambda_l^2\right)\left(\tilde{g}^2\frac{\partial^3\widetilde{W}}{\partial\tilde{x}^3}-\left(\frac{\tilde{g}^2}{(\lambda_c^2\xi_1+\lambda_l^2)}+1\right)\frac{\partial\widetilde{W}}{\partial\tilde{x}}\right) + \left(\lambda_c^2\xi_1+\lambda_l^2\right)\left(\left(\widetilde{N}^T+\widetilde{N}^H\right)\frac{\partial^3\widetilde{W}}{\partial\tilde{x}^3}-\frac{\partial^2}{\partial\tilde{x}^2}\left(\widetilde{N}\frac{\partial\widetilde{W}}{\partial\tilde{x}}\right)\right) + \left(\widetilde{N}-\widetilde{N}^T-\widetilde{N}^H\right)\frac{\partial\widetilde{W}}{\partial\tilde{x}} \tag{4.101}$$

The analytical solution of the governing equation of the flexural spatial mode shape Eq. 4.95 can be expressed by:

$$\widetilde{W}(\tilde{x}) = \sum_{k=1}^{6} q_k e^{\tilde{x}\,\beta_k} \tag{4.102}$$

wherein $\beta_k$ are the roots of the characteristic equation, and $q_k$ are six unknown constants to be determined by imposing suitable boundary conditions. Note that, the six unknown constants can be obtained by satisfying boundary conditions Eqs. 4.96-4.99. Lastly, the linear fundamental natural frequencies of a porous FG nanobeam consists into solving the eigenvalue problem expressed in terms of a six-dimensional array, $q = \{q_1, .., q_6\}$. It can be noted that the corresponding characteristic equation is strongly nonlinear and is numerically solved by using a Wolfram language code written by the author in Mathematica.

### 4.4.2. Higher-order Hamiltonian approach to nonlinear free vibrations: solution procedure

On the basis of the Galerkin method, the transverse displacement function $\tilde{w}(\tilde{x}, t)$ in Eq. 4.84 can be defined by:

$$\tilde{w}(\tilde{x}, t) = \sum_{i=1}^{N} W_i(\tilde{x})\, W_i(t) \tag{4.103}$$

where $W_i(\tilde{x})$ is the i-*th* test function which depends on the assigned boundary conditions and $W_i(t)$ is the unknown i-*th* time-dependent coefficient.

**Remark 4.3.** *In this study, the test function was assumed to be equal to L/NStressGH linear mode shape* $(i = 1)$.

Thererefore, Eq. 4.103 can be rewritten as:

$$\tilde{w}(\tilde{x}, t) = W_1(\tilde{x})\, W_1(t) \tag{4.104}$$

- *First-order Hamiltonian Approach*

Based on the First-order Hamiltonian Approach introduced by He in [102], the time base function, $W_1(t)$, is given by the following approximate cosine solution:

$$W_1(t) = \mathcal{A}_w cos(\omega_1 t) \tag{4.105}$$

being $\omega_1$ the first nonlinear vibration frequency, $\mathcal{A}_w$ the amplitude of the nonlinear oscillator; moreover $W_1(\tilde{x})$ is assumed to be equal to the linear spatial mode based on the L/NStressGH model of elasticity:

$$\begin{aligned} W_1(\tilde{x}) = q_1 e^{-\tilde{x}\beta_1} + q_2 e^{\tilde{x}\beta_1} + q_3 e^{-\tilde{x}\beta_2} + q_4 e^{\tilde{x}\beta_2} + q_5 e^{-\tilde{x}\beta_3} \\ + q_6 e^{\tilde{x}\beta_3} \end{aligned} \tag{4.106}$$

Now, by substituting Eq. 4.105 into Eq. 4.84 and multiplying the resulting equation with the fundamental vibration mode $W_1(\tilde{x})$, then integrating across the length of the nanobeam, leads to the following equation:

$$\delta_0 + \delta_1 W_1(t) + \delta_2 W_1^2(t) + \delta_3 W_1^3(t) + W_1{}''(t) = 0 \tag{4.107}$$

where $\delta_0, \delta_1, \delta_2$ and $\delta_3$ are four coefficients obtained by splitting up the terms.

Finally, in agreement with Hamiltonian Approach to nonlinear oscillators [103], it is easy to establish a variational principle for Eq. 4.107:

$$\begin{aligned} H = \int_0^{\mathcal{T}/4} \Bigg( \delta_0 W_1(t) + \frac{1}{2}\delta_1 W_1^2(t) + \frac{1}{3}\delta_2 W_1(t) + \frac{1}{4}\delta_3 W_1(t) \\ - \frac{1}{2} W_1{}'(t)^2 \Bigg) dt \end{aligned} \tag{4.108}$$

where $\mathcal{T}$ is period of the nonlinear oscillator.

The frequency–amplitude relationship can be obtained from the following equation:

$$\omega_1 = \frac{\sqrt{-48\delta_0 - 12\pi\mathcal{A}_w\delta_1 - 32\mathcal{A}_w^2\delta_2 - 9\pi\mathcal{A}_w^3\delta_3}}{2\sqrt{3\pi}\sqrt{\mathcal{A}_w}} \tag{4.109}$$

Note that the linear vibration frequency of a porous FG nanobeam can be determined from the previous Eq. 4.109 by setting $\mathcal{A}_w = 0$.

- *Second-order Hamiltonian Approach*

In order to find the Second-order approximate solution and frequency, we assume that a Second-order trial solution can be expressed by:

$$W_1(t) = \mathcal{A}_1 cos(\omega_1 t) + \mathcal{A}_2 cos(3\omega_1 t) \tag{4.110}$$

with the following initial condition:

$$\mathcal{A}_w = \mathcal{A}_1 + \mathcal{A}_2 \tag{4.111}$$

Applying the mathematical resolution method previously introduced for the First-order Hamiltonian Approach [104], we obtain the following system of equations:

$$\begin{cases} \dfrac{\partial}{\partial \mathcal{A}_1}\left(\dfrac{\partial H}{\partial \dfrac{1}{\omega_1}}\right) = 0 \\ \dfrac{\partial}{\partial \mathcal{A}_2}\left(\dfrac{\partial H}{\partial \dfrac{1}{\omega_1}}\right) = 0 \end{cases} \tag{4.112}$$

Solving Eq. 4.112 and Eq. 4.111 simultaneously, and assuming Eq. 4.110, one can obtain the Second-order solution and the approximate frequency $\omega_1$ according to the Hamiltonian Approach.

- *Third-order Hamiltonian Approach*

The accuracy of the results will be further improved by consider the following equation as the response of the system:

$$W_1(t) = \mathcal{A}_1 cos(\omega_1 t) + \mathcal{A}_2 cos(3\omega_1 t) + \mathcal{A}_3 cos(5\omega_1 t) \tag{4.113}$$

where the initial condition is:

$$\mathcal{A}_w = \mathcal{A}_1 + \mathcal{A}_2 + \mathcal{A}_3 \tag{4.114}$$

By using the same procedure explained above, the following system of equations follows:

$$\begin{cases} \dfrac{\partial}{\partial \mathcal{A}_1}\left(\dfrac{\partial H}{\partial \dfrac{1}{\omega_1}}\right) = 0 \\ \dfrac{\partial}{\partial \mathcal{A}_2}\left(\dfrac{\partial H}{\partial \dfrac{1}{\omega_1}}\right) = 0 \\ \dfrac{\partial}{\partial \mathcal{A}_3}\left(\dfrac{\partial H}{\partial \dfrac{1}{\omega_1}}\right) = 0 \end{cases} \tag{4.115}$$

Similarly, by solving Eq. 4.115 simultaneously with Eq. 4.114, the amplitude-frequency relation up to the Third-order approximation is obtained.

### 4.4.3. Convergence and comparison study

In order to validate the accuracy and reliability of the proposed approach, three numerical examples are presented in this paragraph.

To this purpose, both a uniform temperature rise, $T(z) = T_0 + \Delta T,$ and a moisture concentration, $H(z) = H_0 + \Delta H,$ between the bottom $(z = -h/2)$ and the top surface $(z = h/2)$ of porous FG nanobeam cross-section are considered, being $T_0 = 300$ [K] and $H_0 = 0\ [\mathrm{wt.\%\ H_2O}]$ the reference values of the temperature and moisture concentration at the bottom surface, respectively, and $\Delta T,\ \Delta H$ their increments.

In the first two comparison examples, the linear normalized frequency ratio between the linear $(\mathcal{A}_w = 0)$ dimensionless nonlocal fundamental frequency, $\widetilde{\omega}$, and the dimensionless local natural frequency, $\widetilde{\omega}_{loc}$, of a Clamped-Clamped (C-C) porous FG nanobeam in a hygrothermal environment were compared (Tables 4.3, 4.4) with the results obtained by Penna et al. in [27], for $\lambda_c = 0.2$ and assuming: for $\lambda_l = 0.0$ or $0.1$; $\xi_1 = 0.0$ or $0.5$; $\Delta T_{UTR} = 0, 50, 100$ [K]; $\Delta H = 2$ [wt.% $H_2O$].

In the third example (Table 4.5), the present approach is compared with the model proposed by Barretta et al. in [113] for a (C-C) porous FG nanobeam in absence of hygrothermal loads for $\lambda_l = 0.1$, varying $\lambda_c$, in the set $\{0.0^+, 0.2, 0.4, 0.6, 0.8, 1.0\}$ and assuming $\xi_1 = 0.0$ or $0.5$, and the gyration radius, $\tilde{g}$, equal to 1/20.

Note that the dimensionless local natural frequency, $\tilde{\omega}_{loc}$, has been obtained assuming $n = 0, \zeta = 0$ (pure ceramic), $\Delta T = \Delta H = 0$ and considering a value of the non-dimensional gyration radius, $\tilde{g}$, equal to zero.

**Table 4.3.** Linear dimensionless natural frequencies of porous FG Clamped-Clamped (C-C) nanobeam.

| | $\xi_1 = 0.0$, $\mathcal{A}_w = 0$, $\lambda_c = 0.20$ | | | | | |
|---|---|---|---|---|---|---|
| $\lambda_l$ | $\Delta T_{UTR} = 0$ | | $\Delta T_{UTR} = 50$ | | $\Delta T_{UTR} = 100$ | |
| | *Present Approach* | *Ref.* [27] | *Present Approach* | *Ref.* [27] | *Present Approach* | *Ref.* [27] |
| 0.00 | 1.83226 | 1.83226 | 1.82706 | 1.82706 | 1.82313 | 1.82313 |
| 0.10 | 1.57333 | 1.57333 | 1.56718 | 1.56718 | 1.56254 | 1.56254 |

**Table 4.4.** Linear dimensionless natural frequencies of porous FG Clamped-Clamped (C-C) nanobeam.

| | $\xi_1 = 0.5$, $\mathcal{A}_w = 0$, $\lambda_c = 0.20$ | | | | | |
|---|---|---|---|---|---|---|
| $\lambda_l$ | $\Delta T_{UTR} = 0$ | | $\Delta T_{UTR} = 50$ | | $\Delta T_{UTR} = 100$ | |
| | *Present Approach* | *Ref.* [27] | *Present Approach* | *Ref.* [27] | *Present Approach* | *Ref.* [27] |
| 0.00 | 1.23148 | 1.23148 | 1.22424 | 1.22424 | 1.21876 | 1.21876 |
| 0.10 | 1.13883 | 1.13883 | 1.13089 | 1.13089 | 1.12487 | 1.12487 |

**Table 4.5.** Normalized linear fundamental flexural frequency of Clamped-Clamped (C-C) nanobeam for $\Delta T = \Delta H = 0$.

| | $\Delta T = \Delta H = \mathcal{A}_w = 0$ | | | | | | | | | | | |
|---|---|---|---|---|---|---|---|---|---|---|---|---|
| $\frac{\tilde{\omega}}{\tilde{\omega}_{loc}}$ | $\xi_1 = 0.0$ | | | | | | $\xi_1 = 0.5$ | | | | | |
| | $\lambda_l = 0.1$ | *Ref.* [113] | $\lambda_l = 0.3$ | *Ref.* [113] | $\lambda_l = 0.5$ | *Ref.* [113] | $\lambda_l = 0.1$ | *Ref.* [113] | $\lambda_l = 0.3$ | *Ref.* [113] | $\lambda_l = 0.5$ | *Ref.* [113] |
| $0.0^+$ | 0.89165 | 0.89165 | 0.52522 | 0.52522 | 0.34619 | 0.34619 | 0.88416 | 0.88416 | 0.52314 | 0.52314 | 0.34529 | 0.34529 |
| 0.2 | 1.58127 | 1.58127 | 0.89822 | 0.89822 | 0.58545 | 0.58545 | 1.14531 | 1.14531 | 0.77938 | 0.77938 | 0.54126 | 0.54126 |
| 0.4 | 2.57577 | 2.57577 | 1.38724 | 1.38724 | 0.93713 | 0.93713 | 1.28946 | 1.28946 | 1.02374 | 1.02374 | 0.77625 | 0.77625 |
| 0.6 | 3.61940 | 3.61940 | 2.01640 | 2.01640 | 1.30727 | 1.30727 | 1.34633 | 1.34633 | 1.16750 | 1.16750 | 0.95453 | 0.95453 |
| 0.8 | 4.67784 | 4.67784 | 2.59796 | 2.59796 | 1.68291 | 1.68291 | 1.37237 | 1.37237 | 1.24944 | 1.24944 | 1.07846 | 1.07846 |
| 1.0 | 5.74258 | 5.74258 | 3.18308 | 3.18308 | 2.06089 | 2.06089 | 1.38608 | 1.38608 | 1.29819 | 1.29819 | 1.16320 | 1.16320 |

### 4.4.4. Results and discussion

In this paragraph, the dynamic response of a Clamped-Clamped non-porous and porous Bernoulli-Euler FG nanobeam, with length $L=10nm$ and square cross-section ($b=h=L/10$) subjected to a hygrothermal environment is investigated via Local/Nonlocal Stress Gradient Hygrothermal formulation here proposed. As said before, starting from a reference value of temperature equal to $T_0 = 300\ [K]$ and an initial value of moisture concentration $H_0 = 0.0\ [wt.\%\mathrm{H_2O}]$, both a uniform temperature rise and a heat-conduction have been considered in the parametric thermo-elastic analysis. The convergence of series in Eq.6 has been ensured by setting $k = 10$.

For greater understanding, below is a brief summary of the tables that collect the main results of the parametric analysis.

In particular, the effects of nonlocal parameter, $\lambda_c$, and the gradient length parameter, $\lambda_l$, as well as the mixture parameter, $\xi_1$, on normalized linear fundamental flexural frequencies have been summarized in the following Tables 4.6-4.17:

**Table 4.6.** Normalized linear fundamental flexural frequency of Clamped-Clamped (C-C) non-porous FG nanobeam assuming: $\mathcal{A}_w = 0.0,\ \xi_1 = 0.0,\ n = 1,\ \Delta T_{UTR} = 50\ [K]$ and $\Delta H = 0.1\ [\mathrm{wt.\%\ H_2O}]$.

| $\lambda_c$ | $\tilde{\omega}/\tilde{\omega}_{loc}$ | | | | | |
|---|---|---|---|---|---|---|
| | $\lambda_l = 0.0$ | $\lambda_l = 0.01$ | $\lambda_l = 0.02$ | $\lambda_l = 0.03$ | $\lambda_l = 0.04$ | $\lambda_l = 0.05$ |
| $0.0^+$ | 0.98945 | 0.98980 | 0.98687 | 0.98369 | 0.97927 | 0.97368 |
| 0.01 | 1.01062 | 1.00903 | 1.00431 | 0.99659 | 0.98608 | 0.97303 |
| 0.02 | 1.03462 | 1.03298 | 1.02812 | 1.02016 | 1.00933 | 0.99589 |
| 0.03 | 1.06146 | 1.05977 | 1.05474 | 1.04651 | 1.03532 | 1.02144 |
| 0.04 | 1.09110 | 1.08935 | 1.08413 | 1.07562 | 1.06402 | 1.04965 |
| 0.05 | 1.12346 | 1.12164 | 1.11623 | 1.10739 | 1.09536 | 1.08045 |

**Table 4.7.** Normalized linear fundamental flexural frequency of Clamped-Clamped (C-C) non-porous FG nanobeam assuming: $\mathcal{A}_w = 0.0,\ \xi_1 = 0.0,\ n = 1,\ \Delta T_{UTR} = 100\ [K]$ and $\Delta H = 0.1$ [wt. % $\mathrm{H_2O}$].

| $\lambda_c$ | $\tilde{\omega}/\tilde{\omega}_{loc}$ | | | | | |
|---|---|---|---|---|---|---|
| | $\lambda_l = 0.0$ | $\lambda_l = 0.01$ | $\lambda_l = 0.02$ | $\lambda_l = 0.03$ | $\lambda_l = 0.04$ | $\lambda_l = 0.05$ |
| $0.0^+$ | 0.97952 | 0.97885 | 0.97681 | 0.97345 | 0.96880 | 0.96289 |
| 0.01 | 1.00073 | 0.99912 | 0.99434 | 0.98651 | 0.97585 | 0.96263 |
| 0.02 | 1.02482 | 1.02316 | 1.01823 | 1.01017 | 0.99919 | 0.98557 |
| 0.03 | 1.05179 | 1.05007 | 1.04498 | 1.03666 | 1.02532 | 1.01126 |
| 0.04 | 1.08160 | 1.07983 | 1.07456 | 1.06594 | 1.05420 | 1.03965 |
| 0.05 | 1.11417 | 1.11233 | 1.10686 | 1.09792 | 1.08575 | 1.07067 |

**Table 4.8.** Normalized linear fundamental flexural frequency of Clamped-Clamped (C-C) non-porous FG nanobeam assuming: $\mathcal{A}_w = 0.0,\ \xi_1 = 0.0,\ n = 1,\ \Delta H = 0.1$ [wt. % $\mathrm{H_2O}$], $\Delta T_{HC}$ corresponding to $T_m = 350\ [K], T_c = 300\ [K]$.

| $\lambda_c$ | $\tilde{\omega}/\tilde{\omega}_{loc}$ | | | | | |
|---|---|---|---|---|---|---|
| | $\lambda_l = 0.0$ | $\lambda_l = 0.01$ | $\lambda_l = 0.02$ | $\lambda_l = 0.03$ | $\lambda_l = 0.04$ | $\lambda_l = 0.05$ |
| $0.0^+$ | 0.98988 | 0.98924 | 0.98732 | 0.98414 | 0.97974 | 0.97416 |
| 0.01 | 1.01106 | 1.00947 | 1.00475 | 0.99704 | 0.98653 | 0.97349 |
| 0.02 | 1.03505 | 1.03342 | 1.02856 | 1.02060 | 1.00977 | 0.99634 |
| 0.03 | 1.06188 | 1.06019 | 1.05517 | 1.04965 | 1.03576 | 1.02188 |
| 0.04 | 1.09151 | 1.08976 | 1.08455 | 1.07604 | 1.06445 | 1.05009 |
| 0.05 | 1.12387 | 1.12205 | 1.11664 | 1.10780 | 1.09578 | 1.08088 |

**Table 4.9.** Normalized linear fundamental flexural frequency of Clamped-Clamped (C-C) non-porous FG nanobeam assuming: $\mathcal{A}_w = 0.0,\ \xi_1 = 0.0,\ n = 1,\ \Delta H = 0.1$ [wt. % $\mathrm{H_2O}$], $\Delta T_{HC}$ corresponding to $T_m = 400\ [K], T_c = 300\ [K]$.

| $\lambda_c$ | $\tilde{\omega}/\tilde{\omega}_{loc}$ | | | | | |
|---|---|---|---|---|---|---|
| | $\lambda_l = 0.0$ | $\lambda_l = 0.01$ | $\lambda_l = 0.02$ | $\lambda_l = 0.03$ | $\lambda_l = 0.04$ | $\lambda_l = 0.05$ |
| $0.0^+$ | 0.98546 | 0.98480 | 0.98283 | 0.97957 | 0.97506 | 0.96934 |
| 0.01 | 1.00664 | 1.00504 | 1.00030 | 0.99254 | 0.98196 | 0.96885 |
| 0.02 | 1.03068 | 1.02903 | 1.02414 | 1.01614 | 1.00525 | 0.99174 |
| 0.03 | 1.05756 | 1.05586 | 1.05081 | 1.04255 | 1.03129 | 1.01734 |
| 0.04 | 1.08727 | 1.08551 | 1.08028 | 1.07172 | 1.06007 | 1.04562 |
| 0.05 | 1.11972 | 1.11789 | 1.11246 | 1.10357 | 1.09149 | 1.07651 |

**Table 4.10.** Normalized linear fundamental flexural frequency of Clamped-Clamped (C-C) non-porous FG nanobeam assuming: $\mathcal{A}_w = 0.5,\ \xi_1 = 0.0,\ n = 1,\ \Delta T_{UTR} = 50\ [K]$ and $\Delta H = 0.1$ [wt. % $H_2O$].

| $\lambda_c$ | $\widetilde{\omega}/\widetilde{\omega}_{loc}$ | | | | | |
|---|---|---|---|---|---|---|
| | $\lambda_l = 0.0$ | $\lambda_l = 0.01$ | $\lambda_l = 0.02$ | $\lambda_l = 0.03$ | $\lambda_l = 0.04$ | $\lambda_l = 0.05$ |
| $0.0^+$ | 0.98945 | 0.98801 | 0.98687 | 0.98369 | 0.97927 | 0.97368 |
| 0.01 | 0.99983 | 0.99829 | 0.99370 | 0.98619 | 0.97597 | 0.96328 |
| 0.02 | 1.01114 | 1.00960 | 1.00503 | 0.99754 | 0.98734 | 0.97467 |
| 0.03 | 1.02326 | 1.02173 | 1.01717 | 1.00972 | 0.99956 | 0.98693 |
| 0.04 | 1.03604 | 1.03452 | 1.03000 | 1.02259 | 1.01248 | 0.99992 |
| 0.05 | 1.04934 | 1.04783 | 1.04335 | 1.03600 | 1.02597 | 1.01349 |

**Table 4.11.** Normalized linear fundamental flexural frequency of Clamped-Clamped (C-C) non-porous FG nanobeam assuming: $\mathcal{A}_w = 0.5,\ \xi_1 = 0.0,\ n = 1,\ \Delta T_{UTR} = 100\ [K]$ and $\Delta H = 0.1$ [wt. % $H_2O$].

| $\lambda_c$ | $\widetilde{\omega}/\widetilde{\omega}_{loc}$ | | | | | |
|---|---|---|---|---|---|---|
| | $\lambda_l = 0.0$ | $\lambda_l = 0.01$ | $\lambda_l = 0.02$ | $\lambda_l = 0.03$ | $\lambda_l = 0.04$ | $\lambda_l = 0.05$ |
| $0.0^+$ | 0.97952 | 0.97885 | 0.97681 | 0.97345 | 0.96880 | 0.96289 |
| 0.01 | 0.98993 | 0.98836 | 0.98371 | 0.97610 | 0.96573 | 0.95286 |
| 0.02 | 1.00128 | 0.99972 | 0.99509 | 0.98750 | 0.97716 | 0.96431 |
| 0.03 | 1.01347 | 1.01192 | 1.00731 | 0.99975 | 0.98945 | 0.97665 |
| 0.04 | 1.02634 | 1.02480 | 1.02022 | 1.01272 | 1.00248 | 0.98974 |
| 0.05 | 1.03974 | 1.03822 | 1.03368 | 1.02624 | 1.01608 | 1.00343 |

**Table 4.12.** Normalized linear fundamental flexural frequency of Clamped-Clamped (C-C) non-porous FG nanobeam assuming: $\mathcal{A}_w = 0.5,\ \xi_1 = 0.0,\ n = 1,\ \Delta H = 0.1$ [wt. % $H_2O$], $\Delta T_{HC}$ corresponding to $T_m = 350\ [K], T_c = 300\ [K]$.

| $\lambda_c$ | $\widetilde{\omega}/\widetilde{\omega}_{loc}$ | | | | | |
|---|---|---|---|---|---|---|
| | $\lambda_l = 0.0$ | $\lambda_l = 0.01$ | $\lambda_l = 0.02$ | $\lambda_l = 0.03$ | $\lambda_l = 0.04$ | $\lambda_l = 0.05$ |
| $0.0^+$ | 0.98988 | 0.98924 | 0.98732 | 0.98414 | 0.97974 | 0.97416 |
| 0.01 | 1.00027 | 0.99872 | 0.99414 | 0.98664 | 0.97462 | 0.96374 |
| 0.02 | 1.01157 | 1.01004 | 1.00547 | 0.99799 | 0.98779 | 0.97513 |
| 0.03 | 1.02369 | 1.02216 | 1.01761 | 1.01016 | 1.00000 | 0.98738 |
| 0.04 | 1.03647 | 1.03495 | 1.03043 | 1.02303 | 1.01293 | 1.00037 |
| 0.05 | 1.04976 | 1.04826 | 1.04377 | 1.03643 | 1.02641 | 1.01393 |

**Table 4.13.** Normalized linear fundamental flexural frequency of Clamped-Clamped (C-C) non-porous FG nanobeam assuming: $\mathcal{A}_w = 0.5,\ \xi_1 = 0.0,\ n = 1,\ \Delta H = 0.1$ [wt.% $H_2O$], $\Delta T_{HC}$ corresponding to $T_m = 400\ [K], T_c = 300\ [K]$.

| $\lambda_c$ | $\tilde{\omega}/\tilde{\omega}_{loc}$ | | | | | |
|---|---|---|---|---|---|---|
| | $\lambda_l = 0.0$ | $\lambda_l = 0.01$ | $\lambda_l = 0.02$ | $\lambda_l = 0.03$ | $\lambda_l = 0.04$ | $\lambda_l = 0.05$ |
| $0.0^+$ | 0.98546 | 0.98480 | 0.98283 | 0.97957 | 0.97506 | 0.96934 |
| 0.01 | 0.99584 | 0.99429 | 0.98968 | 0.98214 | 0.97185 | 0.95909 |
| 0.02 | 1.00717 | 1.00562 | 1.00103 | 0.99350 | 0.98324 | 0.97050 |
| 0.03 | 1.01932 | 1.01778 | 1.01320 | 1.00571 | 0.99549 | 0.98279 |
| 0.04 | 1.03214 | 1.03061 | 1.02606 | 1.01862 | 1.00846 | 0.99582 |
| 0.05 | 1.04548 | 1.04396 | 1.03945 | 1.03207 | 1.02199 | 1.00944 |

**Table 4.14.** Normalized linear fundamental flexural frequency of Clamped-Clamped (C-C) non-porous FG nanobeam assuming: $\mathcal{A}_w = 1.0,\ \xi_1 = 0.0,\ n = 1,\ \Delta T_{UTR} = 50\ [K]$ and $\Delta H = 0.1$ [wt.% $H_2O$].

| $\lambda_c$ | $\tilde{\omega}/\tilde{\omega}_{loc}$ | | | | | |
|---|---|---|---|---|---|---|
| | $\lambda_l = 0.0$ | $\lambda_l = 0.01$ | $\lambda_l = 0.02$ | $\lambda_l = 0.03$ | $\lambda_l = 0.04$ | $\lambda_l = 0.05$ |
| $0.0^+$ | 0.98945 | 0.98880 | 0.98687 | 0.98369 | 0.97927 | 0.97368 |
| 0.01 | 0.98945 | 0.98795 | 0.98349 | 0.97618 | 0.96623 | 0.95387 |
| 0.02 | 0.98945 | 0.98800 | 0.98368 | 0.97662 | 0.96698 | 0.95499 |
| 0.03 | 0.98945 | 0.98805 | 0.98389 | 0.97108 | 0.96777 | 0.95619 |
| 0.04 | 0.98945 | 0.98810 | 0.98411 | 0.97757 | 0.96862 | 0.95746 |
| 0.05 | 0.98945 | 0.98816 | 0.98434 | 0.97807 | 0.96949 | 0.95878 |

**Table 4.15.** Normalized linear fundamental flexural frequency of Clamped-Clamped (C-C) non-porous FG nanobeam assuming: $\mathcal{A}_w = 1.0,\ \xi_1 = 0.0,\ n = 1,\ \Delta T_{UTR} = 100\ [K]$ and $\Delta H = 0.1$ [wt.% $H_2O$].

| $\lambda_c$ | $\tilde{\omega}/\tilde{\omega}_{loc}$ | | | | | |
|---|---|---|---|---|---|---|
| | $\lambda_l = 0.0$ | $\lambda_l = 0.01$ | $\lambda_l = 0.02$ | $\lambda_l = 0.03$ | $\lambda_l = 0.04$ | $\lambda_l = 0.05$ |
| $0.0^+$ | 0.97952 | 0.97885 | 0.97681 | 0.97345 | 0.96880 | 0.96289 |
| 0.01 | 0.97952 | 0.97800 | 0.97348 | 0.96608 | 0.95598 | 0.94344 |
| 0.02 | 0.97952 | 0.97805 | 0.97368 | 0.96651 | 0.95673 | 0.94457 |
| 0.03 | 0.97952 | 0.97811 | 0.97389 | 0.96698 | 0.95754 | 0.94579 |
| 0.04 | 0.97952 | 0.97816 | 0.97412 | 0.94748 | 0.95840 | 0.94708 |
| 0.05 | 0.97952 | 0.97822 | 0.97435 | 0.96799 | 0.95928 | 0.94842 |

**Table 4.16.** Normalized linear fundamental flexural frequency of Clamped-Clamped (C-C) non-porous FG nanobeam assuming: $\mathcal{A}_w = 1.0,\ \xi_1 = 1.0,\ n = 1,\ \Delta H = 0.1\ [\text{wt.\%}\ H_2O],\ \Delta T_{HC}$ corresponding to $T_m = 350\ [K], T_c = 300\ [K]$.

| $\lambda_c$ | $\tilde{\omega}/\tilde{\omega}_{loc}$ | | | | | |
|---|---|---|---|---|---|---|
| | $\lambda_l = 0.0$ | $\lambda_l = 0.01$ | $\lambda_l = 0.02$ | $\lambda_l = 0.03$ | $\lambda_l = 0.04$ | $\lambda_l = 0.05$ |
| $0.0^+$ | 0.98988 | 0.98924 | 0.98732 | 0.98414 | 0.97974 | 0.97416 |
| 0.01 | 0.98988 | 0.98839 | 0.98393 | 0.97663 | 0.96669 | 0.95433 |
| 0.02 | 0.98988 | 0.98843 | 0.98412 | 0.97706 | 0.96743 | 0.95545 |
| 0.03 | 0.98988 | 0.98849 | 0.98433 | 0.97753 | 0.96823 | 0.95665 |
| 0.04 | 0.98988 | 0.98854 | 0.98456 | 0.97801 | 0.96907 | 0.95792 |
| 0.05 | 0.98988 | 0.98860 | 0.98478 | 0.97852 | 0.96994 | 0.95924 |

**Table 4.17.** Normalized linear fundamental flexural frequency of Clamped-Clamped (C-C) non-porous FG nanobeam assuming: $\mathcal{A}_w = 1.0,\ \xi_1 = 1.0,\ n = 1,\ \Delta H = 0.1\ [\text{wt.\%}\ H_2O],\ \Delta T_{HC}$ corresponding to $T_m = 400\ [K], T_c = 300\ [K]$.

| $\lambda_c$ | $\tilde{\omega}/\tilde{\omega}_{loc}$ | | | | | |
|---|---|---|---|---|---|---|
| | $\lambda_l = 0.0$ | $\lambda_l = 0.01$ | $\lambda_l = 0.02$ | $\lambda_l = 0.03$ | $\lambda_l = 0.04$ | $\lambda_l = 0.05$ |
| $0.0^+$ | 0.98546 | 0.98480 | 0.98283 | 0.97957 | 0.97506 | 0.96934 |
| 0.01 | 0.98546 | 0.98395 | 0.97946 | 0.97212 | 0.96211 | 0.94968 |
| 0.02 | 0.98546 | 0.98400 | 0.97966 | 0.97255 | 0.96586 | 0.95080 |
| 0.03 | 0.98546 | 0.98405 | 0.97987 | 0.97302 | 0.96366 | 0.95201 |
| 0.04 | 0.98546 | 0.98411 | 0.98009 | 0.97351 | 0.96451 | 0.95329 |
| 0.05 | 0.98546 | 0.98416 | 0.98032 | 0.97402 | 0.96539 | 0.95461 |

Moreover, the coupled effects of porosity volume fraction, $\zeta$, and material gradient index, $n$, on normalized linear fundamental flexural frequencies of Clamped-Clamped (C-C) porous FG nanobeam are listed in the following Tables 4.18, 4.19:

**Table 4.18.** Coupled effects of porosity volume fraction, ζ, and material gradient index, n, on normalized linear fundamental flexural frequency of Clamped-Clamped (C-C) porous FG nanobeam assuming $\xi_1 = 0.5, \lambda_c = 0.01, \lambda_l = 0.01$ and $\Delta H = 0.1$ [wt. % $H_2O$] for two different values of a uniform temperature rise $\Delta T_{UTR} = 50{,}100\ [K]$.

| $\zeta$ | $\tilde{\omega}/\tilde{\omega}_{loc}$ | | | | | |
|---|---|---|---|---|---|---|
| | $\Delta T_{UTR} = 50\ [K]$ | | | $\Delta T_{UTR} = 100\ [K]$ | | |
| | $n = 1$ | $n = 3$ | $n = 5$ | $n = 1$ | $n = 3$ | $n = 5$ |
| 0.00 | 0.99829 | 0.99552 | 0.99542 | 0.98836 | 0.98710 | 0.98667 |
| 0.10 | 0.99888 | 0.99620 | 0.99615 | 0.98975 | 0.98858 | 0.98821 |
| 0.20 | 0.99942 | 0.99684 | 0.99687 | 0.99109 | 0.99002 | 0.98973 |

**Table 4.19.** Coupled effects of porosity volume fraction, ζ, and material gradient index, n, on normalized linear fundamental flexural frequency of Clamped-Clamped (C-C) porous FG nanobeam assuming $\xi_1 = 0.5, \lambda_c = 0.01, \lambda_l = 0.01$ and $\Delta H = 0.1$ [wt. % $H_2O$] for two different values of heat-conduction rise, $\Delta T_{HC}$, corresponding to: $\{T_m = 350\ [K], T_c = 300\ [K].\}$ and $\{T_m = 400\ [K], T_c = 300\ [K]\}$.

| $\zeta$ | $\tilde{\omega}/\tilde{\omega}_{loc}$ | | | | | |
|---|---|---|---|---|---|---|
| | $T_m = 350\ [K], T_c = 300\ [K]$ | | | $T_m = 400\ [K], T_c = 300\ [K]$ | | |
| | $n = 1$ | $n = 3$ | $n = 5$ | $n = 1$ | $n = 3$ | $n = 5$ |
| 0.00 | 0.99872 | 0.99881 | 0.99928 | 0.99429 | 0.99400 | 0.99445 |
| 0.10 | 0.99896 | 0.99912 | 0.99933 | 0.99491 | 0.99468 | 0.99489 |
| 0.20 | 0.99915 | 0.99939 | 0.99966 | 0.99548 | 0.99533 | 0.99560 |

Furthermore, in the scientific literature, the effect of gyration radious, $\tilde{g}$, is sometimes omitted to simplify computational calculations. Next, the normalized linear fundamental flexural frequencies with and without the effect of $\tilde{g}$, expressing the differences in terms of percentage changes, are condensed in the following Tables 4.20-4.23:

**Table 4.20.** Coupled effects of porosity volume fraction, $\zeta$, material gradient index, $n$, and dimensionless gyration radious, $\tilde{g}$, on normalized linear fundamental flexural frequency of Clamped-Clamped (C-C) porous FG nanobeam assuming $\xi_1 = 0.5, \lambda_c = 0.01, \lambda_l = 0.01$ and $\Delta H = 0.1$ [wt. % $H_2O$] for a uniform temperature rise $\Delta T_{UTR} = 50\ [K]$.

| $n$ | $\Delta T_{UTR} = 50\ [K]$ | | | | | | | | |
|---|---|---|---|---|---|---|---|---|---|
| | $\zeta = 0.00$ | | | $\zeta = 0.10$ | | | $\zeta = 0.20$ | | |
| | $\tilde{g} \neq 0$ | $\tilde{g} = 0$ | $\Delta_{err}[\%]$ | $\tilde{g} \neq 0$ | $\tilde{g} = 0$ | $\Delta_{err}[\%]$ | $\tilde{g} \neq 0$ | $\tilde{g} = 0$ | $\Delta_{err}[\%]$ |
| 1 | 0.99829 | 0.99552 | 0.57 | 0.99888 | 1.0048 | 0.59 | 0.99942 | 1.00555 | 0.61 |
| 3 | 0.99888 | 0.99620 | 0.52 | 0.99620 | 1.00144 | 0.52 | 0.99684 | 1.00221 | 0.54 |
| 5 | 0.99942 | 0.99684 | 0.49 | 0.99615 | 1.00113 | 0.50 | 0.99687 | 1.00191 | 0.50 |

**Table 4.21.** Coupled effects of porosity volume fraction, $\zeta$, material gradient index, $n$, and dimensionless gyration radious, $\tilde{g}$, on normalized linear fundamental flexural frequency of Clamped-Clamped (C-C) porous FG nanobeam assuming $\xi_1 = 0.5, \lambda_c = 0.01, \lambda_l = 0.01$ and $\Delta H = 0.1$ [wt. % $H_2O$] for a uniform temperature rise $\Delta T_{UTR} = 100\ [K]$.

| $n$ | $\Delta T_{UTR} = 100\ [K]$ | | | | | | | | |
|---|---|---|---|---|---|---|---|---|---|
| | $\zeta = 0.00$ | | | $\zeta = 0.10$ | | | $\zeta = 0.20$ | | |
| | $\tilde{g} \neq 0$ | $\tilde{g} = 0$ | $\Delta_{\text{err}}[\%]$ | $\tilde{g} \neq 0$ | $\tilde{g} = 0$ | $\Delta_{\text{err}}[\%]$ | $\tilde{g} \neq 0$ | $\tilde{g} = 0$ | $\Delta_{\text{err}}[\%]$ |
| 1 | 0.98836 | 0.99405 | 0.57 | 0.98975 | 0.99559 | 0.59 | 0.99109 | 0.99712 | 0.60 |
| 3 | 0.98710 | 0.99219 | 0.51 | 0.98858 | 0.99375 | 0.52 | 0.99002 | 0.99530 | 0.53 |
| 5 | 0.98667 | 0.99155 | 0.49 | 0.98821 | 0.99313 | 0.50 | 0.98973 | 0.99471 | 0.50 |

**Table 4.22.** Coupled effects of porosity volume fraction, $\zeta$, material gradient index, $n$, and dimensionless gyration radious, $\tilde{g}$, on normalized linear fundamental flexural frequency of Clamped-Clamped (C-C) porous FG nanobeam assuming $\xi_1 = 0.5, \lambda_c = 0.01, \lambda_l = 0.01$ and $\Delta H = 0.1$ [wt. % $H_2O$] for a heat-conduction temperature rise corresponding to: $T_m = 350\ [K], T_c = 300\ [K]$.

| $n$ | $T_m = 350\ [K], T_c = 300\ [K]$ | | | | | | | | |
|---|---|---|---|---|---|---|---|---|---|
| | $\zeta = 0.00$ | | | $\zeta = 0.10$ | | | $\zeta = 0.20$ | | |
| | $\tilde{g} \neq 0$ | $\tilde{g} = 0$ | $\Delta_{\text{err}}[\%]$ | $\tilde{g} \neq 0$ | $\tilde{g} = 0$ | $\Delta_{\text{err}}[\%]$ | $\tilde{g} \neq 0$ | $\tilde{g} = 0$ | $\Delta_{\text{err}}[\%]$ |
| 1 | 0.99872 | 1.00452 | 0.58 | 0.99896 | 1.00491 | 0.59 | 0.99915 | 1.00531 | 0.61 |
| 3 | 0.99881 | 1.00400 | 0.52 | 0.99912 | 1.00439 | 0.52 | 0.99939 | 1.00479 | 0.54 |
| 5 | 0.99928 | 1.00393 | 0.46 | 0.99933 | 1.00433 | 0.50 | 0.99966 | 1.00473 | 0.50 |

**Table 4.23.** Coupled effects of porosity volume fraction, $\zeta$, material gradient index, $n$, and dimensionless gyration radious, $\tilde{g}$, on normalized linear fundamental flexural frequency of Clamped-Clamped (C-C) porous FG nanobeam assuming $\xi_1 = 0.5, \lambda_c = 0.01, \lambda_l = 0.01$ and $\Delta H = 0.1$ [wt. % $H_2O$] for a heat-conduction temperature rise corresponding to: $T_m = 400\ [K], T_c = 300\ [K]$.

| $n$ | $T_m = 400\ [K], T_c = 300\ [K]$ | | | | | | | | |
|---|---|---|---|---|---|---|---|---|---|
| | $\zeta = 0.00$ | | | $\zeta = 0.10$ | | | $\zeta = 0.20$ | | |
| | $\tilde{g} \neq 0$ | $\tilde{g} = 0$ | $\Delta_{\text{err}}[\%]$ | $\tilde{g} \neq 0$ | $\tilde{g} = 0$ | $\Delta_{\text{err}}[\%]$ | $\tilde{g} \neq 0$ | $\tilde{g} = 0$ | $\Delta_{\text{err}}[\%]$ |
| 1 | 0.99429 | 1.00006 | 0.58 | 0.99491 | 1.00082 | 0.59 | 0.99448 | 1.00159 | 0.71 |
| 3 | 0.99400 | 0.99915 | 0.52 | 0.99468 | 0.99991 | 0.52 | 0.99533 | 1.00068 | 0.53 |
| 5 | 0.99445 | 0.99908 | 0.46 | 0.99489 | 0.99985 | 0.50 | 0.99560 | 1.00063 | 0.50 |

Finally, nonlinear dimensionless natural frequencies of the porous FG nanobeam under investigation corresponding to the First-, Second-, and Third- Order approximate solutions are reported in the following Tables 4.24-4.32:

**Table 4.24.** Nonlinear dimensionless natural frequencies of porous FG clamped-clamped (C-C) nanobeam for $\xi_1 = 0.0$ in the case of First-Order Hamiltonian Approach.

| $\xi_1 = 0.0$ | $\mathcal{A}_w$ | $\Delta T_{UTR} = 0$ | | $\Delta T_{UTR} = 50$ | | $\Delta T_{UTR} = 100$ | |
|---|---|---|---|---|---|---|---|
| | | $\lambda_l = 0.0$ | $\lambda_l = 0.10$ | $\lambda_l = 0.0$ | $\lambda_l = 0.10$ | $\lambda_l = 0.0$ | $\lambda_l = 0.10$ |
| $\lambda_c = 0.1$ | 0.00 | 1.33333 | 1.15406 | 1.32613 | 1.14551 | 1.32070 | 1.13904 |
| | 0.01 | 1.33469 | 1.15575 | 1.32761 | 1.14769 | 1.32236 | 1.14117 |
| | 0.05 | 1.36706 | 1.19553 | 1.36270 | 1.19886 | 1.36164 | 1.19121 |
| | 0.10 | 1.46359 | 1.31211 | 1.46697 | 1.34630 | 1.47766 | 1.33554 |
| $\lambda_c = 0.2$ | 0.00 | 1.84414 | 1.58369 | 1.83894 | 1.57754 | 1.83504 | 1.57291 |
| | 0.01 | 1.84464 | 1.58430 | 1.83950 | 1.57821 | 1.83564 | 1.57364 |
| | 0.05 | 1.85680 | 1.59886 | 1.85269 | 1.59406 | 1.85004 | 1.59117 |
| | 0.10 | 1.89429 | 1.64355 | 1.89333 | 1.64262 | 1.89435 | 1.64471 |

**Table 4.25.** Nonlinear dimensionless natural frequencies of porous FG clamped-clamped (C-C) nanobeam for $\xi_1 = 0.5$ in the case of First-Order Hamiltonian Approach.

| $\xi_1 = 0.5$ | $\mathcal{A}_w$ | $\Delta T_{UTR} = 0$ | | $\Delta T_{UTR} = 50$ | | $\Delta T_{UTR} = 100$ | |
|---|---|---|---|---|---|---|---|
| | | $\lambda_l = 0.0$ | $\lambda_l = 0.10$ | $\lambda_l = 0.0$ | $\lambda_l = 0.10$ | $\lambda_l = 0.0$ | $\lambda_l = 0.10$ |
| $\lambda_c = 0.1$ | 0.00 | 1.12891 | 1.01093 | 1.12085 | 1.00166 | 1.11477 | 0.99464 |
| | 0.01 | 1.13040 | 1.01267 | 1.12250 | 1.00362 | 1.11666 | 0.99695 |
| | 0.05 | 1.16559 | 1.05373 | 1.16131 | 1.04952 | 1.16128 | 1.05087 |
| | 0.10 | 1.26930 | 1.17279 | 1.27499 | 1.18153 | 1.29082 | 1.20390 |
| $\lambda_c = 0.2$ | 0.00 | 1.23896 | 1.14585 | 1.23170 | 1.13789 | 1.22623 | 1.13187 |
| | 0.01 | 1.23965 | 1.14660 | 1.23247 | 1.13872 | 1.22711 | 1.13284 |
| | 0.05 | 1.25622 | 1.16447 | 1.25082 | 1.15865 | 1.24806 | 1.15590 |
| | 0.10 | 1.30663 | 1.21862 | 1.30650 | 1.21884 | 1.31137 | 1.22516 |

**Table 4.26.** Nonlinear dimensionless natural frequencies of porous FG clamped-clamped (C-C) nanobeam for $\xi_1 = 1.0$ in the case of First-Order Hamiltonian Approach.

| $\xi_1 = 1.0$ | $\mathcal{A}_w$ | $\Delta T_{UTR} = 0$ | | $\Delta T_{UTR} = 50$ | | $\Delta T_{UTR} = 100$ | |
|---|---|---|---|---|---|---|---|
| | | $\lambda_l = 0.0$ | $\lambda_l = 0.10$ | $\lambda_l = 0.0$ | $\lambda_l = 0.10$ | $\lambda_l = 0.0$ | $\lambda_l = 0.10$ |
| $\lambda_c = 0.1$ | 0.00 | 0.99999 | 0.91331 | 0.99115 | 0.90336 | 0.98444 | 0.89581 |
| | 0.01 | 1.00161 | 0.91514 | 0.99296 | 0.90544 | 0.98658 | 0.89832 |
| | 0.05 | 1.03951 | 0.95786 | 1.03544 | 0.95401 | 1.03662 | 0.95670 |
| | 0.10 | 1.14994 | 1.08052 | 1.15820 | 1.09195 | 1.17937 | 1.11968 |
| $\lambda_c = 0.2$ | 0.00 | 1.11740 | 0.94718 | 1.13331 | 0.93774 | 1.14511 | 0.93058 |
| | 0.01 | 1.11837 | 0.94804 | 1.13444 | 0.93872 | 1.14645 | 0.93176 |
| | 0.05 | 1.14139 | 0.96837 | 1.16110 | 0.96200 | 1.17811 | 0.95983 |
| | 0.10 | 1.21050 | 1.02932 | 1.24073 | 1.03137 | 1.27198 | 1.04266 |

**Table 4.27.** Nonlinear dimensionless natural frequencies of porous FG clamped-clamped (C-C) nanobeam for $\xi_1 = 0.0$ in the case of Second-Order Hamiltonian Approach.

| $\xi_1 = 0.0$ | $\mathcal{A}_w$ | $\Delta T_{UTR} = 0$ | | $\Delta T_{UTR} = 50$ | | $\Delta T_{UTR} = 100$ | |
|---|---|---|---|---|---|---|---|
| | | $\lambda_l = 0.0$ | $\lambda_l = 0.10$ | $\lambda_l = 0.0$ | $\lambda_l = 0.10$ | $\lambda_l = 0.0$ | $\lambda_l = 0.10$ |
| $\lambda_c = 0.1$ | 0.00 | 1.33333 | 1.15406 | 1.32613 | 1.14551 | 1.32070 | 1.13904 |
| | 0.01 | 1.33469 | 1.15575 | 1.32761 | 1.14769 | 1.32236 | 1.41117 |
| | 0.05 | 1.36699 | 1.19542 | 1.36263 | 1.19868 | 1.36154 | 1.19103 |
| | 0.10 | 1.46272 | 1.31073 | 1.46596 | 1.34421 | 1.47644 | 1.33352 |
| $\lambda_c = 0.2$ | 0.00 | 1.84414 | 1.58369 | 1.83894 | 1.57754 | 1.83504 | 1.57291 |
| | 0.01 | 1.84464 | 1.58430 | 1.83950 | 1.57821 | 1.83564 | 1.57364 |
| | 0.05 | 1.85679 | 1.59885 | 1.85268 | 1.59405 | 1.85003 | 1.59115 |
| | 0.10 | 1.89418 | 1.64338 | 1.89320 | 1.64241 | 1.89421 | 1.64447 |

**Table 4.28.** Nonlinear dimensionless natural frequencies of porous FG clamped-clamped (C-C) nanobeam for $\xi_1 = 0.5$ in the case of Second-Order Hamiltonian Approach.

| $\xi_1 = 0.5$ | $\mathcal{A}_w$ | $\Delta T_{UTR} = 0$ | | $\Delta T_{UTR} = 50$ | | $\Delta T_{UTR} = 100$ | |
|---|---|---|---|---|---|---|---|
| | | $\lambda_l = 0.0$ | $\lambda_l = 0.10$ | $\lambda_l = 0.0$ | $\lambda_l = 0.10$ | $\lambda_l = 0.0$ | $\lambda_l = 0.10$ |
| $\lambda_c = 0.1$ | 0.00 | 1.12891 | 1.01093 | 1.12085 | 1.00166 | 1.11477 | 0.99464 |
| | 0.01 | 1.13040 | 1.01267 | 1.12250 | 1.00362 | 1.11666 | 0.99695 |
| | 0.05 | 1.16550 | 1.05359 | 1.16199 | 1.04935 | 1.16133 | 1.05064 |
| | 0.10 | 1.26817 | 1.17121 | 1.27364 | 1.17962 | 1.28911 | 1.20143 |
| $\lambda_c = 0.2$ | 0.00 | 1.23896 | 1.14585 | 1.23170 | 1.13789 | 1.22623 | 1.13187 |
| | 0.01 | 1.23965 | 1.14660 | 1.23247 | 1.13872 | 1.22711 | 1.13284 |
| | 0.05 | 1.25620 | 1.16445 | 1.25080 | 1.15862 | 1.24802 | 1.15585 |
| | 0.10 | 1.30635 | 1.21828 | 1.30616 | 1.21842 | 1.31904 | 1.22461 |

**Table 4.29.** Nonlinear dimensionless natural frequencies of porous FG clamped-clamped (C-C) nanobeam for $\xi_1 = 1.0$ in the case of Second-Order Hamiltonian Approach.

| $\xi_1 = 0.0$ | $\mathcal{A}_w$ | $\Delta T_{UTR} = 0$ | | $\Delta T_{UTR} = 50$ | | $\Delta T_{UTR} = 100$ | |
|---|---|---|---|---|---|---|---|
| | | $\lambda_l = 0.0$ | $\lambda_l = 0.10$ | $\lambda_l = 0.0$ | $\lambda_l = 0.10$ | $\lambda_l = 0.0$ | $\lambda_l = 0.10$ |
| $\lambda_c = 0.1$ | 0.00 | 0.99999 | 0.91331 | 0.99115 | 0.90336 | 0.98444 | 0.89581 |
| | 0.01 | 1.00161 | 0.91514 | 0.99296 | 0.90544 | 0.98658 | 0.89832 |
| | 0.05 | 1.03939 | 0.95769 | 1.03529 | 0.95380 | 1.03641 | 0.95640 |
| | 0.10 | 1.14854 | 1.07872 | 1.15650 | 1.08974 | 1.17716 | 1.11674 |
| $\lambda_c = 0.2$ | 0.00 | 1.11740 | 0.94718 | 1.13331 | 0.93774 | 1.14511 | 0.93058 |
| | 0.01 | 1.11837 | 0.94804 | 1.13444 | 0.93872 | 1.14645 | 0.93176 |
| | 0.05 | 1.14135 | 0.96833 | 1.16105 | 0.96195 | 1.17804 | 0.95975 |
| | 0.10 | 1.20955 | 1.02882 | 1.24003 | 1.03073 | 1.27104 | 1.04178 |

**Table 4.30.** Nonlinear dimensionless natural frequencies of porous FG clamped-clamped (C-C) nanobeam for $\xi_1 = 0.0$ in the case of Third-Order Hamiltonian Approach.

| $\xi_1 = 0.0$ | $\mathcal{A}_w$ | $\Delta T_{UTR} = 0$ | | $\Delta T_{UTR} = 50$ | | $\Delta T_{UTR} = 100$ | |
|---|---|---|---|---|---|---|---|
| | | $\lambda_l = 0.0$ | $\lambda_l = 0.10$ | $\lambda_l = 0.0$ | $\lambda_l = 0.10$ | $\lambda_l = 0.0$ | $\lambda_l = 0.10$ |
| $\lambda_c = 0.1$ | 0.00 | 1.33333 | 1.15406 | 1.32613 | 1.14551 | 1.32070 | 1.13904 |
| | 0.01 | 1.33469 | 1.15575 | 1.32761 | 1.14769 | 1.32236 | 1.14117 |
| | 0.05 | 1.36699 | 1.19542 | 1.36262 | 1.19867 | 1.36154 | 1.19102 |
| | 0.10 | 1.46271 | 1.31070 | 1.46595 | 1.34416 | 1.47642 | 1.33347 |
| $\lambda_c = 0.2$ | 0.00 | 1.84414 | 1.58369 | 1.83894 | 1.57754 | 1.83504 | 1.57291 |
| | 0.01 | 1.84464 | 1.58430 | 1.83850 | 1.57821 | 1.83564 | 1.57364 |
| | 0.05 | 1.85679 | 1.59885 | 1.85268 | 1.59405 | 1.85003 | 1.59115 |
| | 0.10 | 1.89417 | 1.64337 | 1.89319 | 1.64241 | 1.89420 | 1.64446 |

**Table 4.31.** Nonlinear dimensionless natural frequencies of porous FG clamped-clamped (C-C) nanobeam for $\xi_1 = 0.5$ in the case of Third-Order Hamiltonian Approach.

| $\xi_1 = 0.5$ | $\mathcal{A}_w$ | $\Delta T_{UTR} = 0$ | | $\Delta T_{UTR} = 50$ | | $\Delta T_{UTR} = 100$ | |
|---|---|---|---|---|---|---|---|
| | | $\lambda_l = 0.0$ | $\lambda_l = 0.10$ | $\lambda_l = 0.0$ | $\lambda_l = 0.10$ | $\lambda_l = 0.0$ | $\lambda_l = 0.10$ |
| $\lambda_c = 0.1$ | 0.00 | 1.12891 | 1.01093 | 1.12085 | 1.00166 | 1.11477 | 0.99464 |
| | 0.01 | 1.13040 | 1.01267 | 1.12250 | 1.00362 | 1.11666 | 0.99695 |
| | 0.05 | 1.16550 | 1.05359 | 1.16199 | 1.04935 | 1.16113 | 1.05087 |
| | 0.10 | 1.26815 | 1.17117 | 1.27362 | 1.17958 | 1.28907 | 1.20390 |
| $\lambda_c = 0.2$ | 0.00 | 1.23896 | 1.14585 | 1.23170 | 1.13789 | 1.22623 | 1.13187 |
| | 0.01 | 1.23965 | 1.14660 | 1.23247 | 1.13872 | 1.22711 | 1.13284 |
| | 0.05 | 1.25620 | 1.16445 | 1.25080 | 1.15862 | 1.24802 | 1.15585 |
| | 0.10 | 1.30634 | 1.21827 | 1.30615 | 1.21841 | 1.31093 | 1.22460 |

**Table 4.32.** Nonlinear dimensionless natural frequencies of porous FG clamped-clamped (C-C) nanobeam for $\xi_1 = 1.0$ in the case of third-Order Hamiltonian Approach.

| $\xi_1 = 1.0$ | $\mathcal{A}_w$ | $\Delta T_{UTR} = 0$ | | $\Delta T_{UTR} = 50$ | | $\Delta T_{UTR} = 100$ | |
|---|---|---|---|---|---|---|---|
| | | $\lambda_l = 0.0$ | $\lambda_l = 0.10$ | $\lambda_l = 0.0$ | $\lambda_l = 0.10$ | $\lambda_l = 0.0$ | $\lambda_l = 0.10$ |
| $\lambda_c = 0.1$ | 0.00 | 0.99999 | 0.91331 | 0.99115 | 0.90336 | 0.98444 | 0.89581 |
| | 0.01 | 1.00161 | 0.91514 | 0.99296 | 0.90544 | 0.98658 | 0.89832 |
| | 0.05 | 1.03939 | 0.95769 | 1.03529 | 0.95380 | 1.03641 | 0.95640 |
| | 0.10 | 1.14851 | 1.07868 | 1.15646 | 1.08968 | 1.17711 | 1.11665 |
| $\lambda_c = 0.2$ | 0.00 | 1.11740 | 0.94718 | 1.13331 | 0.93774 | 1.14511 | 0.93058 |
| | 0.01 | 1.11837 | 0.94804 | 1.13444 | 0.93872 | 1.14645 | 0.97176 |
| | 0.05 | 1.14135 | 0.96833 | 1.16105 | 0.96195 | 1.17804 | 0.95975 |
| | 0.10 | 1.20954 | 1.02881 | 1.24002 | 1.03072 | 1.27103 | 1.04176 |

The main results of parametric analysis can be summarized as follows:

- *Influence of nonlocal parameter, gradient length parameter and mixture parameter.*

From Tables 4.6-4.17 and Tables 4.24-4.32, on one hand, it can be seen that an increase in the values of $\lambda_c$ results in an increase of the frequency ratio, $\widetilde{\omega}/\widetilde{\omega}_{loc}$ but on the other, it can be found that as $\lambda_l$ increases, the values of the aforementioned frequency ratio decrease. It is also possible to note that the ratio $\widetilde{\omega}/\widetilde{\omega}_{loc}$, decreases by increasing the mixture parameter $\xi_1$.

- *Influence of hygrothermal loads.*

From the numerical evidence of Tables 4.6-4.32, it is possible to underline that the values of the linear ( $\mathcal{A}_w = 0$) normalized fundamental flexural frequency based on local/nonlocal stress-driven hygrothermal gradient theory of elasticity decrease as the temperature rise increases. Furthermore, from the Tables 4.24-4.32, in the range of values here considered, an opposite trend is obtained for the normalized nonlinear ( $\mathcal{A}_w \neq 0$) fundamental flexural frequency as $\mathcal{A}_w$ and $\Delta T_{UTR}$ increase. Furthermore, for the cases studies examines, a uniform temperature rise always shows smaller values of the normalized fundamental flexural frequency than those obtained by heat-conduction.

- *Influence of material gradient index and porosity volume fraction.*

From Tables 4.18-4.23, it can be observed that in the case of a uniform temperature rise, an increase in the material gradient index always leads to a decrease in the values of the normalized fundamental flexural frequency. However, for the case of heat-conduction, a more general response is exhibited by the L/NStressGH model of elasticity. In particular, for small values of heat-conduction rise, as the material gradient index increases, the normalized fundamental flexural frequency increases. On the contrary, for high values of heat-conduction, it decreases. Furthermore, an increase in the porosity volume fraction always provides an increase in the normalized fundamental flexural frequency.

- *Influence of gyration radious.*

As reported in Tables 4.20-4.23, neglecting the gyration radious results in a slight overestimation of the normalized linear fundamental flexural frequency values, with an error consistently below 0.8% for the examined cases in this analysis.

- *Influence of Higher-Order Hamiltonian Approach.*

Finally, the nonlinear dimensionless natural frequencies of the porous FG nanobeam under investigation corresponding to the First-, Second-, and Third-order approximate solutions are summarized in Tables 4.24-4.32, varying the nonlinear oscillator amplitude in the set $\{0.0, 0.01, 0.05, 0.10\}$. From these tables, it can be seen that the aforementioned flexural frequency always increases as the amplitude of the nonlinear oscillator increases, while they decrease as the order of the Hamiltonian Approach increases. The above parametrical analysis assumes relevance in the study of the nonlinear vibrations of porous FG nanobeams because their behavior is influenced by the dimensionless term $\tilde{r}^2$, which is proportional to the ratio between the axial and the bending stiffness of the nanobeam cross-section, both depending on the porosity distribution of the structure of the nanobeam material and on the temperature increment and the material gradient index. Moreover, the term $\tilde{r}^2$ allows us to take into account the nonlinear response due to the mid-plane stretching effect.

### 4.4.5. Summary and conclusions

In this section, both linear and nonlinear dynamic behavior of a Bernoulli–Euler nano-beam made of a metal-ceramic functionally graded porous material in a hygrothermal environment, with von Kármán type nonlinearity, has been studied, employing the local/nonlocal stress-driven hygrothermal theory of elasticity (L/NStressGH). The free vibration analysis is carried out by considering a Clamped-Clamped (C-C) static scheme. The governing equations have been reduced to a nonlinear ordinary differential equation by using the Galerkin method. Then, the higher-order Hamiltonian approach to nonlinear oscillators was employed. In particular, the effects of several parameters on both the thermo-elastic material properties and the structural response of the FG nanobeams, such as the porosity volume fraction and the material gradient index, the nonlocal parameter, the gradient length parameter and the mixture parameter, the nonlinear oscillator amplitude, the gyration radious, as well as the hygrothermal loadings, have been investigated by using a Wolfram language code developed in Mathematica. Moreover, a comparison between the results of the present approach with those already available in current literature has been successfully presented.

In view of the numerical results obtained in the present study, the following main conclusions may be formulated:

- as nonlocal parameter increasing the normalized fundamental flexural frequencies increase, while an opposite is shown by the L/NStressGH theory when both the gradient length parameter and the mixture parameter are increased;
- on the one hand an increase in the temperature rise always leads to a decrease in the values of normalized linear fundamental flexural frequencies but on the other hand an opposite trend is obtained for the normalized nonlinear fundamental flexural frequencies as the temperature rise increases;
- in the case of a uniform temperature rise, an increase in the material gradient index always leads to a decrease in the values of the normalized fundamental flexural frequency. However, for the case of heat-conduction, a more general response is exhibited by the L/NStressGH model of elasticity. In particular, for small values of heat-conduction rise, as the material gradient index increases, the normalized fundamental flexural frequency increases. On the contrary, for high values of heat-conduction, it decreases;
- an increase in the porosity volume fraction always provides an increase in the normalized fundamental flexural frequency;
- neglecting the gyration radious results in a slight overestimation of the normalized linear fundamental flexural frequency values, with an error consistently below 0.8% for the examined cases in this analysis;
- the flexural frequency always increases as the amplitude of the nonlinear oscillator increases, while they decrease as the Order of the Hamiltonian Approach increases.

The results obtained in the study confirm that stress-driven local/non-local hygrothermal gradient formulations are capable of simulating both size-dependent softening and stiffening not only for static analysis but also for the dynamic response of the FG Bernoulli-Euler nanobeam with uniform internal porosity under severe thermal loads.

In conclusion, the proposed approach, based on L/NStressGH plays an important role in revealing stiffness-hardening or stiffness-softening mechanical and dynamic behaviors in small-scaled structures, especially in temperature-dependent porous FG nanobeams.

## Chapter 5

## On the combined effects of nonlocality and surface energy

As extensively discussed in previous chapters, nanostructures exhibit unique and remarkable properties due to their small size. A key feature is the gradual attenuation of interatomic forces regarding the overall geometric size of nanostructures [114], which requires the application of nonlocal elasticity theories presented in Section 3. In addition, the small size introduces another significant feature of nanostructures: a substantially increased surface-to-bulk ratio. The surface of a solid is a region of practically negligible thickness, characterized by an atomic arrangement and properties distinct from the bulk. Indeed, in a macroscopic solid, surface effects are typically neglected since the ratio between the surface region to bulk is insignificant. However, as illustrated in Figure 5.1, this surface-to-bulk ratio increases significantly as the size decreases.

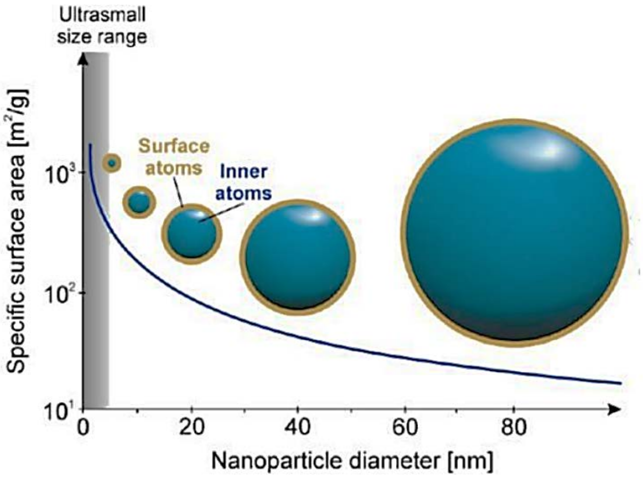

**Figure 5.1.** Increase in fraction of surface atoms as size of particle decreases. [115]

Furthermore, due to changes in the atomic environment, materials in the surface layer exhibit different behavior compared to bulk materials. Therefore, the energy of atoms close to the surface cannot be neglected, resulting in the formation of surface residual stresses and elastic properties distinct from those of the bulk material [116]. In support of this, various mechanical experiments have been conducted on nanobeams and nanoplates, revealing that the effective strength properties of nanostructures depend heavily on their size [117].

Therefore, for an optimal study of the structural response of nanostructures, it is necessary to use of nonlocal theories that take into account the significant contribution of surface effects. To analyze surface effects, several continuous theories have been formulated to describe the surface with different properties and constitutive laws compared to those of the bulk material. One of the earliest mathematical theories that incorporates surface effects was developed by Gurtin and Murdoch [118,119] for isotropic materials, based on rational principles of mechanics, and is commonly known as the Surface Elasticity Theory (SET). In this theory, the surface layer of a solid is modeled as a membrane with negligible thickness, perfectly adhered to the underlying bulk but endowed with different elastic properties and constitutive laws. The theory of surface elasticity has been extensively employed in the literature to investigate the static and dynamic response of nanostructures [120-139].

In the scientific literature, the surface elasticity theory is often combined with Eringen's purely nonlocal theory (EDM) and Lim's gradient theory (NStrainG) [122-129] to better predict surface effects and small-scale effects in the static and dynamic response of nanostructures. However, it is important to highlight that Gurtin and Murdoch's surface elasticity theory does not consider the flexural rigidity of the surface and, in some cases, as demonstrated in [130], may lead to deviations from atomistic simulations. To address this problem, Steigmann and Ogden in [131] proposed an extension of the surface elasticity theory that also incorporates flexural rigidity with a dependence on surface energy curvature. Both theories mentioned above are limited to local interactions between the surface and bulk, neglecting the nonlocal contribution [114]. Moreover, it has recently been demonstrated [127] that there is an intrinsic correlation between non-locality and surface elasticity, leading to what is referred to in the literature as the pre-coupling problem. Finally, Jiang et al. in [114] demonstrate the existence of an incompatibility problem between the two-dimensional settings in surface theories and the three-dimensional setting in local elasticity theory, creating difficulties in evaluating local interactions. To overcome these problems, they have developed a new model that couples Eringen's nonlocal theory and the Steigmann-

Ogden model through a new interpretation of surface parameters and restoring surface thickness through dependence on the curvature of surface energy.

However, as discussed earlier in Chapter 3, Eringen's elasticity model and Lim's gradient model provide a mathematically inconsistent approach for the study of static and dynamic analyses of nanobeams. In order to overcome these mathematical discrepancies, Penna in [132] combined Romano & Barretta's SDM model with Gurtin and Murdoch's surface elasticity theory, introducing the Surface Stress-Driven Model (SSDM) for the analysis of the bending behavior of functionally graded nanobeams with two types of cross-sections (rectangular and circular) subjected to a uniformly distributed load. This approach provided a well-posed mathematical model with a reasonable computational cost. Yang et al. in [133] combined non-local theories, N/LStressG and L/NStrainG, with surface elasticity theory to investigate the dynamic response of nanobeams.

Despite the simplifications mentioned earlier, the Surface Elasticity Theory (SET) continues to be widely used by researchers to understand surface effects in the study of the structural response of nanostructures. The use of this theory has allowed for the identification of particular and highly significant effects to fully comprehend the potential at the nanoscale. In particular, it has been observed that when the surface is modeled using positive elastic constants, such as the surface Young's modulus and surface residual stress, deformations decrease while critical load and natural frequency increase. Conversely, an opposite behavior is observed for negative elastic constants [132]. Chen et al. in [133] explained that surface stress depends on two components: the first is an intrinsic characteristic, namely surface residual stress, while the second depends on structural strain and hence surface elasticity. It is important to note that the surface elastic modulus in the second component can be either positive or negative since a surface cannot exist without the bulk, and the total energy (bulk and surface) must satisfy the positivity condition [134].

In this chapter, the novel approach proposed by Penna [132], based on the coupling of the stress-driven model [85] and surface elasticity theory [118,119], used for the bending analysis of functionally graded nanobeams under uniformly distributed loads, is first extended to analyze their response in the case of internal load discontinuities

(Section 5.1.) and then further extended to the study of cracked functionally graded nanobeams (Section 5.2.).

## 5.1. Bending analysis of functionally graded nanobeams with loading discontinuities

In the present paragraph, the surface stress-driven model [132], in which the stress-driven model and the surface elasticity theory are coupled, is enriched for the bending analysis of Bernoulli-Euler nanobeams with loading discontinuities. According to the procedure proposed by Vaccaro et al. in [132] and Barretta et al. in [133], continuity constitutive boundary conditions are needed at nanobeam internal point where loading discontinuity occurs. The paragraph is structured as follows. The problem formulation is summarized in Section 5.1.1. In 5.1.2. the equations that govern the problem of elastostatic bending in the presence of discontinuities are reported. In addition, the constitutive law and equations governing the problem of elastostatic bending in the presence of a discontinuity due to external loads are formulated in Section 5.1.3. Finally, the results of the parametric analysis are discussed in Section 5.1.4.

### 5.1.1. Problem formulation

Let us consider an FG straight nanobeam with length $L$ and a rectangular cross-section $\Sigma$ $(b \times h)$ made of a bulk volume ($B$), composed of a mixture of metal ($m$) and ceramic ($c$), and a thin surface layer ($S$) perfectly adhered to the bulk continuum (Figure 5.2).

According to the power-law distributions introduced by Shahab et al. in [128], the elastic modulus of the bulk material, denoted as $E^B = E^B(z)$, the surface elastic modulus, represented as $E^S = E^S(z)$, and the residual surface stress, indicated as $\tau^S = \tau^S(z)$, continuously vary in the transverse direction, $z$, as follows:

$$E^B(z) = E_m + (E_c - E_m)\left(\frac{1}{2} + \frac{z}{h}\right)^n \tag{5.1}$$

$$E^S(z) = \ E^S_m + (E^S_c \ - E^S_m)\left(\frac{1}{2}+\frac{z}{h}\right)^n \tag{5.2}$$

$$\tau^S(z) = \ \tau^S_m + (\tau^S_c \ - \tau^S_m)\left(\frac{1}{2}+\frac{z}{h}\right)^n \tag{5.3}$$

where $n$ denotes the gradient index of the FG material $(n \geq 0)$. The Poisson's ratio is here assumed to be constant $(\nu^B = \nu^S = \nu)$.

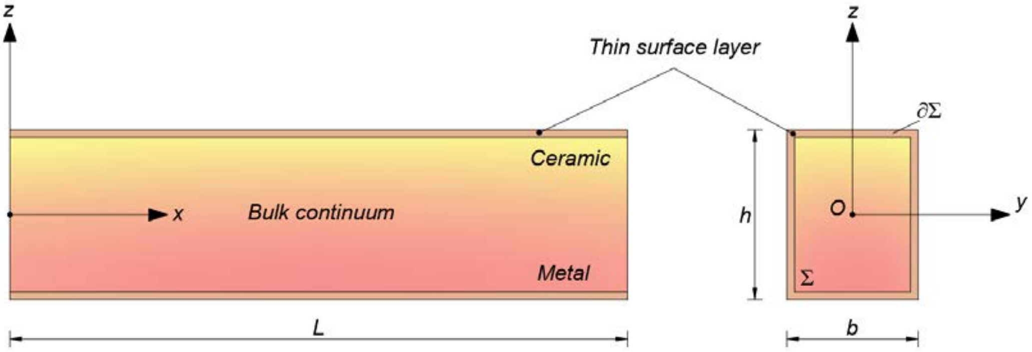

**Figure 5.2.** Coordinate system and configuration of the FG nanobeam: bulk continuum (mixture of ceramic and metal) and surface layer. [138]

The material properties of the FG material are listed in Table 5.1.

**Table 5.1.** Material parameters of metal (*m*) and ceramic (*c*). [137]

| Material | Parameters | Values | Unit |
|---|---|---|---|
| Ceramic | $E^B_c$ | 210 | [GPa] |
| | $E^S_c$ | -10.6543 | [N/m] |
| (Si) | $\tau^S_c$ | 0.6048 | [N/m] |
| Metal | $E^B_m$ | 70 | [GPa] |
| | $E^S_m$ | 5.1882 | [N/m] |
| (Al) | $\tau^S_m$ | 0.9108 | [N/m] |

The Cartesian components $u_x \ = u_x(x,z)$ and $u_z = u_z(x,z)$ of the displacement field of the FG nanobeam along $x$ and $z$ directions, respectively, in presence of a loading discontinuity at the point of abscissa $x = d$ (Figure 5.3) can be expressed as:

$$u_x = -z\frac{\partial w_1}{\partial x} \qquad u_z(x,z) = w_1 \qquad 0 \leq x \leq d \tag{5.4}$$

$$u_x = -z\frac{\partial w_2}{\partial x} \qquad u_z(x,z) = w_2 \qquad 0 \leq x \leq d \tag{5.5}$$

where $w_1 = w_1(x)$ and $w_2 = w_2(x)$ are the transverse displacements of the geometric center $O$ belonging to the first and the second part of the FG nanobeam, respectively.

The corresponding non-zero strain, $\varepsilon_x = \varepsilon_x(x,z)$, can be expressed, respectively, as:

$$\varepsilon_x = -z\frac{\partial^2 w_1}{\partial x^2} = -z\,\chi_1(x) \qquad 0 \leq x \leq d \tag{5.6}$$

$$\varepsilon_x = -z\frac{\partial^2 w_2}{\partial x^2} = -z\,\chi_2(x) \qquad 0 \leq x \leq d \tag{5.7}$$

being $\chi_i(x)$ the geometrical bending curvature ($i = 1,2$).

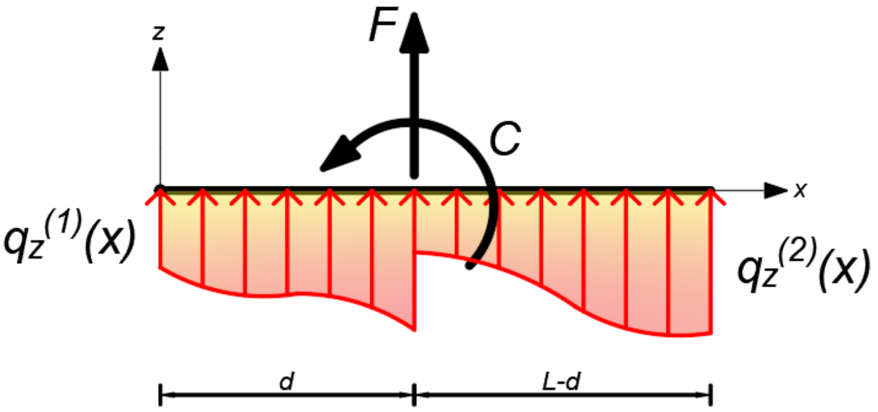

**Figure 5.3.** Geometry and loads of an FG nanobeam with loading discontinuities at the abscissa *d*. [138]

### 5.1.2. Governing equation

According to surface elasticity theory, the surface of the nanobeam is modelled as zero-thickness membrane perfectly bonded to the underlying material and the bulk continuum and surface layer are characterized by different stress states: a uniaxial stress state for the bulk, $\sigma_x^B = \sigma_x^B(x,z)$, and two stress state for the surface. $\sigma_x^S = \sigma_x^S(x,z)$ and $\tau_{zx}^S = \tau_{zx}^S(x,z)$, respectively. Furthermore, unlike classical Bernoulli-

Euler beam theory, the component of the bulk stress in transverse direction $z$, $\sigma_z^B = \sigma_z^B(x,z)$, which describes the surface layer and bulk interaction, is not negligible due to surface effects.

As described in [138] for a FG material in order to satisfy the surface equilibrium equations introduced by Gurtin and Murdoch it is necessary to assume that the $\sigma_z^B$ component to vary cubically along the nanobeam thickness according to the following equation:

$$\sigma_z^B = f(z)\left[-(\tau_c^S - \tau_m^S)\frac{\partial^2 w}{\partial x^2}\right] + \frac{1}{2}\left[(\tau_c^S - \tau_m^S)\frac{\partial^2 w}{\partial x^2}\right] \tag{5.8}$$

where

$$f(z) = z\left(\frac{z}{h}\right)\left[\left(\frac{z}{h}\right)^2 - \frac{3}{4}\right] \tag{5.9}$$

$$\mathrm{w} := \begin{cases} w_1 & 0 \le x < d \\ w_2 & d < x \le L \end{cases} \tag{5.10}$$

Note that a linear distribution for $\sigma_z^B$ is not adequate for FG nanobeams with high gradient in material properties for satisfying the surface equilibrium equations of Gurtin and Murdoch [118,119].

By manipulating Eq. 5.6 and Eq. 5.7, with Eq. 5.7 it is obtained:

$$\sigma_z^B = \left[\frac{f(z)}{z}(\tau_c^S + \tau_m^S) - \frac{1}{2\,z}(\tau_c^S - \tau_m^S)\right]\varepsilon_x \tag{5.11}$$

In accordance with the surface elasticity theory, the stress at point $x$ is proportional to the corresponding strain at the same point. Consequently, the bulk stress-strain relation can be expressed as:

$$\sigma_x^B = E^B\varepsilon_x + \nu\,\sigma_z^B \tag{5.12}$$

For the surface layer, the two relevant constitutive relations can be formulated as:

$$\sigma_x^S = \tau^S + E^S\varepsilon_x \tag{5.13}$$

$$\tau_{zx} = \tau^S\frac{\partial u_z}{\partial x} \tag{5.14}$$

The governing equations of the elastostatic bending problem for each part of the FG nanobeam are derived by using the virtual work principle, that can be expressed as:

$$\delta(U+W)=0 \tag{5.15}$$

The expression of the virtual strain energy, $\delta U$, is expressed as:

$$\begin{gathered}\delta U=\int_0^L\left(\int_\Sigma \sigma_x^B\,\delta\varepsilon_x d\Sigma+\oint_{\partial\Sigma}\sigma_x^S\,\delta\varepsilon_x d\sigma\right)dx+\int_0^L\oint_{\partial\Sigma}\tau_{zx}^S\frac{\partial^2\delta w}{\partial x^2}d\sigma dx=\\ -\int_0^L M\frac{\partial^2\delta w}{\partial x^2}dx+\int_0^L T^S\frac{\partial w}{\partial x}\frac{\partial\delta w}{\partial x}dx\end{gathered} \tag{5.16}$$

where

$$M=\int_\Sigma \sigma_x^B\,zd\Sigma+\oint_{\partial\Sigma}\sigma_x^S\,zd\sigma \tag{5.17}$$

$$T^S=\oint_{\partial\Sigma}\tau^S\,d\sigma \tag{5.18}$$

It can be noted that the quantity $T^S$ is a constant and for FG nanobeams with rectangular cross-section can be expressed as:

$$T^S=2\,b\,\tau_c^S+\frac{2h(n\,\tau_m^S+\tau_c^S)}{1+n} \tag{5.19}$$

For a homogenous material ($n=0$), $T^S$ becomes equal to $T^S=2(b+h)\tau_c^S$.

The expression of the virtual work, $\delta W$, done by external force, is expressed as:

$$\delta W=-\int_0^L q_z\,\delta w\,dx \tag{5.20}$$

By substituting Eq. 5.16 and Eq. 5.20 into Eq. 5.15 and applying the fundamental Lemma of variational calculus, the following governing equation for each part of the FG nanobeam:

$$\frac{\partial^2 M_1}{\partial x^2}+T^S\frac{\partial^2 w}{\partial x^2}+q_z^{(1)}=0 \qquad 0\le x\le d \tag{5.21}$$

$$\frac{\partial^2 M_2}{\partial x^2} + T^S \frac{\partial^2 w}{\partial x^2} + q_z^{(2)} = 0 \qquad d \le x \le L \tag{5.22}$$

The corresponding boundary conditions at the FG nanobeam ends ($x = 0,L$) can be chosen by specifying one element of each of the following two pairs of standard boundary conditions, SBCs (kinematic and static boundary conditions):

$$\left[\frac{\partial w_1}{\partial x}\right]_{x=0} = \left[\frac{\partial w_1^*}{\partial x}\right]_{x=0} \quad \text{or} \quad [M_1]_{x=0} = [M_1^*]_{x=0} \tag{5.23}$$

$$[w_1]_{x=0} = [w_1^*]_{x=0} \quad \text{or} \quad \left[\frac{\partial M_1}{\partial x} + T^S \frac{\partial w_1}{\partial x}\right]_{x=0} = [V_1^*]_{x=0} \tag{5.24}$$

$$\left[\frac{\partial w_2}{\partial x}\right]_{x=L} = \left[\frac{\partial w_2^*}{\partial x}\right]_{x=L} \quad \text{or} \quad [M_2]_{x=L} = [M_2^*]_{x=L} \tag{5.25}$$

$$[w_2]_{x=L} = [w_2^*]_{x=L} \quad \text{or} \quad \left[\frac{\partial M_2}{\partial x} + T^S \frac{\partial w_2}{\partial x}\right]_{x=L} = [V_2^*]_{x=L} \tag{5.26}$$

In addition, it is necessary to satisfy the internal compatibility boundary conditions (ICBs) at the abscissa *d:*

$$w_1(d) = w_2(d) \tag{5.27}$$

$$\frac{\partial w_1(d)}{\partial x} = \frac{\partial w_2(d)}{\partial x} \tag{5.28}$$

$$M_1(d) - C = M_2(d) \tag{5.29}$$

$$T_1(d) - F = T_2(d) \tag{5.30}$$

being $M_1^*, M_2^*$ and $V_1^*, V_2^*$ assigned moments and vertical forces acting at the nanobeam ends ($x = 0, L$), respectively, and $w_1^*, w_2^*$ an assigned vertical displacements at the nanobeam ends; $M_1$, $M_2$ , $T_1$, $T_2$ , $q_z^{(1)}$ and $q_z^{(2)}$ the bending moments, the shear stress and the transverse distributed loads associated to the first and second part of the FG nanobeam, respectively, and where $C$ and $F$ represent a concentrated couple and a concentrated force applied at the abscissa *d*.

### 5.1.3. Constitutive law (SSDM)

The bending curvature $\chi$ at a point of FG nanobeam at the abscissa $x$ in absence of concentrated loads is defined as the following integral convolution according to Penna in [132]:

$$\chi = \int_{0}^{L} \Phi_{L_c}(x-\xi, L_c)\left(-\frac{M(\xi)-M^{\tau}}{I_E^{*}}\right) d\xi \tag{5.31}$$

where $M$ is the bending moment, $\Phi_{L_c}$ represents an averaging kernel depending on the small-scale parameter $L_c$, and $I_E^{*}$ is the equivalent bending stiffness defined as:

$$\begin{aligned} I_E^{*} = & \int_{\Sigma} \left(E^{B} + \nu\left(\frac{f(z)}{z}(\tau_c^{S} + \tau_m^{S}) - \frac{1}{2\,z}(\tau_c^{S} - \tau_m^{S})\right)\right) z^{2} d\Sigma \\ & + \oint_{\partial\Sigma} E^{S} z^{2}\, d\sigma \end{aligned} \tag{5.32}$$

and

$$M^{\tau} = \oint_{\partial\Sigma} \tau^{S} z\, d\sigma \tag{5.33}$$

The extended form expressions of $I_E^{*}$ and $M^{\tau}$, for a rectangular cross-section, are respectively:

$$\begin{aligned} I_E^{*} = & \frac{1}{60(1+n)(2+n)(3+n)} h^{2}(30bE_c^{S}(1+n)(2+n)(3+n) \\ & + 15bE_c^{B}h(2+n+n^{2}) + 5bE_m^{B}hn(8+n(3+n)) \\ & + 10h(3E_c^{S}(2+n+n^{2}) + E_m^{S}n(8+n(3+n))) - 6b(1 \\ & + n)(2+n)(3+n)\nu(\tau_m^{S} + \tau_c^{S})) \end{aligned} \tag{5.34}$$

$$M^{\tau} = -\frac{h^{2}n(\mathrm{\tau}_{\mathrm{m}}^{\mathrm{S}} - \mathrm{\tau}_{\mathrm{c}}^{\mathrm{S}})}{(1+n)(2+n)} + bh\,\mathrm{\tau}_{\mathrm{c}}^{\mathrm{S}} \tag{5.35}$$

In the case of homogenous material ($n = 0$) Eq. 5.34 and Eq. 5.35 are reduce respectively to:

$$I_E^* = \frac{bh^3}{12} E_c^B - \frac{bh^2}{5} \nu \, \tau_c^S + \left( \frac{h^3}{6} + \frac{bh^2}{2} \right) E_c^S \tag{5.36}$$

$$M^\tau = bh \, \tau_c^S \tag{5.37}$$

Note that if the Poisson's effect is neglected, the expression of Eq. 5.36 coincide whit those given in [139].

In presence of a loading discontinuity and/or concentrated loads (force and couple) at an interior point of abscissa *d*, Eq. 5.31 can be rewritten as:

$$\chi_1 = \int_0^d \Phi_{L_c}(x - \xi, L_c) \left( -\frac{M_1(\xi) - M^\tau}{I_E^*} \right) d\xi \qquad 0 \le x \le d \tag{5.38}$$

$$\chi_2 = \int_d^L \Phi_{L_c}(x - \xi, L_c) \left( -\frac{M_2(\xi) - M^\tau}{I_E^*} \right) d\xi \qquad d \le x \le L \tag{5.39}$$

As it is well-known, by choosing a special function kernel $\Phi_{L_c}$ equal to:

$$\Phi_{L_c}(x, L_c) = \frac{1}{2L_c} \exp\left( -\frac{|x|}{L_c} \right) \tag{5.40}$$

the convolutions in Eqs. 5.38 and 5.39 are equivalent to following second-order differential equations according to Penna in [132]:

$$\left( 1 - L_c^2 \frac{\partial^2}{\partial x^2} \right) \chi_1 = -\frac{M_1 - M^\tau}{I_E^*} \qquad 0 \le x \le d \tag{5.41}$$

$$\left( 1 - L_c^2 \frac{\partial^2}{\partial x^2} \right) \chi_2 = -\frac{M_2 - M^\tau}{I_E^*} \qquad d \le x \le L \tag{5.42}$$

if and only if the conventional constitutive boundary conditions (CBCs) of the stress-driven nonlocal theory [85] and continuity constitutive boundary conditions (CCBCs) introduced by Vaccaro et al. in [140] e Barretta et al. in [141] are satisfied:

$$\frac{\partial \chi_1(0)}{\partial x} - \frac{1}{L_c}\chi_1(0) = 0 \tag{5.43}$$

$$\chi_1(d) = \chi_2(d) \tag{5.44}$$

$$\frac{\partial \chi_1(d)}{\partial x} = \frac{\partial \chi_2(d)}{\partial x} \tag{5.45}$$

$$\frac{\partial \chi_2(L)}{\partial x} + \frac{1}{L_c}\chi_2(L) = 0 \tag{5.46}$$

By manipulating Eqs. 5.41 and 5.42, the expressions of the stress-driven nonlocal resultant moments incorporating surface effects can be obtained as:

$$M_1 = -I_E^*\frac{\partial^2 w_1}{\partial x^2} + I_E^* L_c^2\frac{\partial^4 w_1}{\partial x^4} + M^\tau \qquad 0 \leq x \leq d \tag{5.47}$$

$$M_2 = -I_E^*\frac{\partial^2 w_2}{\partial x^2} + I_E^* L_c^2\frac{\partial^4 w_2}{\partial x^4} + M^\tau \qquad d \leq x \leq L \tag{5.48}$$

Finally, by substituting Eq. 5.47 and 5.48 into Eq. 5.21 and 5.22, respectively, the governing equations incorporating surface energy effect in terms of transverse displacement for the first and the second part of an inflected FG nanobeam are obtained as:

$$I_E^* L_c^2\frac{\partial^6 w_1}{\partial x^6} - I_E^*\frac{\partial^4 w_1}{\partial x^4} + T^S\frac{\partial^2 w_1}{\partial x^2} + q_z^{(1)} = 0 \qquad 0 \leq x \leq d \tag{5.49}$$

$$I_E^* L_c^2\frac{\partial^6 w_2}{\partial x^6} - I_E^*\frac{\partial^4 w_2}{\partial x^4} + T^S\frac{\partial^2 w_2}{\partial x^2} + q_z^{(1)} = 0 \qquad d \leq x \leq L \tag{5.50}$$

with the corresponding constitutive and constitutive continuity boundary conditions (Eqs. 5.43-5.46) in conjunction with the standard and compatibility boundary conditions (Eqs. 5.23-5.30). Now, by introducing the following dimensionless quantities:

$$\tilde{x} = \frac{x}{L} \qquad \tilde{w} = \frac{w}{L} \qquad \tilde{w}_1^* = \frac{w_1^*}{L} \qquad \tilde{w}_2^* = \frac{w_2^*}{L} \qquad \tilde{d} = \frac{d}{L}$$

$$\tilde{V}^* = \frac{V^* L^2}{I_E^*} \qquad \tilde{M}^* = \frac{M^* L}{I_E^*} \qquad \tilde{q}_z^{(1)} = \frac{q_z^{(1)} L^3}{I_E^*} \qquad \tilde{q}_z^{(2)} = \frac{q_z^{(2)} L^3}{I_E^*} \qquad \theta = \frac{T^S L^2}{I_E^*} \tag{5.51}$$

$$\widetilde{M}^{\tau}=\frac{M^{\tau}L}{I_E^{*}}\qquad \lambda_c=\frac{L_c}{L}\qquad \tilde{C}=\frac{C\,L}{I_E^{*}}\qquad \tilde{F}=\frac{F\,L^2}{I_E^{*}}$$

the dimensionless governing equations incorporating surface energy effect of the bending problem for the two parts of the FG nanobeam can be formulated as follow:

$$\lambda_c^2\frac{\partial^6\widetilde{w}_1}{\partial\tilde{x}^6}-\frac{\partial^4\widetilde{w}_1}{\partial\tilde{x}^4}+\theta\frac{\partial^2\widetilde{w}_1}{\partial\tilde{x}^2}+\tilde{q}_z^{(1)}=0\qquad 0\le\tilde{x}\le\tilde{d}\qquad (5.52)$$

$$\lambda_c^2\frac{\partial^6\widetilde{w}_2}{\partial\tilde{x}^6}-\frac{\partial^4\widetilde{w}_2}{\partial\tilde{x}^4}+\theta\frac{\partial^2\widetilde{w}_2}{\partial\tilde{x}^2}+\tilde{q}_z^{(2)}=0\qquad \tilde{d}\le\tilde{x}\le 1\qquad (5.53)$$

with the following boundary conditions in terms of dimensionless transverse displacements:

- SBCs

$$\left[\frac{\partial\widetilde{w}_1}{\partial\tilde{x}}\right]_{\tilde{x}=0}=\left[\frac{\partial\widetilde{w}_1^{*}}{\partial\tilde{x}}\right]_{\tilde{x}=0}\quad\text{or}\quad \left[\widetilde{M}_1\right]_{x=0}=\left[\widetilde{M}\right]_{x=0}\qquad (5.54)$$

$$[\widetilde{w}_1]_{\tilde{x}=0}=[\widetilde{w}_1^{*}]_{x=0}\quad\text{or}\quad \left[\frac{\partial\widetilde{M}_1}{\partial x}+\theta\frac{\partial\widetilde{w}_1}{\partial x}\right]_{x=0}=[\tilde{V}^{*}]_{x=0}\qquad (5.55)$$

$$\left[\frac{\partial\widetilde{w}_2}{\partial\tilde{x}}\right]_{\tilde{x}=L}=\left[\frac{\partial\widetilde{w}_2^{*}}{\partial\tilde{x}}\right]_{\tilde{x}=1}\quad\text{or}\quad \left[\widetilde{M}_2\right]_{\tilde{x}=1}=\left[\widetilde{M}\right]_{\tilde{x}=1}\qquad (5.56)$$

$$[\widetilde{w}_2]_{\tilde{x}=L}=[\widetilde{w}_2^{*}]_{\tilde{x}=1}\quad\text{or}\quad \left[\frac{\partial\widetilde{M}_2}{\partial\tilde{x}}+\theta\frac{\partial\widetilde{w}_2}{\partial\tilde{x}}\right]_{\tilde{x}=1}=[\tilde{V}^{*}]_{\tilde{x}=1}\qquad (5.57)$$

- ICBCs

$$\widetilde{w}_1(\tilde{d})=\widetilde{w}_2(\tilde{d})\qquad (5.58)$$

$$\frac{\partial\widetilde{w}_1(\tilde{d})}{\partial\tilde{x}}=\frac{\partial\widetilde{w}_2(\tilde{d})}{\partial\tilde{x}}\qquad (5.59)$$

$$\widetilde{M}_1(\tilde{d})-\tilde{C}=M_2(\tilde{d})\qquad (5.60)$$

$$\tilde{T}_1(\tilde{d})-\tilde{F}=\tilde{T}_2(\tilde{d})\qquad (5.61)$$

- CBCs

$$\frac{\partial^3\widetilde{w}_1(0)}{\partial\tilde{x}^3}-\frac{1}{\lambda_c}\frac{\partial^2\widetilde{w}_1(0)}{\partial\tilde{x}^2}=0\qquad (5.62)$$

$$\frac{\partial^3 \widetilde{w}_2(1)}{\partial \tilde{x}^3}+\frac{1}{\lambda_c}\frac{\partial^2 \widetilde{w}_2(1)}{\partial \tilde{x}^2}=0 \tag{5.63}$$

- CCBCs

$$\frac{\partial^2 \widetilde{w}_1(\tilde{d})}{\partial \tilde{x}^2}=\frac{\partial^2 \widetilde{w}_2(\tilde{d})}{\partial \tilde{x}^2} \tag{5.64}$$

$$\frac{\partial^3 \widetilde{w}_1(\tilde{d})}{\partial \tilde{x}^3}=\frac{\partial^3 \widetilde{w}_2(\tilde{d})}{\partial \tilde{x}^3} \tag{5.65}$$

being

$$\widetilde{M}_1=-\frac{\partial^2 \widetilde{w}_1}{\partial \tilde{x}^2}+\lambda_c^2\frac{\partial^4 \widetilde{w}_1}{\partial \tilde{x}^4}+\widetilde{M}^\tau \qquad 0\le \tilde{x}\le \tilde{d} \tag{5.66}$$

$$\widetilde{M}_2=-\frac{\partial^2 \widetilde{w}_2}{\partial \tilde{x}^2}+\lambda_c^2\frac{\partial^4 \widetilde{w}_2}{\partial \tilde{x}^4}+\widetilde{M}^\tau \qquad \tilde{d}\le \tilde{x}\le 1 \tag{5.67}$$

$$\tilde{T}_1=-\frac{\partial^3 \widetilde{w}_1}{\partial \tilde{x}^3}+\lambda_c^2\frac{\partial^5 \widetilde{w}_1}{\partial \tilde{x}^5}+\theta\frac{\partial \widetilde{w}_1}{\partial \tilde{x}} \qquad 0\le \tilde{x}\le \tilde{d} \tag{5.68}$$

$$\tilde{T}_2=-\frac{\partial^3 \widetilde{w}_2}{\partial \tilde{x}^3}+\lambda_c^2\frac{\partial^5 \widetilde{w}_2}{\partial \tilde{x}^5}+\theta\frac{\partial \widetilde{w}_2}{\partial \tilde{x}} \qquad \tilde{d}\le \tilde{x}\le 1 \tag{5.69}$$

### 5.1.4. Results and discussion

In this paragraph, the results of a parametric analysis are presented to show the effectiveness of the surface stress-drivel model (SSDM) for the study of the bending behavior of a straight Bernoulli-Euler FG nanobeam, with length *L=10 nm*, $b=h=0.1L$, in presence of discontinuous loads.

In order to validate the proposed SSDM model, a numerical analysis has been carried out for a Simply-Supported (S-S) FG nanobeam by considering three different loading configurations: *(i)* a non-uniform distributed load $\left(q_z^{(1)}=0.1\frac{N}{m}\ for\ 0\le x<d\,, q_z^{(2)}=10\frac{N}{m}\ for\ d\le x<l\right)$, *(ii)* a concentrated force at the abscissa *d* $(F=10\ nN)$ and *(iii)* a concentrated couple at the abscissa $d$ $(C=100\ nNnm)$ in terms of dimensionless deflection. The obtained numerical results have been always

compared to those derived by employing the Stress-Driven Model (SDM) without considering surface energy effects.

In Figures 5.4-5.6 the curves of the non-dimensional deflections corresponding to the SSDM (continuous) and SDM (dashed) are plotted for each statical scheme by setting $\lambda_c \in \{0.10, 0.30, 0.50\}$ and $n \in \{1, 2\}$ and show the combined effects of the nonlocal parameter, $\lambda_c$, of the surface energy and of the material gradient index, $n$, on the bending behavior of the FG nanobeams.

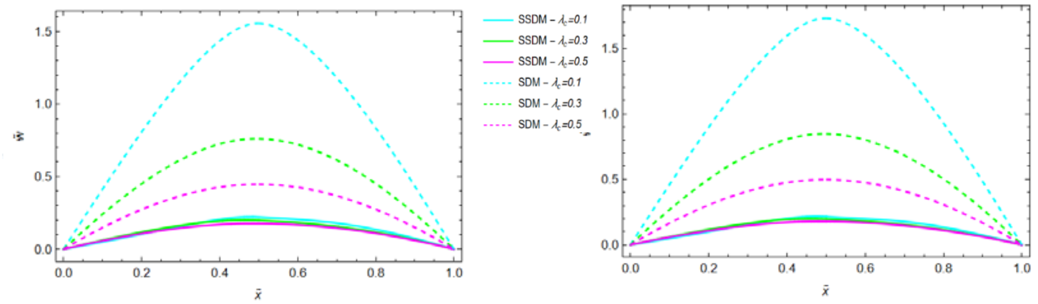

(a) (b)

**Figure 5.4.** Combined effects of the nonlocal parameter, $\lambda_c$, the surface energy and the material gradient index, k, on non-dimensional deflection, $\tilde{w}$, of a Simply-Supported (S-S) FG nanobeam subjected to a transverse discontinuous distributed load for both SSDM and SDM models of elasticity for *n =1* (a) and *n =2* (b).

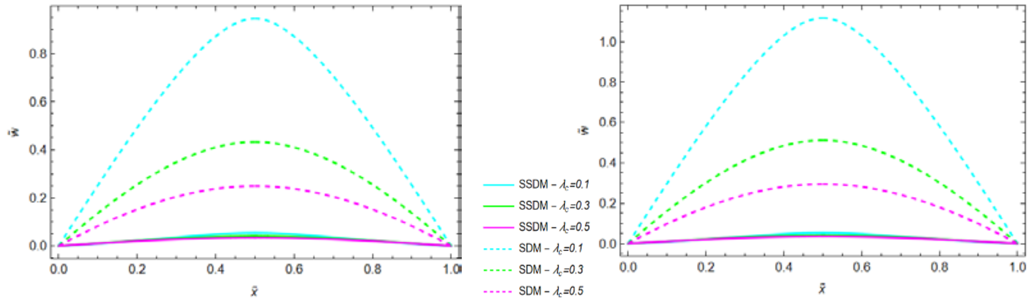

(a) (b)

**Figure 5.5.** Combined effects of the nonlocal parameter, $\lambda_c$, the surface energy and the material gradient index, k, on non-dimensional deflection, $\tilde{w}$, of a Simply-Supported (S-S) FG nanobeam subjected to a concentrated load for both SSDM and SDM models of elasticity for *n =1* (a) and *n =2* (b).

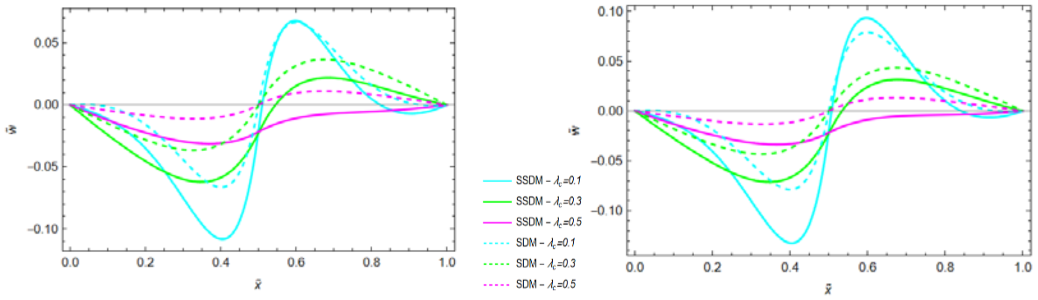

(a) (b)

**Figure 5.6.** Combined effects of the nonlocal parameter, $\lambda_c$, the surface energy and the material gradient index, k, on non-dimensional deflection, $\tilde{w}$, of a Simply-Supported (S-S) FG nanobeam subjected to a concentrated couple for both SSDM and SDM models of elasticity for *n=1* (a) and *n=2* (b).

### 5.1.5. Summary and conclusions

The main outcomes of the present section may be summarized as follows:

- the effective surface parameters $(E^S, \tau^S)$ depend on the variation of the material gradient, k, as well as on those of the bulk volume;
- as the value of the nonlocal parameter increases, the value of the deflection decreases both for the SSDM (with surface energy effects) model and for the SDM model (without surface energy effects);
- the values of the SSDM deflections evaluated in presence of surface effects are always lower than those obtained by the SDM model (without surface energy effects).

In conclusion, the novel proposed surface stress-driven model, which combine the stress-driven formulation of elasticity with the surface elasticity theory, is here extended in order to analyses the coupled effects of the nonlocal parameter, $\lambda_c$, the surface energy and the material gradient index, $n$, on the bending response of Bernoulli-Euler FG nanobeams with internal load discontinuities such as a non-uniform distributed load and/or a concentrated force or couple at an internal point of the nanobeam axis.

## 5.2. Application of SSDM theory of elasticity for the study of the bending response of FG cracked nanobeams

The Surface Stress-Driven Model (SSDM) recently proposed by Penna in [132] for uncracked FG nanobeams, in which the stress-driven model and the surface elasticity theory are coupled, is here enriched for the bending analysis of Bernoulli-Euler FG cracked nanobeams.

As is well known, the presence of cracks in structures and nanostructures has a significant effect on their mechanical and stiffness properties. Many researchers are studying the static and dynamic response of cracked structures [142-158]. In particular, the study of the static and dynamic responses of cracked beams can be developed by using both 2-D and 3-D numerical analysis based on the Finite Element Method. In literature, several simplified methods have been also proposed, which lead to lower computational efforts. For example, in the model proposed by Christides and Barr [142], as well as in the one by Shen and Pierre [143,144] a crack function representing the perturbation in the stress field induced by the rotational discontinuity is considered. Other simplified theories assume that a cracked beam is composed of two segments connected by a rotational spring whose stiffness can be related to the length of the crack using the Fracture Mechanics Theory [145-152]. The rotational hinge model assumes a linear elastic response of the beam material and neglects any interactions with other parts of the structure. Furthermore, the model does not account for the potential effects of local stresses, stress concentration and crack propagation. Its validity depends largely on the geometry of the crack and provides good results when the crack dimension is very small or negligible in size compared to the total length of the beam. Therefore, despite the simplifications made to the rotational hinge model, it can be used since, within the previously mentioned hypotheses, it provides an estimate of the effect of cracks through simple analysis models.

The present paragraph is structured as follows. The problem formulation is summarized in Section 5.2.1. In Section 5.2.2. is reported the constitutive law and the nonlocal governing equations of the elastostatic bending problem in the presence of a discontinuity due to a crack. Results of the parametric analysis are discussed in Section 5.3. Some closing remarks are given in Section 5.4.

### 5.2.1. Problem formulation

Let us consider an FG straight nanobeam with length $L$ and a rectangular cross-section $\Sigma$ $(b \times h)$ made of a bulk volume ($B$), composed of a mixture of metal ($m$) and ceramic ($c$), and a thin surface layer ($S$) perfectly adhered to the bulk continuum (Figure 5.7).

According to the power law distributions proposed by Shahab et al. in [128], the bulk elastic modulus of elasticity, $E^B = E^B(z)$, the surface modulus of elasticity, $E^S = E^S(z)$ and the residual surface stress, $\tau^S = \tau^S(z)$, continuously vary along transverse direction, $z$, as described in Eqs. 5.1-5.3.

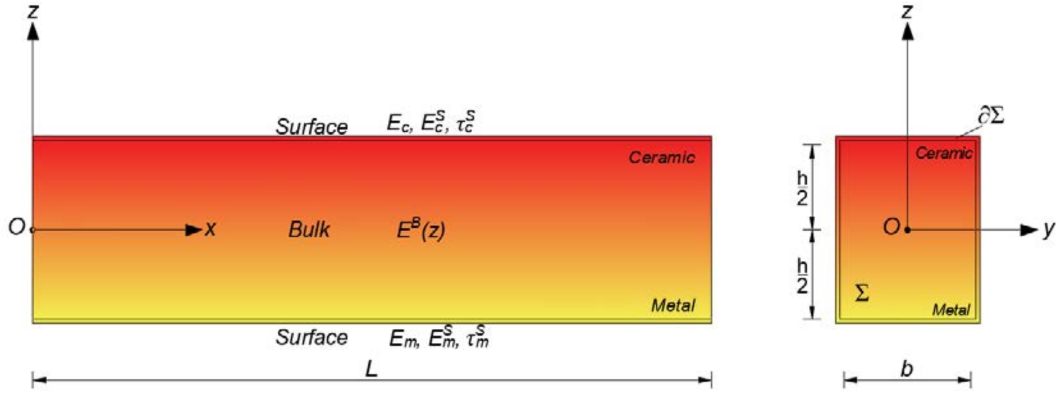

**Figure 5.7.** Coordinate system and configuration of the FG nanobeam: bulk continuum (mixture of ceramic and metal) and surface layer.

Let us suppose that the FG nanobeam presents a crack of depth $a$ at the abscissa $x = d$ which divides the nanobeam into two parts $\boldsymbol{B_1}$ and $\boldsymbol{B_2}$ respectively (Figure 5.8). Therefore, the Cartesian components $u_x = u_x(x,z)$ and $u_z = u_z(x,z)$ of the displacement field of the FG nanobeam along $x$ and $z$ directions, respectively, can be expressed as:

$$u_x = -z\frac{\partial w_1}{\partial x} \qquad u_z(x,z) = w_1 \qquad x \in [0,d] \tag{5.70}$$

$$u_x = -z\frac{\partial w_2}{\partial x} \qquad u_z(x,z) = w_2 \qquad x \in [d,L] \tag{5.71}$$

where $w_1(x)$ and $w_2(x)$ are the transverse displacements of the geometric center O belonging to the first and the second part of the FG nanobeam, respectively.

The corresponding non-zero strain, $\varepsilon_x = \varepsilon_x(x,z)$, can be expressed, respectively, as:

$$\varepsilon_x = -z\frac{\partial^2 w_1}{\partial x^2} = -z\,\chi_1(x) \qquad x \in [0,d] \tag{5.72}$$

$$\varepsilon_x = -z\frac{\partial^2 w_2}{\partial x^2} = -z\,\chi_2(x) \qquad x \in [d,L] \tag{5.73}$$

being $\chi_i(x)$ the geometrical bending elastic curvature ($i = 1{,}2$).

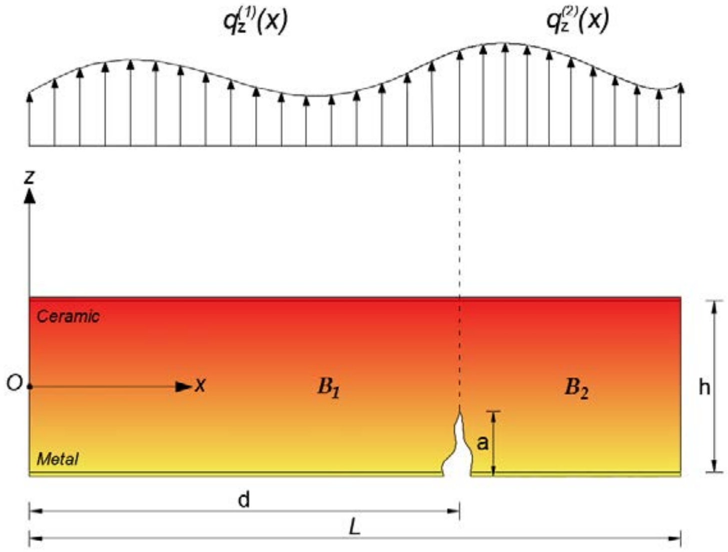

**Figure 5.8.** FG nanobeam with discontinuities (a crack) at the abscissa $x = d$.

By repeating the same steps done in the previous paragraph, applying the principle of virtual work, it is possible to obtain the following governing equations for each part of the FG nanobeam:

$$\frac{\partial^2 M_1}{\partial x^2} + T^S\frac{\partial^2 w}{\partial x^2} + q_z^{(1)} = 0 \qquad x \in [0,d] \tag{5.74}$$

$$\frac{\partial^2 M_2}{\partial x^2} + T^S\frac{\partial^2 w}{\partial x^2} + q_z^{(2)} = 0 \qquad x \in [d,L] \tag{5.75}$$

with the corresponding standard boundary conditions previously defined in Eqs. 5.23-5.26. As said before, it is also necessary to satisfy the following internal compatibility boundary conditions (ICBs) at the abscissa *d:*

$$w_1(d) = w_2(d) \tag{5.76}$$

$$\frac{\partial w_1(d)}{\partial x} = \frac{\partial w_2(d)}{\partial x} \tag{5.77}$$

$$M_1(d) = M_2(d) \tag{5.78}$$

$$T_1(d) = T_2(d) \tag{5.79}$$

being $M_1 = M_1(x)$, $M_2 = M_2(x)$, $T_1 = T_1(x)$, $T_2 = T_2(x)$, $q_z^{(1)} = q_z^{(1)}(x)$ and $q_z^{(2)} = q_z^{(2)}(x)$ the bending moments, the shear stress and the transverse distributed loads associated to the first and second part of the FG nanobeam, respectively. Moreover, the quantity $T^S$ was previously defined in Eq. 5.18.

### 5.2.2. Constitutive law

This section is divided in two parts: the first one presents an extension of the novel approach proposed by Penna in [124], in order to study the size-dependent bending response of FG cracked nanobeams in case of discontinuities; in the second part, the modeling of a cracked FG nanobeam with discontinuity is discussed in depth.

Now, we recall the differential constitutive law introduced by Penna in [124] for uncracked FG nanobeams:

$$\chi = \int_0^L \Phi_{L_c}(x-\xi, L_c)\left(-\frac{M(\xi)-M^\tau}{I_E^*}\right)d\xi \qquad x \in [0, L] \tag{5.80}$$

where $M$ is the bending moment, $\Phi_{L_c}$ represents an averaging kernel (Eq. 5.40) depending on the small-scale parameter, $L_c = \lambda_c L$, which describes the nonlocal effects and is function of nonlocal parameter, $\lambda_c$, while $I_E^*, M^\tau$ are the quantity previously defined in Eq. 5.32 and Eq. 5.33, respectively.

Due to the presence of a crack at an interior point of abscissa $d$, the assemblage domain $[0, L]$ is partitioned into two parts $[0, d]$ and $[d, L]$ (with $[0, L] = [0, d] \cup [d, L]$, and Eq. 5.80 can be rewritten as:

$$\chi = \int_0^L \Phi_{L_c}(x-\xi, L_c)\left(-\frac{M(\xi)-M^\tau}{I_E^*}\right)d\xi = \begin{cases} \chi_1(x), & x \in [0, d] \\ \chi_2(x), & x \in [d, L] \end{cases} \tag{5.81}$$

**Remark 5.1.** *By assuming that the nonlocal effects in one subdomain are reflected only in that subdomain, the elastic curvature* $\chi$*, as expressed by Eq. 5.83, results in being the unique solution of a constitutive differential problem with conventional constitutive boundary conditions* [85] *applied to the boundaries of the two subdomains. Hence, the constitutive continuity boundary conditions introduced in* [140,141] *are not necessary.*

Consequently, the constitutive problem is described by the equivalent system of second-order differential equations:

$$\left(1 - L_c^2\frac{\partial^2}{\partial x^2}\right)\chi_1 = -\frac{M_1 - M^\tau}{I_E^*} \qquad x \in [0, d] \tag{5.82}$$

$$\left(1 - L_c^2\frac{\partial^2}{\partial x^2}\right)\chi_2 = -\frac{M_2 - M^\tau}{I_E^*} \qquad x \in [d, L] \tag{5.83}$$

if and only if the two pairs of conventional constitutive boundary conditions (CBCs) of the stress-driven nonlocal theory [85] are satisfied at the two nanobeams ends ($[0, d] \cup [d, L]$):

$$\frac{\partial \chi_1(0)}{\partial x} - \frac{1}{L_c}\chi_1(0) = 0 \tag{5.84}$$

$$\frac{\partial \chi_1(d)}{\partial x} + \frac{1}{L_c}\chi_1(d) = 0 \tag{5.85}$$

$$\frac{\partial \chi_2(d)}{\partial x} - \frac{1}{L_c}\chi_2(d) = 0 \tag{5.86}$$

$$\frac{\partial \chi_2(L)}{\partial x} + \frac{1}{L_c}\chi_2(L) = 0 \tag{5.87}$$

Now, repeating the steps performed in the previous paragraph, the dimensionless governing equations incorporating the surface energy effects in terms of transverse displacement for the first and second parts of an inflected cracked FG nanobeam are obtained as:

$$\lambda_c^2\frac{\partial^6\widetilde{w}}{\partial\tilde{x}^6}-\frac{\partial^4\widetilde{w}}{\partial\tilde{x}^4}+\theta\frac{\partial^2\widetilde{w}}{\partial\tilde{x}^2}+\tilde{q}_z^{(1)}=0 \qquad \tilde{x}\in\left[0,\tilde{d}\right] \tag{5.88}$$

$$\lambda_c^2\frac{\partial^6\widetilde{w}}{\partial\tilde{x}^6}-\frac{\partial^4\widetilde{w}}{\partial\tilde{x}^4}+\theta\frac{\partial^2\widetilde{w}}{\partial\tilde{x}^2}+\tilde{q}_z^{(2)}=0 \qquad \tilde{x}\in\left[\tilde{d},1\right] \tag{5.89}$$

with the corresponding dimensionless conventional constitutive boundary conditions:

$$\frac{\partial^3\widetilde{w}_1(0)}{\partial\tilde{x}^3}-\frac{1}{\lambda_c}\frac{\partial^2\widetilde{w}_1(0)}{\partial\tilde{x}^2}=0 \tag{5.90}$$

$$\frac{\partial^3\widetilde{w}_1\left(\tilde{d}\right)}{\partial\tilde{x}^3}+\frac{1}{\lambda_c}\frac{\partial^2\widetilde{w}_1\left(\tilde{d}\right)}{\partial\tilde{x}^2}=0 \tag{5.91}$$

$$\frac{\partial^3\widetilde{w}_2\left(\tilde{d}\right)}{\partial\tilde{x}^3}-\frac{1}{\lambda_c}\frac{\partial^2\widetilde{w}_2\left(\tilde{d}\right)}{\partial\tilde{x}^2}=0 \tag{5.92}$$

$$\frac{\partial^3\widetilde{w}_2(1)}{\partial\tilde{x}^3}+\frac{1}{\lambda_c}\frac{\partial^2\widetilde{w}_2(1)}{\partial\tilde{x}^2}=0 \tag{5.93}$$

In conjunction with the dimensionless standard and internal compatibility boundary conditions (Eqs. 5.54-5.61).

### 5.2.3. Cracked FG nanobeam modeling

Let us consider a crack in the FG nanobeam located at a distance d from origin of axes ($x=0$). As already said, the cracked FG nanobeam is here modelled as two nanobeams (***B₁*** and ***B₂***) connected by a rotational elastic spring characterized by a flexibility constant denoted by $C_m$ (Figure 5.9).

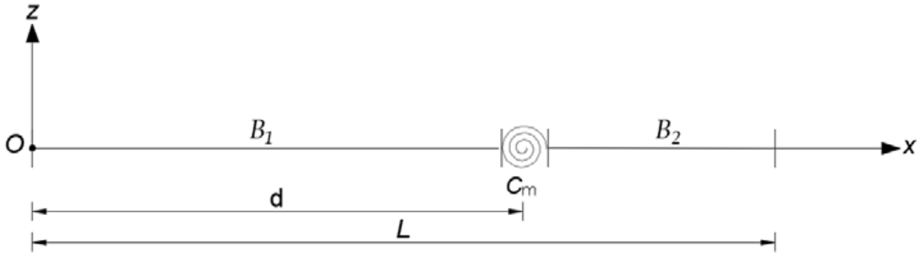

**Figure 5.9.** Model of the cracked FG nanobeam.

The method proposed by Freund and Herrmann in [47] and followed by other authors in [148-153] assumes that the discontinuity in the slope, $\Delta\emptyset$, depends on the flexibility constant.

Consequently, Eq. 5.77, can be rewritten as:

$$\Delta\emptyset = \frac{\partial w_2(d)}{\partial x} - \frac{\partial w_1(d)}{\partial x} = C_m \frac{\partial^2 w_1(d)}{\partial x^2} \tag{5.94}$$

in which the spring flexibility constant $C_m$ can be calculated by:

$$C_m = \frac{h}{I_E^*}\Theta(\bar{\alpha}, cross - section\ geometry) \tag{5.95}$$

where $I_E^*$ is the equivalent bending stiffness of the un-cracked nanobeam and $\Theta(\bar{\alpha})$ is a function depending on the crack ratio $\bar{\alpha} = \frac{a}{h}$ and on the nanobeam cross-section geometry. The function $\Theta(\bar{\alpha})$ can be evaluated by using the Fracture Mechanics Theory and, in the case of a rectangular or square cross-section, can be expressed as [158]:

$$\Theta(\bar{\alpha}) = 2\left(\frac{\bar{\alpha}}{1-\bar{\alpha}}\right)(5{,}93 - 19{,}69\bar{\alpha} + 37{,}14\bar{\alpha}^2 - 35{,}84\bar{\alpha}^3 + 13{,}12\bar{\alpha}^4) \tag{5.96}$$

The boundary condition related to the jump in the bending slope, $\widetilde{\Delta\emptyset}$, in terms of dimensionless deflection, can be rewritten as:

$$\widetilde{\Delta\emptyset} = \frac{\partial \tilde{w}_2(\tilde{d})}{\partial \tilde{x}} - \frac{\partial \tilde{w}_1(\tilde{d})}{\partial \tilde{x}} = \mathcal{K}\frac{\partial^2 \tilde{w}_1(\tilde{d})}{\partial \tilde{x}^2} \tag{5.97}$$

where

$$\mathcal{K} = \frac{h}{L}\Theta(\bar{\alpha}) \tag{5.98}$$

The other kinematic conditions to satisfy are the continuity of displacements, the continuity of the bending moments and of the shear forces:

$$\widetilde{w}_1(\tilde{d}) = \widetilde{w}_2(\tilde{d}) \tag{5.99}$$

$$\widetilde{M}_1(\tilde{d}) = \widetilde{M}_2(\tilde{d}) \tag{5.100}$$

$$\tilde{T}_1(\tilde{d}) = \tilde{T}_2(\tilde{d}) \tag{5.101}$$

### 5.2.4. Applications

In this paragraph, the results of a parametric analysis are presented to show the effectiveness of the surface stress-drivel model (SSDM) for the study of the bending behavior of a cracked Bernoulli-Euler FG nanobeam, with length $L$=10nm and $b = h = 0.1L$. The material properties of the FG nanobeam are listed in Table 5.1.

The analysis has been carried out for three different boundary conditions at the ends of the FG nanobeam: Simply-Supported (S-S), Clamped-Clamped (C-C) and Clamped-Pinned (C-P), under a uniformly distributed load $\left(q_z^{(1)} = q_z^{(2)} = \text{const} = 10\frac{nN}{nm}\right)$ across the complete span, assuming that FG nanobeam presents a crack at the abscissa $x = d = \frac{L}{2}$.

For each example, the SSDM (continuous line) and SDM (dashed curves) of the non-dimensional deflections, illustrated in Figures 5.10-5.12 for $\lambda_c = 0.10$ and $\bar{\alpha} \in \{0.25,\ 0.50,\ 0{,}75\}$, show the combined effects of the nonlocal parameter, $\lambda_c$, the surface energy, the material gradient index, $n$, and the crack ratio, $\alpha$, on the static behavior of the cracked FG nanobeam.

In addition, for both SSDM and SDM, Tables 5.2-5.4 collect the dimensionless midpoint deflection, $\widetilde{w}\left(\frac{1}{2}\right)$, for three values of crack ratio, $\bar{\alpha} = \{0.25, 0.50, 0.75\}$, varying $n$ and $\lambda_c$ in the sets {0, 1, 2} and {$0.00^+$, 0.02, 0.04, 0.06, 0.08, 0.10}, respectively.

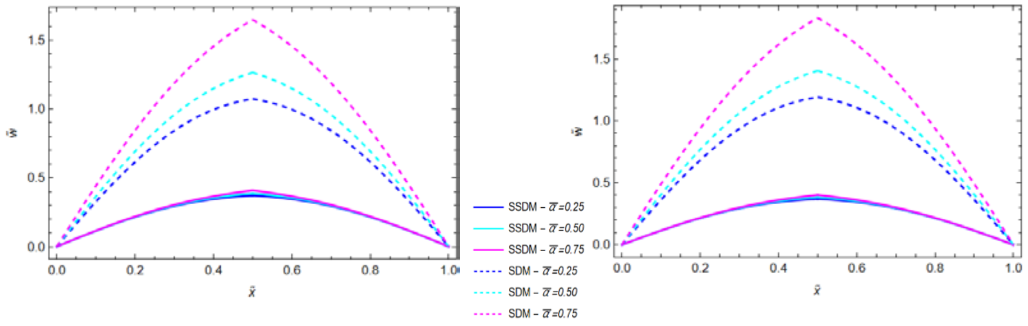

(a) (b)

**Figure 5.10.** Combined effects of the nonlocal parameter, $\lambda_c$, the surface energy, the material gradient index, $k$, and the crack ratio, a, on the non-dimensional deflection, $\tilde{w}$, of a Simply-Supported (S-S) cracked FG nanobeam subjected to a uniformly transverse distributed load for both SSDM and SDM models of elasticity for $n=1$ (a) and $n=2$ (b).

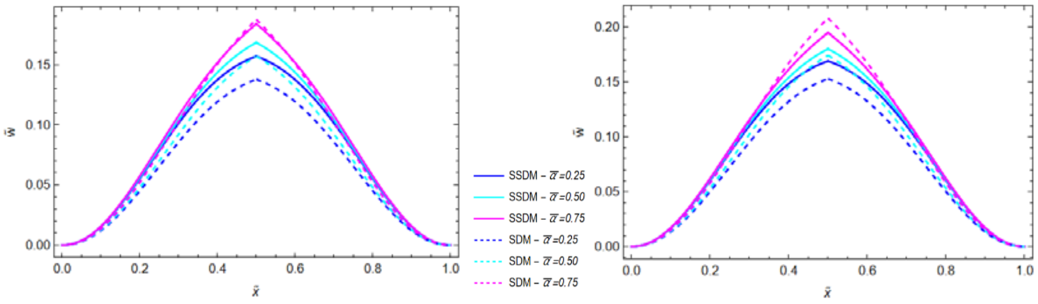

(a) (b)

**Figure 5.11.** Combined effects of the nonlocal parameter, $\lambda_c$, the surface energy, the material gradient index, $k$, and the crack ratio, a, on the non-dimensional deflection, $\tilde{w}$, of a Doubly-Clamped (C-C) cracked FG nanobeam subjected to a uniformly transverse distributed load for both SSDM and SDM models of elasticity for $n=1$ (a) and $n=2$ (b).

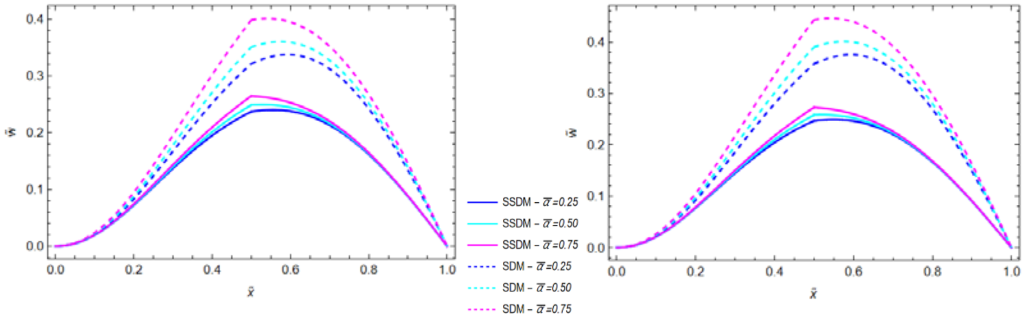

(a) (b)

**Figure 5.12.** Combined effects of the nonlocal parameter, $\lambda_c$, the surface energy, the material gradient index, *k*, and the crack ratio, a, on the non-dimensional deflection, $\tilde{w}$, of a Clamped-Pinned (C-P) cracked FG nanobeam subjected to a uniformly transverse distributed load for both SSDM and SDM models of elasticity for *n=1* (a) and *n=2* (b).

**Table 5.2.** Dimensionless midpoint deflection of (S-S) FG nanobeam vs. nonlocal parameter $\lambda_c$, varying $n$ in the set (0, 1, 2), for three different values of the crack ratio $\bar{\alpha} = \{0.25, 0.50, 0.75\}$.

| $\lambda_c$ | | $\bar{\alpha}$ = 0.25 | | | $\bar{\alpha}$ = 0.50 | | | $\bar{\alpha}$ = 0.75 | | |
|---|---|---|---|---|---|---|---|---|---|---|
| | | $n = 0$ | $n = 1$ | $n = 2$ | $n = 0$ | $n = 1$ | $n = 2$ | $n = 0$ | $n = 1$ | $n = 2$ |
| $0.00^+$ | SDM | 1.08527 | 1.62598 | 1.80743 | 1.35829 | 2.04009 | 2.26776 | 1.91151 | 2.87101 | 3.19140 |
| | SSDM | 0.39417 | 0.39441 | 0.38861 | 0.41387 | 0.40506 | 0.39722 | 0.43632 | 0.41596 | 0.40577 |
| 0.02 | SDM | 0.87673 | 1.31681 | 1.46376 | 1.01415 | 1.52321 | 1.69319 | 1.28987 | 1.93734 | 2.15353 |
| | SSDM | 0.37201 | 0.38120 | 0.37789 | 0.38440 | 0.39247 | 0.38720 | 0.41207 | 0.40548 | 0.39779 |
| 0.04 | SDM | 0.83662 | 1.25656 | 1.39679 | 0.97271 | 1.46097 | 1.62400 | 1.24578 | 1.87111 | 2.07991 |
| | SSDM | 0.36765 | 0.37913 | 0.37612 | 0.37435 | 0.39122 | 0.38654 | 0.41205 | 0.40691 | 0.39971 |
| 0.06 | SDM | 0.79531 | 1.19452 | 1.32782 | 0.92921 | 1.39563 | 1.55137 | 1.19787 | 1.79915 | 1.99992 |
| | SSDM | 0.36273 | 0.37658 | 0.37415 | 0.36203 | 0.39007 | 0.38590 | 0.41107 | 0.40779 | 0.40094 |
| 0.08 | SDM | 0.75414 | 1.13269 | 1.25909 | 0.88504 | 1.32930 | 1.47764 | 1.14769 | 1.72378 | 1.91614 |
| | SSDM | 0.35743 | 0.37377 | 0.37197 | 0.34890 | 0.38858 | 0.38496 | 0.40939 | 0.40824 | 0.40180 |
| 0.10 | SDM | 0.71425 | 1.07277 | 1.19248 | 0.84152 | 1.26393 | 1.40498 | 1.09690 | 1.64749 | 1.83134 |
| | SSDM | 0.35182 | 0.37068 | 0.36953 | 0.33585 | 0.38670 | 0.39369 | 0.40703 | 0.40819 | 0.40223 |

**Table 5.3.** Dimensionless midpoint deflection of (C-C) FG nanobeam vs. nonlocal parameter $\lambda_c$, varying $n$ in the set (0, 1, 2), for three different values of the crack ratio $\bar{\alpha} = \{0.25, 0.50, 0.75\}$.

| $\lambda_c$ | | $\bar{\alpha}$ = 0.25 | | | $\bar{\alpha}$ = 0.50 | | | $\bar{\alpha}$ = 0.75 | | |
|---|---|---|---|---|---|---|---|---|---|---|
| | | $n = 0$ | $n = 1$ | $n = 2$ | $n = 0$ | $n = 1$ | $n = 2$ | $n = 0$ | $n = 1$ | $n = 2$ |
| $0.00^+$ | SDM | 0.19642 | 0.29501 | 0.32793 | 0.22524 | 0.33830 | 0.37606 | 0.26686 | 0.40081 | 0.44553 |
| | SSDM | 0.18518 | 0.22951 | 0.23914 | 0.19675 | 0.23793 | 0.24638 | 0.20982 | 0.24653 | 0.25356 |
| 0.02 | SDM | 0.15630 | 0.23475 | 0.26095 | 0.17360 | 0.26704 | 0.28984 | 0.20207 | 0.30350 | 0.33737 |
| | SSDM | 0.16128 | 0.20724 | 0.21811 | 0.15303 | 0.21526 | 0.22596 | 0.18349 | 0.22595 | 0.23486 |
| 0.04 | SDM | 0.13812 | 0.20745 | 0.23060 | 0.15457 | 0.23215 | 0.25806 | 0.18144 | 0.27251 | 0.30292 |
| | SSDM | 0.14881 | 0.19449 | 0.20563 | 0.12327 | 0.20381 | 0.21425 | 0.17346 | 0.21587 | 0.22513 |
| 0.06 | SDM | 0.12095 | 0.18166 | 0.20193 | 0.13631 | 0.20473 | 0.22757 | 0.16120 | 0.24212 | 0.26914 |
| | SSDM | 0.13626 | 0.18182 | 0.19340 | 0.09726 | 0.19209 | 0.20306 | 0.16209 | 0.20555 | 0.21543 |
| 0.08 | SDM | 0.10536 | 0.15825 | 0.17591 | 0.11945 | 0.17940 | 0.19942 | 0.14210 | 0.21343 | 0.23725 |
| | SSDM | 0.12404 | 0.16922 | 0.18122 | 0.07684 | 0.18026 | 0.19178 | 0.15043 | 0.19488 | 0.20547 |
| 0.10 | SDM | 0.09168 | 0.13770 | 0.15306 | 0.10443 | 0.15684 | 0.17435 | 0.12477 | 0.18740 | 0.20832 |
| | SSDM | 0.11243 | 0.15682 | 0.16912 | 0.06141 | 0.16837 | 0.18036 | 0.13874 | 0.18382 | 0.19508 |

**Table 5.4.** Dimensionless midpoint deflection of (C-P) FG nanobeam vs. nonlocal parameter $\lambda_c$, varying $n$ in the set (0, 1, 2), for three different values of the crack ratio $\overline{\alpha} = \{0.25, 0.50, 0.75\}$.

| $\lambda_c$ |  | $\overline{\alpha} = 0.25$ |  |  | $\overline{\alpha} = 0.50$ |  |  | $\overline{\alpha} = 0.75$ |  |  |
|---|---|---|---|---|---|---|---|---|---|---|
|  |  | $n = 0$ | $n = 1$ | $n = 2$ | $n = 0$ | $n = 1$ | $n = 2$ | $n = 0$ | $n = 1$ | $n = 2$ |
| $0.00^+$ | SDM | 0.39058 | 0.58663 | 0.65210 | 0.45068 | 0.67690 | 0.75244 | 0.54313 | 0.81576 | 0.90679 |
|  | SSDM | 0.26403 | 0.29796 | 0.30255 | 0.27845 | 0.30728 | 0.31037 | 0.29477 | 0.31681 | 0.31812 |
| 0.02 | SDM | 0.31931 | 0.47959 | 0.53311 | 0.35220 | 0.52898 | 0.58802 | 0.40833 | 0.61329 | 0.68173 |
|  | SSDM | 0.23924 | 0.27833 | 0.28749 | 0.23399 | 0.28743 | 0.29283 | 0.26748 | 0.29900 | 0.30285 |
| 0.04 | SDM | 0.29084 | 0.43683 | 0.48558 | 0.32063 | 0.48158 | 0.53532 | 0.37086 | 0.55702 | 0.61918 |
|  | SSDM | 0.22746 | 0.26829 | 0.27550 | 0.20326 | 0.27838 | 0.28462 | 0.25714 | 0.29144 | 0.29614 |
| 0.06 | SDM | 0.26316 | 0.39526 | 0.43937 | 0.28959 | 0.43495 | 0.48349 | 0.33358 | 0.50102 | 0.55693 |
|  | SSDM | 0.21541 | 0.25812 | 0.26617 | 0.17351 | 0.26906 | 0.27624 | 0.24587 | 0.28340 | 0.28914 |
| 0.08 | SDM | 0.23726 | 0.35635 | 0.39612 | 0.26023 | 0.39085 | 0.43446 | 0.29794 | 0.44749 | 0.49743 |
|  | SSDM | 0.20320 | 0.24763 | 0.25655 | 0.14816 | 0.25916 | 0.26736 | 0.23358 | 0.27444 | 0.28315 |
| 0.10 | SDM | 0.21383 | 0.32117 | 0.35701 | 0.23347 | 0.35066 | 0.38979 | 0.26530 | 0.39846 | 0.44293 |
|  | SSDM | 0.19111 | 0.23691 | 0.24663 | 0.12762 | 0.24871 | 0.25788 | 0.22060 | 0.26449 | 0.27262 |

## 5.2.5. Results and discussion

Several computational experiments have been carried out to investigate the size-dependent behavior due to the nature of nonlocal elasticity and surface effects. In particular, a Wolfram language code in Mathematica was written to carry out the parametric investigation for different boundary conditions including Simply-Supported, Doubly-Clamped and Clamped-Pinned conditions. Different materials, with different material gradient index, were used to study the effects of surface elastic constants on the bending behavior of the FG nanobeams. Moreover, a parametric investigation of the bending response for cracked FG nanobeams is presented by varying the nonlocal parameter and the material gradient index for both SDM and SSDM model.

The main outcomes of the present study can be summarized as follows:

- as the nonlocal parameter increases, a stiffening nonlocal behavior has been observed, with and without surface effects, for all static boundary conditions considered;
- as the material gradient index increases, a softening response always occurs for the SDM model. However, the modified static boundary conditions introduced to incorporate surface energy effects result in a more general bending behavior, depending on the coupled effects of the nonlocal parameter and the material gradient index, as well as on the crack ratio;
- when the crack ratio increases, the value of the dimensionless midpoint deflection increases for both SSDM and SDM model;

In conclusion, the results obtained in this study show that the proposed approach is capable of describing the static behavior of Bernoulli-Euler functionally graded nanobeams in presence of crack and represent a valuable reference point for engineers and researchers.

# Conclusions

The research conducted in this thesis has addressed the study of nonlocal elasticity theories, which represent an important theoretical framework for understanding and analyzing the behavior of elastic materials on a small-scale, particularly in nanostructures. The growing interest in nanoscience, nanoengineering and nanotechnology has made the development of coherent nonlocal formulations essential to address the challenges posed by such structures, where long-range interactions cannot be neglected.

The thesis explored the theoretical foundations of nonlocal elasticity theories, highlighting how these theories provide a more complete and accurate framework for describing the behavior of elastic materials on a small-scale. In particular, it has been demonstrated that these theories are particularly useful in nanostructures, where nonlocal and surface effects play a predominant role in the mechanical behavior of materials.

Another area of interest within the thesis was functionally graded materials, which represent an innovative solution to address complex challenges in the field of materials engineering. It was examined how controlled variations of physical and chemical properties within a single component can lead to materials with extraordinary performance. Furthermore, micromechanical and physical models have been applied to consider how the thermos-elastic properties of a material are affected by temperature.

A significant contribution of this research is the proposed one-dimensional approach for modeling cracks in a functionally graded nanobeam. This model considers not only the nonlocal effect but also the influence of surface effects, thus providing a more accurate understanding of the behavior of nanostructures with defects.

In summary, this thesis provides a comprehensive overview of nonlocal elasticity theories, highlighting the challenges and opportunities that these theories present. It also highlights the crucial role of nonlocal theories in the engineering and materials science of the future. The work carried out represents a significant contribution to the understanding and application of these theories in a rapidly evolving context such as that of nanostructures and functionally graded materials.

# Bibliography

[1] Feynman R. Eng Sci 1960;23.

[2] Taniguchi N. On the Basic Concept of Nano-Technology. Proc. Intl. Conf. Prod. Eng. Tokyo. Part II. Japan Society of Precision Engineering. 1974.

[3] Alagarasi, A. Chapter – Introduction to nanomaterials

[4] https://euon.echa.europa.eu/it/general-information

[5] Tawfik A. Saleh. Nanomaterials: Classification, properties, and environmental toxicities. Environmental Technology & Innovation 20 (2020) 101067

[6] L. Giorgi, E. Salernitano. Produzione di nanomateriali-tecnologie chimiche e fisiche - n. 1-2 Gennaio-Aprile 2015 - Spazio aperto

[7] Andrea Li Bassi. Nanotecnologie e Nanomateriali.

[8] Khan, Y.; Sadia, H.; Ali Shah, S.Z.; Khan, M.N.; Shah, A.A.; Ullah, N.; Ullah, M.F.; Bibi, H.; Bafakeeh, O.T.; Khedher, N.B.; et al. Classification, Synthetic, and Characterization Approaches to Nanoparticles, and Their Applications in Various Fields of Nanotechnology: A Review. Catalysts 2022, 12, 1386. https://doi.org/ 10.3390/catal12111386

[9] Aslam, A.A.; Aslam, A.A.; Aslam, M.S.; Quazi, S. An Overview on Green Synthesis of Nanomaterials and Their Advanced Applications in Sustainable Agriculture. Preprints 2022, 2022020315. https://doi.org/10.20944/preprints202202.0315.v1

[10] Kaizar Hossain & Shaik Rameeja. Importance of Nanotechnology in Civil Engineering. European Journal of Sustainable Development (2015), 4, 1, 161-166 ISSN: 2239-5938. Doi: 10.14207/ejsd.2015.v4n1p161

[11] Sanchez, Florence, and Konstantin Sobolev. "Nanotechnology in concrete--a review." Construction and Building Materials Nov. 2010.

[12] Mohan, Prem. "Civil Engineering Seminar Topics: Significance Of Nanotechnology In Construction Engineering.".p., 17 Sept. 2011.

[13] Valentina Rognoli, Laura Anselmi, Sofia Duarte. Ricerca di nuovi materiali: efficienza, sicurezza e sostenibilità nell'ambito del design. Manifacturing. 2011.

[14] Adam Drazin and Susanne Küchler (eds.) 2015. The social life of materials: studies in materials and society. London and New York: Bloomsbury. 301 pp. Pb.: £24.99. ISBN: 978-1-4725-9264-4.

[15] Rasheedat Modupe Mahamood, Esther Titilayo Akinlabi. Functionally Graded Materials. Topics in Mining, Metallurgy and Materials Engineering Series Editor: Carlos P. Bergmann. Springer.

[16] M. B. Bever, P. E. Duwez (1970). On Gradient Composites. Preliminary Reports, Memoranda and Technical Notes of the ARPA Materials Summer Conference, 117–140.

[17] M. Shen, M.B. Bever (1972). Gradients in polymeric materials. J. Mater. Sci, 7 (7), 741-746.

[18] Koizumi, M. F. G. M. (1997). FGM activities in Japan. Composites Part B: Engineering, 28(1-2), 1-4.

[19] Bassiouny Saleh, Jinghua Jiang, Reham Fathi, Tareq Al-hababi, Qiong Xu, Lisha Wang, Dan Song, Aibin Ma, 30 Years of functionally graded materials: An overview of manufacturing methods, Applications and Future Challenges, Composites Part B: Engineering, Volume 201, 2020, 108376, ISSN 1359-8368,H ttps://doi.org/10.1016/j.compositesb.2020.108376.

[20] Koizumi, M., Niino, M.: Overview of FGM research in Japan. MRS Bull. 20(1995), 19–24(1995)

[21] Amira SADGUI. Modeling of Functionally Graded structures behavior. PhD Thesis (2022).

[22] R. Mahamood, TC Jen, S. Akinlabi, S. Hassan, M. Shatalov, E. Murashkin, E. Akinlabi. (2021) Functionally Graded Materials: An Introduction. In Functionally Graded Materials (FGMs) Fabrication, Properties, Applications, and Advancements, 1-10. CRC Press.

[23] Y. Miyamoto, W. A. Kaysser, B. H. Rabin, A. Kawasaki, R. G. Ford (Eds.), Functionally Graded Materials: design, processing and applications. (Springer US, Boston (MA), 1999).

[24] S. K. Sarangi (2021). Modeling and Analysis of Smart Functionally Graded Structures. In Functionally Graded Materials (FGMs), 139-168. CRC Press.

[25] Chi Zhang, Fei Chen, Zhifeng Huang, Mingyong Jia, Guiyi Chen, Yongqiang Ye, Yaojun Lin, Wei Liu, Bingqing Chen, Qiang Shen, Lianmeng Zhang, Enrique J. Lavernia. Additive manufacturing of functionally graded materials: A review, Materials Science and Engineering: A, Volume 764, 2019, 138209, ISSN 0921-5093, https://doi.org/10.1016/j.msea.2019.138209.

[26] Penna, R.; Lovisi, G.; Feo, L. Hygro-thermal bending behavior of porous FG nano-beams via local/nonlocal strain and stress gradient theories of elasticity. Compos. Struct., 2021, 263, 113627. https://doi.org/10.1016/j.compstruct.2021.113627

[27] Penna, R.; Feo, L.; Lovisi, G. Fabbrocino, F;. Hygro-Thermal Vibrations of Porous FG Nano-Beams Based on Local/Nonlocal Stress Gradient Theory of Elasticity. Nanomaterials, 2021, 11(4), 910. https://doi.org/10.3390/nano11040910

[28] Penna, R.; Lovisi, G.; Feo, L. Dynamic Response of Multilayered Polymer Functionally Graded Carbon Nanotube Reinforced Composite (FG-CNTRC) Nano-Beams in Hygro-Thermal Environment. Polymers 2021, 13, 2340. https://doi.org/10.3390/polym13142340

[29] Penna, R.; Feo, L.; Lovisi, G.; Fabbrocino, F. Application of the Higher-Order Hamilton Approach to the Nonlinear Free Vibrations Analysis of Porous FG Nano-Beams in a Hygrothermal Environment

Based on a Local/Nonlocal Stress Gradient Model of Elasticity. Nanomaterials 2022, 12, 2098. https://doi.org/10.3390/nano12122098

[30] Rosa Penna, Luciano Feo, Giuseppe Lovisi, Arturo Pascuzzo. A stress-driven model incorporating surface energy effects for the bending analysis of functionally graded nanobeams with loading discontinuities. 27th International Conference on Fracture and Structural Integrity (IGF27). https://doi.org/10.1016/j.prostr.2023.07.040

[31] R. M. Mahamood, E. T. Akinlabi, M. Shukla, S. Pityana (2012). Functionally Graded Material, An Overview. Proceedings of the World Congress on Engineering, III, London, U.K.

[32] V. Cannillo, L. Lusvarghi, T. Manfredini, M. Montorsi, C. Siligardi, A. Sola (2007). Glass-alumina functionally graded materials produced by plasma spraying. In Key Engineering Materials, 333, 227-230. Trans Tech Publications Ltd.

[33] S. A. Lajevardi, T. Shahrabi, J. A. Szpunar (2013). Synthesis of functionally graded nano Al2O3–Ni composite coating by pulse electrodeposition. Applied Surface Science, 279, 180-188.

[34] S. Put, J. Vleugels, O. Van der Biest (2001). Functionally graded WC–Co materials produced by electrophoretic deposition. Scripta materialia, 45(10), 1139-1145.

[35] G.S. Was, J.W. Jones, C. E. Kalnas, L.J. Parfitt, M. Goldiner (1994). Role of ion beam assisted deposition in the synthesis and fracture of metal-ceramic multilayers. Surf Coat Technol, 65(1-3): 77-83.

[36] A. L. Dumont, J. P. Bonnet, T. Chartier, J. M. Ferreira (2001). MoSi2/Al2O3 FGM: elaboration by tape casting and SHS. Journal of the European Ceramic Society, 21(13), 2353-2360.

[37] A. Shahrjerdi, F. Mustapha, M. Bayat, S. M. Sapuan, D. L. A. Majid (2011). Fabrication of functionally graded hydroxyapatite-titanium by applying optimal sintering procedure and powder metallurgy. International Journal of Physical Sciences, 6(9), 2258-2267.

[38] Y. Watanabe, N. Yamanaka, Y. Fukui (1998). Control of composition gradient in a metal-ceramic functionally graded material manufactured by the centrifugal method. Composites Part A: Applied Science and Manufacturing, 29(5-6), 595-601.

[39] T. Katayama, S. Sukenaga, N. Saito, H. Kagata, K. Nakashima (2011). Fabrication of Al2O3-W functionally graded materials by slip casting method. In 3rd International Congress on Ceramics, ICC 2011, IOP Conference Series: Materials Science and Engineering, Osaka; Japan.

[40] J.G. Yeo, Y.G. Jung, S.C. Choi (1998). Design and microstructure of ZrO2/SUS316 functionally graded materials by tape casting. Mater. Lett, 37 (6) 304–311.

[41] R.M. Mahamood, E.T. Akinlabi, M. Shukla, S. Pityana (2014). Evolutionary additive manufacturing: an overview. Lasers in Engineering 27, 161–178.

[42] Bajaj K, Shrivastava Y, Dhoke P. Experimental study of functionally graded beam with fly ash. J Inst Eng Ser A 2013;94:219–27. doi:10.1007/s40030-014-0057

[43] Herrmann, M and Sobek, W. Functionally graded concrete: Numerical design methods and experimental tests of mass-optimized structural Components. Structural Concrete. 2017; 18: 54-66.

[44] Ming Dao, Pei Gu, Akhilesh Maewal and R. J. Asaro. A micromechanical study of residual stresses in functionally graded materials. Acta mater. vol. 45, no. 8, pp. 3265-3276, 1997.

[45] Pushkaraj M. Deshmukh. Modeling error estimation and adaptive modeling of FGM. A Thesis submitted to the Division of Research and dvanced Studies of the University of Cincinnati in partial fulfillment of the requirements for the degree of Master of science

[46] W. Voigt (1889). Ueber die Beziehung zwischen den beiden Elasticitätsconstanten isotroper Körper. Annalen der physik, 274(12), 573-587.

[47] A. Reuss (1929). Berechnung der fließgrenze von mischkristallen auf grund der plastizitätsbedingung für einkristalle. ZAMM-Journal of Applied Mathematics and Mechanics/Zeitschrift für Angewandte Mathematik und Mechanik, 9(1), 49-58.

[48] Z. Hashin (1960). The elastic moduli of heterogeneous materials. HARVARD UNIV CAMBRIDGE MA.

[49] Z. Hashin, S. Shtrikman (1963). A variational approach to the theory of the elastic behavior of multiphase materials. Journal of the Mechanics and Physics of Solids, 11(2), 127-140.

[50] T. Mori, K. Tanaka (1973). Average stress in matrix and average elastic energy of materials with misfitting inclusions. Acta metallurgica, 21(5), 571-574.

[51] R. Hill (1965). A self-consistent mechanics of composite materials. Journal of the Mechanics and Physics of Solids, 13(4), 213-222.

[52] K. Wakashima, H. Tsukamoto (1991). Mean-field micromechanics model and its application to the analysis of thermomechanical behavior of composite materials. Materials Science and Engineering: A, 146(1-2), 291-316.

[53] J. C. Halpin (1969). Effects of Environmental Factors on Composite Materials. Air Force Materials Lab Wright-Patterson AFB OH.

[54] I. Tamura (1973). Strength and ductility of Fe-Ni-C alloys composed of austenite and martensite with various strength. In Proceedings of the third international conference on strength of metals and alloys, 1, 611-615. Cambridge, Institute of Metals.

[55] J. H. Kim, G. H. Paulino (2003). An accurate scheme for mixed-mode fracture analysis of functionally graded materials using the interaction integral and micromechanics models. International Journal for Numerical Methods in Engineering, 58(10), 1457-1497.

[56] A. R. Nemati, M. J. Mahmoodabadi (2020). Effect of micromechanical models on stability of functionally graded conical panels resting on Winkler–Pasternak foundation in various thermal environments. Archive of Applied Mechanics, 90(5), 883-915.

[57] J. R. Zuiker (1995). Functionally graded materials: choice of micromechanics model and limitations in property variation. Composites Engineering, 5(7), 807-819.

[58] T. Reiter, G. J. Dvorak (1998). Micromechanical modeling of functionally graded materials. In IUTAM Symposium on Transformation Problems in Composite and Active Materials (pp. 173-184). Springer, Dordrecht.

[59] B. Klusemann, B. J. T. M. Svendsen (2010). Homogenization methods for multi-phase elastic composites: Comparisons and benchmarks. Technische Mechanik-European Journal of Engineering Mechanics, 30(4), 374-386.

[60] B. Karami, D. Shahsavari, M. Janghorban, L. Li (2019). Influence of homogenization schemes on vibration of functionally graded curved microbeams. Composite Structures, 216, 67-79

[61] K. Wakashima, T. Hirano, M. Niino (1990). Functionally Gradient Materials (Fgm) Architecture: A New Type of Ceramic-Metal Assemblage Designed for Hot Structural Components.

[62] Lee, Y.D., Erdogan, F., 1995. Residual/thermal stress in FGM and laminated thermal barrier coatings. International Journal of Fracture 69, 145–165

[63] Bao, G., Wang, L., 1995. Multiple cracking in functionally graded ceramic/metal coatings. International Journal of Solids and Structure 32, 2853–2871.

[64] Chung, Y.L., Chi, S.H., 2001. The residual stress of functionally graded materials. Journal of the Chinese Institute of Civil and Hydraulic Engineering 13, 1–9.

[65] Shyang-Ho Chi, Yen-Ling Chung. Mechanical behavior of functionally graded material plates under transverse load—Part I: Analysis. International Journal of Solids and Structures 43 (2006) 3657–3674.

[66] J. H. Kim, G. H. Paulino (2002). Finite element evaluation of mixed mode stress intensity factors in functionally graded materials. International Journal for Numerical Methods in Engineering, 53(8), 1903-1935.

[67] Yijie Liua, Shengkai Sua , Huaiwei Huangb, Yingjing Lianga. Thermal-mechanical coupling buckling analysis of porous functionally graded sandwich beams based on physical neutral plane. Composites Part B: Engineering Volume 168, 1 July 2019, Pages 236-242

[68] Nuttawit Wattanasakulpong , Arisara Chaikittiratana. Flexural vibration of imperfect functionally graded beams based on Timoshenko beam theory: Chebyshev collocation method. Meccanica (2015) 50:1331–1342. DOI 10.1007/s11012-014-0094-8

[69] TouloukianYS.Thermophysicalpropertiesofhightemperaturesolidmateri- als. New York: Macmillan;1967.

[70] Reddy, J. N. , & Chin, C. D. (1998). Thermomechanical analysis of functionally graded cylinders and plates. Journal of Thermal Stresses, 21 (6), 593–626 .

[71] M.A. Eltaher, A.E. Alshorbagy, F.F. Mahmoud. Determination of neutral axis position and its effect on natural frequencies of functionally graded macro/nanobeams. Composite Structures Volume 99, May 2013, Pages 193-201

[72] Malagù, M.; Benvenuti, E.; Simone, A. One-dimensional nonlocal elasticity for tensile single-walled carbon nanotubes: A molecular structural mechanics characterization. Eur. J. Mech.—A/Solids 2015, 54, 160–170.

[73] Duan, K.; Li, L.; Hu, Y.; Wang, X. Enhanced interfacial strength of carbon nanotube/copper nanocomposites via Ni-coating: Molecular-dynamics insights. Phys. E Low-Dimens. Syst. Nanostructures 2017, 88, 259–264.

[74] Bartolomeo Chiara. Nonlocal Elastic Modelling of Carbon Nanotubes for Free Vibrations Problems. Doctoral Thesis in energy science and engineering. (2020)

[75] Barretta, R.; Marotti de Sciarra, F.; Vaccaro, M.S. Nonlocal Elasticity for Nanostructures: A Review of Recent Achievements. Encyclopedia 2023, 3, 279-310.

[76] Rogula D., 1965. Influence of spatial acoustic dispersion on dynamical properties of dislocations, Bull. Acad. Pol. Sci. Ser. Sci. Tech. 13, 337-343.

[77] Rogula D., 1982. Introduction to nonlocal theory of material media. Nonlocal theory of material media, CISM courses and lectures, Springer, Wien, 268, 125-222.

[78] Eringen A.C., 1972. Linear theory of nonlocal elasticity and dispersion of plane waves, International Journal of Engineering Science 10(5), 425-435.

[79] Eringen, A.C., 1983. On differential equations of nonlocal elasticity and solutions of screw dislocation and surface waves, Journal of Applied Physics 54, 4703.

[80] Peddieson J., Buchanan G.R., McNitt R.P., 2003. Application of nonlocal continuum models to nanotechnology. International Journal of Engineering Science 41(3-5), 305-312.

[81] Challamel N., Wang C.M., 2008. The small length scale effect for a nonlocal cantilever beam: a paradox solved, Nanotechnology 19, 345703.

[82] Li C., Yao L., Chen W., Li S., 2015. Comments on nonlocal effects in nanocantilever beams, International Journal of Engineering Science 87, 47-57.

[83] Romano G., Barretta R., Diaco M., Marotti de Sciarra F., 2017. Constitutive boundary conditions and paradoxes in nonlocal elastic nano-beams, International Journal of Mechanical Sciences 121, 151-156.

[84] Eringen A.C., 1987. Theory of nonlocal elasticity and some applications, Res Mechanica 21, 313-342.

[85] Romano G., Barretta R., 2017. Nonlocal elasticity in nanobeams: the stress-driven integral model, International Journal of Engineering Science 115, 14-27.

[86] Barretta R., Fabbrocino F., Luciano R., Marotti de Sciarra F., 2018. Closed-form solutions in stress-driven two-phase integral elasticity for bending of functionally graded nano-beams, Physica E: Low-dimensional Systems and Nanostructures 97, 13-30.

[87] Lim C.W., Zhang G., Reddy J.N., 2015. A higher-order nonlocal elasticity and strain gradient theory and its applications in wave propagation, Journal of the Mechanics and Physics of Solids 78, 298-313.

[88] Mindlin RD. Micro-structure in linear elasticity. Arch Ration Mech Anal 1964; 16:51–78.

[89] Mindlin RD. Second gradient of strain and surface-tension in linear elasticity. Int. J. Solids Struct.1 1965;417–438.

[90] Zaera R, Serrano Ó, Fernández-Sáez R. On the consistency of the nonlocal strain gradient elasticity. International Journal of Engineering Science 2019;138:65–81.

[91] Barretta R, Marotti de Sciarra F. Variational nonlocal gradient elasticity for nano-beams. International Journal of Engineering Science 2019;143:73–91.

[92] Pinnola FP, Faghidian SA Barretta R, Marotti de Sciarra F. Variationally consistent dynamics of nonlocal gradient elastic beams. International Journal of Engineering Science 2020;149:103220.

[93] Tanga Y, Ding Q. Nonlinear vibration analysis of a bi-directional functionally graded beam under hygro-thermal loads. Compos Struct 2019;225:111076.

[94] Lee CY, Kim JH. Hygrothermal postbuckling behavior of functionally graded plates. Compos Struct 2013;95:278–82.

[95] Shen HS. Nonlinear analysis of functionally graded fiber reinforced composite laminated beams in hygrothermal environments, Part I: Theory and solutions. Compos Struct 2015;125:698–705.

[96] Shen HS. Nonlinear analysis of functionally graded fiber reinforced composite laminated beams in hygrothermal environments, Part II: numerical results. Compos Struct 2015;125:706–12.

[97] Nguyen TK, Nguyen BD, Vo TP, Thai HT. Hygro-thermal effects on vibration and thermal buckling behaviours of functionally graded beams. Compos Struct 2017;176:1050–60.

[98] Bouazza M, Zenkour AM. Hygro-thermo-mechanical buckling of laminated beam using hyperbolic refined shear deformation theory. Compos Struct 2020;252:112689.

[99] Amir Mehdi, Dehrouyeh-Semnani. On boundary conditions for thermally loaded FG beams. International Journal of Engineering Science Volume 119, October 2017, Pages 109-127

[100] Jouneghanim FZ, Dimitri R, Tornabene F. Structural response of porous FG nanobeams under hygro-thermo-mechanical loadings. Compos B 2017;152:71–8.

[101] Dastjerdi S, Malikan M, Dimitri R, Tornabene F. Nonlocal elasticity analysis of moderately thick porous functionally graded plates in a hygro-thermal environment. Compos Struct 2021;255:112925.

[102] He, J.-H. Hamiltonian approach to nonlinear oscillators. Phys. Lett. A 2010, 374, 2312–2314.

[103] He, J.-H. Variational approach for nonlinear oscillators. Chaos Solitons Fractals 2007, 34, 1430–1439.

[104] Ismail, G.; Cveticanin, L. Higher order Hamiltonian approach for solving doubly clamped beam type N/MEMS subjected to the van der Waals attraction. Chin. J. Phys. 2021, 72, 69–77.

[105] Akbarzade, M.; Kargar, A. Application of the Hamiltonian approach to nonlinear vibrating equations. Math. Comput. Model. 2011, 54, 2504–2514.

[106] A. M. Dehrouyeh-Semnani. On boundary conditions for thermally loaded FG beams. International Journal of Engineering Science. Volume 119, October 2017, Pages 109-127.

[107] Zhao, F.-q , Wang, Z.-m. , & Liu, H.-z. (2007). Thermal post-bunkling analyses of functionally graded material rod. Applied Mathematics and Mechanics, 28 (1), 59–67 .

[108] Ma, L. S. , & Lee, D. W. (2011). A further discussion of nonlinear mechanical behavior for FGM beams under in-plane thermal loading. Composite Structures, 93 (2), 831–842 .

[109] Ma, L. S. , & Lee, D. W. (2012). Exact solutions for nonlinear static responses of a shear deformable FGM beam under an in-plane thermal loading. European Journal of Mechanics - A/Solids, 31 (1), 13–20 .

[110] Esfahani, S. E. , Kiani, Y. , & Eslami, M. R. (2013a). Non-linear thermal stability analysis of temperature dependent FGM beams supported on non-linear hardening elastic foundations. International Journal of Mechanical Sciences, 69 , 10–20 .

[111] Esfahani, S. E. , Kiani, Y. , Komijani, M. , & Eslami, M. R. (2013b). Vibration of a temperature-dependent thermally pre/postbuckled FGM beam over a nonlinear hardening elastic foundation. Journal of Applied Mechanics, 81 (1) 011004-011004-011013.

[112] Barretta R, Canadija M, Feo L, Luciano R, Marotti de Sciarra F, Penna R. Exact solutions of inflected functionally graded nano-beams in integral elasticity. Compos. B 2018; 142:273–86.

[113] Pinnola, F.P.; Faghidian, S.A.; Barretta, R.; Marotti de Sciarra, F. Variationally consistent dynamics of nonlocal gradient elastic beams. Int. J. Eng. Sci. 2020, 149, 103220.

[114] Yiyuan Jiang, Li Li, Yujin Hu. A nonlocal surface theory for surface–bulk interactions and its application to mechanics of nanobeams. International Journal of Engineering Science Volume 172, 1 March 2022, 103624.

[115] K. Zarschler, L. Rocks, N. Licciardello, L. Boselli, E. Polo, K.P. Garcia, L. De Cola, H. Stephan, K.A. Dawson, Nanomed-Nanotechnol 12, 1663-1701 (2016).

[116] Wang J, Duan H.L, Huang Z.P and Karihaloo B.L. 2006. A scaling law for properties of nano-structured materialsProc. R. Soc. A.4621355–1363

[117] R. E. Miller and V. B. Shenoy, Size-dependent elastic properties of nanosized structural elements, Nanotechnology, 11 (3) (2000) 139-147

[118] Gurtin M., Murdoch A. (1975) A continuum theory of elastic material surfaces. Arch Ration Mech Anal 57(4):291–323.

[119] Gurtin M., Murdoch A. (1978) Surface stress in solids. Int J Solids Struct 14(6):431–440.

[120] Jin He and Carmen M. Lilley. Surface Effect on the Elastic Behavior of Static Bending Nanowires. Nano Lett. 2008, 8, 7, 1798–1802.

[121] Gang-Feng Wang and Xi-Qiao Feng 2009. Timoshenko beam model for buckling and vibration of nanowires with surface effects. J. Phys. D: Appl. Phys. 42 155411

[122] Ghadiri, M., Shafiei, N., & Akbarshahi, A. (2016). Influence of thermal and surface effects on vibration behavior of nonlocal rotating Timoshenko nanobeam. Appl. Phys. A, 122, 673. 10.1007/s00339-016-0196-3.

[123] Mohammad Hashemian, Shahin Foroutan, Davood Toghraie. Comprehensive beam models for buckling and bending behavior of simple nanobeam based on nonlocal strain gradient theory and surface effects. Mechanics of Materials Volume 139, December 2019, 103209.

[124] Sourani P., Mohammad Hashemian, Mostafa Pirmoradian, Davood Toghraie. A comparison of the Bolotin and incremental harmonic balance methods in the dynamic stability analysis of an Euler–Bernoulli nanobeam based on the nonlocal strain gradient theory and surface effects. Mechanics of Materials Volume 145, June 2020, 103403.

[125] F. F. Mahmoud, M. A. Eltaher, A. E. Alshorbagy, E. I. Meletis. Static analysis of nanobeams including surface effects by nonlocal finite element. Journal of Mechanical Science and Technology volume 26, pages3555–3563 (2012).

[126] Lingyu Li, Lin Cheng, Ri Sa, Xian Qiu, Libo Chen, Real-world insights into the efficacy and safety of tyrosine kinase inhibitors against thyroid cancers, Critical Reviews in Oncology/Hematology, Volume 172, 2022, 103624, ISSN 1040-8428, https://doi.org/10.1016/j.critrevonc.2022.103624.

[127] Li Li, Rongming Lin, Teng Yong Ng, Contribution of nonlocality to surface elasticity, International Journal of Engineering Science, Volume 152, 2020, 103311, ISSN 0020-7225, https://doi.org/10.1016/j.ijengsci.2020.103311.

[128] Shahab Saffari, Mohammad Hashemian⁎, Davood Toghraie. Dynamic stability of functionally graded nanobeam based on nonlocal Timoshenko theory considering surface effects. Physica B 520 (2017) 97–105.

[129] Parviz Malekzadeh, Mohamad Shojaee. Surface and nonlocal effects on the nonlinear free vibration of non-uniform nanobeams. Composites: Part B 52 (2013) 84–92.

[130] Chhapadia, P., Mohammadi, P., & Sharma, P. (2011). Curvature-dependent surface energy and implications for nanostructures. Journal of the Mechanics and Physics of Solids, 59(10), 2103–2115.

[131] Steigmann D. J. And Ogden R. W. 1999Elastic surface—substrate interactions Proc. R. Soc. Lond. A.455437–474http://doi.org/10.1098/rspa.1999.0320.

[132] Rosa Penna, Bending analysis of functionally graded nanobeams based on stress-driven nonlocal model incorporating surface energy effects, International Journal of Engineering Science, Volume 189, 2023, 103887, ISSN 0020-7225, https://doi.org/10.1016/j.ijengsci.2023.103887.

[133] Weidong Yang, Shuo Wang, Wenbing Kang, Tao Yu, Yan Li, A unified high-order model for size-dependent vibration of nanobeam based on nonlocal strain/stress gradient elasticity with surface effect, International Journal of Engineering Science, Volume 182, 2023, 103785, ISSN 0020-7225, https://doi.org/10.1016/j.ijengsci.2022.103785.

[134] Qiang Chen, Nicola Pugno, Zhiyong Li, Influence of surface stress on elastic constants of nanohoneycombs, Physica E: Low-dimensional Systems and Nanostructures, Volume 53, 2013, Pages 217-222, ISSN 1386-9477, https://doi.org/10.1016/j.physe.2013.05.001.

[135] Shenoy Vijay B. Atomistic calculations of elastic properties of metallic fcc crystal surfaces Phys. Rev. B 71, 094104 – Published 18 March 2005; Erratum Phys. Rev. B 74, 149901 (2006)

[136] Giuseppe Lovisi, Application of the surface stress-driven nonlocal theory of elasticity for the study of the bending response of FG cracked nanobeams, Composite Structures, Volume 324, 2023, 117549, ISSN 0263-8223, https://doi.org/10.1016/j.compstruct.2023.117549.

[137] Rosa Penna, Luciano Feo, Giuseppe Lovisi, Arturo Pascuzzo, A stress-driven model incorporating surface energy effects for the bending analysis of functionally graded nanobeams with loading discontinuities, Procedia Structural Integrity, Volume 47, 2023, Pages 789-799, ISSN 2452-3216, https://doi.org/10.1016/j.prostr.2023.07.040.

[138] Shahrokh Hosseini-Hashemi, Reza Nazemnezhad, An analytical study on the nonlinear free vibration of functionally graded nanobeams incorporating surface effects, Composites Part B: Engineering, Volume 52, 2013, Pages 199-206, ISSN 1359-8368, https://doi.org/10.1016/j.compositesb.2013.04.023.

[139] Hui, D. W., & Gang-Feng, W. (2011). Surface Effects on the Vibration and Buckling of Double-Nanobeam-Systems. Hindawi Publishing Corporation Journal of Nanomaterials Volume. https://doi.org/10.1155/2011/518706. Article ID 518706, 7 pages.

[140] Vaccaro, M.S., Marotti De Sciarra, F., Barretta, R. On the regularity of curvature fields in stress-driven nonlocal elastic beams. Acta Mech 232, 2595–2603 (2021). https://doi.org/10.1007/s00707-021-02967-w

[141] Barretta, R., Caporale, A., Luciano, R., Vaccaro, M.S. Nonlocal gradient mechanics of nanobeams for non-smooth fields. International Journal of Engineering ScienceVolume 1891 August 2023 Article number 103879. 10.1016/j.ijengsci.2023.103879

[142] Christides, S., Barr, A.D.S. One-dimensional theory of cracked Bernoulli–Euler beams, International Journal of the Mechanical Sciences 26 (1984) 639–648.

[143] Shen, M., Pierre, C. Natural modes of Bernoulli–Euler beams with symmetric cracks, Journal of Sound and Vibration 138 (1990) 115–134.

[144] Shen, M., Pierre, C. Free vibrations of beams with a single-edge crack, Journal of Sound and Vibration 170 (1994) 237–259

[145] Adams, R. D., Cawley, P., Pye, C. J., Stone, B. J. A vibration technique for non-destructively assessing the integrity of structures. J. Mech. Eng. Sci. 20, 93 s1978

[146] Cawley, P., Adams, R.D. The locations of defects in structures from measurements of natural frequencies, Journal of Strain Analysis 14 (1979) 49–57.

[147] Freund, L. B., Herrmann, G. Dynamin fracture of a beam or plate in plane bending. J. Appl. Mech. 76-APM-15, 112 s1976d.

[148] Valiente, A., Elices, M., Ustáriz, F. Determinacion de esfuerzos y movimientos en estructuras lineales con secciones fisuradas. Anales de mecanica de la fractura vol.7 (1990).

[149] Fernandez-Saez, J., Rubio, L., Navarro, C. Approximate calculation of the fundamental frequency for bending vibrations of cracked beams. Sound Vib. 225, 345s1999d.

[150] Fernandez-Saez, J., Navarro, C. Fundamental frequency of cracked beams in bending vibrations: an analytical approach. J. Sound Vib. 256, 17 s2002d, 2002.

[151] Loya, J., Rubio, L., Fernandez-Saez, J. Natural frequencies for bending vibrations of Timoshenko cracked beams. J. Sound Vib. 290, 640 s2006d.

[152] Ariaa, A.I., Friswellb, M.I., Rabczukc, T. Thermal vibration analysis of cracked nanobeams embedded in an elastic matrix using finite element analysis. Composite Structures. Volume 212, 15 March 2019, Pages 118-128

[153] Ismail, E., Cevat, Ö., Eltaher, M.A. Free vibration of a cracked FG microbeam embedded in an elastic matrix and exposed to magnetic field in a thermal environment. Composite Structures. Volume 261, 1 April 2021, 113552

[154] Kienzler, R. Energy changes in elastic plates due to holes and cracks. Proceedings of the Estonian Academy of Sciences, 2008, 57, 1, 26–33 doi: 10.3176/proc.2008.1.03

[155] Rohde, L., Kienzler, R. Numerical computation and analytical estimation of stress-intensity factors for strips with multiple edge cracks. Arch Appl Mech (2005) 74: 846–852 DOI 10.1007/s00419-005-0397-2

[156] Fischer, F.D., Predan, J., Kienzler, R. An easy-to-use estimate of the energy-release rate for crack arrays. Arch Appl Mech (2014) 84:1325–1337 DOI 10.1007/s00419-014-0872-8

[157] Rohde, L., Kienzler, R., Herrmann, G. On a new method for calculating stress-intensity factors of multiple edge cracks. ISSN 1478–6435 print/ISSN 1478–6443

[158] Tada, H., Paris, P., Irwin, G. The Stress Analysis of Cracks Handbook. St Louis: Paris Productions, Inc., third edition, 1985.

## Appendix A

- *Even porosity distribution*

$$A_E = -\frac{bh((-2+\zeta+n\zeta)E_c+(n(-2+\zeta)+\zeta)E_m)}{2(1+n)} \tag{A1}$$

$$S_E = 0 \tag{A2}$$

$$I_E = \frac{bh^3(12E_c^2+4n(7+4n+n^2)E_cE_m+n^2(7+4n+n^2)E_m^2)}{12(2+n)^2(3+n)(E_c+nE_m)} \tag{A3}$$

$$A_\rho = -\frac{bh((-2+\zeta+n\zeta)\rho_c+(n(-2+\zeta)+\zeta)\rho_m)}{2(1+n)} \tag{A4}$$

$$S_\rho = \frac{bh^2n(-1+\zeta)(E_m\rho_c-E_c\rho_m)}{(2+n)((-2+\zeta+n\zeta)E_c+(n(-2+\zeta)+\zeta)E_m)} \tag{A5}$$

$$\begin{aligned} I_\rho = -((bh^3(e_m^2((-24n^2(7+n(4+n))+4n(24+n(9+n)(7\\ &+n(4+n)))\zeta-2(1+n)(2+n)(6+n(5+n)(3\\ &+2n))\zeta^2+(1+n)^2(2+n)^2(3+n)\zeta^3)\rho_c+(n(-2\\ &+\zeta)+\zeta)(4n^2(7+n(4+n))-4n(2+n)(7+n(4\\ &+n))\zeta+(1+n)(2+n)^2(3+n)\zeta^2)\rho_m)\\ &+2e_ce_m((n(-2+\zeta)+\zeta)(48+(2+n)\zeta(-8(3+n(2\\ &+n))+(1+n)(2+n)(3+n)\zeta))\rho_c+(-2+\zeta\\ &+n\zeta)(4n^2(7+n(4+n))-4n(2+n)(7+n(4+n))\zeta\\ &+(1+n)(2+n)^2(3+n)\zeta^2)\rho_m)+e_c^2((-2+\zeta\\ &+n\zeta)(48+(2+n)\zeta(-8(3+n(2+n))+(1+n)(2\\ &+n)(3+n)\zeta))\rho_c+(-32n(2+n)^2+8(6+n(24\\ &+n(31+n(10+n))))\zeta-2(1+n)(2+n)(12\\ &+n(18+n(5+n)))\zeta^2+(1+n)^2(2+n)^2(3\\ &+n)\zeta^3)\rho_m)))/(24(2+n)^2(3\\ &+n)((-2+\zeta+n\zeta)e_c+(n(-2+\zeta)+\zeta)e_m)^2)) \end{aligned} \tag{A6}$$

- *Uneven porosity distribution*

$$A_E = \frac{b(4hE_c - h\zeta E_c - hn\zeta E_c + 4hnE_m - h\zeta E_m - hn\zeta E_m)}{4(1+n)} \tag{A7}$$

$$S_E = 0 \tag{A8}$$

$$\begin{aligned} I_E = -\Big(bh^3\Big(\big(&384 \\ &+ (2+n)\zeta(-72 - 4n(11+7n) \\ &+ (1+n)(2+n)(3+n)\zeta)\big)e_c^2 \\ &+ 2\big(64n\big(7+n(4+n)\big) - 6(1+n)(2+n)^2(3+n)\zeta \\ &+ (1+n)(2+n)^2(3+n)\zeta^2\big)e_c e_m \\ &+ \big(32n^2\big(7+n(4+n)\big) \\ &- 4n(2+n)\big(22+n(11+3n)\big)\zeta \\ &+ (1+n)(2+n)^2(3+n)\zeta^2\big)e_m^2\Big)\Big)/(96(2+n)^2(3 \\ &+ n)((-4+\zeta+n\zeta)e_c + (n(-4+\zeta)+\zeta)e_m))) \end{aligned} \tag{A9}$$

$$A_\rho = \frac{b(4h\rho_c - h\zeta\rho_c - hn\zeta\rho_c + 4hn\rho_m - h\zeta\rho_m - hn\zeta\rho_m)}{4(1+n)} \tag{A10}$$

$$S_\rho = \frac{b(-2h^2nE_m\rho_c + h^2n\zeta E_m\rho_c + 2h^2nE_c\rho_m - h^2n\zeta E_c\rho_m)}{(2+n)(-4E_c + \zeta E_c + n\zeta E_c - 4nE_m + \zeta E_m + n\zeta E_m)} \tag{A11}$$

$$
\begin{aligned}
I_\rho = -((bh^3(E_m^2((-384n^2(7+n(4+n)) + 16n(48+n(114+n(5 \\
&+ n)(14+n)))\zeta - 8(1+n)(2+n)(6+n(9+n(8 \\
&+ n)))\zeta^2 + (1+n)^2(2+n)^2(3+n)\zeta^3)\rho_c + (n(-4 \\
&+ \zeta) + \zeta)(32n^2(7+n(4+n)) - 4n(2+n)(22 \\
&+ n(11+3n))\zeta + (1+n)(2+n)^2(3+n)\zeta^2)\rho_m) \\
&+ 2E_cE_m((n(-4+\zeta)+\zeta)(384+(2+n)\zeta(-72 \\
&- 4n(11+7n) + (1+n)(2+n)(3+n)\zeta))\rho_c + (-4 \\
&+ \zeta + n\zeta)(32n^2(7+n(4+n)) - 4n(2+n)(22 \\
&+ n(11+3n))\zeta + (1+n)(2+n)^2(3+n)\zeta^2)\rho_m) \\
&+ E_c^2((-4+\zeta+n\zeta)(384+(2+n)\zeta(-72-4n(11 \\
&+ 7n) + (1+n)(2+n)(3+n)\zeta))\rho_c \\
&+ (-512n(2+n)^2 + 16(12+n(80+n(117+n(39 \\
&+ 4n))))\zeta - 8(1+n)(2+n)(6+n(13+n(4 \\
&+ n)))\zeta^2 + (1+n)^2(2+n)^2(3 \\
&+ n)\zeta^3)\rho_m)))/(96(2+n)^2(3 \\
&+ n)((-4+\zeta+n\zeta)E_c + (n(-4+\zeta)+\zeta)E_m)^2))
\end{aligned}
\tag{A12}
$$